‘BIOINSPIRED’ TOTAL SYNTHESIS OF AGELASTATIN A AND DERIVATIVES FOR CELLULAR TARGET IDENTIFICATION; SYNTHESES OF ^{15}N-LABELED OROIDIN AND KERAMADINE ANALOG FOR ‘METABIOSYNTHETIC’ STUDIES

A Dissertation

by

JEREMY CHRIS PUNZALAN REYES

Submitted to the Office of Graduate and Professional Studies of
Texas A&M University
in partial fulfillment of the requirements for the degree of

DOCTOR OF PHILOSOPHY

Chair of Committee,	Daniel Romo
Committee Members,	David E. Bergbreiter
	Daniel A. Singleton
	Thomas D. McKnight
Head of Department,	David H. Russell

December 2013

Major Subject: Chemistry

ABSTRACT

Numerous marine-derived pyrrole 2-aminoimidazole alkaloids (P-2-AIs), including the highly potent antitumor natural product agelastatin A, are presumed to be derived from the simple precursor oroidin and related stuctures. The molecular complexity of P-2AIs, significant biological activities, as well as the interesting biosynthetic routes proposed for their origin has made this family of alkaloids the subject of numerous synthetic investigations.

Herein, a bioinspired total synthesis of agelastatin A is described premised on the isolation of two other P-2AIs, keramadine and nagelamide J. Two biosynthetically relevant cyclizations rapidly convert a linear precursor, resembling an oxidized keramadine, to agelastatin A. A facile and highly diastereoselective C-ring formation via a 5-*exo*-trig cyclization or a Nazarov 4π-electrocyclization, proceeding through a deep-red colored *N*-acyliminium intermediate, constructs the three contiguous stereocenters of the cyclopentane core found in the agelastatins and nagelamide J. A possible templating effect was discovered in a silica gel-assisted reaction that enables the final B-ring closure. The described synthesis provided access to various agelastatin A derivatives leading to a bioactive biotin probe that is proving to be useful for cellular target identification.

In an effort toward understanding the biosynthesis of P-2-AIs, a synthesis of ^{15}N-oroidin labeled oroidin was developed and pulse labeling and analysis by 1D ^{1}H-^{15}N HSQC NMR and FTMS experiments was validated as a direct method for measurement

of ^{15}N incorporation into P2-AIs. Studies toward the synthesis of a ^{15}N-keramadine analog, which will be used to investigate the biosynthetic origin of agelastatin A, are also described.

DEDICATION

To my son, Jairus Benjamin

ACKNOWLEDGEMENTS

First and foremost, I would like to thank my advisor/committee chair, Prof. Daniel Romo, for his guidance and support all throughout graduate school and for his confidence that I could take on challenging projects. I am forever grateful to him for providing me with the research resources and the opportunity to learn other subfields of chemistry, more than synthetic organic chemistry. Looking back to when I started graduate school, it has truly been a rewarding educational experience working in his laboratories. Special thanks to the Romo family as well for welcoming me and my wife into their home for group gatherings and reminding me a lot of my own family.

My sincere gratitude also goes to Prof. Daniel Singleton and Prof. David Bergbreiter for serving on my advisory committee and most especially for teaching me organic chemistry. Your enthusiasm and dedication to teaching is truly inspirational. My wife and I also appreciate the pieces of advice you have given both of us the past years.

I am also grateful to Prof. Thomas McKnight for accommodating my short notice request to serve on my committee and to Prof. Jean-Philippe Pellois for being my non-departmental committee member for my preliminary proposal defense.

I owe special thanks to my undergraduate mentors Prof. Flerida Cariño and Prof. Florecita de Guzman for teaching me biochemistry and organic chemistry, and for all their invaluable help in the preparation of my graduate school applications.

Thanks also to my friends and colleagues in the Romo research group – previous and current members. You guys have been my family away from home. To Dr. Yonggang Wang, Dr. Chunxiao Xu, and Dr. Manuel Zancanella – you guys are true inspiration of diligence and excellence. To Dr. Gang Liu for being an older brother to me – you are one of the best chemists I know. To Dr. Fred Briones, thanks for adding more fun to my last year in the group, you are a true friend. To Dr. Sreekumar Velallath and Dr. Omar Robles, thanks for the friendship and advice. To RaeLynn, Natalie, and Khoi – you guys are siblings I never had. To Morgan and Mikail, the 'seniors' in the lab, its been fun alongside you both the past few years. To Angie, thanks for being the best administrative assistant our group have ever seen. To Dr. Mingzhao Zhu, thanks for being a good friend and providing a home to RJ when my wife and I are away. To Dr. Supakarn Chamni, Dr. Changsuk Lee, Dr. Henry Nguyen, Dr. Kay Morris, and Dr. Carolyn Leveret, Dr. Jing Li, and more recently Dr. Ken Hull thanks for the camaraderie.

To my College Station family, the Filipino Graduate Students Association (FIGSA), thank you all for your support and encouragement. To Kat, Aldrin, baby Noelle, Jess, Alnald, Jo, Madz, baby Lian, Fred, Jewel, Kuya Gally, Paul, Monet, Christian, Froi, Ate Gaya, Bjorn, Noah, Rose – thanks making CS a home away from home - you guys are amazing. To the Zamora, Go, and Capareda families, thanks for serving as our elders.

To my parents Manuel Rodrigo and Ma. Consuelo Reyes, thank you for the life lessons you've taught me. They have served as my guiding principle through the years.

To my brothers Michael Angelo, Jonah Matthew, Leo Martin and Mark Emmanuel, trying to set a good example for all of you has been my anchor throughout this process. To Jennifer and Jan Madeline, welcome to our family.

Most especially, thanks to my wife, Larisa Mae Quijano Reyes, for almost 11 years of unconditional love, patience, and support. Thanks to "UP Chemistry" for bringing our paths together. To my son, Jairus Benjamin, our very own natural product, this is for you. I may not have been there all the time for you and your mom as you were growing inside her womb, but I sure will do my best to make up for it. Mom and Dad are excited to see you. I hope one day you'll get the chance to read this.

Finally, thanks to God Almighty, for all the blessings He has showered my family especially this year.

TABLE OF CONTENTS

		Page
ABSTRACT		ii
DEDICATION		iv
ACKNOWLEDGEMENTS		v
TABLE OF CONTENTS		viii
LIST OF FIGURES		x
LIST OF TABLES		xii
CHAPTER		
I	INTRODUCTION	1
	1.1 The Pyrrole 2-Aminoimidazole (P-2-AI) Alkaloids	1
	1.2 Previous Total Syntheses of Agelastatin A	3
	1.3 Application of *N*-Acyliminium Intermediates in Bioinspired Total Syntheses	9
II	BIOINSPIRED TOTAL SYNTHESIS OF AGELASTATIN A	13
	2.1 Introduction	13
	2.2 Syntheses of the Imidazolone Fragments	24
	2.3 Syntheses of the Pyrrole Fragments	32
	2.4 Coupling of Fragments	36
	2.5 Synthesis of *N*-Acyliminium Cyclization Precursor: Investigation of the Proposed Key Step	39
	2.6 Final Cyclization Investigations: Completion of Synthesis	53
	2.7 Conclusions	57
III	STRUCTURE-ACTIVITY RELATIONSHIP (SAR) AND CELLULAR TARGET IDENTIFICATION STUDIES	58
	3.1 Introduction	58
	3.2 Syntheses and Bioactivity of Agelastatin A Derivatives	60
	3.3 Synthesis of a Potent Biotin Conjugate	67

CHAPTER Page

3.4 Initial Studies on the Identification of the Cellular Target of Agelastatin A 68

IV SYNTHESES OF ^{15}N-OROIDIN AND ^{15}N-KERAMADINE ANALOG FOR BIOSYNTHESIS/ METABIOSYNTHETIC STUDIES …….. 74

4.1 Introduction 74
4.2 Synthesis of ^{15}N-Oroidin 77
4.3 Synthesis of ^{15}N-Keramadine Analog 80
4.4 Evaluation of the Utility of ^{15}N-Oroidin for Biosynthetic Studies by HSQC and FTMS 83
4.5 Biosynthetic Feeding Experiments and 'Metabiosynthetic' Studies 91

V CONCLUSIONS 96

REFERENCES 98

APPENDIX A EXPERIMENTAL AND SELECTED SPECTRAL DATA 111

APPENDIX B LETTERS OF PERMISSION 212

LIST OF FIGURES

FIGURE		Page
1.1	The pyrrole-2-aminoimidazole (P-2-AI) alkaloids	2
2.1	The agelastatin family of alkaloids	13
2.2	Agelastatin A and pre-agelastatin motifs in other P-2-AIs	19
2.3	Ambivalent reactivity of 2-imidazolones	20
2.4	Calculated HOMO and LUMO of the red-colored *N*-acyliminium **2.87** and the π→π* transition proposed to be responsible for this color based on TD-DFT calculations. Isovalue for surface = 0.04	49
3.1	Cytotoxicity data (IC_{50}, μM) against L1210 mouse lymphocytic leukemia cells and summary of essential moieties in agelastatin A	59
3.2	Effects of agelastatin A on DNA, RNA, and protein synthesis using incorporation of [^{3}H]-thymidine, [^{3}H]-uridine, and [^{35}S]-methionine. IC_{50} values listed next to the corresponding curves	69
3.3	Effects of cycloheximide (CHX) on DNA, RNA, and protein synthesis using incorporation of [^{3}H]-thymidine, [^{3}H]-uridine, and [^{35}S]-methionine. IC50 values listed next to the corresponding curves	70
3.4	Dose-dependent inhibition of [^{35}S]-methionine incorporation by agelastatin A in an in vitro translation system. Agelastatin A was added to a rabbit reticulocyte lysate cocktail that included luciferase poly(A) control mRNA and [^{35}S]-methionine	71
3.5	Dual luciferase translation inhibition by agelastatin A using HCV IRES dual reporter in an in vitro RRL translation system in the presence of different concentrations of agelastatin A and 4 μM CHX	72
4.1	MALDI FTMS (7T) expansions of the pseudomolecular ion $[M+H]^+$ of oroidin for (a) natural **1.1** ($C_{11}H_{12}Br_2{}^{14}N_5O$) and 7-^{15}N-oroidin (**1.1b**). $C_{11}H_{12}Br_2{}^{14}N_4{}^{15}NO$, >98% atom ^{15}N. Mass accuracy = 1ppm	80

FIGURE Page

4.2 MALDI FTMS (7T) expansions of *m/z* and peak height, *h*, for the 'M+1' peak of the pseudomolecular ions of oroidin ($C_{11}H_{11}Br_2N_5O$). Mass accuracy = 1 ppm (R = 240,000). (a) natural **1.1**. (b) **1.1** + **1.1b** (0.04 mol equiv). (c) **1.1** + **1.1b** (0.10 mol equiv). Peak assignments of $[M+H]^+$ in (c): *m/z* 388.94372, $^{12}C_{10}{}^{13}CH_{12}Br_2N_5O^+$; *m/z* 388.93739; $^{12}C_{11}H_{12}Br_2N_4{}^{15}NO^+$. The unrelated peak at *m/z* 388.9305 (indicated with an '*') is tentatively assigned to some loss of H from the dominant $^{79}Br/^{81}Br$ isotopomer, $C_{11}H_{10}{}^{79}Br^{81}BrN_5O^+$ ($[M]^+$, Δmmu = –0.5). 85

4.3 2D ^1H-^{15}N HSQC (600 MHz, 1:1 DMSO-d_6/benzene-d_6) of natural oroidin (**1.1**, depicted tautomer is arbitrary). N locants are labeled following the numbering scheme of Assman and Köck[50]. ns = 16, T2, T1 = 2K x 256; F2, F1 = 2K x 1K; d1 =1.5s 88

4.4 1D ^1H-^{15}N HSQC experiments (^1H δ, 1.7 mm microcryoprobe, 600 MHz) of **1.1** with N-H assignments. Labels indicate N atom assignments made from a separate ^1H-^{15}N HMBC experiment (not shown). (a) 1500 µg of **1.1**, no added [^{15}N]-**1.1b**. (b) 1500 µg **1.1** +10 µg **1.1b**. (c) 1500 µg **1.1** + 5.0 µg **1.1b**. (d) 1500 µg **1.1** + 2.5 µg. Relaxation delay, d1 = 1.50 s, optimized for $^1J_{N\text{-}H}$ = 90 Hz; ^1H π/2 pulse = 12 µS, ^{15}N π/2 pulse = 34 µS; NA = 6K; dummy scans = 16; NI = 1; T2 = F2= 8K points (no zero fill) 89

4.5 Linear regression of ^1H-^{15}N HSQC NH(C=O) cross-peak integral ratio, $(I–I_0)/I_0$, of 'mock' pulse labeling experiments with natural abundance **1.1** (1500 µg, I_0) spiked with measured aliquots of **1.1b** (µg, 'x-scale'). Observed I' values for the NH-C=O ^1H-^{15}N couplet are normalized to the intensity of the pyrrole N-H cross peak, I_0 = 1.00 (I or $I_0 = I'/I_p$). Error bars are ± SD..... 90

S1 Single crystal X-ray structure (ORTEP) of cyclization precursor **2.84** 143

S2 Single crystal X-ray structure (ORTEP) of DMB aldehyde **2.58b** 145

S3 UV-Vis spectrum of the reaction (**2.84→2.88**) in CH_2Cl_2 147

S4 Experimental versus TD-DFT predicted absorption bands 150

LIST OF TABLES

TABLE		Page
2.1	Characterization of 2-imidazolone **2.47**	26
2.2	Screening of conditions for decarboxylative bromination	27
2.3	Screening of conditions for Fischer esterification	30
2.4	Electrophilic aromatic substitution of pyrrole carboxamide **2.39**	33
2.5	Characterization of monocyclized adduct **2.89**	48
2.6	Screening of chiral Brønsted acids	50
4.1	Integrals from ^{1}H-^{15}N 1D HSQC of natural oroidin (**1.1**, 1.5 mg/ 30 μL) and **1.1** 'spiked ' with **1.1b**. Integrals of H-N couplets corresponding to N-12, N-14 and N-16 vary due to tautomerism	88
S1	Comparison of ^{1}H NMR data of natural and synthetic agelastatin A in CD_3OD	140
S2	Comparison of ^{13}C NMR data of natural and synthetic agelastatin A in CD_3OD	141
S3	Comparison of ^{1}H NMR data of 4,5-bis-*epi*-agelastatin A in CD_3OD	142
S4	Absorbance maxima of tosyl and pyrrole moieties in dichloromethane	148
S5	Experimental versus TD-DFT predicted absorption bands.	149
S6	Orbital pairs involved in each transition.	151

CHAPTER I

INTRODUCTION

1.1 The Pyrrole-2-Aminoimidazole (P-2-AI) Alkaloids

Nitrogen-rich alkaloids containing multiple heterocyclic motifs rank high among the most challenging targets in synthetic organic chemistry. One such example is the ever growing family of pyrrole-2-aminoimidazole (P-2-AI) alkaloids (Figure 1.1).[1] Their structural complexity, compact stereochemical content, high nitrogen to carbon ratio, and widely varied biological activities have gained significant attention from a number of scientists from different fields worldwide. The simplest members of this family, oroidin **1.1** and its congeners hymenidine **1.2** and clathrodin **1.3**, are proposed to be the key biosynthetic precursor of more complex members *via* diverse sequences of cyclization and dimerization. To date, the Romo group has completed the enantioselective total syntheses of monomeric P-2-AI alkaloids, (+)-dibromophakellstatin **1.5**[2] and (+)-monobromophakellin **1.7**[3]. Our ongoing unified synthetic strategy towards dimeric P-2-AI alkaloids, palau'amine **1.11** and the axinellamines **1.10**, has revealed fascinating chemistry that plausibly mimics Nature's elegant assembly of these metabolites through its complex machinery. While more than one hundred and fifty members isolated and characterized, many new congeners still continue to be detected aside from identification of new sources of known metabolites. Although biosynthetic evidence are scarce, successful implementation of synthetic strategies premised on speculative biosynthetic proposals[1] have provided indirect

evidence of feasibility of biosynthetic pathways. Among P-2-AIs, agelastatin A **1.8**, is arguably the most popular within the synthetic community not only because of the challenge imposed by its highly compact structure but also due to the fact that it is arguably the most bioactive P-2-AI reported to date.

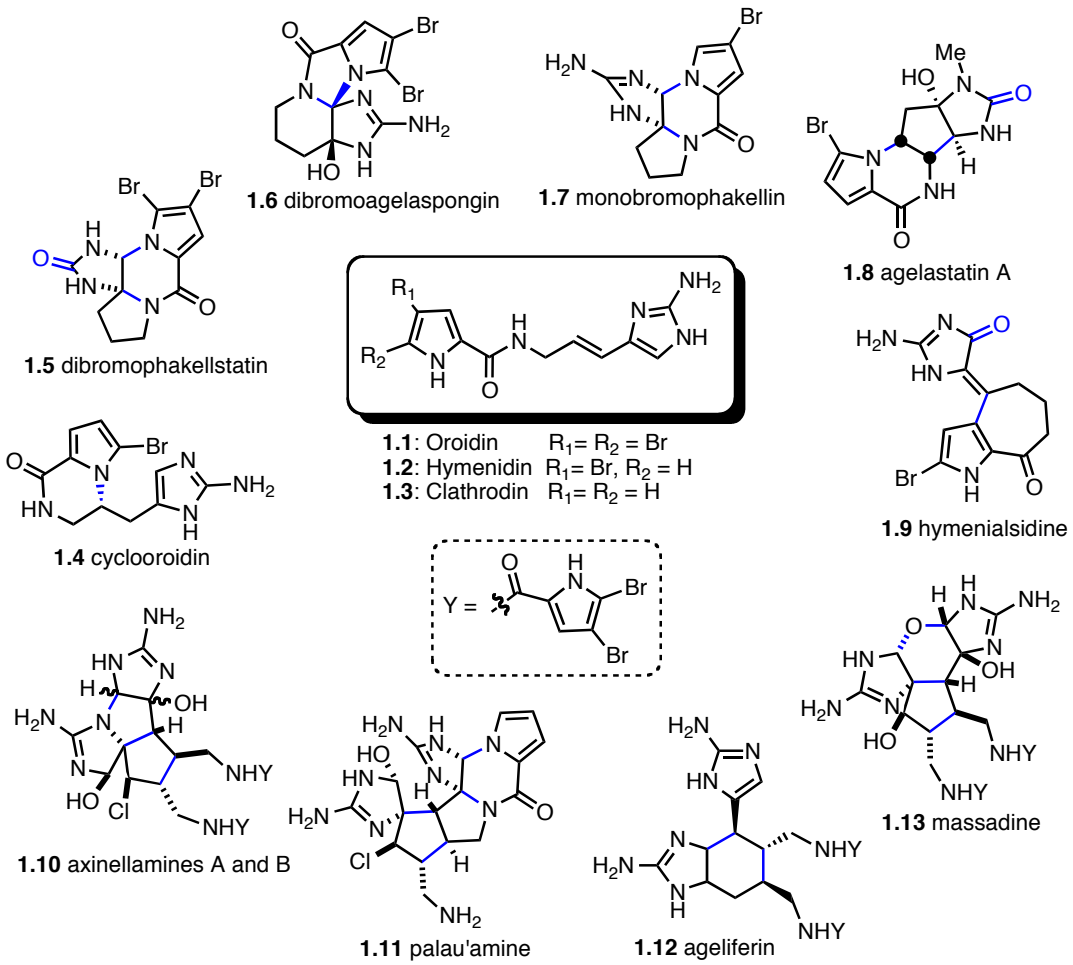

Figure 1.1 The pyrrole-2-aminoimidazole (P-2-AI) alkaloids

1.2 Previous Total Syntheses of Agelastatin A

To date, a number of research groups worldwide have disclosed their own approaches to the total synthesis of agelastatin A.[4] A variety of strategies have been employed to construct the unusual 5-6-5-5 tetracyclic ring system of the agalestatins. With all stereocenters in the molecule found decorating the cyclopentane C-ring, a common theme in most synthetic strategies is the construction of this ring with one or two of its stereocenters followed by substrate-controlled installation of the remaining stereocenters. The most notable syntheses are revisited herein focusing on key strategies used that enabled synthesis completion.

1.2.1 Weinreb's Racemic Synthesis of Agelastatin A

The Weinreb group has set the bar in this endeavor with their first total synthesis of racemic agelastatin A.[4a,4b] Their synthesis utilized several pericyclic reactions to construct the functionalized C-ring, starting off with a Hetero-Diels-Alder 4+2 cyloaddition between diene **1.14** and dienophile **1.15** to give bicycle **1.16**, which was immediately treated with phenyl magnesium bromide to produce allylic sulfoxide **1.17** (Scheme 1.1). With HMPT in methanol at elevated temperature, sulfoxide **1.17** underwent a [2,3]-sigmatropic rearrangement with the intermediacy of sulfenate ester **1.18**, which spontaneously cyclizes to afford cyclopentene-fused oxazolidinone **1.20**. Application of a Sharpless/Kresze allylic amination using **1.19** with refluxing toluene produced allylic sulfonamide **1.22** as a single regio- and stereoisomer. This transformation presumably occurs *via* an ene reaction that generates **1.21** followed by a [2,3]-sigmatropic rearrangement to give **1.22**. After deprotection steps, acylation with 2-

trimethylsilyl pyrrole acyl chloride, hydrolysis of cyclic carbamate, and pyridinium dichromate oxidation, **1.22** was converted to enone **1.23**. Treatment of **1.23** with $CsCO_3$ provided the piperazinone B-ring **1.24**. It is noteworthy that this aza-Michael cyclization strategy developed by the Weinreb group has been utilized by other subsequent efforts toward agelastatins.

Scheme 1.1

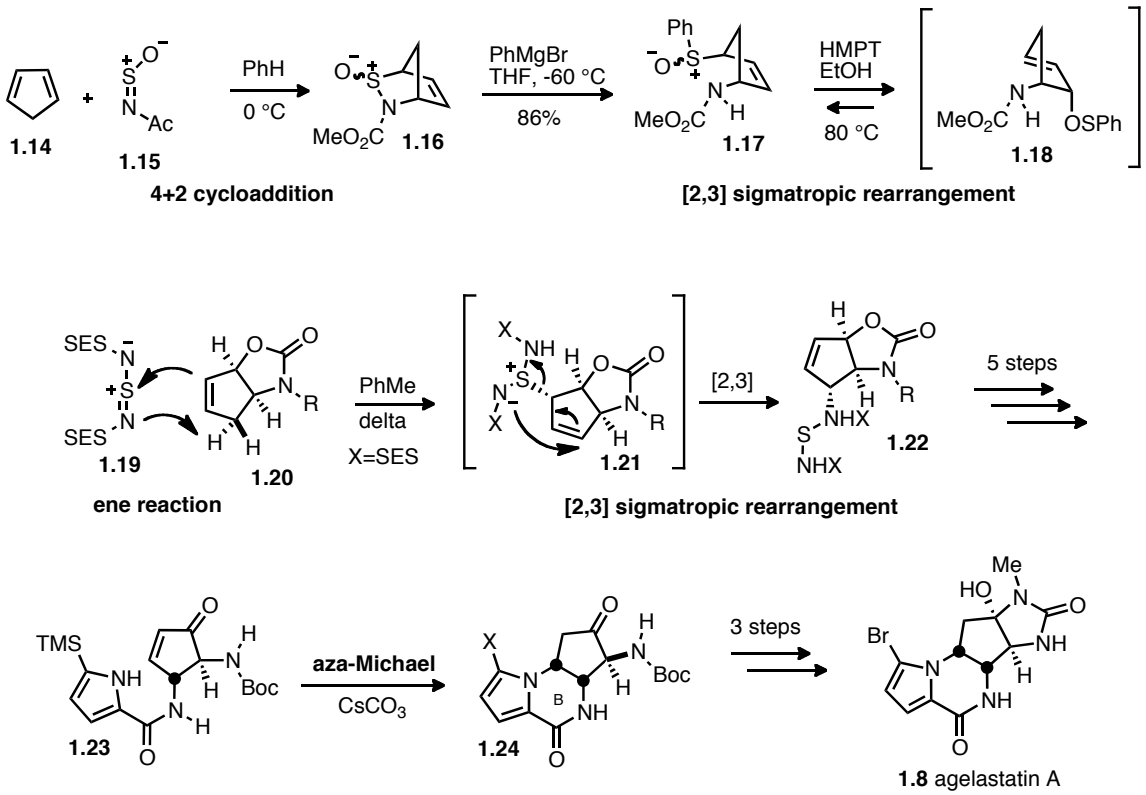

1.2.2 Feldman's Synthesis of (–)-Agelastatins A and B

The Feldman group accomplished the first enantioselective syntheses of both (–)-agelastatins A and B in 2002.[4c,4d] Alkynyliodonium salt **1.26** was prepared from chiral epoxide **1.25** (Scheme 1.2). Nucleophilic treatment of **1.26** with *p*-toluenesulfinate salt (TsNa) resulted in alkylidene-carbene **1.27**, which underwent a substrate-controlled diastereoselective C-H insertion giving cyclopentene **1.28**. This step closed the C-ring with one stereocenter in place. Another stereochemical setting step utilized in their approach is a convex face aza-Michael addition of *ortho*-nitrobenzylamine to vinyl sulfone **1.28**. Acylation with pyrrole acyl chloride gives **1.29**, which is converted to agelastatins A and B in 3 or 4 steps. Feldman's late-stage bromination procedure has also been adopted in many subsequent efforts.

Scheme 1.2

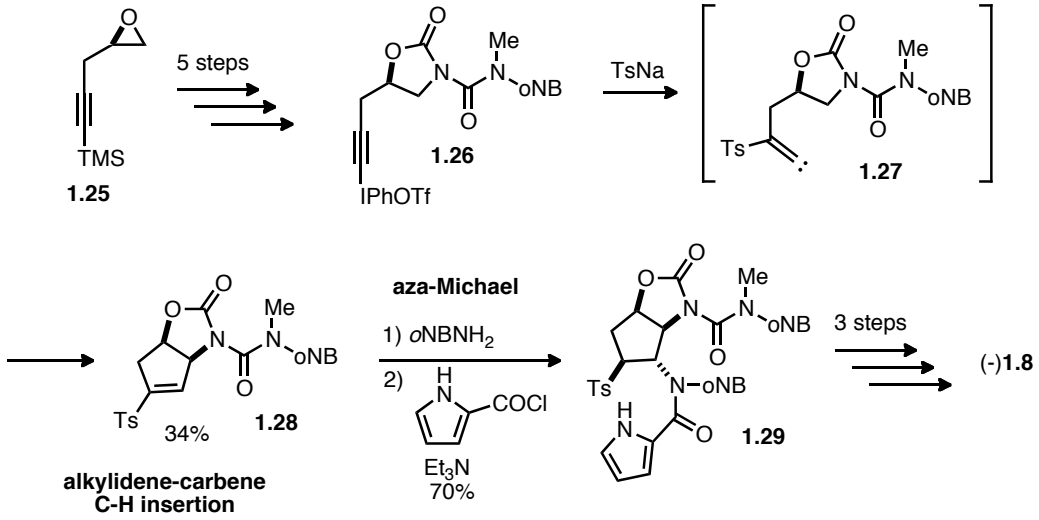

1.2.3 Du Bois's Synthesis of (–)-Agelastatin A

Du Bois and Wehn accomplished a robust route towards agelastatin A in 2006.[4r] From optically enriched lactam **1.30**, an efficient 3-step route converts this material to sulfamate **1.31** (Scheme 1.3). Using a methodology developed in their group, a substrate-controlled rhodium-catalyzed intramolecular aziridination yielded **1.32** as a single diastereomer in 95% yield using as low as 0.06 mol% catalyst loading. Treatment of **1.32** with NaN_3 allows regioselective attack at C(4) giving **1.33**, which after a PhSe nucleophilic attack and *N*-acylation provides a fully functionalized C-ring **1.34**, with all the requisite stereocenters in place. The A-ring was then installed *via* a Paal-Knorr pyrrole synthesis while the B-ring was installed via an amidation reaction. A 4-step sequence then converts urea **1.36** to agelastatin A **1.8**.

Scheme 1.3

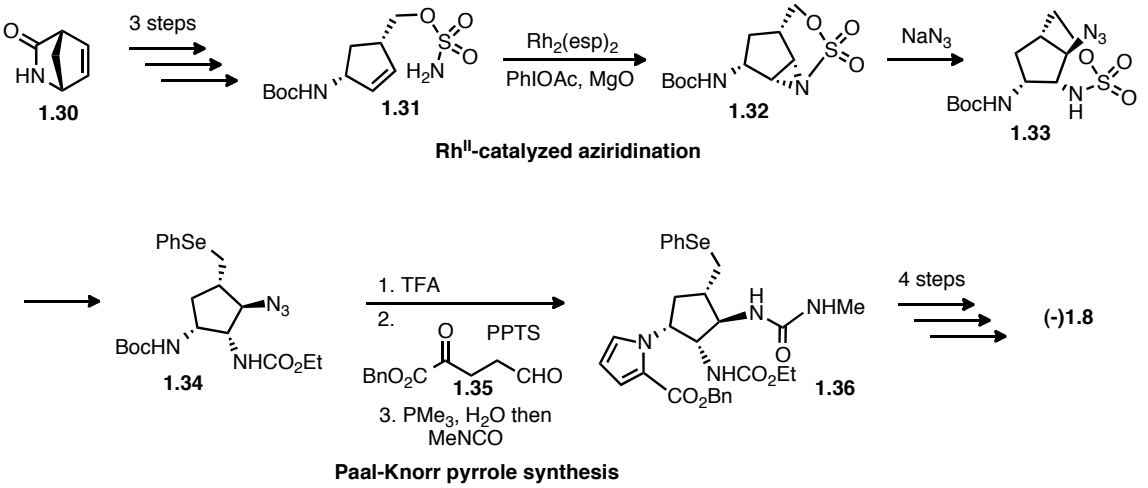

1.2.4 Trost's Stereodivergent Synthesis of Both (+) and (–)-Agelastatin A

Trost and Dong developed a stereodivergent strategy to access both enantiomers of agelastatin A.[4j,4m] Through the use *N*-methoxy amide pyrrole **1.37** and carbonate **1.38** under Pd-catalyzed AAA conditions using standard Trost ligand **1.39** provided ABC ring tricycle **1.40** as a single regio- and stereoisomer (Scheme 1.4). Mechanistically, this indicates a double allylic alkylation with the methoxyamide serving as the first nucleophile. A Kresze-type allylic amination reaction then installs N(3) and jumpstarts the introduction of the D-ring. Subsequent acylation of **1.42** with methyl isocyanate followed by formal hydration provides **1.43**, which is elaborated to (-)-agelastatin A in 2 steps. Using the same stereoinducing catalyst **1.39**, (+)-agelastatin A was also synthesized by sequential Pd-catalyzed AAA methodology.

Scheme 1.4

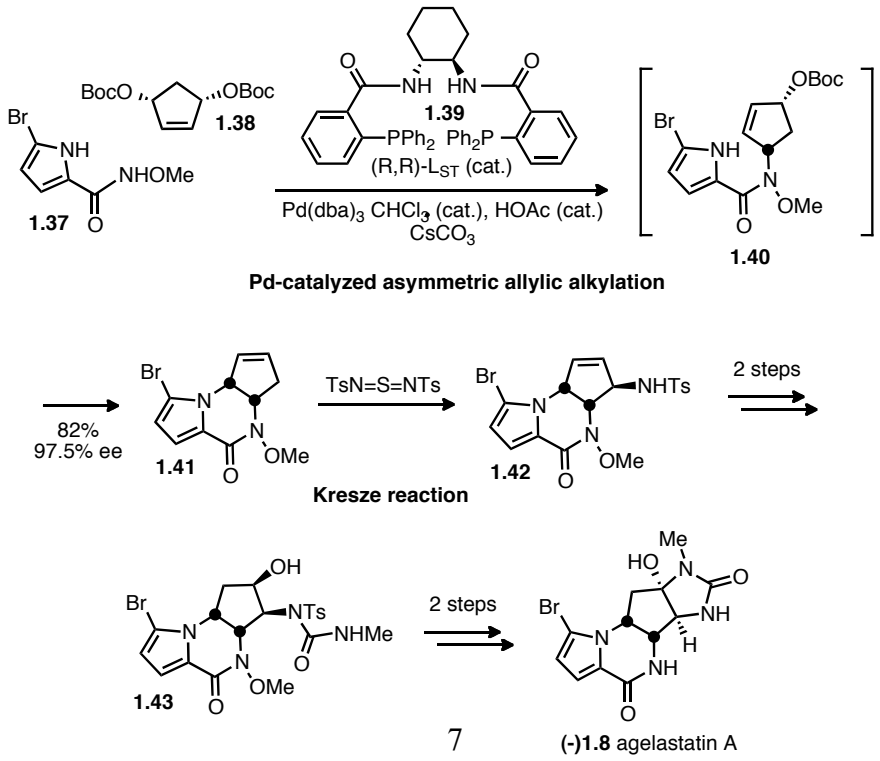

1.2.5 Movassaghi's Synthesis of (–)-Agelastatins A-F

The Movassaghi group in 2010 reported the first bioinspired total synthesis of agelastatin A and congeners.[4s] Their strategy, premised on the isolation of P-2-AI cyclooroidin,[5] commenced with chiral pool material *D*-aspartic acid dimethyl ester **1.44**, which was converted to pyrrole **1.46** (Scheme 1.5). This material was readily converted to cabinolamide **1.47** in 3 straighforward steps. Conversion of methyl ester **1.47** to imidazolone **1.49** was achieved through formation of a thioester, a Cu-promoted ketone synthesis using urea stannane **1.48**, and dehydration with HCl in methanol. Finally, the C-ring was introduced via a 5-*exo*-trig cyclization of imidazolone to the *N*-acyliminium formed from **1.49** under acidic conditions in water. This overall strategy led to the synthesis of all agelastatins with adaptation of some protocols from Pietra.[6]

Scheme 1.5

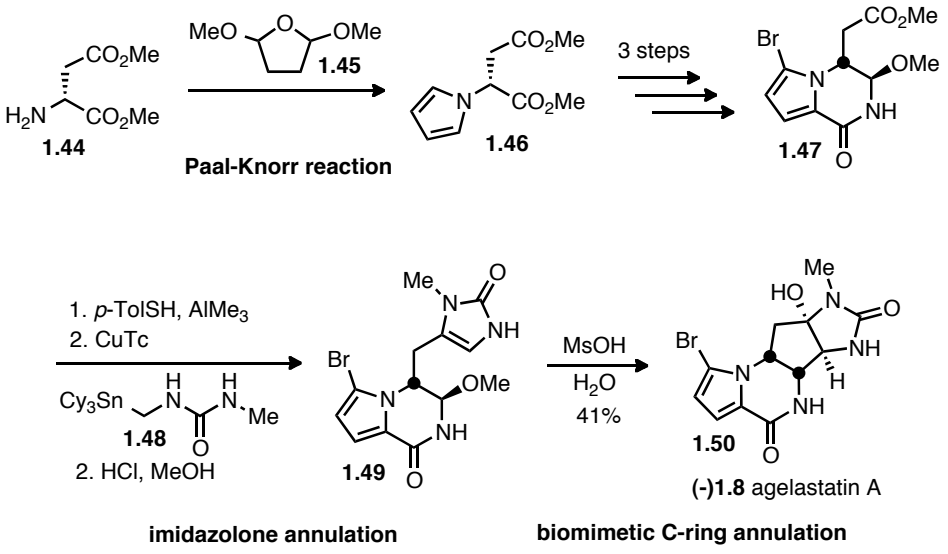

1.3 Application of *N*-Acyliminium Intermediates in Bioinspired Total Syntheses

Iminium ions are important reactive species for the formation of carbon-carbon and carbon-heteroatom bonds. The Mannich and Pictet-Spengler reactions have played a dramatic role in the advancement of synthetic organic chemistry in the past century. *N*-Acylation of the iminium ions further enhances its electron-attracting property, making *N*-acyliminium ions much more reactive electrophiles when compared to their *N*-alkyliminium counterparts. Because of its synthetic utility, several reviews on methodologies and applications of *N*-acyliminium chemistry have appeared in the literature.[7] This section focuses on representative examples of the utility of *N*-acyliminium intermediates in synthetic strategies premised on biosynthetic proposals.

In the biosynthesis of stemoamide **1.54**, spermidine **1.51** was proposed to be the penultimate biosynthetic precursor.[8] The proposal suggests that the azepine ring is constructed *via* iminium ion **1.52** (Scheme 1.6). It also suggests that preorganization of the reacting partners in an enzyme pocket is involved in the stereochemical setting step. A bioinspired approach based on this proposal was accomplished by Hong and coworkers in 2011.[8] Their 8-step synthesis with a straightforward coupling of propargyl TMS **1.55** and bromo aldehyde **1.56** followed by TBS protection to give **1.57**. Succinimide substitution followed by $NaBH_4$ reduction furnishes carbinolamide **1.58**. After extensive experimentation they ultimately found that anhydrous $FeCl_3$ successfully induced the formation of *N*-acyliminium **1.59**, which underwent a facile 7-*endo*-trig cyclization to give allene **1.60** containing of the 7-5 ring system of stemoamide. Following a tetrabutylammonium fluoride (TBAF) desilylation of the the TBS group, a

remarkable cyclocarbonylation transformation converts **1.61** to lactone **1.62**, installing the final lactone ring. A final nickel-catalyzed reaction readily transforms enone **1.62** to stemoamide **1.64**.

Scheme 1.6

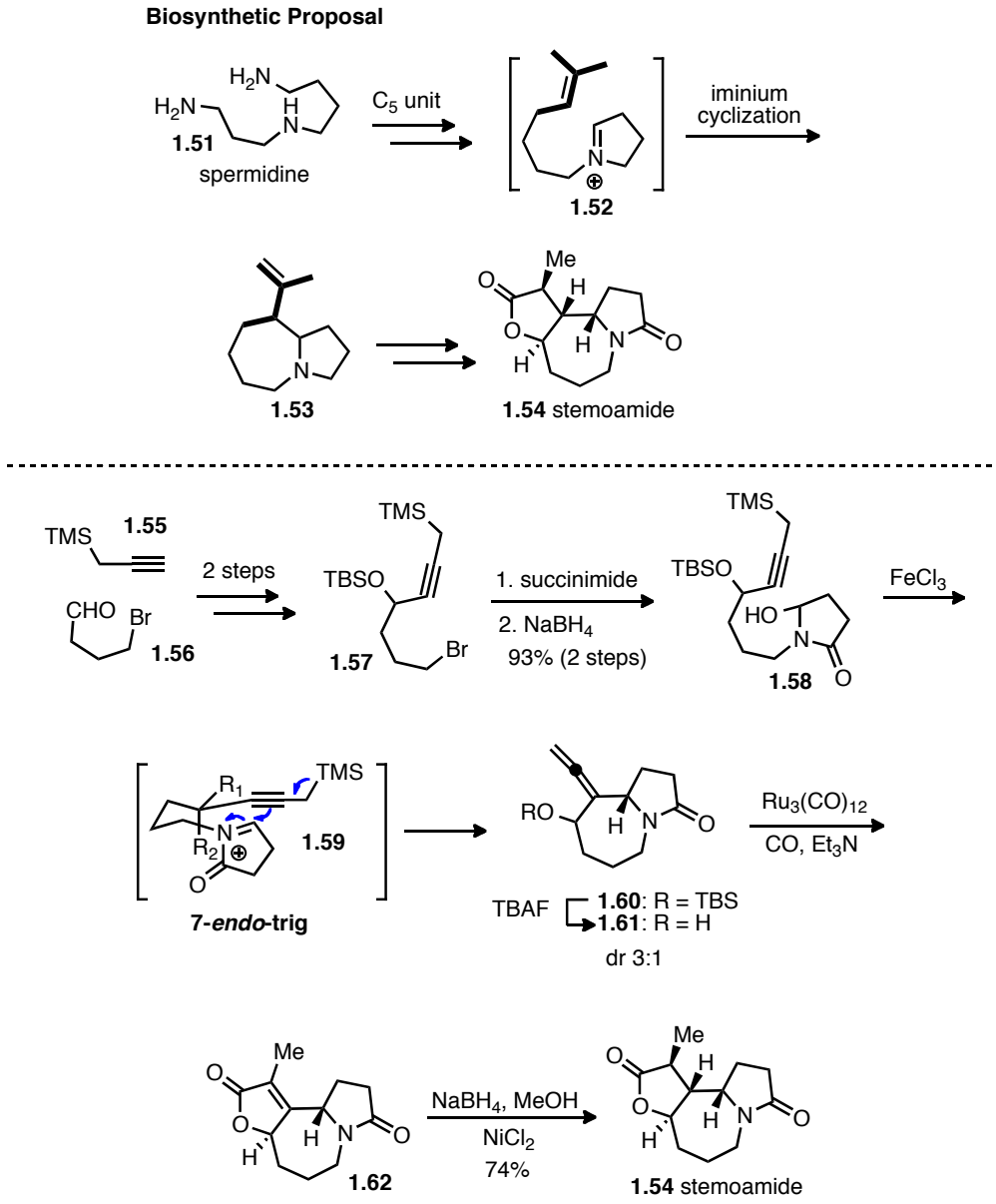

As part of an attempt to access the fumiquinazoline family of structurally related alkaloids, Hart and coworkers[9] reported a biomimetic synthesis of *ent*-alantrypinone (*ent*-**1.66**). The group proposed that alantrypinone could arise from fumiquinazoline F *via* intramolecular indole cyclization of *N*-acyliminium **1.64** to form bicylcle **1.65** (Scheme 1.7). This yields alantrypinone **1.66** *via* an oxidative ring contraction reaction of **1.65**. Relying on this biosynthetic proposal, L-tryptophan methyl ester **1.67**, S-methyl L-cysteine **1.68**, and isatoic anhydride **1.69** was coupled in a robust 4-step sequence to supply **1.70**. Cyclodehydration of **1.70** to iminobenzoxazine **1.71** was accomplished by treatment with PPh_3-I_2 in the presence of *i*Pr_2NEt. Exposure to lithium trimethyl(phenylsulfido)-aluminate (Li[Me_3AlSPh]) effected the rearrangement of iminobenzoxazine **1.71** to quinazoline **1.72**. Fmoc deprotection with piperidine occurs with concomitant amidation to give **1.73**. Oxidation of **1.73** with *m*-CPBA provided a sulfoxide, which upon heating with triphenylphosphine in benzene furnished enamide **1.74**. Trifluoroacetic acid (TFA) promoted the proposed cyclization to bicycle formation of **1.75**, presumably through an intramolecular nucleophilic attack of the indole onto the *N*-acyliminium. Oxidative rearrangement of indole **1.75** was effected using NBS and TFA in THF/water to give polybrominated indolinone, which following hydrogenation utilizing platinum on carbon gave *ent*-alantrypinone (*ent*-**1.66**) along with oxoindole epimer **1.76**. Hart's 10-step synthesis proceeds in 12% overall yield and confirmed the absolute configuration of the natural product.

Scheme 1.7

Biosynthetic Proposal

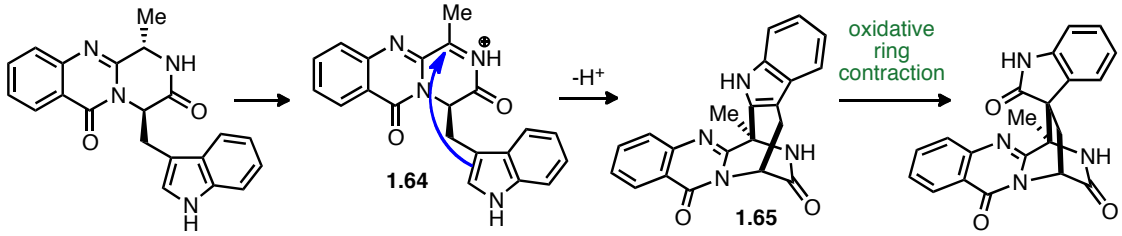

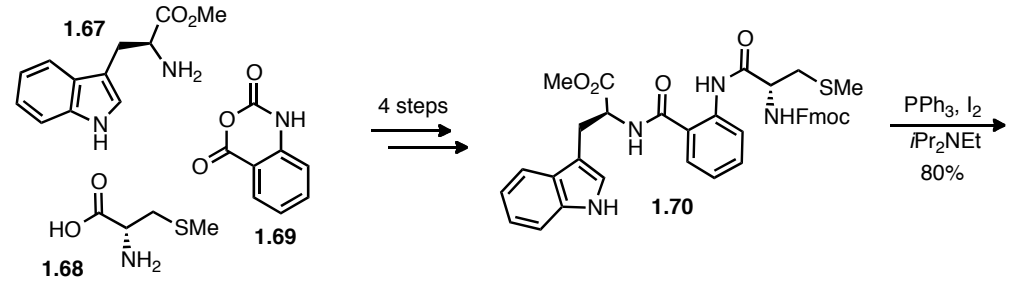

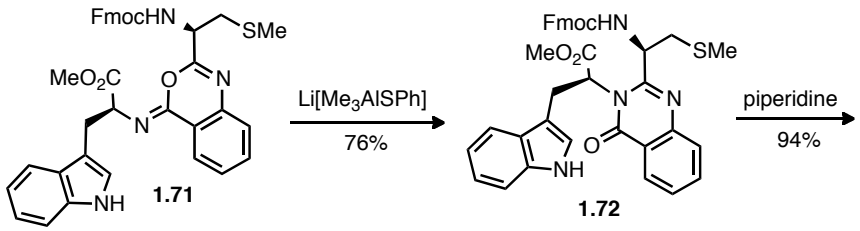

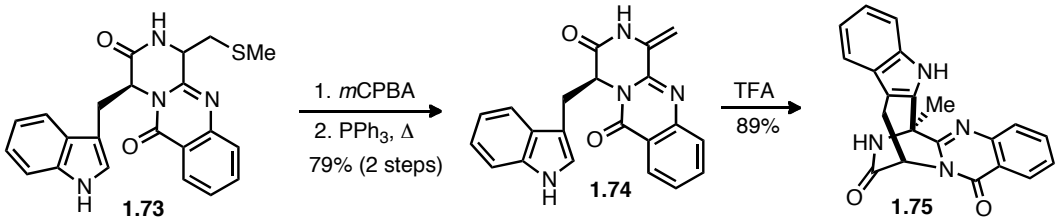

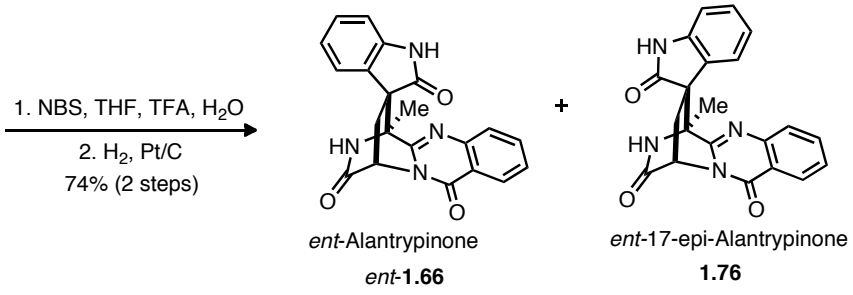

CHAPTER II

BIOINSPIRED TOTAL SYNTHESIS OF AGELASTATIN A*

2.1 Introduction

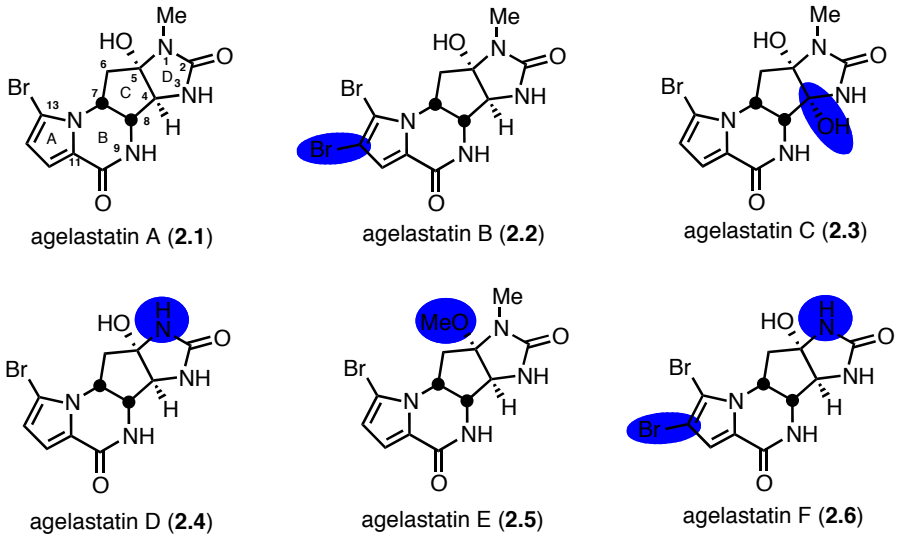

Figure 2.1 The agelastatin family of alkaloids

Agelastatin A (**2.1**) is a unique tetracyclic member of the growing family of pyrrole-2-aminoimidazole alkaloids (PAIs)[1] that was first isolated by Pietra and co-workers[10,6] in 1993 from the axinellid sponge *Agelas dendromorpha* (bioyield 1.2% of dry sponge-150

---

* Part of this chapter is reprinted with permission from [Bioinspired Total Synthesis of Agelastatin A" by Reyes, J. C. P.; Romo, D. *Angew. Chem. Int. Ed.* **2012**, *51*, 6870-6873. *Angew. Chem.* **2012**, *124*, 6976-6979.] Copyright [2012] Wiley-VCH Verlag GmbH & Co. KGaA.

mg initially isolated) contaminated with a small amount of a dibromo analog, agelastatin B (**2.2**) (Figure 2.1). Exhaustive methylation of the mixture was necessary to effect separation and full characterization of agelastatin B as a trimethyl derivative. In 1998, two other congeners, agelastatins C (**2.3**) and D (**2.4**), were isolated from the West Australian axinellid sponge *Cymbastela sp.* by Molinski and co-workers.[11] Twelve years later, in 2010, Al Mourabit and co-workers isolated two additional members from *Agelas dendromopha* named agelastatins E (**2.5**) and F (**2.6**).[12] The intriguing biogenesis of these alkaloids, which can be traced back to simple precursors (*e.g.* oroidin/clathrodin), has inspired several biosynthetic proposals but culminated in only one purely bioinspired and elegant total synthesis recently described by Movassaghi.[4s] This is surprising given the fact that there are numerous total syntheses reported to date spurred by its challenging structure and also the fact that it is arguably the most bioactive member of the P-2-AI family reported to date.

The structure as well as the absolute configuration of the four stereogenic centers of the C-ring (8S,7S,5S,4R),[10b] and conformational preferences of this novel, highly-fused tetracyclic cytotoxic alkaloid, agelastatin A **2.1**, were elucidated by extensive 1D and 2D NMR experiments,[10a] degradation studies, molecular mechanics calculations, and exciton splitting for some of its derivatives. Structure-activity relationship studies show that unsubstituted OH-C(5), H-N(9), and H-N(3) moieties are essential in the B/D transoid configuration for high cytotoxicity. These positions do not tolerate methylation or acetylation. Reductive debromination of the pyrrole C(13) bromine also leads to a significant loss in potency. This is hypothesized to not necessarily mean the importance

of the bromine atom in the aromaticity of the pyrrole but could merely be due to conformational change in the tetracycle in its absence.[10b]

Agelastatin A **2.1** was first reported to be highly cytotoxic against L1210 mouse lymphocytic leukemia cells (IC_{50} 0.097 μM), its doxorubicin-resistant variant (IC_{50} 1.37 μM) and against KB nasopharyngeal tumor cells (IC_{50} 0.220 μM).[6] It also exhibited potent anti-tumor activity against murine P388 leukemia cells (IC_{50} 0.152 μM) and a panel of human cancer cell lines (IC_{50} 0.097-0.703 μM) including pancreas (IC_{50} 0.261-0.498 μM) and breast adenocarcinoma (IC_{50} 0.097-0.161 μM), CNS glioblastoma (IC_{50} 0.111-0.243 μM), lung large cell (IC_{50} 0.105-0.120 μM), colon adenocarcinoma (IC_{50} 0.164-0.258 μM), prostate carcinoma (IC_{50} 0.123-0.170 μM), neuroblastoma (IC_{50} 0.352 μM), and anaplastic thyroid (IC_{50} 0.703 μM) and pharynx squamous carcinoma (IC_{50} 0.223 μM).[13] Antiangiogenic activity against human umbilical vein endothelial cells (HUVEC) was also observed.[14] Most recently, it was found to inhibit osteopontin (OPN), a glycoprotein implicated in aggravating neoplastic transformation, cancer cell progression, and metastasis. Its antimetastatic activity stems from inhibition of OPN-mediated malignant transformation through inhibition of Wnt signaling and prevention of progression of the cell cycle.[15] It selectively inhibits glycogen synthase kinase-3β (GSK-3β) over other kinases thought to be associated with Alzheimer's disease. As a GSK-3β inhibitor, it could also act as a potential insulino-mimetic and have possible antidiabetic properties.[16] Significant insecticidal activity against larvae of the beet army worm and the corn root worm has also been determined.[4] Despite these promising biological activities, the cellular receptor of agelastatin has not been determined.

There are two biosynthetic proposals put forth in literature for the biosynthesis of agelastatin A. Pietra and co-workers[10a], in 1993, envisioned that a hymenidine-like precursor **2.7**, through an an enzyme driven C(8) attack at C(4), forms the C(4)-C(8) bond of the C-ring (Scheme 2.1). The developing partial positive charge at C(7) of **2.8** is then quenched by the pyrrole N(12) nitrogen to complete the C(7)-N(12) bond of the B-ring of **2.9**. Refunctionalization at C(4) and C(5) possibly through the intermediacy of imidazolone **2.10** followed by an acid catalyzed hydration then gives agelastatin A.

Scheme 2.1

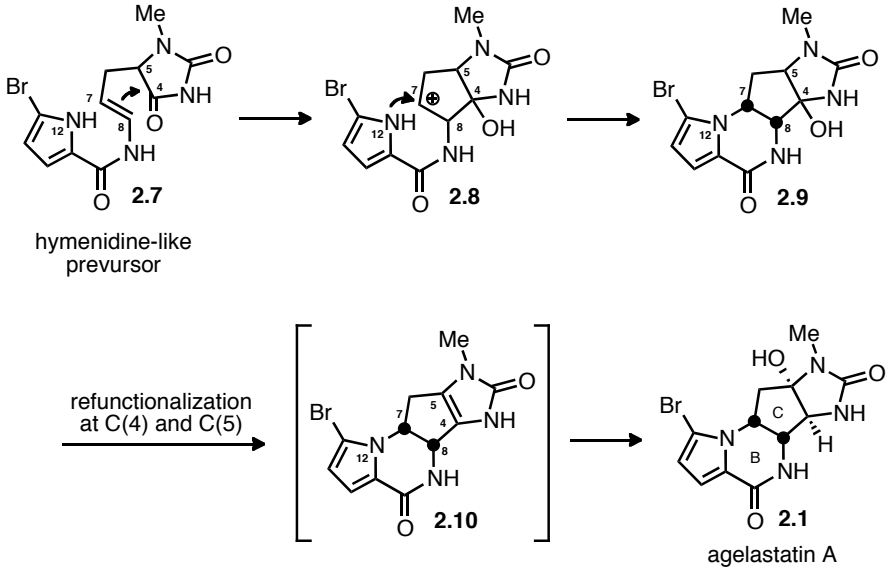

In 2001, Al-Mourabit and Potier[17] proposed the biosynthesis of agelastatin A starting with the union of a 5-bromopyrrole-2-carboxylic acid **2.11** and a tautomer of 3-amino-1-(2-aminoimidazolyl)-prop-1-ene (AAPE) **2.12** giving rise to a linear agelastatin

precursor **2.13** (Scheme 2.2). Oxidation of the 2-aminoimidazole core then gives **2.14** and creates an electrophilic center, which undergoes a 5-*exo*-trig cyclization forming C(4)-C(8) bond to give **2.15**. Nucleophilic attack of the pyrrole nitrogen N(12) at C(7) through a 6-*exo*-trig cyclization gives tetracycle **2.16**, which after tautomerisation, C(5) hydration, N(1) methylation, and C(2) hydrolysis furnishes agelastatin A. The first cyclization mode proposed herein was later on validated in 2007 by the isolation of the dimeric oroidin natural product, Nagelamide J (*cf.* **2.21**), by Kobayashi and co-workers.[18]

Scheme 2.2

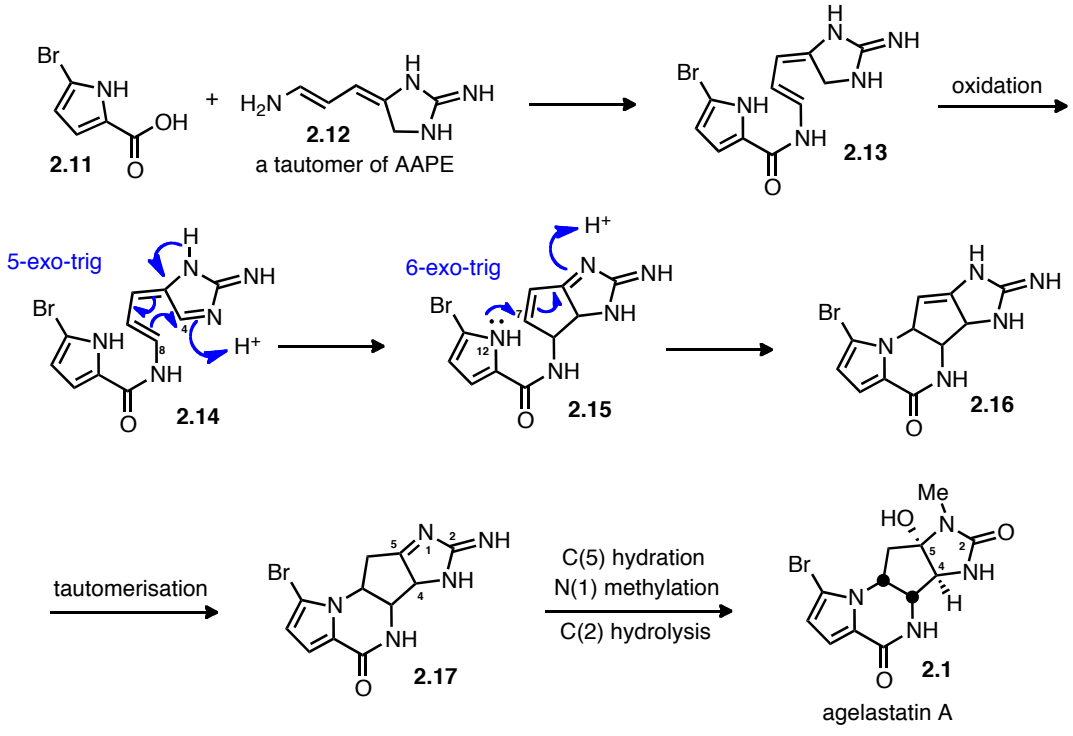

In 2010, Movassaghi and co-workers[4s], envisioned a biosynthesis proposal starting from the unnatural C(7) enantiomer *ent*-cyclooroidin derivative **2.18** (Scheme 2.3). They reason that downstream biosynthetic enzymes may preferentially bind to *ent*-cyclooroidin for the synthesis of agelastatins. Early installation of the N(1) methyl, C(2) hydrolysis, and C(8) oxidation then gives rise to an *N*-acyliminium intermediate **2.19** that undergoes C-ring cyclization followed by nucleophilic trapping with water to give agelastatin A.

Scheme 2.3

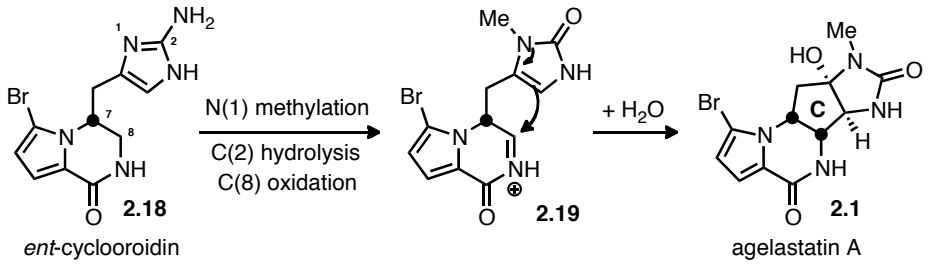

The C-ring, which contains all four stereogenic centers found in the natural product, is clearly the most challenging aspect of this molecule. In fact, most previous synthetic strategies focused on building the functionalized cyclopentane C-ring followed by subsequent construction of the B and D rings. As part of our efforts to investigate the biogenesis of PAIs,[19] this chapter describes our synthetic studies that ultimately led to a concise, bioinspired approach to agelastatin A that is premised on the isolation of the structurally related natural product, nagelamide J (*cf.* **2**.**21**).[18]

Two distinct and plausible biosynthetic presursors of agelastatin A isolated to date are cyclooroidin **2.20**[20] and nagelamide J **2.21**[18] (Figure 2.2). These natural products each support a different order of B-ring and C-ring formation. Although the absolute configuration of **2.21** is unknown, it is worth noting that **2.20** bears the opposite configuration at C(7) compared to agelastatin A. Movassaghi recently described a strategy premised on formation of an *ent*-cyclooroidin-like compound (*cf.* **2.18**) followed by C-ring cyclization to deliver (–)-agelastatin A. In contrast, the synthetic strategy described herein highlights an alternative biogenetic pathway inspired by the nagelamide J structural motif suggesting a biogenetic sequence involving initial C-ring formation followed by B-ring formation.

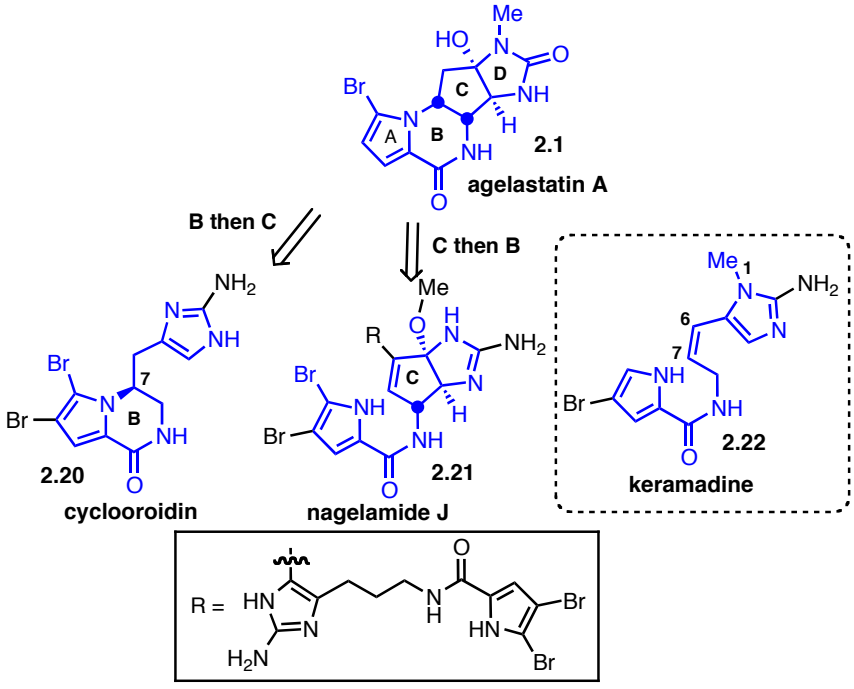

Figure 2.2 Agelastatin A and pre-agelastatin motifs in other P-2-AIs

Our bioinspired approach to agelastatin A was also guided by our previous experience with the ambivalent reactivity of the 2-imidazolone nucleus, observed in our studies toward dimeric P-2-AIs (Figure 2.3).[21] The core structure **2.23** is quite nucleophilic and can react with an electrophile, with the concomitant formation of a reactive *N*-acyliminium **2.24**, which could then be trapped subsequently with a nucleophile. The overall process leads to a formal addition across the imidazolone olefin providing **2.25**.

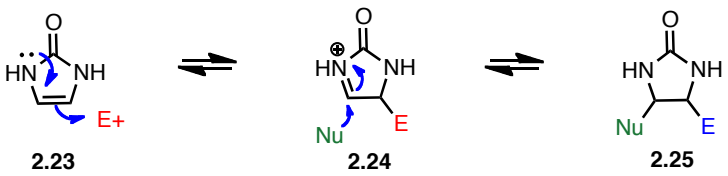

Figure 2.3 Ambivalent reactivity of 2-imidazolones

In our efforts towards the total syntheses of dimeric oroidin alkaloids palau'amine (*cf.* **1.11**) and axinellamines (*cf.* **1.10**), reaction of imidazolone **2.26** with dimethyldioxirane leads to epoxide **2.27** (Scheme 2.4). This then cleaves through electron pushing from the nitrogen to give *N*-acyliminium **2.28**, which in the absence of a nucleophile, undergoes tautomerisation to give enamide **2.29**. We then take this intermediate to a chlorination-ring-contraction sequence to give the 5-5 spiro-ring core **2.31** found in palau'amine and other dimeric oroidin alkaloids.

Scheme 2.4

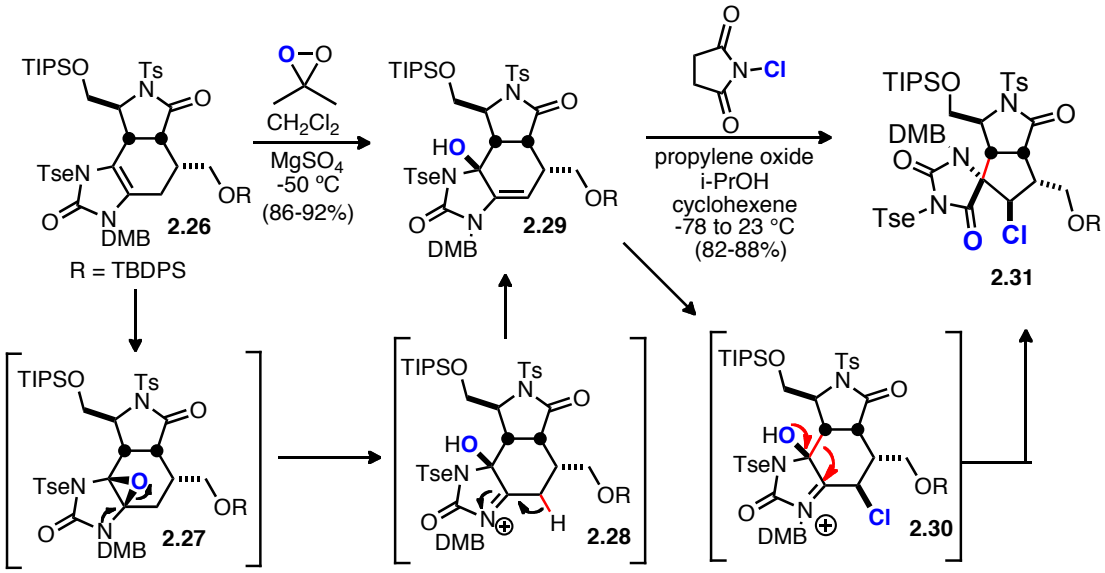

This imidazolone reactivity is in stark contrast to what is commonly invoked for the biogenesis of these targets, wherein an oxidized imidazolone or aminoimidazole serves as an electrophile in subsequent cyclization events.[10a,17] Based on this reactivity pattern we put forth our own biosynthetic proposal starting from a keramadine analog **2.31** (Scheme 2.5). Keramadine[22] **2.22** is the only isolated, monomeric PAI, also from an *Agelas* sponge, known to posses a stable *Z*-configured olefin and notably bears the requisite N1-methyl group found in the agelastatins. Early hydrolysis at C(2), followed by oxidation at C(8) gives carbinolamide **2.32**. *N*-acyliminium formation then provides **2.33** ready for nucleophilic attack by the imidazolone in a 5-*exo*-trig fashion or through its resonance structure **2.34** undergo a 4π electrocyclization process. Either of this process leads to a conjugated *N*-acyliminium intermediate **2.35**, which can be trapped by

the pendant pyrrole nitrogen. Overall this leads to sequential C and B ring formation via an *N*-acyliminium-initiated, diastereoselective, bis-cyclization cascade exploiting the 'umpolung' reactivity of the imidazolone nucleus. Following a hydration step, this sequence provides agelastatin A.

Scheme 2.5

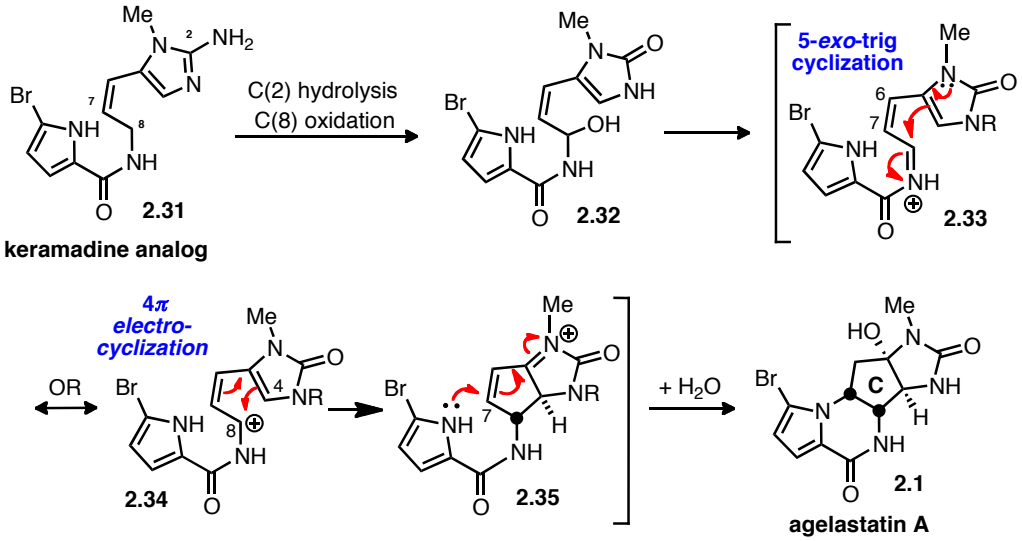

Based on the above biosynthetic proposal, our retrosynthetic strategy starts with a hydration step from 'dehydroagelastatin A' **2.36** to install the stable carbinolurea moiety in the target (Scheme 2.6). Two strategic bond disconnections on the C and B rings, at the C4-C8 and C7-N12 bonds, reveal a linear precursor **2.37** with pendant A and D rings. We envisioned that a key *N*-acyliminium intermediate could be derived from **2.37**, utilizing a Brønsted or Lewis acid. The C6-C7 *Z*-olefin was introduced to

exert conformational bias and assist in the formation of the C4-C8 bond *via* a 5-*exo*-trig cyclization or via a a Nazarov 4π electrocyclization. The *Z*-configured olefin of the key cyclization precursor **2.37** will then be introduced using a Lindlar reduction of alkyne **2.38**, which in turn arises from the coupling of an appropriate imidazolone alkyne fragment and a pyrrole carboxamide fragment.

Scheme 2.6

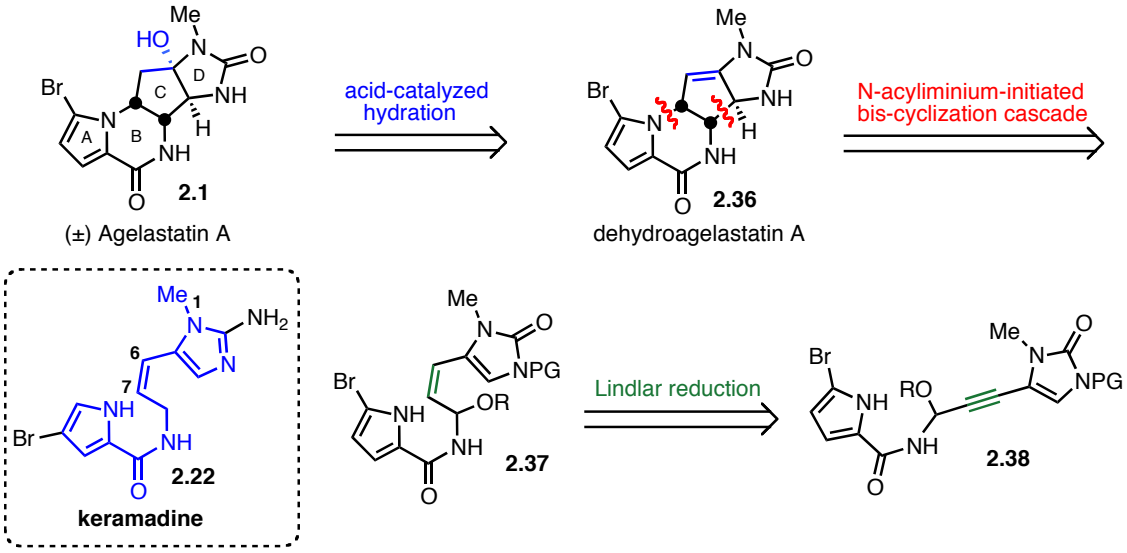

With the synthetic plan layed out, the rest of this chapter presents our synthetic investigations that ultimately led to a concise 'bio-inspired' total synthesis of agelastatin A utilizing an imidazolone intermediate bearing an allylic *N*-acylcarbinolamide. This synthesis enabled cellular receptor isolation studies through synthesis of designed

derivatives bearing novel sites for probe attachment, taking some lessons from literature SAR data. These investigations are detailed in chapter III.

Retrosynthetic analysis of key coupling adduct **2.38** led us to two different disconnections detailed in Scheme 2.7. The syntheses of the possible fragments **2.39-2.44** for this coupling reaction are detailed in the next two subsections.

Scheme 2.7

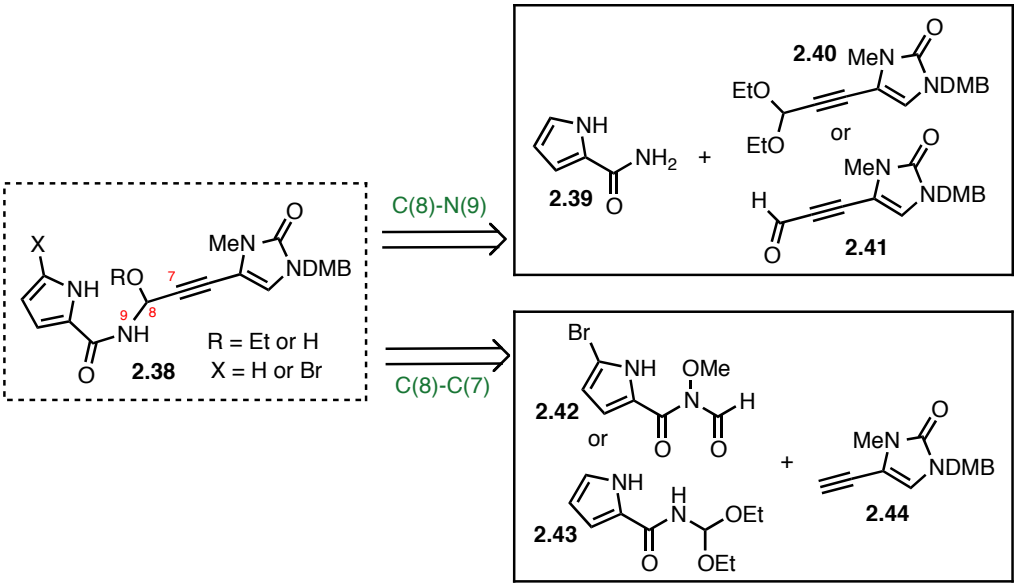

2.2 Syntheses of the Imidazolone Fragments

The imidazolone fragment synthesis starts with a modified literature procedure that involves the condensation of N-methyl urea **2.45** and tartaric acid **2.46** (Scheme 2.8). Modification in the procedure included the use of 95-98% sulfuric acid (H_2SO_4) instead of 16% H_2SO_4 decribed in the literature.[23] After heating at 80 °C for 3 hours,

precipitation in ice water lead to isolation of **2.47** as tan solids. Regioselective placement of the methyl group at N1 was verified by 1D NOE correlations (Scheme 2.8). The 1D NOE difference spectra showed that irradiation of either N3-H or C4-H shows enhancement of the other. Irradiation of the N1-Me protons, on the other hand did not show any enhancement of other proton signals as expected since it is not within proximal distance to other protons within the compound. While the values of 2.52% and 3.73% enhancements do qualitatively prove the proximity of N3-H and C4-H, these are low values due to the limitations of 1D NOESY measurements and some relaxation of signal during the mixing time is expected.

Scheme 2.8

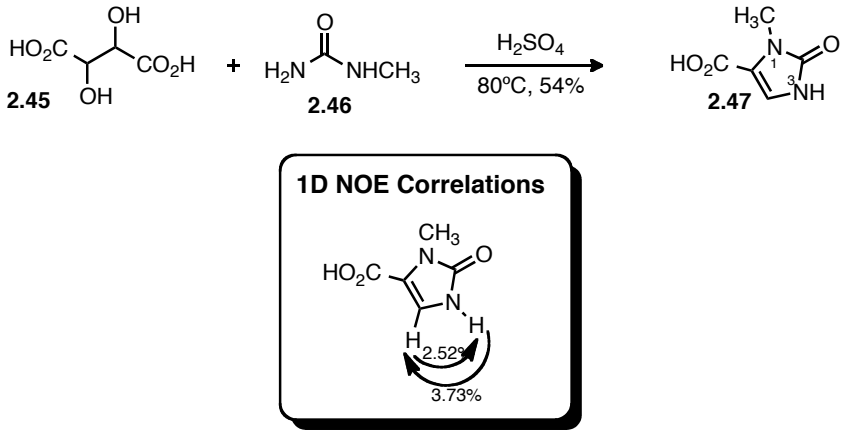

The regioselectivity was further verified by correlation of the proton chemical shifts with literature values of both plausible regioisomers (Table 2.1).[23a] While the observed chemical shift of C4-H does not match well with either compounds, the

chemical shift of N1-CH_3 (3.28 ppm) and N3-H (10.83 ppm) in **2.47** does indeed correlate better with 1-methyl-2-oxo-imidazoline-5-carboxylic acid.

Table 2.1 Characterization of 2-imidazolone **2.47**.

Compound	δ (ppm)		
	NH	**=CH**	**NCH_3**
3-Methyl-2-oxo-imidazoline-5-carboxylic acid	10.33	7.16	3.08
1-Methyl-2-oxo-imidazoline-5-carboxylic acid	10.60	7.13	3.25
Compound **2.47**	10.83	7.27	3.28

With the N1-methyl imidazolone acid **2.47** in hand, the next challenge was to install the appropriate bromine pendant through a decarboxylative bromination (Scheme 2.9). This will be coupled to an appropriate alkyne *via* a Sonogashira cross coupling reaction to provide imidazolone alkyne fragments **2.49a** and **2.49b**.

Scheme 2.9

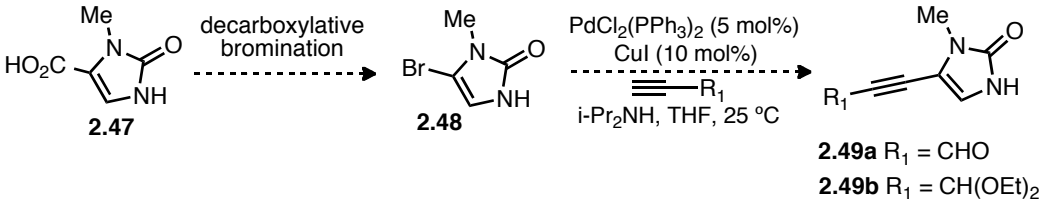

Several procedures were screened for the decarboxylative bromination step (Table 2.2). These however did not produce any of the desired product **2.48** and the crude ^{13}C NMR showed the loss of the olefinic carbon signals in most cases. The only

promising result was that of entry 2 where the pyridine nitrogen is attached to the imidazolone core as a pyridinium salt providing **2.50a**. This product was verified my mass spectrometry and NMR spectroscopy. From these results, it is apparent that the imidazolone olefin is still quite nucleophilic even in the presence of a conjugated acid moiety. The absence of olefinic carbon signals indicates a bis-bromo product or a bis-aminal product of the general structure **2.50b**. This possibly occurs through a mechanism similar to the addition of a bromine across an olefin and is a consequnce of the dual reactivity of the imidazolone core as discussed previously. The bis-aminal product is the addition of water to the *N*-acyliminum formed after extrusion of the bromines. These proposed structures, however, were not unambiguously assigned.

Table 2.2 Screening of conditions for decarboxylative bromination.

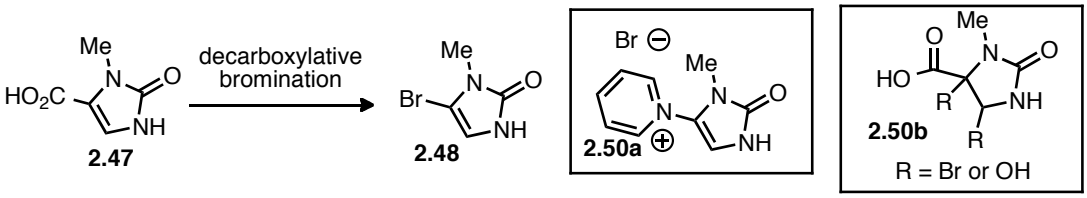

Entry	Conditions	Outcome
1	i. KOH, $AgNO_3$, H_2O; ii. Br_2, CCl_4	Single product 16% yield; No olefinic ^{13}C signal
2	$PyHBr_3$, CH_2Cl_2	Product **2.50a**
3	LiOAc, NBS, $MeCN/H_2O$, 50 °C	Multiple products; No olefinic ^{13}C signal
4	K_2CO_3, NBS, DMF	Multiple products; No olefinic ^{13}C signal
5	Br_2, AcOH	2 products; No olefinic ^{13}C signal

The pyridium product **2.50a** was then tested for bromine substitution using sodium bromide (NaBr) in water and DMSO as solvents (Scheme 2.10). However, the starting material seemed to be resistant to substitution and is stable to bromide nucleophiles and the conditions tested did not yield any bromoimidazolone **2.48**.

Scheme 2.10

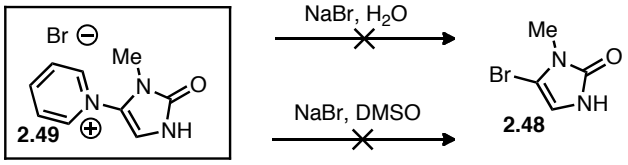

The next strategy then relied on more classical functional group interconversion of an acid moiety to an alkyne (Scheme 2.11). This involved an esterification step, a reduction step to alcohol **2.53**, oxidation to aldehyde **2.54** and finally a homologation to yield alkyne **2.55**.

Scheme 2.11

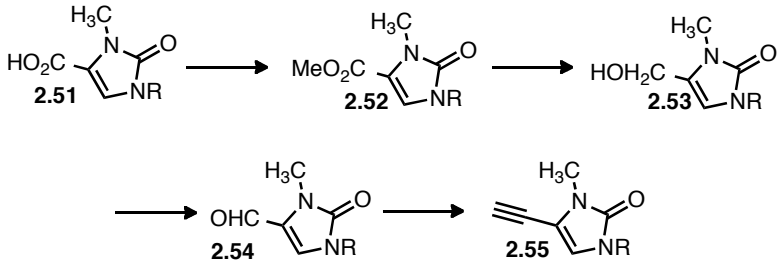

Conversion of acid **2.47** to methyl ester **2.56** *via* a Fischer esterification with methanol proved not to be as straightforward as it seemed (Table 2.3). A mixture of thionyl chloride ($SOCl_2$) in methanol provides hydrochloric acid (HCl) that catalyzes a Fisher esterification to yield methyl ester **2.56**. However, it was found that with 1.5 – 3.0 equivalents of thionyl chloride, the reaction required heating to effect conversion to product **2.56** with concomitant decarboxylation byproduct **2.57** (entries 1-4). While high tempreratures was necessary for dissolution, it also promoted the decarboxylation pathway. A mixture of dimethyl formamide (DMF) and methanol (MeOH), while making the reaction more homogenous at room temperature (entry 5), however, provided no reaction product at 23 °C and even at 50 °C indicating that an excess of methanol is necessary to push the reaction forward. Sulfuric acid (H_2SO_4) and acetyl chloride (AcCl) were then screened as an alternative to thionyl chloride but still led to about a 1:1 mixture of the desired methyl ester **2.56** and decarboxylation product **2.57** (Entries 6 and 7). Lowering the equivalents of sulfuric acid while maintaining reflux conditions or a temperature of 60 °C either led to no reaction or still a mixture of products (Entries 8-10). Finally, it was found that 50 equivalents of sulfuric acid promoted the reaction effectively producing only the desired esterification product **2.56** in 41% yield (Entry 11).

Table 2.3 Screening of conditions for Fischer esterification.

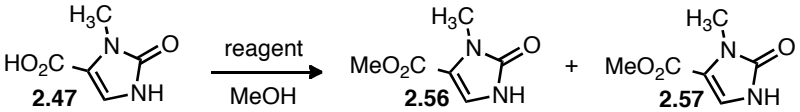

Entry	Conditions	Temp.	Time	Ratio 2.56:2.57
1	$SOCl_2$ (2 equiv.)	reflux	12h	~1:1
2	$SOCl_2$ (2 equiv.)	55ºC	12h	~1:1
3	$SOCl_2$ (3 equiv.)	52ºC	3h	~1:1 (45% conversion)
4	$SOCl_2$ (1.5 equiv.)	60ºC	12h	4:5 (74%conversion)
5	$SOCl_2$ (2 equiv.)	rt	6h	No reaction
	(DMF/MeOH 3:1)	42ºC	6h	No reaction
		50ºC	10h	No reaction
6	AcCl (20 equiv.)	reflux	12h	~1:1
7	H_2SO_4 (20 equiv.)	reflux	12h	~1:1
8	H_2SO_4 (0.1 equiv.)	reflux	12h	No reaction
9	H_2SO_4 (0.6 equiv.)	reflux	6h	2:3 (15% conversion)
10	H_2SO_4 (10 equiv.)	60ºC	12h	~1:1
11	**H_2SO_4 (50 equiv.)**	**rt**	**12h**	**1:0 (41% yield)**

With ester **2.56** in hand, the next step was protection of imidazolone N(3) with a tosylethyl group, a protecting group popularized by the Romo group for the ease of preparation of the required reagent, tosylethyl mesylate, and facile removal through the use of a variety of bases. We also explored the dimethoxybenzyl (DMB) protecting group.

Scheme 2.12

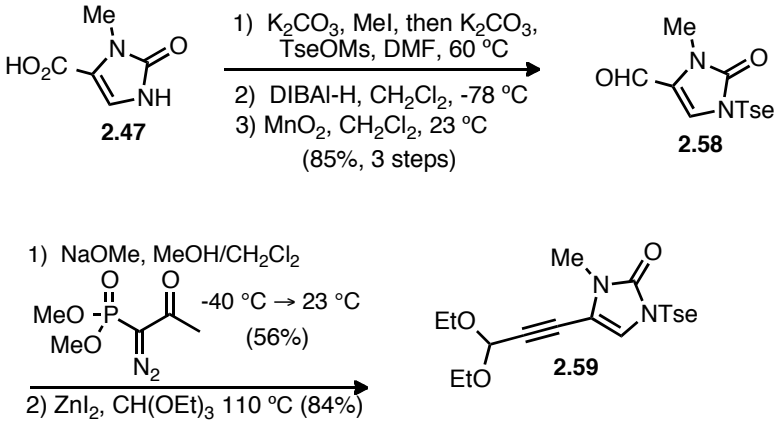

We eventually discovered that esterification acid **2.47** was easily achieved under basic conditions (K_2CO_3) using methyl iodide while in the same pot protecting N(3) with a tosylethyl moiety using the same base (Scheme 2.12). Conversion of resulting methyl ester to aldehyde **2.58** was accomplished in a two-step process involving reduction with DIBAl-H, and oxidation with manganese(IV) oxide (MnO_2). Modified Seyferth-Gilbert conditions using Ohira-Bestmann reagent[24] and sodium methoxide[25] in a 1:1 mixture of methanol and dichloromethane as solvent gave the desired alkyne. Addition of dichloromethane as cosolvent helped solubilize the aldehyde starting material. This transformation required low temperatures with extended reaction times to give the best yields. Overall, the conversion of **2.47** to **2.58** occurs in 85% yield over three-steps. A subsequent Zn(II)-mediated acetalization[26] furnished the targeted alkynyl acetal **2.59**, and this entire 5-step sequence could be readily performed on multigram scale. DMB

protected alkyne **2.44** was also synthesized in the same manner (Scheme 2.13). Subsequent acetalization and formylation (*n*-BuLi/DMF) of this intermediate resulted in the requisite imidazolone fragments **2.40** and **2.41**, respectively, to be screened for the key coupling reaction described in section 2.4.

Scheme 2.13

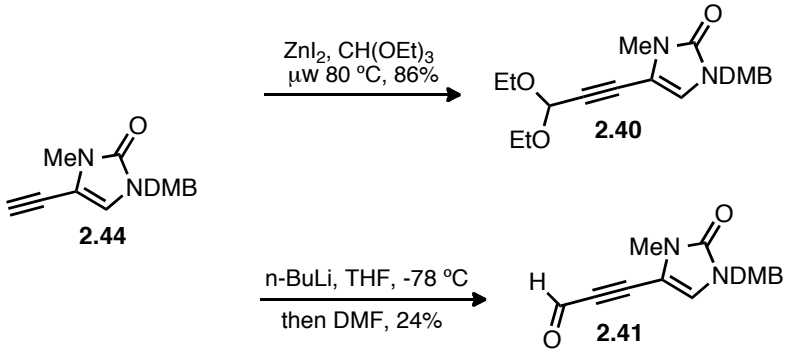

2.3 Syntheses of the Pyrrole Fragments

The synthesis of bromopyrrole fragment **2.61** starts with trichloroacetyl pyrrole **2.60** (Table 2.4). Amidation reaction of **2.60** with ammonia led to quantitative conversion to pyrrole amide **2.39**. However, regioselective bromination of **2.39** proved to be problematic leading to products **2.60a**, **2.60b**, and **2.60c** (Table 2.4). Sub-stoichiometric amounts (0.3 equivalents) of brominating agents were used in the screening process to reduce the risk of overbromination. Once a pyrrole position is brominated, it results to activation towards electrophilic aromatic bromination. Screening of solvents with *N*-bromosuccinimide (NBS) revealed that THF/MeOH and

acetonitrile both gave a ratio of 3:1:0 in favor of the desired product ----. On the other hand, using methanol also gave bis-brominated product **2.60c**. THF/MeOH proved to be superior to acetonitrile in terms of solubilization of the starting material. Using other sources of electrophilic bromine, namely tetrabromocyclohexadienone and pyridinium bromide perbromide (entries 4 and 5) gave inferior results. Further optimization of entry 3 was done by slowing down the bromination process by lowering the reaction temperature (entries 6-8). A 5-hour reaction at -5 °C was found to be optimal giving a 4:1:0 ratio of the bromopyrrole products. Lowering the reaction temperature further, only resulted with inferior ratio of products. While the optimized ratio of products is reasonable to get sufficient quantities of the desired product **2.60a**, purification of the mixture proved to be difficult.

Table 2.4 Electrophilic aromatic substitution of pyrrole carboxamide **2.39**.

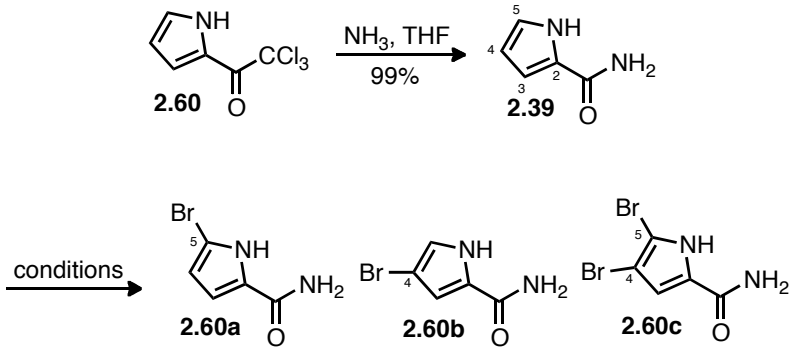

Table 2.4 Continued.

Conditions	Product Ratio (2.60a : 2.60b : 2.60c)
NBS (0.3 equiv), MeOH, 0ºC to rt	2:1:1
NBS (0.3 equiv), CH_3CN, 0ºC to rt	3:1:0
NBS (0.3 equiv), THF/MeOH, 0ºC to rt	3:1:0
Tetrabromocyclohexadienone (0.3 equiv) 0ºC to rt THF/MeOH	1.67:1:0.6
Pyridinium bromide perbromide (0.3 quiv) 0ºC to rt THF/MeOH	0.8:1:0.2
NBS (0.3 equiv), THF/MeOH, -5ºC (5h) to rt	4:1:0
NBS (0.3 equiv), THF/MeOH, -78ºC (5h) to rt	2.5:1:0.3
NBS (0.3 equiv), THF/MeOH, -30ºC (7days)	3.2:1:0.5

Since regioselectivity of electrophilic aromatic bromination is highly dependent on the overall electronics of the aromatic ring, we sought to decrease the electron withdrawing effect of the acyl group of the amide. To this end, reaction of O-methylhydroxylamine hydrochloride salt with trichloroacetyl pyrrole **2.60** using triethylamine as solvent led to quantitative conversion to N-methoxy amide **2.61** (Scheme 2.14).[4j] Reaction of **2.61** with NBS in THF/MeOH led to regioselective bromination of the pyrrole 5-position in 96% yield.

Scheme 2.14

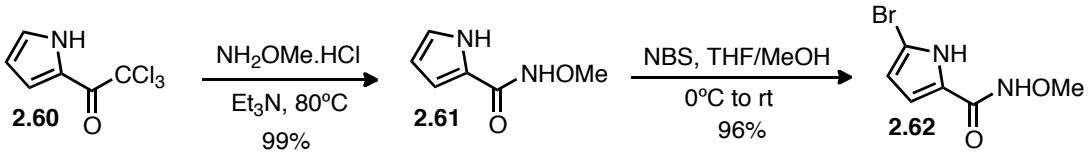

Chemoselective formylation of N-methoxy amido pyrrole **2.62** was successfully accomplished with 2-chloro-4,6-dimethoxy-1,3,5-triazine (CDMT), formic acid, 4-(dimethylamino)pyridine (DMAP) and N-methylmorpholine (NMM) to give formylated compound **2.42** (Scheme 2.15). Interestingly, a similar N-formyl amide **2.63** was isolated from the marine sponge *Agelas oroides.*[27]

Scheme 2.15

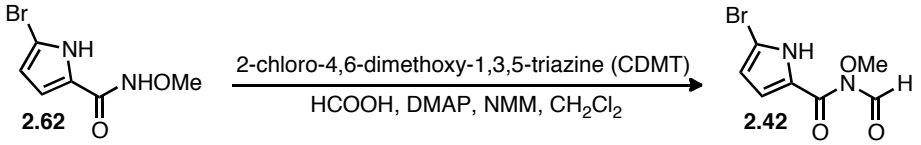

1.1 equiv HCOOH 49% yield
1.3 equiv HCOOH 51% yield
2.5 equiv HCOOH 92% yield

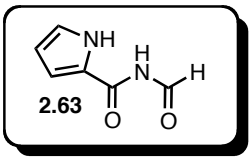

- a pyrrole derivative isolated from *Agelas oroides*

Acetalization of amides **2.62** and **2.39** leads to other possible pyrrole fragments for the key coupling reaction (Scheme 2.16). Surprisingly, **2.62** was not able to react with triethylorthoformate to give any of the desired product **2.64**. However, amide **2.39** successfully reacted with triethylorthoformate in acetic acid to give acetal **2.43**, in low conversion albeit easily separable from the starting material. Heating of this reaction led to multiple products. The use of potential pyrrole fragments **2.42** and **2.43** are described in section 2.4.

Scheme 2.16

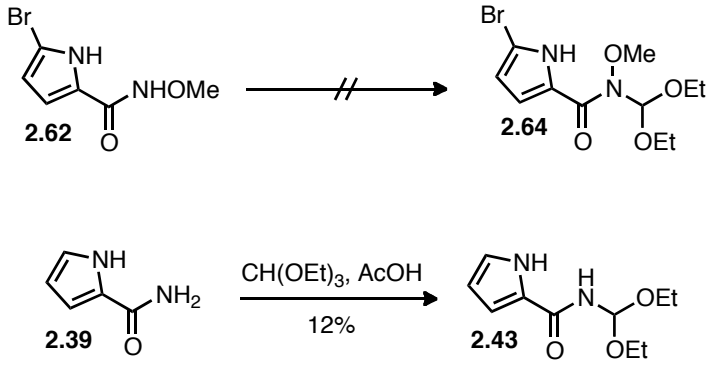

2.4 Coupling of Fragments

With the proposed pyrrole amide and alkynyl imidazolone fragments synthesized, we continued with our studies on the key coupling reaction leading to a product containing all the requisite carbons found in agelastatin A. Our first disconnection relied on the coupling of imidazolone alkyne **2.68** onto activated carbonyl

equivalents **2.66** and **2.67** (Scheme 2.17). Screening of conditions revealed that the carbonyl equivalents **2.66** and **2.67** were prone to hydrolysis giving amides **2.62** and **2.39**, respectively. In some cases where the desired C-C bond was formed, only the formal formyl transfer adduct **2.41** was isolated.

Scheme 2.17

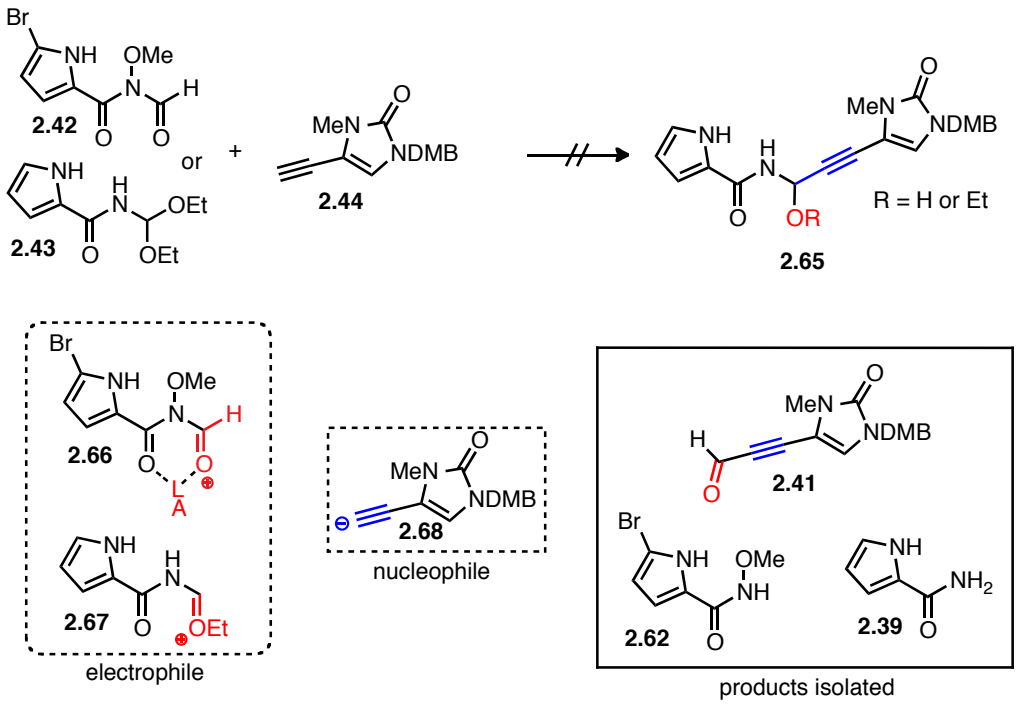

Alternative disconnection of the C(8)-N(9) bond leads to pyrrole fragments **2.39** and alkynyl imidazolone fragments **2.40** and **2.41**(Scheme 2.17). Amide **2.39** was expected to behave as a vinylogous urea, due to delocalization of pyrrole N electrons, and thus have enhanced nucleophilicity. Activated acyl equivalents **2.70** and **2.71**, on the

other hand served as the electrophiles upon activation with Lewis or Brønsted acids. After extensive experimentation with a variety of activators, we found that amide **2.39** is quite inert or that the addition reaction is reversible. In most cases, reaction conditions only returned starting materials or some decomposition of the imidazolone fragments as well as hydrolysis of **2.71**.

Scheme 2.18

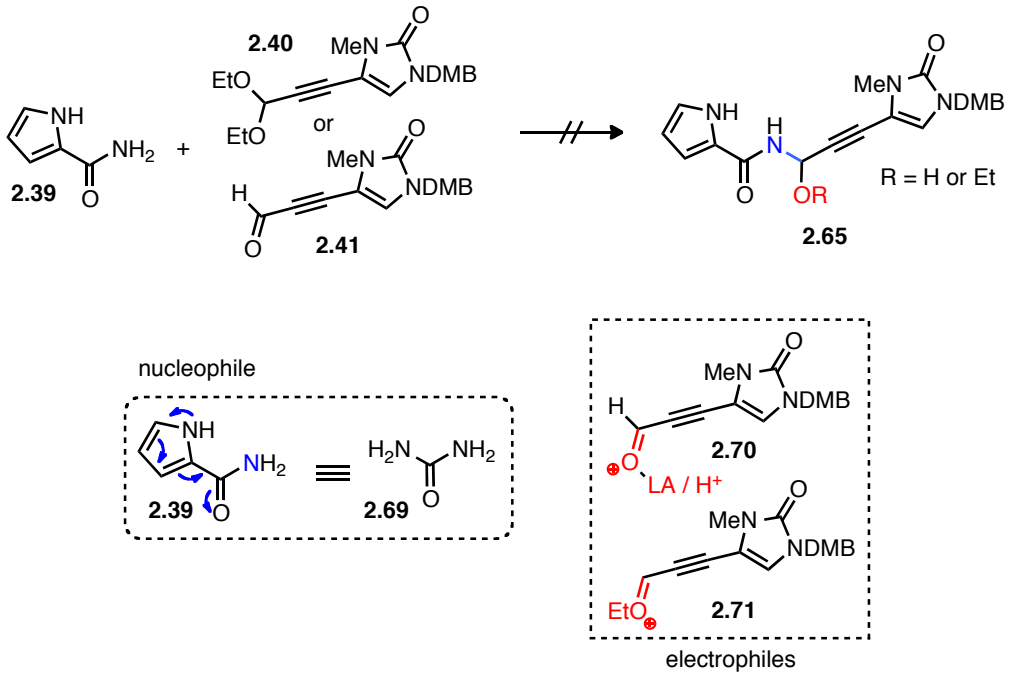

At this point, focus was directed towards searching for an appropriate nitrogen nucleophile to alkynyl imidazolone **2.40**, which could be accessed in gram quantities. After screening several nitrogen nucleophiles and Lewis acids, successful coupling of fragments was finally achieved using N-methoxy amide **2.62** and alkyne acetal **2.40**

using $SnCl_4$ as a catalyst (Scheme 2.19). A substoichiometric amount (0.25 equiv) of $SnCl_4$ and a 3 h reaction time provided the best results in terms of avoiding further decomposition and enabling optimal recovery of unreacted alkynyl acetal **11** and pyrrole amide **12.** The 'alpha effect' of the adjacent methoxy group on the amide nitrogen allowed regioselective reactivity of the amide nitrogen over the pyrrole nitrogen toward the oxocarbenium **2.71** to give the desired coupling adduct **2.72**.

Scheme 2.19

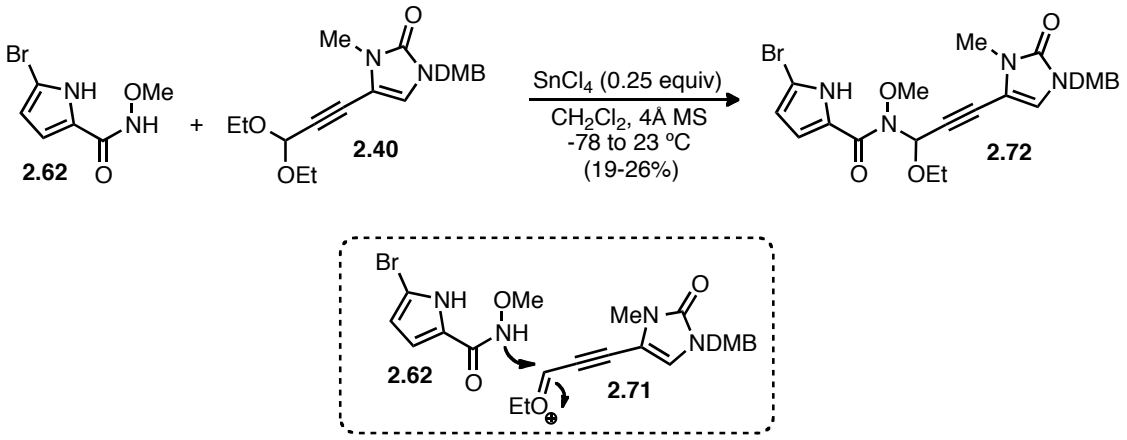

2.5 Synthesis of *N*-Acyliminium Cyclization Precursor: Investigation of the Proposed Key Step

Lindlar reduction of coupling adduct **2.72** provided bis-cyclization precursor **2.73** (Scheme 2.20). We sought not to optimize this reaction at this point and investigated the proposed *N*-acyliminium biscyclization cascade. Treatment of precursor **2.73** with $SnCl_4$ surprisingly did not yield the desired *N*-acylimminium **2.74**,

which is supposed to undergo the 5-*exo*-trig cyclization followed by the 6-*exo*-trig cyclization. Instead of delivering dehydroagelastatin **2.76**, the compound broke apart into two fragments releasing pyrrole amide **2.62** and oxocarbenium **2.77**, which in turn hydrolysed and isomerized to enal **2.78**. Reduction cleavage of the N-methoxy group in **2.72** was postponed since we reasoned that aside from keeping the nitrogen protected, it could also serve as a suitable coordinating atom for further activating *N*-acyliminium **2.74**. As the results showed, bis-coordination of the Lewis only activated **2.73** towards oxocarbenium formation instead. The methoxy group also lowers the pKa of amide **2.62**, making its conjugate base a weaker base and therefore a better leaving group.

Scheme 2.20

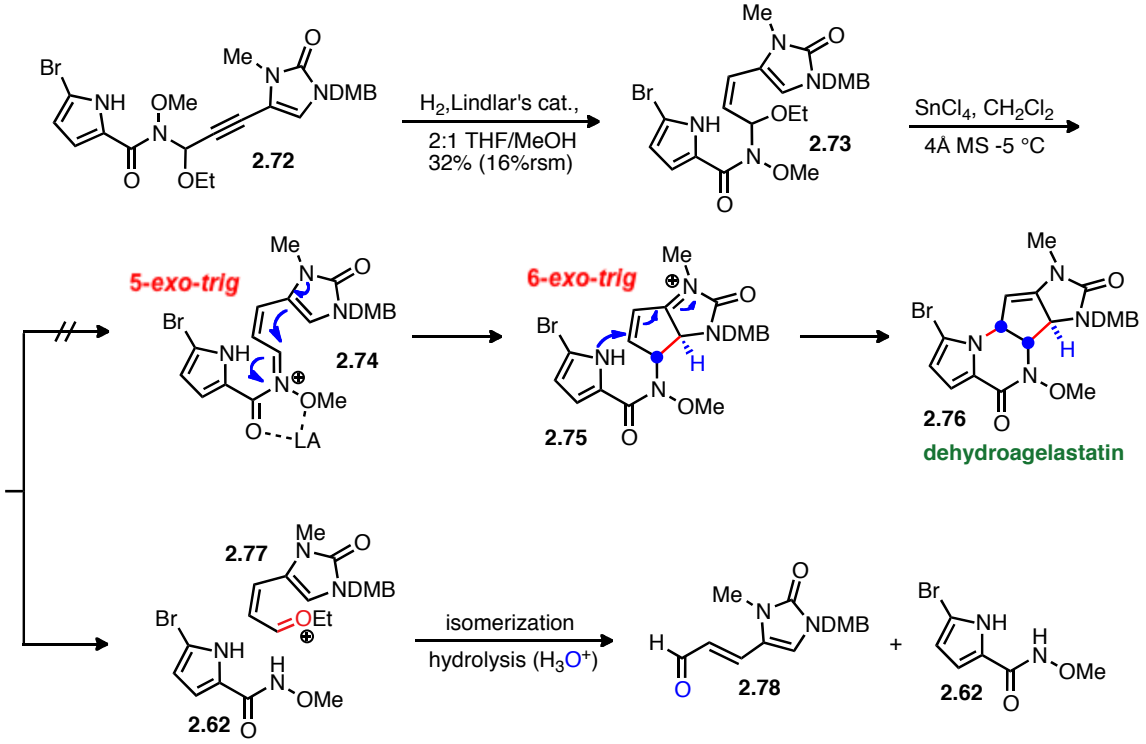

To further verify that an oxocarbenium **2.71** (Scheme 2.21), instead of an *N*-acyliminium **2.79** is formed from an N-methoxycarbinolamide motif, **2.72** was subjected to tin(IV) tetrachloride ($SnCl_4$) and the resulting intermediate (either **2.71** or **2.79**) was then trapped with allyl TMS. NMR or LCMS analysis found none of the expected product **2.80** from *N*-acyliminium **2.79**. Not surprisingly, the reaction yielded only product **2.81**, which was observed in 80% yield, as a result of allyl TMS trapping of oxocarbenium **2.71**. The reaction also returned pyrrole amide coupling partner **2.62**.

Scheme 2.21

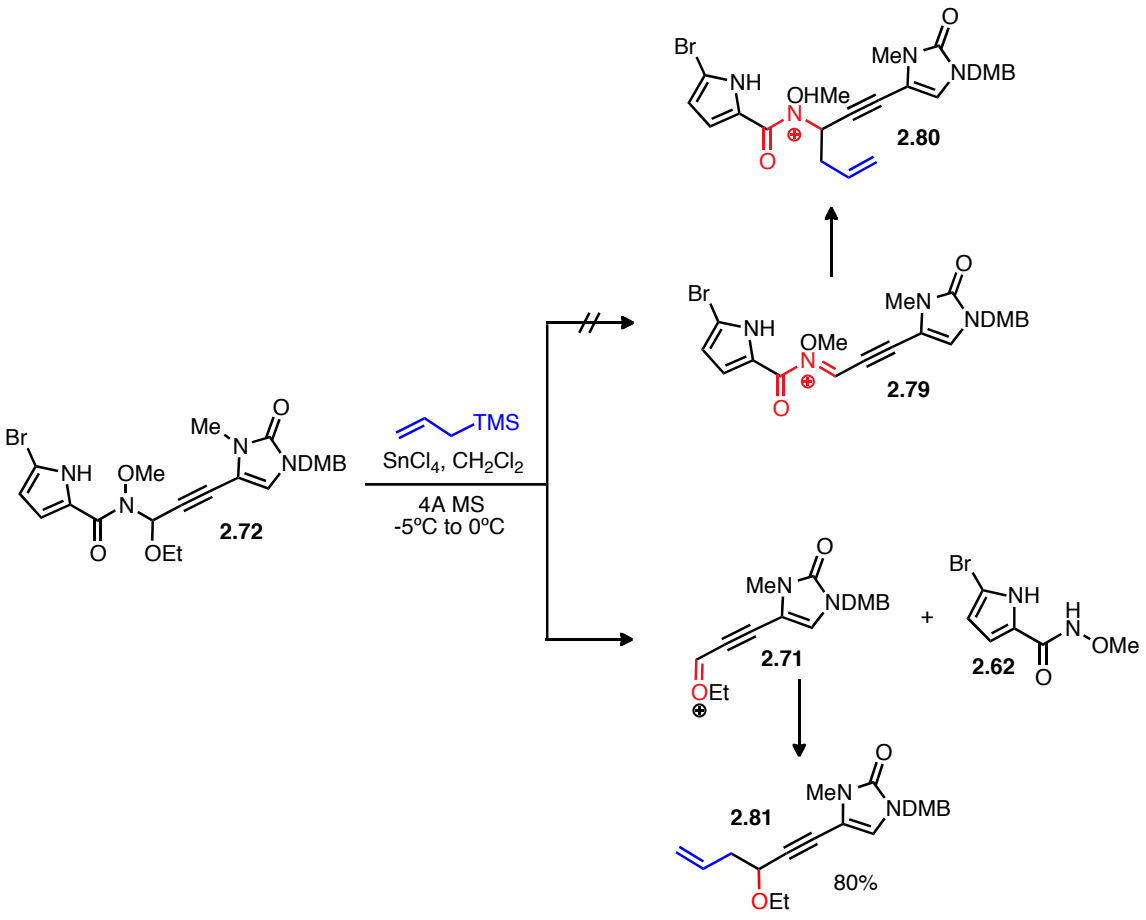

To avoid the detrimental effects of the N-methoxy group in our proposed key step, we elected to reductively cleave the N-methoxy bond earlier than what we originally planned. To this end, coupling adduct **2.82**, now bearing an N-tosylethyl protecting group, was subjected to samarium (II) iodide (SmI_2) to cleave the N-O bond (Scheme 2.22). Performing this reaction at -20 °C prevented debromination of the pyrrole as a byproduct, which occurs when the reaction is done at 23 °C. Inconsistencies in conversion, yield, and selectivity of the Lindlar reaction in the formation of **2.84** due to catalyst inactivity or overactivity was solved through the use of 2,2′-(Ethylenedithio)diethanol as a palladium poison. As low as 10 ppt of poison was sufficient to effect a more consistent reaction yield and chemoselectivity, furnishing biscyclization precursor **2.84**. Screening of manufacturers of Lindlar's catalyst revealed that Strem Chemicals consistently gave active palladium catalysts when compared to Sigma-Aldrich. The use of a 1:1 mixture of THF-methanol was also key in solubilization of the starting material **2.83**, giving a faster conversion to the desired alkene product **2.84**. X-ray crystallographic analysis[28] of this intermediate confirmed the Z-olefin configuration and the chemoselective addition of the amide nitrogen over the pyrrole nitrogen in the coupling step.

Scheme 2.22

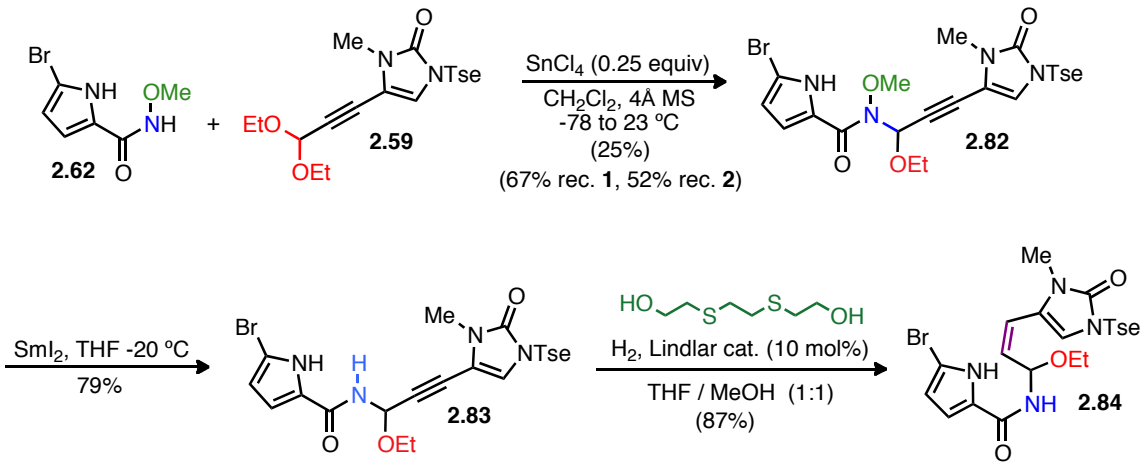

Treatment of **2.84** with Brønsted or Lewis acids, however, still did not deliver the desired biscyclization adduct dehydroagelastatin A **2.85**. Interestingly, formation of *N*-acyliminium **2.86** was favored and underwent a facile 5-*exo*-trig cyclization or a Nazarov 4π electrocyclization involving the pseudoaromatic imidazolone (Scheme 2.23).[29] The deep red solution formed in this process was postulated at this point to be due to the highly conjugated N-acyliminium intermediate **2.87**. The 6-*exo*-trig attack of the pyrrole nitrogen, however, did not occur and **2.87** seemed to be stable until quenched with a nucleophile (*e.g.* water) to give monocyclized adduct **2.88**. Quenching with methanol or ethanol gives the corresponding methoxy and ethoxy carbinolamines, respectively (not shown). Formation of the C-ring was quite facile as complete conversion occurred in < 5 min at low temperatures and delivered three contiguous stereocenters with a relative configuration corresponding to the agelastatins and

nagelamide J. However, the second cyclization envisioned to complete the synthesis, involving nucleophilic addition of the pyrrole nitrogen to C7 of the extended *N*-acyliminium **23**, did not proceed under a variety of conditions including prolonged reaction times, addition of non-nucleophilic bases, or exposure to elevated temperatures. Under most conditions, the dark red intermediate, which is presumably *N*-acyliminium **2.87** was easily regenerated from **2.88** with both Lewis and Brønsted acids and again persisted until quenched with a nucleophile (*e.g.* water, methanol) leading back to carbinolamine **2.88**.

Scheme 2.23

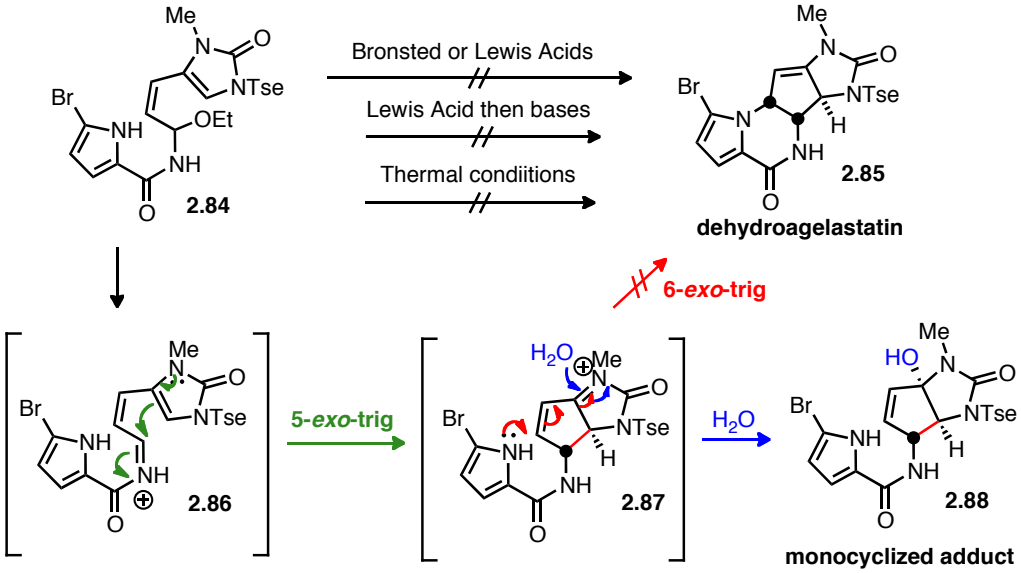

Conformational analysis of intermediate **2.87** suggests that the C6-C7 olefin is out of plane with respect to the *N*-acyliminium by ~25° resulting in a low degree of conjugation which in turn is responsible for the low electrophilicity at C7 (Scheme 2.24).[30] This may also explain why intermolecular addition of nucleophiles occurred exclusively at the more electrophilic C5 carbon. Moreover, DFT calculations[31] predicted that products **2.90** and **2.91** arising from nucleophilic trapping at C7 were energetically disfavored by ~2 kcal/mol relative to trapping at C5.

Scheme 2.24

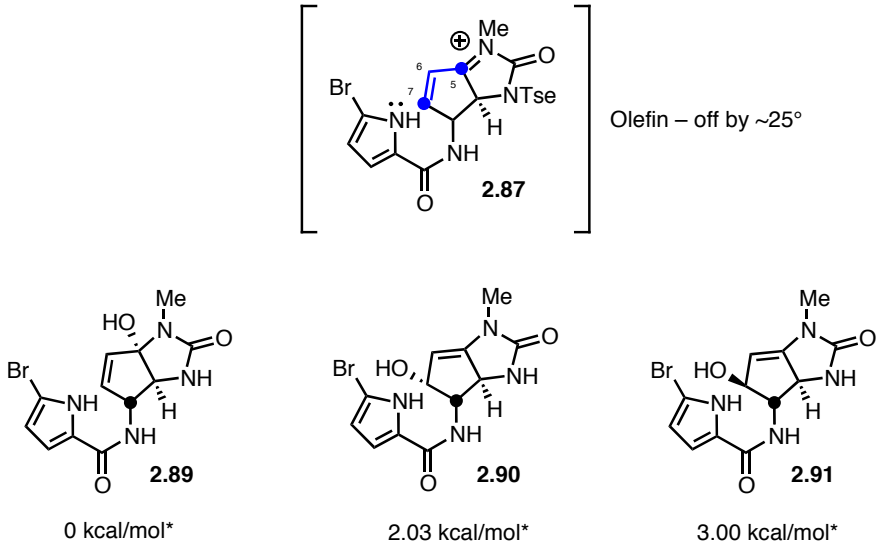

N-acyliminium precursor **2.84** (Scheme 2.25) was also found to be highly sensitive to even traces of Brønsted acids (*e.g.* traces of HCl in $CDCl_3$). This occurs

with a transient persistence of faint red color that rapidly disappears within seconds. It undergoes facile cyclization with the ethanol byproduct of *N*-acyliminium formation readily quenching **2.87** to form ethoxy cabinolamine **2.92** and returns the acidic proton for another catalytic cycle. Lewis acids on the other hand traps the ethoxy group that is cleaved off of precursor **2.87**, and allows the formation of either **2.88** or **2.92**, with water or ethanol as nucleophiles, respectively.

Scheme 2.25

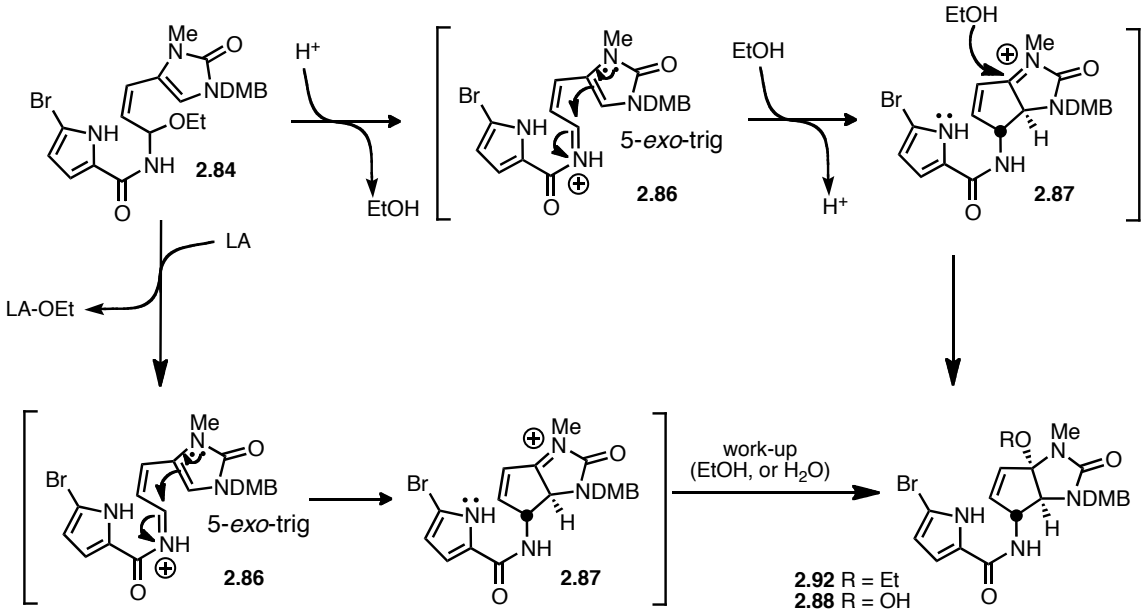

The full characterization as well as confirmation of the relative stereochemistry of the newly formed C-ring was established through a combination of NMR studies and DFT calculations of ^{1}H NMR coupling constants (Table 2.5). The *cis*-fused

configuration of on the 5-5 ring system in **2.93** (Scheme 2.26) was established through the NOESY correlation of C(4)-H and C(5)-OMe. The C(4)-C(8) connectivity that closed the C-ring was verified though COSY correlations of C(4)-H and C(8)-H as well as ^{1}H-^{13}C correlations of C(7)-H to C(4) as well as C(4)-H to C(7). These 2D NMR studies however could not verify the *trans* relationship between C(4)-H and C(8)-H. To this end, the experimental ^{1}H-^{1}H coupling constants were then compared to what is expected when these protons are *cis* or *trans* and is compared to predictions for products **2.89** and **2.92**. Predictions were based on the dihedral angles of these compounds and comparison with the experimental. The predictions of the Karplus plot gave very broad and similar ranges of 6.0-10.3 Hz and 6.5-11.6 Hz despite the large difference in dihedral angles 140.7° and 23.7°, respectively. DFT calculations using Gaussian 09 (B972/6-311g(2d,p)), on the other hand, was quite useful and product **2.92** closely matched the experimental coupling constants. Based on this evidence, C(4)-H and C(8)-H was established to be the desired *trans* configuration.

Scheme 2.26

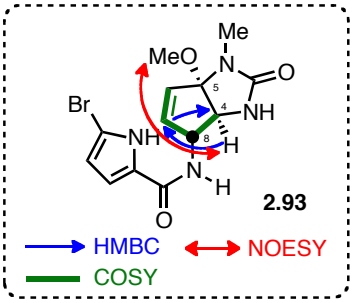

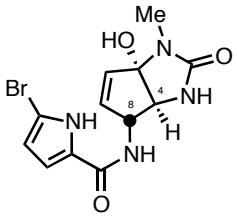

2.89

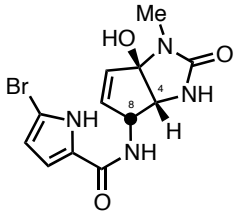

2.92

Table 2.5 Characterization of monocyclized adduct **2.89**.

	2.89	**2.92**
C(4)-H -- C(8)-H dihedral angle	140.7 º	23.7 º
^{3}J , (Karplus Plot)	6.0-10.3 Hz	6.5-11.6 Hz
δ, ^{3}J [C(4)-H -- C(8)-H] (B972/6-311g(2d,p))	3.37 ppm, 2.6 Hz 4.61 ppm, 2.6 Hz	3.66 ppm, 5.6 Hz 5.00 ppm, 5.6 Hz
δ, ^{3}J [C(4)-H -- C(8)-H] (experimental, CD_3OD)	3.67 ppm, 2.0 Hz 4.66 ppm, 2.0 Hz	

We were intrigued by the observed intense red color during the first cyclization event, which occurs immediately upon addition of acid even at low temperatures. Given the absorption of light in the visible region, we suspected that the color may be due to a charge transfer complex involving the *N*-acyliminium intermediate **2.87**. We utilized Time-Dependent Density Functional Theory (TD-DFT) calculations to analyze excited states of this charged intermediate and simpler sub-structures using B3LYP and X3LYP hybrid functionals.[32] We compared these values with those extracted from the experimental UV-VIS spectra of this colored intermediate and related simpler sub-structures. These studies revealed that the red color of intermediate **2.87**, is likely due to a $\pi \rightarrow \pi^*$ transition between the HOMO, which is composed mostly of orbital contributions from the bromopyrrole amide moiety and the LUMO, which is composed mostly of orbital contributions from the *N*-acyliminium moiety (Figure 2.4).

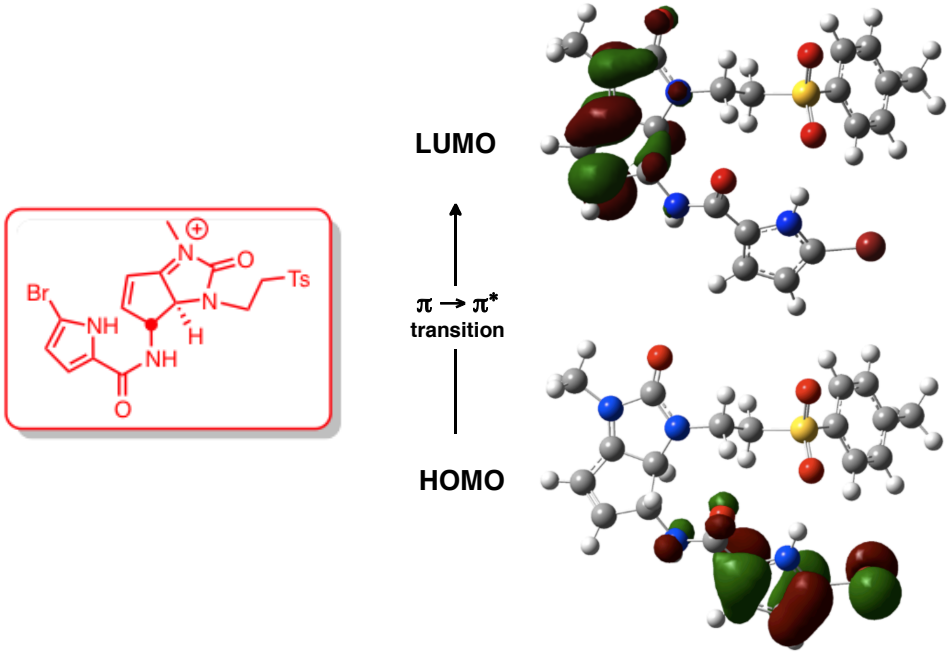

Figure 2.4 Calculated HOMO and LUMO of the red-colored *N*-acyliminium **2.87** and the π→π* transition proposed to be responsible for this color based on TD-DFT calculations. Isovalue for surface = 0.04.

Given that the stereochemical setting step in the synthesis is an acid-catalyzed C-ring formation, which sets three out of four contiguous stereocenters in a highly diastereoselective fashion, we envisioned that the use of chiral acids should set the absolute stereochemistry of the core C-ring. Initial screening of chiral acids shown in Table 2.6 revealed the superiority of BINOL-derived phosphoric acids **2.95** with 3,3'-bistriphenylsilyl-substituted BINOL phosphosphoric acid **2.95c** giving the best enantiomeric excess of 74% (enantiomeric ratio 87:13). Due to limitations in available chiral columns in our laboratories, enantiomeric excess was established by HPLC analysis of the deprotected product **2.89**. Erosion of about 10% ee was observed during

purification of **2.89**. Further screening of catalysts and conditions are necessary to optimize the enantiomeric excess and yield highly enantiopure synthetic natural product.

Table 2.6. Screening of chiral Brønsted acids.

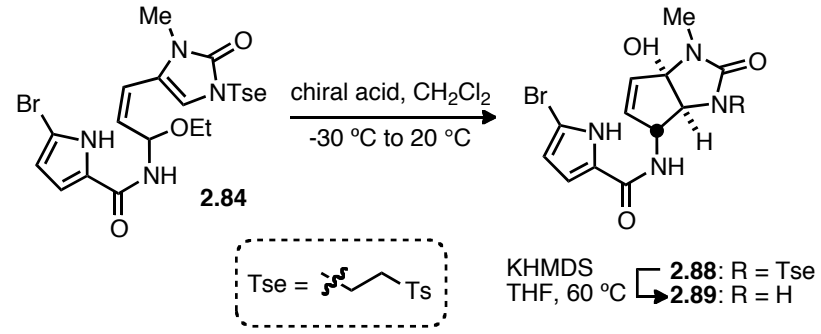

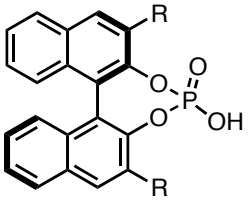

2.95a R = $Ph(CF_3)_2$
2.95b R = $Ph(iPr)_3$
2.95c R = $SiPh_3$

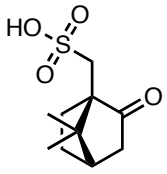

2.93 (+)-CSA

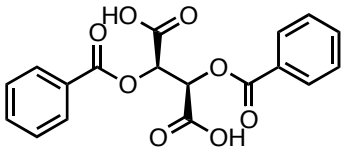

2.94 (-)-Dibenzoyl tartaric acid

Chiral Acid	ee of **2.13**
2.93	2 %
2.94	10 %
2.95a	40 %
2.95b	63 %
2.95c	74 %

We then sought to examine the diastereoselectivity of the C-ring formation. Formation of only the desired diastereomer ----- was observed when N-Tse ----- was subjected to the cyclization conditions (Scheme 2.29). The transformation was clean rest of the mass balance was attributed to some degree of decomposition and none of the undesired bis-*epi* diasteromer **2.96** was observed by NMR. In the absence of the N-Tse protecting group, a mixture of diasteromers **2.89** and **2.92** with a dr of 1:2 in favor of the undesired cyclization product **2.92** was observed.

Scheme 2.29

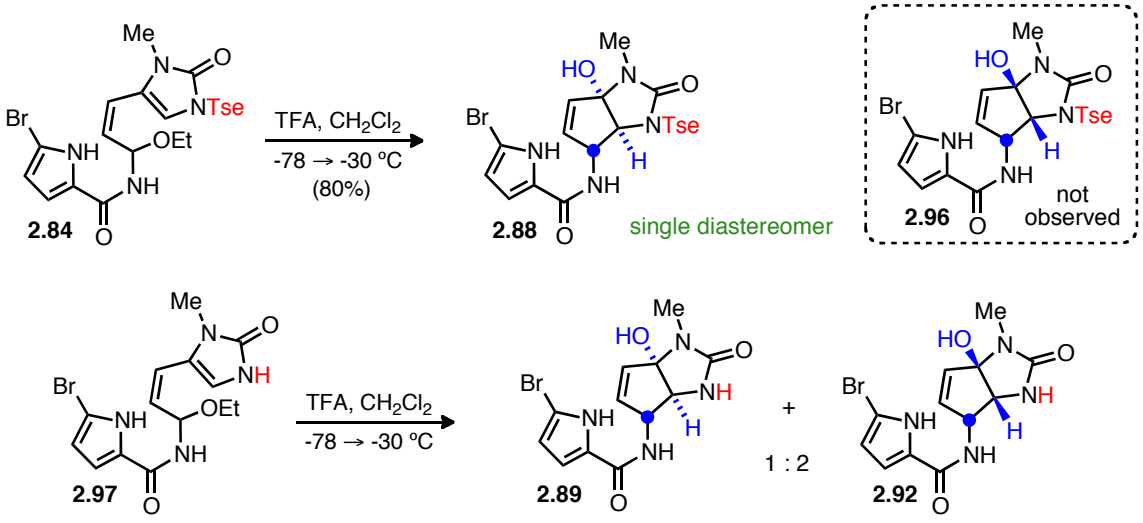

The dependence of the diastereoselective formation of the C-ring on the presence or absence of the Tse protecting group can be attributed to the lower energy, major conformer of the *N*-acyliminium intermediate **2.86** and **2.98** (Scheme 2.30). Particularly, the s-*cis* and s-*trans* conformers formed upon rotation of the C(7)-C(8)

single bond plays a key role whether C(4)-H and C(8)-H ends up cis or trans in the monocyclized adduct (*cf.* **2.88**). With the Tse group present, **s-*trans* 2.86** conformer is favored over the **s-*cis* 2.86** conformer due to steric interactions between the Tse and the bromopyrrole moieties in the latter. This leads to a transition state arrangement ---- leading to the desired trans-C(4)-H-C(8)-H diasteromer **2.88**. On the other hand, the absence of the Tse in **2.98** allowed **s-*cis* 2.98** conformer to be dominant based on the observed results leading to the wrong diastereomer **2.92** (Scheme 2.29) as the major product.

Scheme 2.30

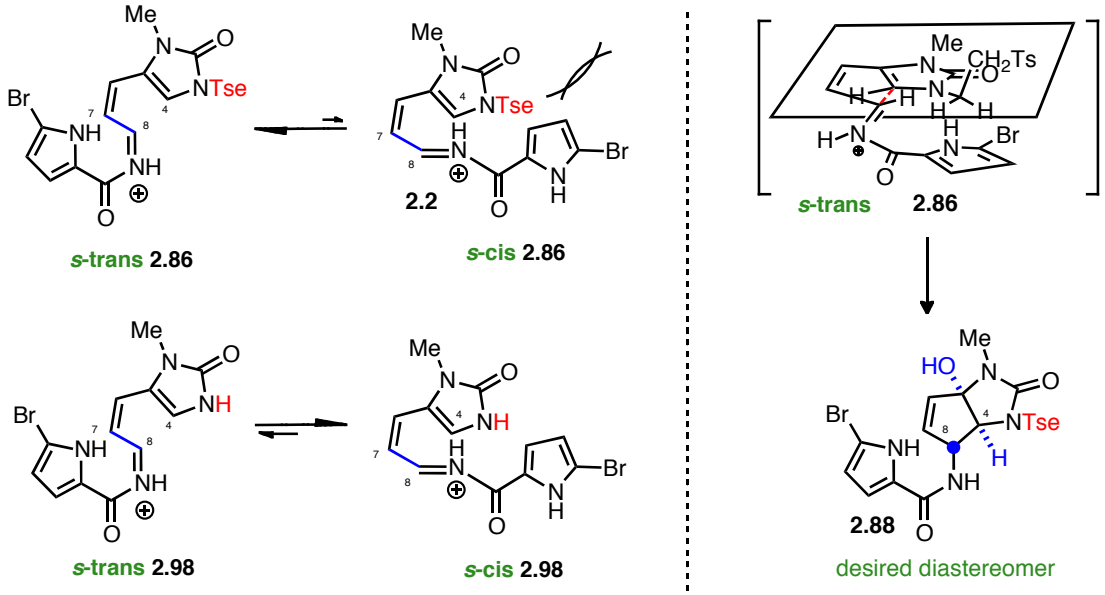

2.6 Final Cyclization Investigations: Completion of Synthesis

At this point, all that remains to be done is to form the final B-ring. As the pyrrole N(12) failed to cyclize onto the conjugated *N*-acyliminium intermediate, we sought different strategies. Since this failure was partly attributed to ineffective conjugation of the C(6)-C(7) olefin with the *N*-acyliminium, we envisioned that electrophilic activation of this double bond should promote nucleophilic trapping with the pyrrole nitrogen. After screening different sources of electrophilic halogens or oxidants (*e.g.* NBS, NIS, mCPBA) to form activated intermediate **2.89**, we found that the C(6)-C(7) olefin was of inferior nucleophilicity compared to the bromopyrrole moiety (Scheme 2.31). In this case the electrophiles preferred to react with the electron-rich pyrrole, which was further activated by the C(13)-Br towards electrophilic aromatic substitution. Alternatively, we also examined the possibility of performing a base-promoted hydroamination. While this approach worked with the alkyne precursor prior to C-ring formation, in this case screening of bases proved to be a dead end. In an attempt to relieve strain in the D ring of *N*-acyliminium intermediate derived from **2.88**, we envisioned that a base should be able to deprotonate the C(5)-OH to induce a transient opening of the D-ring revealing a cyclopentanone that is amenable to an aza-Michael addition. This regenerates the C(5) carbonyl ready for D-ring reclosure by nucleophilic attack of N(1)-Me.

Scheme 2.31

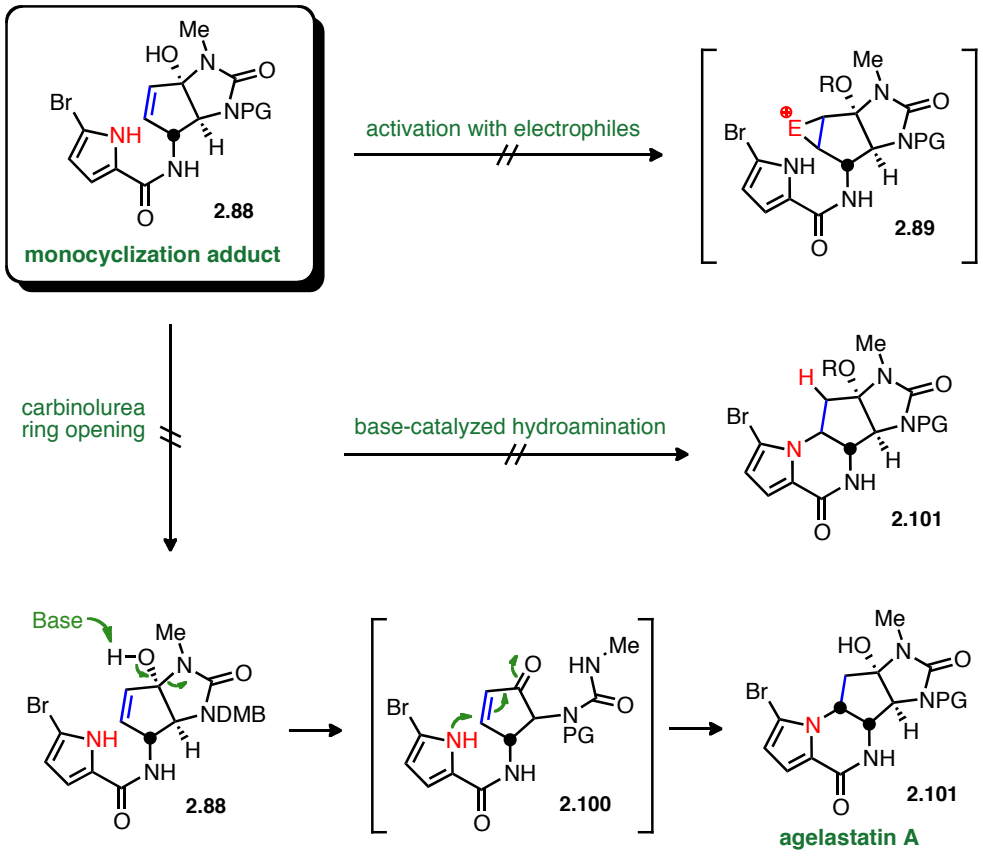

Interestingly, several previous syntheses of agelastatin A requiring late-stage B ring closure, proceeded via an enone intermediate bolstering this idea further.[4a,4h,4i,4k,4o,4q] The monocyclized adduct **2.88**, however, was quite stable to bases and did not yield any desired product **2.101** even at elevated temperatures. We reasoned that the protecting group on N(3) was the key steric issue, preventing D-ring opening. To this end, the Tse protecting group on the urea nitrogen was removed to enable greater conformational mobility and facilitate D-ring cleavage. NaHMDS was found to be the best base for

deprotection over KHMDS, which gave 10% lower yield (Scheme 2.32). After much experimentation, we serendipitously found that bicyclic intermediate **25** is readily converted to agelastatin A **2.1** on silica gel[33] pretreated with triethylamine under solvent-free conditions with mild heating. 4,5-Bis-*epi*-agelastatin A **2.102** was observed as a byproduct of the cyclization, presumably arising from a retro-Nazarov or a retro-5-*exo*-trig ring-opening followed by recyclization. This silica gel-promoted cyclization was scaled up with the use of toluene to assist the uniform heating of silica gel. Inspection of the toluene layer reveals that there is no dissolution of precursor and the transformation happens through an apparent templating effect on the surface of the gel. The precursor **2.89** is adsorbed on regular TLC plates (pretreated by immersion in 10% triethylamine in hexanes) as thick bands and eluted with 10% methanol in dichloromethane for a more uniform distribution on the silica gel surface. When methanol is used as solvent, the precursor is desorbed from the silica gel and no reaction happens. Also, without triethylamine pretreatment of the silica gel used, the starting material cleaves into two fragments occurring probably through a retro-Nazarov or retro-5-*exo*-trig followed by hydrolysis (*cf* **2.103** and **2.104**.)

Scheme 2.32

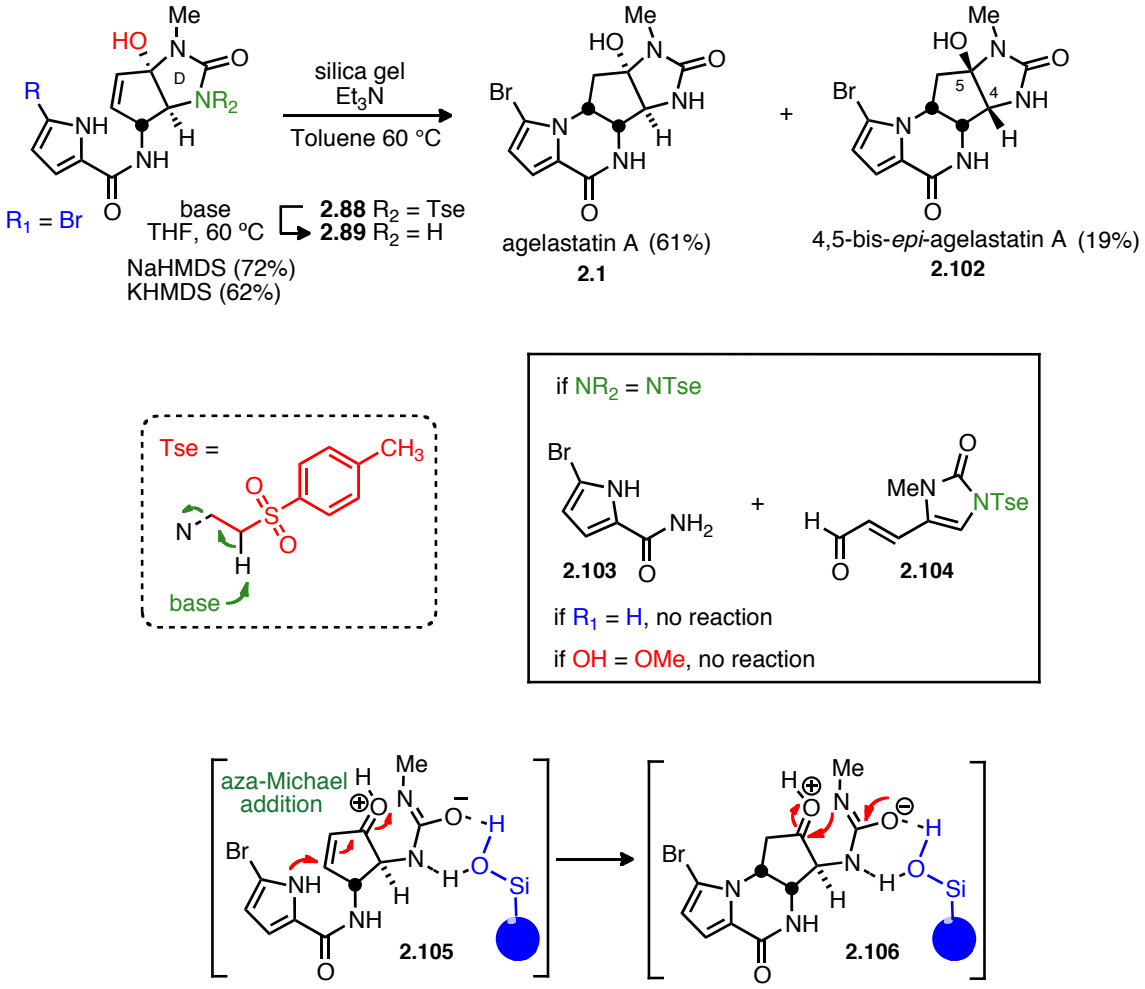

Attempted cyclization with alternative substrates revealed that removal of the Tse group and the presence of unprotected C5-OH and the bromine at C13 of the pyrrole ring of **2.89** were essential for successful cyclization. The importance of the bromine in this cyclization event is quite remarkable since all agelastatin have at least this bromine in the pyrrole. Another interesting aspect is that in the presence of the Tse, the reaction

delivers **2.103** and **2.104**, instead of intramolecular cyclization. This points out to the importance of an unprotected N(3)-H and C(5)-OH for H-bonding. Based on these experiments, we propose that extensive H-bonding is involved in the transition state enabling D-ring opening to give **2.105** followed by an aza-Michael to form the final B-ring giving **2.106**, with concomitant reclosure of the methyl urea to give agelastatin A (Scheme 2.32).

2.7 Conclusions

In summary, a concise total synthesis of agelastatin A **2.1** *via* two sequential, potentially biomimetic cyclizations was completed. The described sequential assembly of the C and B rings provides evidence for the proposed reactivity of a linear alkenyl imidazolone pyrrole leading to the agelastatins and complements other approaches to agelastatin involving initial B ring followed by C ring formation.[4s] C-ring formation, which sets three contiguous centers in a highly diastereoselective fashion, was accompanied by an intense red color that we propose involves a $\pi \rightarrow \pi^*$ transition between the HOMO and LUMO of *N*-acyliminium intermediate **2.86** which is supported by TD-DFT calculations. The final B-ring closure was uniquely successful and occurs on the surface of the silica gel with uniform heating assistance of toluene. The reaction sequence leading from an oxidized keramadine analog (*cf.* **2.84**) through a nagelamide J–like intermediate (*cf.* **2.88**) to agelastatin A is a provocative proposal for the biosynthesis of the agelastatins that inspired the concise route to the natural product reported herein. Further studies of the described strategy, including development of an enantioselective version,[4s] are currently underway.

CHAPTER III

STRUCTURE-ACTIVITY RELATIONSHIP (SAR) AND CELLULAR TARGET IDENTIFICATION STUDIES

3.1 Introduction

The investigation of structure-activity relationships (SARs) of small molecules is a central concept in medicinal chemistry. The aim of any SAR Study pertaining to the use of natural products as potential drug candidates is to reveal which structural features are essential and non-essential to biological activity. This facilitates not only the development of more potent analogs but also provide clues for rational design of a biological probe that can be used to identify the cellular receptor of the natural product in question.

Pietra and co-workers[10b] pioneered the initial SAR data on agelastatin A **2.1**. They synthesized several semisynthetic derivatives (Figure 3.1) of agelastatin A from the material they isolated from *Agelas dendromorpha.* Their studies revealed that unsubstituted C(5)-OH, N(9)-H and N(3)-H moieties are essential in the B/D transoid configuration for high cytotoxicity. Acetylation or methylation of C(5)-OH lead to 20-fold and 116-fold decrease in potency, respectively. Methylation of both N(3) and N(9) showed 280-fold loss of activity. This however begs the question whether only one of these two NHs is essential for bioactivity. Complete reduction of both C(2) ans C(10) carbonyls also resulted in loss of activity (33-fold). The stereochemistry at C(4) and C(5) are quite necessary based on a 3-fold loss of potency. Reductive debromination of

the pyrrole C(13) bromine also lead to a significant loss in potency (6-fold). Although this is hypothesized to not necessarily mean the importance of the bromine atom in the aromaticity of the pyrrole but could merely be due to conformational change in the tetracycle in its absence.

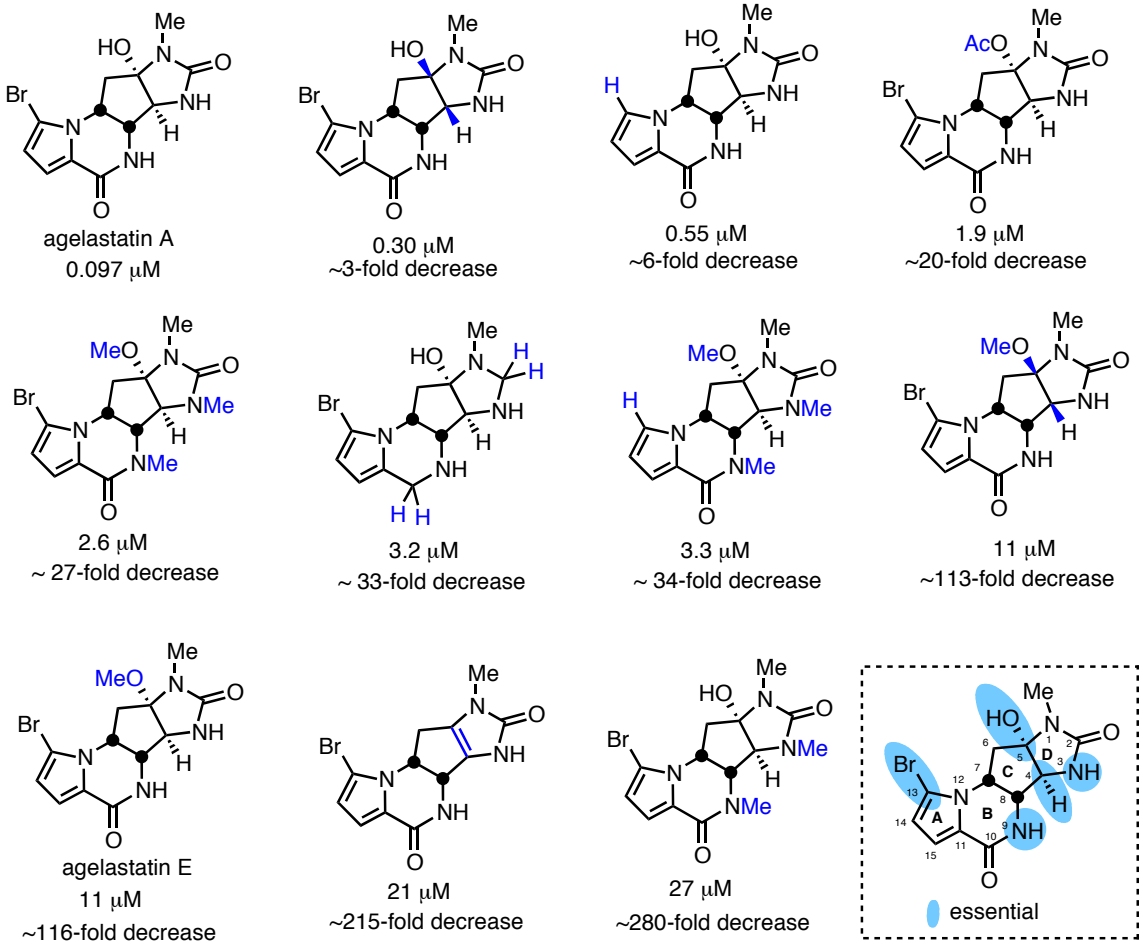

Figure 3.1 Cytotoxicity data (IC_{50}, μM) against L1210 mouse lymphocytic leukemia cells and summary of essential moieties in agelastatin A

3.2 Syntheses and Bioactivity of Agelastatin A Derivatives

We started our SAR studies based on the initial data discussed in the previous section. Cellular target identification, as well as biological activity assays were done at the laboratories of Prof. Jun O. Liu at Johns Hopkins University in collaboration with graduate student Mr. Brandon McClary. HeLa cells were ultimately chosen to be used in the antiproliferation studies since synthetic (±)-agelastatin A was found to have a low IC_{50} of 229 nM with this cancer cell line. All designed derivatives described herein are in racemic form.

Since our synthesis involves sequential biomimetic cyclizations forming the C and B rings, we decided to ascertain whether the B-ring of agelastatin A is necessary for bioactivity. Monocyclized intermediates **3.1** and **3.2** (Scheme 3.1) were subjected to cytotoxicity assay using HeLa cells and showed that while **3.1** had no inhibition, **3.2** retained some bioactivity with an IC_{50} of 2.50 μM. This suggests that the N(3)-H is important for potency and that the uncyclized B-ring is not detrimental to bioactivity. To fully mimic the C-D ring in agelastatin A, the C(6)-C(7) olefin needs to be fully reduced (Scheme 3.1). Using Pearlman's catalyst $Pd(OH)_2/C$, hydrogenation of **3.1** gave **3.3** with fully reduced C-ring and concomitant removal of the bromine atom. Using 2-nitrobenzenesulfonylhydrazide (NBSH), the C(6)-C(7) olefin was chemoselectively reduced to give **3.4**. Bioassays, however, indicated that **3.3** showed no inhibition. This could mean that the activity of **3.2** might be due to *in cellulo* B-ring cyclization leading to appreciable amounts of the parent compound, agelastatin A, and thus **3.2** just serves as a "pro-drug". Following this line of thought, the inactivity of **3.1** could also be due to

its inability to undergo B-ring cyclization as observed in our laboratory investigations. On the other hand, another difference of **3.3** to **3.2** is the absence of the C(13) bromine atom. Although the bromine is quite remote to the C-D ring junction and its effect on the C/D-ring conformation is minimal, its presence in all agelastatins and the importance of a C(13)-bromopyrrole interaction in the active site cannot be dismissed. The pending bioassay of **3.4** should be able to address this question.

Scheme 3.1

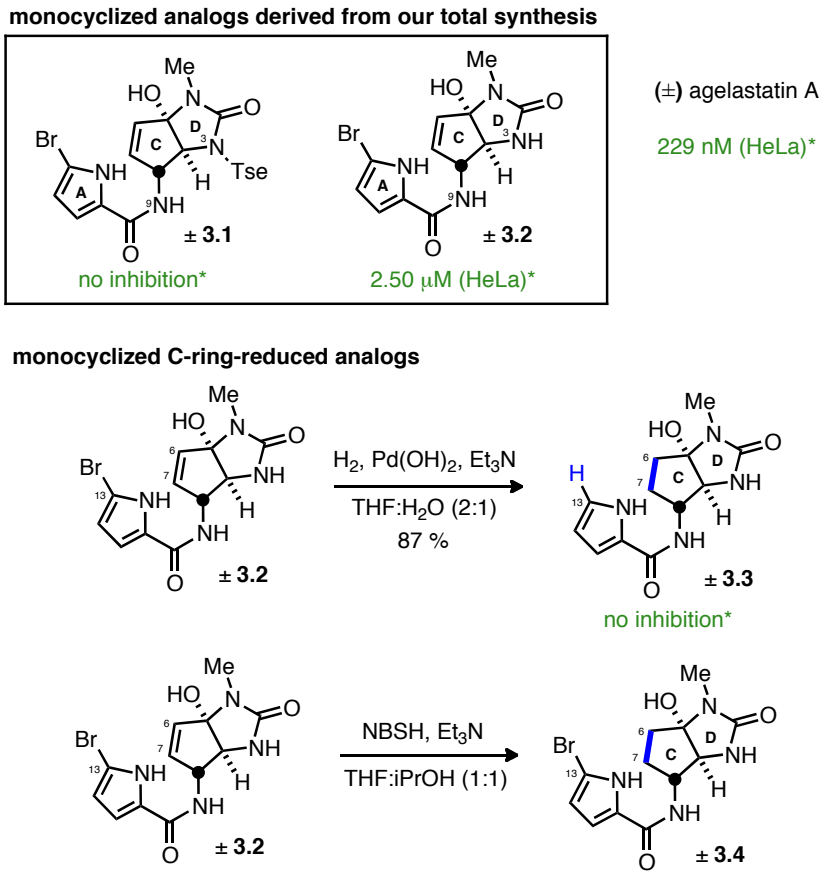

Agelastatin B (**2.2**), a C(14)-bromo analog of agelastatin A, was isolated as a trimethyl derivative. The absence of biological data on **2.2**, as well as the lack of SAR studies of the pyrrole C(14) prompted us to investigate substitution at this position. The electron rich nature of the pyrrole allows it to undergo straightforward electrophilic halogenation reactions. *N*-Bromosuccinimide (NBS) regioselectively brominates the C(14) position to give **2.2** (Scheme 3.2). A mixture of 2:1 THF:water allowed dissolution of the starting material and 2,6-di-*t*-butylpyridine was used to scavenge adventitious acid in the reaction mixture. It also necessitated the addition of NBS as a solid instead of addition as a stock solution. Attempts at using a stock solution lead to regioselectivity issues with bromination presumably due to formation of Br_2 evidenced by slight yellow color change upon dissolution. Iodination, on the other hand, required $In(OTf)_3$ as an activator to produce product **3.5** using *N*-iodosuccinimide (NIS). Iodinated compound **3.5** was then subjected to copper-free Sonogashira cross-coupling with bis-alkyne **3.6** to give alkyne derivative **3.7**. The presence of copper iodide in this reaction led to inconsistent results. The distal terminal TMS-alkyne was designed to serve as a functional handle for an eventual synthesis of a biotin probe. Antiproliferation assays of **2.2**, **3.5**, and **3.7** resulted in IC_{50} values of 5.74 μM, 38.1 μM, and 1.30 μM, respectively. A clear trend is observed when you consider the steric bulk added, with C(14)-iodo-substituted compound **3.5** showing 166-fold loss of activity, followed by C(14)-bromo substituted agelastatin B (**2.2**) showing 25-fold decrease in activity. It is noteworthy, however, that the addition of the linear bis-alkyne at C(14) only showed a 6-fold loss of activity. This could point out that the proximal alkyne handle itself does not

have steric bulk and allows the molecule to still bind to its cellular target. This provides us with a good lead compound for a cellular probe synthesis.

Scheme 3.2

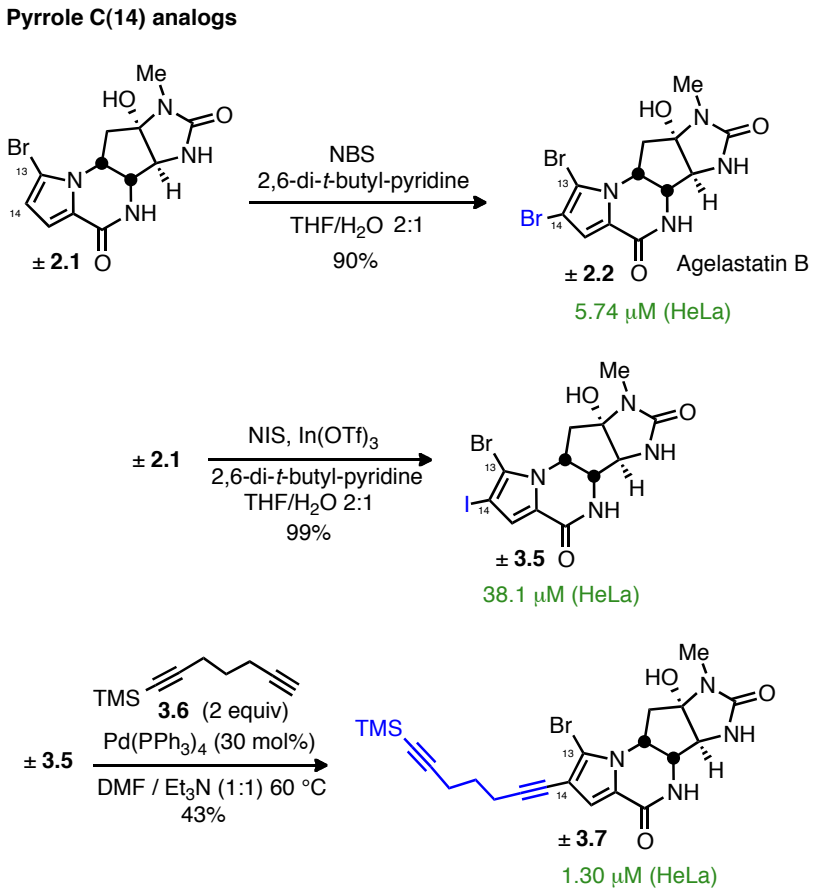

The importance of the C(13)-bromine was not conclusive because its absence, while decreasing potency, was also proposed to result in slight changes in the conformation of the parent tetracyclic structure. Thus, we sought substitutions at C(13) that are either a bioisostere of bromine or a linker that allows synthesis of a biological

probe. Reduction of the bromopyrrole with hydrogen and $Pd(OH)_2/C$ gave **3.8** (Scheme 3.3). Copper-free Sonogashira reaction of agelastatin A (**2.1**) with bis-alkyne **3.6** yielded **3.9**, with a probe linker in place. Debromoagelastatin A **3.8** lost 17-fold of activity based on HeLa cells (IC_{50} 3.81 μM) in contrast to a 6-fold decrease in L1210 leukemia cells. This verifies the importance not necessarily of the presence of a bromine atom but a substituent at C(13). Linker-appended **3.9**, on the other hand, was more active against HeLa cells than **3.8** at an IC_{50} of 2.96 μM .

Scheme 3.3

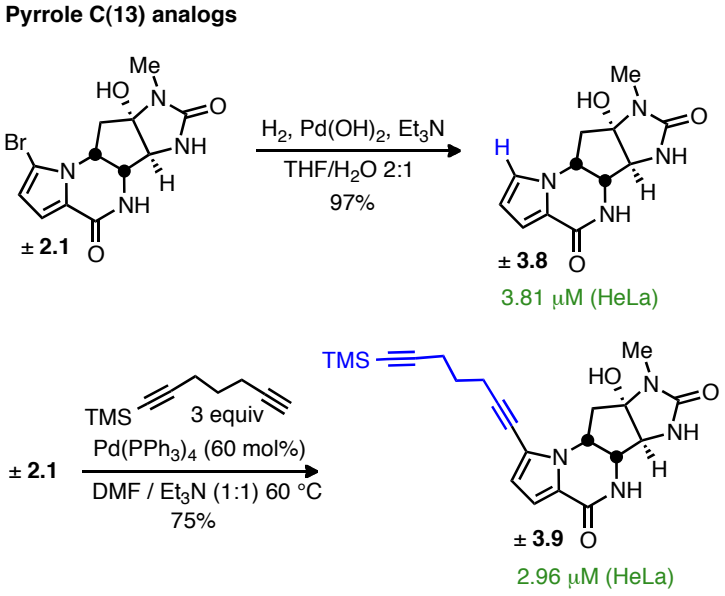

More interesting C(13) derivatives are substitutions of bioisosteres of bromine that maintains similar sterics around the pyrrole region. Methyl derivative **3.10** was synthesized using Stille cross-coupling reaction with tetramethyltin (Scheme 3.4).

Chloroagelastatin A **3.11** and iodoagelastatin A **3.12** were synthesized using $In(OTf)_3$ promoted halogenations using *N*-chlorosuccinimide (NCS) and *N*-iodosuccinimide (NIS). While biological evaluations of **3.10**, **3.11**, and **3.12** are pending, these derivatives are indeed interesting. Chloroagelastatin **3.11** not only reduces sterics but also lowers the molecular weight farther from the maximum ideal limit of 500g/mol. C(13)-Methyl derivative **3.10** on the other hand enhances lipophilicity and solubility.

Scheme 3.4

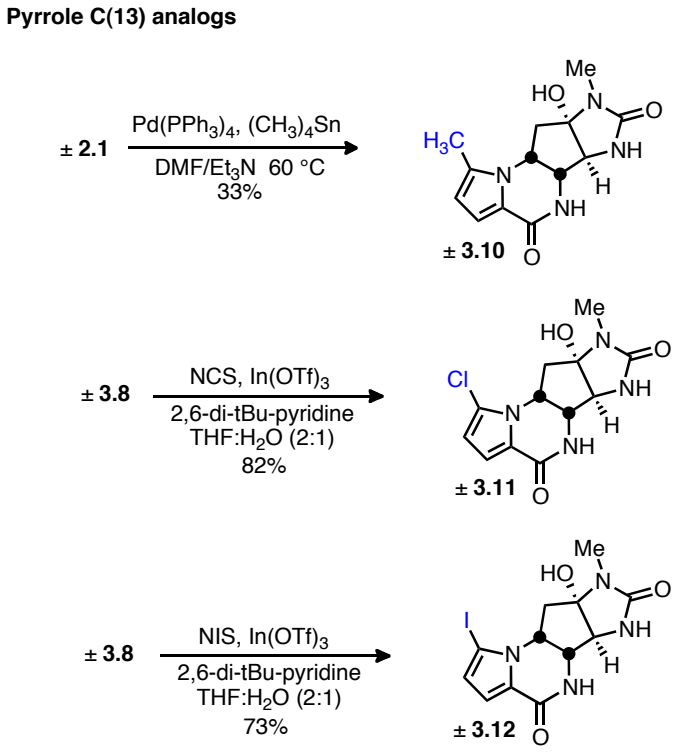

Another possible site of probe attachment is the N(9) position. As alluded to in section 3.1 this position has not been explored. To access singly-substituted N(9)

analog, we took advantage of the increasing pKa of the acidic protons in the molecule (C(5)-OH < N(9)-H < N(3)-H). Deprotonation of the C(5)-OH with LHMDS followed by quenching with TMSCl leads to **3.13** (Scheme 3.5). Another equivalent of LHMDS deprotonates the N(9)-H and the anion is alkylated with methyl iodide to give **3.14**. Finally, the transient TMS protecting group is cleaved with tetrabutylammonium fluoride (TBAF) to give the desired N(9)-methyl analog **3.15**. The methyl attachment at N(9) was verified with HMBC correlatios of the methyl protons with the adjacent carbons. Retention of some bioactivity of **3.15** would lead to an analogous biological probe based on N(9) attachment.

Scheme 3.5

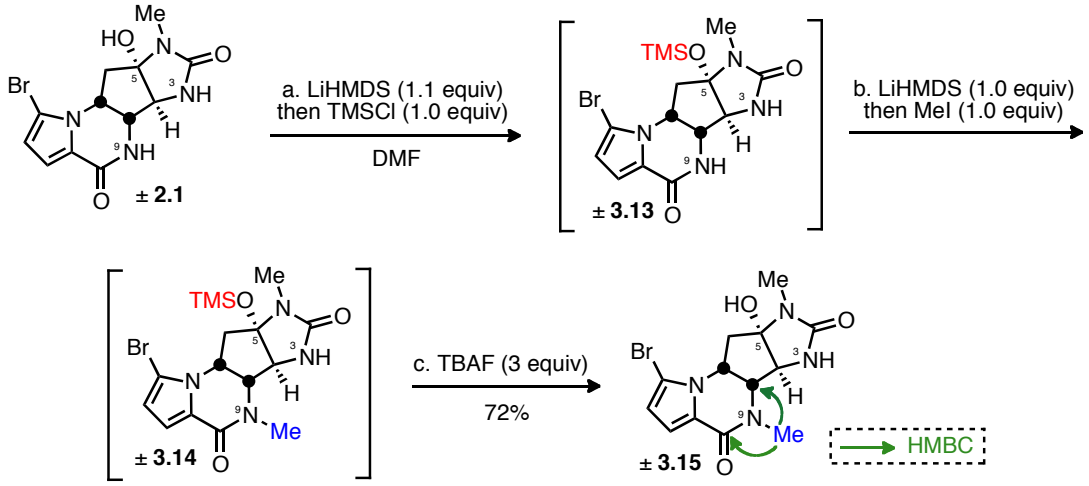

3.3 Synthesis of a Potent Biotin Conjugate

Of all the compounds we tested for bioactivity our best lead compound for the synthesis of a functional probe for receptor isolation studies was compound **3.7**. The ability of this compound to retain activity at 1.30 μM allowed us to extend the linker to include a biotin functionality via a Sharpless-Hüisgen cycloaddition with biotin-azide **3.16** to give the desired biotin conjugate **3.17**. Investigations on the use of **3.17** for pull-down affinity chromatography experiments are currently underway.

Scheme 3.6

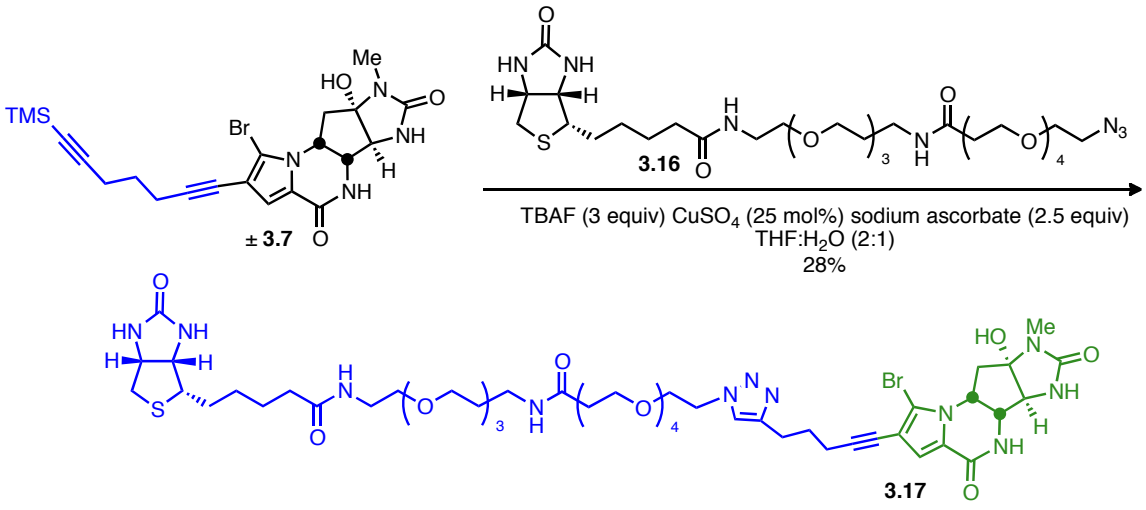

3.4 Initial Studies on the Identification of the Cellular Target of Agelastatin A

To elucidate the cellular mechanism of antitumor activity of agelastatin A (**2.1**), a 'top down approach' was used to determine the specific effect on three major cellular processes: DNA replication, transcription, and translation. The effects of **2.1** on DNA synthesis, RNA synthesis, and global protein synthesis were determined using incorporation of [^{3}H]-thymidine, [^{3}H]-uridine, and [^{35}S]-methionine as readouts, respectively. Treatment of PC3 cells for 1 hour led to a dose-dependent inhibition of [^{3}H]-thymidine incorporation into the DNA backbone with an IC_{50} of 30 nM, and [^{35}S]-methionine incorporation into newly formed proteins with an IC_{50} of 80 nM. This meant that both DNA synthesis and global protein synthesis is inhibited while RNA synthesis was not significantly affected (Figure 3.2). The IC_{50} value for inhibition of PC3 cell proliferation (88 nM) by treatment of agelastatin A for 24 hours correlated well with the IC_{50} value of inhibition of [^{35}S]-methionine incorporation (80 nM). The high correlation between these two values led us to believe that agelastatin A is preferentially inhibiting protein synthesis. However, the IC_{50} value for inhibition of [^{3}H]-thymidine incorporation (30 nM) is lower than the value for [^{35}S]-methionine incorporation (80 nM), which suggests that DNA synthesis is preferentially inhibited. To consolidate these contradicting data, it is quite possible that the synthesis of fast-turnover proteins necessary for DNA replication is rapidly inhibited, contributing to a more significant effect on DNA synthesis at earlier time points. This has been commonly observed with protein synthesis inhibitors.[34]

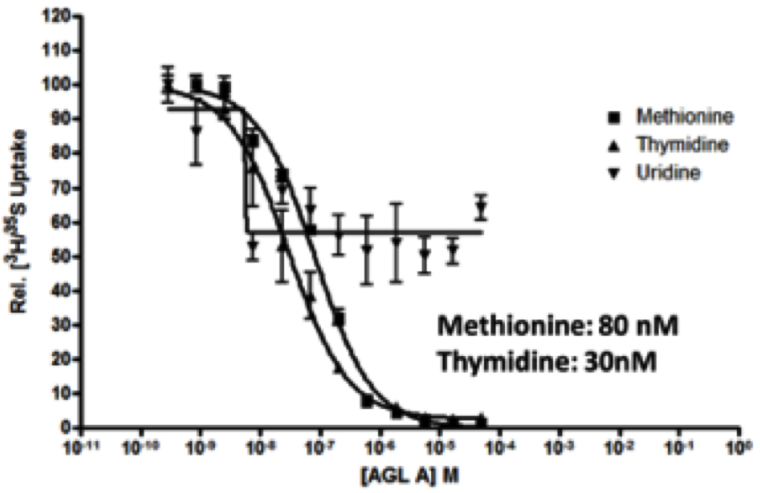

Figure 3.2 Effects of agelastatin A on DNA, RNA, and protein synthesis using incorporation of [^{3}H]-thymidine, [^{3}H]-uridine, and [^{35}S]-methionine. IC_{50} values listed next to the corresponding curves.

To confirm this hypothesis of preferential inhibition of translation with agelastatin A, cycloheximide (CHX)[35], a well-known inhibitor of translation elongation, was subjected to the same PC3 cells inhibition experiment (Figure 3.3). Treatment for 1 hour results in dose-dependent inhibition of [^{3}H]-thymidine incorporation with an IC_{50} of 45 nM, and [^{35}S]-methionine incorporation with an IC_{50} of 59 nM. As expected, RNA synthesis was not significantly affected. It is also interesting that similar to agelastatin A, CHX also has a lower IC_{50} value for DNA synthesis. Based on this evidence, it is hypothesized that (-)-agelastatin A is also an inhibitor of eukaryotic translation, and DNA inhibition effects as commonly observed with translation inhibitors, are likely due to a secondary response to the loss of translation.

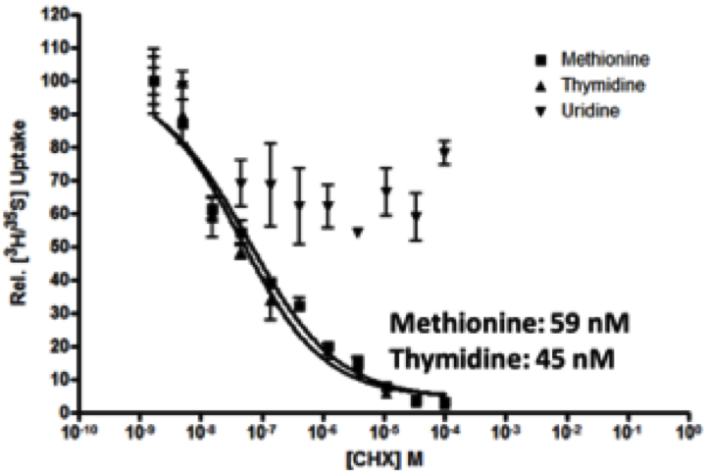

Figure 3.3 Effects of Cycloheximide (CHX) on DNA, RNA, and protein synthesis using incorporation of [^{3}H]-thymidine, [^{3}H]-uridine, and [^{35}S]-methionine. IC_{50} values listed next to the corresponding curves.

To verify that agelastatin A is indeed capable in blocking translation, protein synthesis from control RNA templates in rabbit reticulocyte lysate and [^{35}S]-methionine was analyzed by SDS-PAGE (Figure 3.4). In this *in vitro* system, agelastatin A also inhibits protein synthesis in a dose-dependent manner verifying that agelastatin A does block translation. The difference in the observed IC_{50} values between cell proliferation and translation assays may be attributed to the different drug incubation times and intrinsic sensitivity of the different readouts, as observed with previous work with translation inhibitors.[35-36]

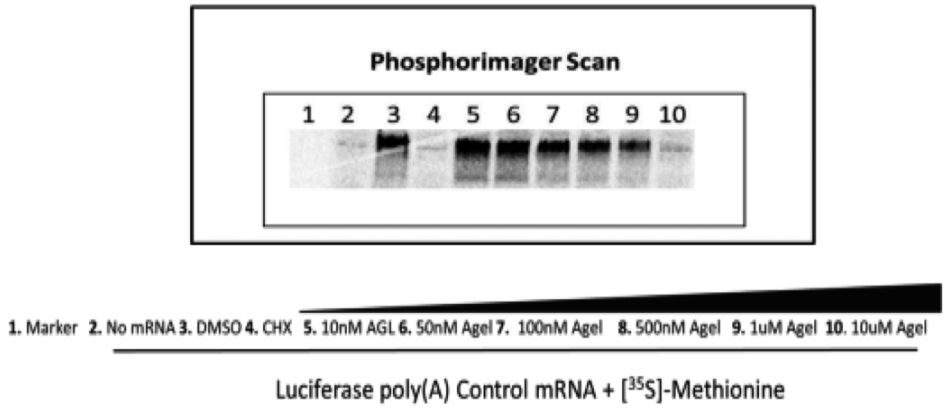

Figure 3.4 Dose-dependent inhibition of [^{35}S]-methionine incorporation by agelastatin A in an *in vitro* translation system. Agelastatin A was added to a rabbit reticulocyte lysate cocktail that included luciferase poly(A) control mRNA and [^{35}S]-methionine.

The specific step at which agelastatin A interferes with translation remains to be determined. A dual luciferase assay using hepatitis C virus (HCV) internal ribosome entry site (IRES) was performed to distinguish between the possibilities of agelastatin A interfering with the initiation or elongation phase of protein synthesis. Many viral mRNAs and a relatively small number of cellular mRNAs are translated as a result of the ribosome attaching to the mRNA at an internal entry site. HCV IRES mediated translation initiation does not require the 5' 7meG-cap structure. By recruiting initiation factors directly to the AUG start codon, HCV can bypass the eIF4F complex, which contains cap-binding factors eIF4E, and initiation factors eIF4A and eIF4G.[37] The dual luciferase reporter assay uses bicistronic *in vitro* reporters with a conventional capped firefly luciferase followed by renilla luciferase under the translational control of an IRES

element, which are resistant to inhibitors of translation initiation. Transcribed HCV IRES dual luciferase reporters were used to perform in vitro translation assays with rabbit reticulocyte lysate. AglA dose-dependently inhibited both cap-dependent translation and IRES-dependent translation of the mRNAs from both dual luciferase reporters. Treatment with CHX at 4 μM resulted in nearly complete inhibition of both cap- and HCV IRES-dependent translation (Figure 3.5). These results suggest that AglA, like CHX, inhibits translation at the elongation phase.

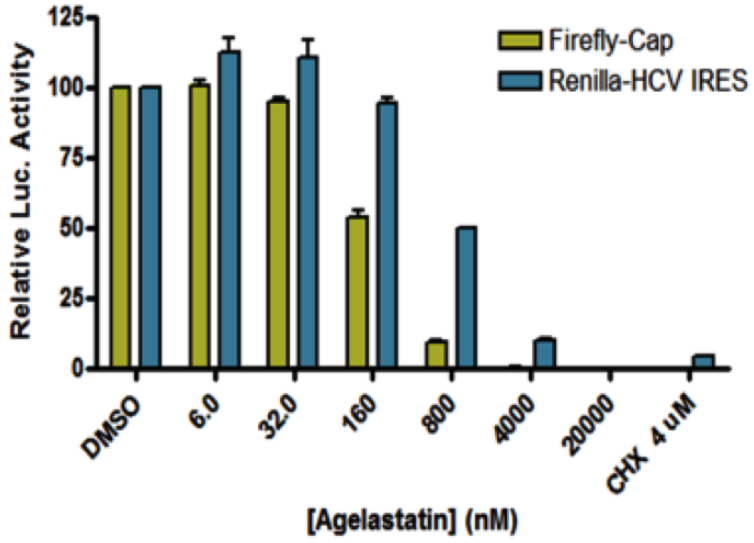

Figure 3.5 Dual luciferase translation inhibition by agelastatin A using HCV IRES dual reporter in an *in vitro* RRL translation system in the presence of different concentrations of agelastatin A and 4 μM CHX.

Agelastatin A may or may not be binding within the ribosome. It is possible that protein/s associated with translation elongation may in fact be the primary target. The

described agelastatin A C(13)-biotin probe described in the previous section is currently being used for affinity chromatography experiments in an effort to isolate the target protein of the natural product. A number of other translation assays is currently being conducted to further elucidate the mechanism of action.

CHAPTER IV

SYNTHESES OF ^{15}N-OROIDIN AND ^{15}N-KERAMADINE ANALOG FOR BIOSYNTHESIS/ METABIOSYNTHETIC STUDIES*

4.1 Introduction

The polycyclic pyrrole-2-aminoimidazole alkaloid (P-2-AI) family has received much attention from the synthetic organic community[1a,1b,38,1c] because of their challenging molecular structure, dense functionality and potential biological activity. All are believed to have been derived from a simple common sponge metabolites; most likely oroidin (**1.1**) and its analogs hymenidin (**1.2**) and clathrodin (**1.3**), or a related monomeric linear structure keramadine (**2.22**) (Scheme 4.1)..[22,17] Representative of the members of this family are the dimeric P-2-AIs sceptrin (**4.1**),[39] ageliferin (**1.12**),[40] massadine (**1.13**),[41] palau'amine (**1.11**)[42] and axinellamines A and B (**1.10a-b**),[43] and higher-order tetrameric P-2-AIs.[44] In addition, compact monomeric polycyclic P-2-AIs, such as agelastatins A-F (**2.1-2.6**),[10-12] and dibromophakellin[45] appear to be derived from oxidative intramolecular cyclizations of keramadine (**2.22**) and oroidin (**1.1**), respectively. P-2-AIs are of contemporary interest due to their potent biological activity

---

* Part of this chapter is reprinted with permission from ["Synthesis of 7-^{15}N-Oroidin and Evaluation of Utility for Biosynthetic Studies of Pyrrole-Imidazole Alkaloids by Microscale ^{1}H-^{15}N HSQC and FTMS" by Wang, Y. G.; Morinaka, B. I.; Reyes, J. C. P.; Wolff, J. H.; Romo, D.; Molinski, T F. *J. Nat. Prod.* **2010**, *73*, 428-434.] Copyright [2010] American Chemical Society (ACS).

and intriguing biosyntheses. For example, (–)-agelastatin A (**2.1**), an antitumor P-2-AI is 1.5-16 times more active than *cis*platin against a range of tumor cell lines[6,13], and potently inhibits osteopontin, an adhesion glycoprotein transcriptionally regulated by the Wnt β-catenin pathway and implicated in tumor progression, dissemination, and metastases.[15]

Scheme 4.1

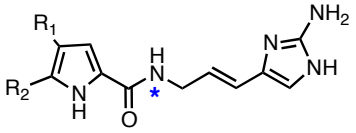

1.1: Oroidin $R_1 = R_2 = Br$
1.2: Hymenidin $R_1 = Br$, $R_2 = H$
1.3: Clathrodin $R_1 = R_2 = H$

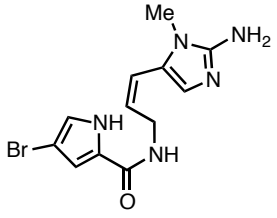

2.22: Keramadine

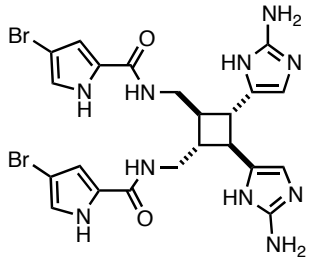

4.1: Sceptrin

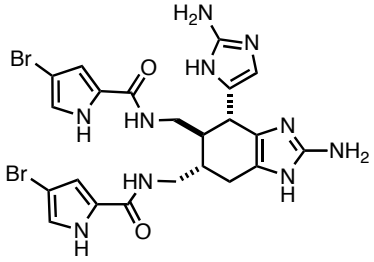

1.12: Ageliferin

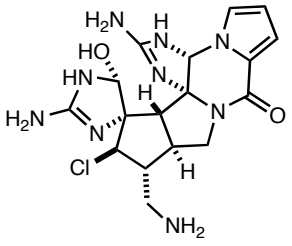

1.11: Palau'amine

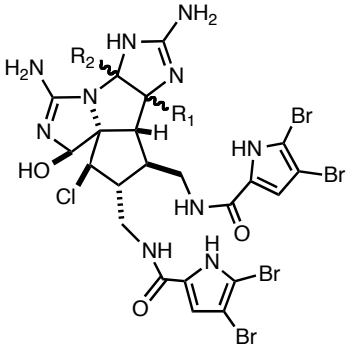

Axinellamines
1.10a: A R_1 = β-OH, R_2 = β-H
1.10b: B R_1 = α-OH, R_2 = α-H

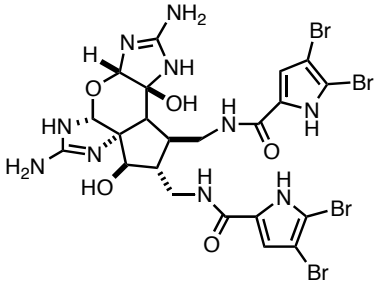

1.13: Massadine

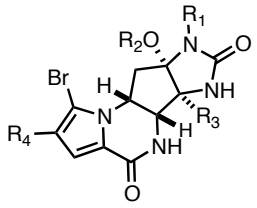

Agelastatins A-E
2.1 R_1 = Me; R_2, R_3, R_4 = H
2.2 R_1 = Me; R_2, R_3 = H; R_4 = Br
2.3 R_1 = Me; R_2, R_4 = H; R_3 = OH
2.4 R_1, R_2, R_3, R_4 = H
2.5 R_1, R_2 = Me; R_3, R_4 = H
2.6 R_1, R_2, R_3 = H; R_4 = Br

The widely accepted hypothesis for biosynthesis of dimeric and tetrameric P-2-AIs, involves dimerization of oroidin (**1.1**) followed by consecutive oxidative transformations leading to more densely functionalized, polycyclic alkaloids. In 1982, Büchi reported a 'biomimetic' synthesis of the simple P-2-AI, racemic dibromophakellin, by oxidative cyclization of 9,10-dihydrooroidin.[45a] The structure of sceptrin (**4.1**) is highly suggestive of a formal [2+2] cycloaddition of two molecules of hymenidin (**1.2**) to **4.1**; however, despite many attempts, Faulkner, Clardy and co-workers were unable to achieve photodimerization of **1.2** to **4.1**[39a], suggesting that an alternative mechanism may be responsible for the biosynthesis. Recent speculation on the order of biosynthesis of **4.1** and **1.12** revolves around ionic mechanisms of ring-expansion, supported by the demonstrated conversion of **4.1** to **1.12** under thermal conditions,[46] or a ring-contraction pathway from an ageliferin-type dimer generated by a Diels Alder type cycloaddition of two molecules of hymenidin (**1.2**).[17] For example, one speculative hypothesis invokes a cycloaddition in the biosynthesis of palau'amine[42b] and axinellamine, followed by a stepwise electrophilic chlorination and ring contraction. However, none of these hypotheses have been tested experimentally in live sponges.

This chapter describes the syntheses of ^{15}N-oroidin (**1.1b)** and an ^{15}N-keramadine analog **2.31a** along with optimization of conditions for detection of ^{15}N-incorporation by microscale FTMS and ^{1}H-^{15}N HSQC using a 'mock' pulse-labeling experiment with **1.1b** and natural oroidin (**1.1**). The limits of detection of these methods are estimated and its suitability for use in field incorporation for biosynthetic studies of complex P-2-AIs with

living sponges is determined. This can be useful to answer biosynthetic questions of the biosynthesis of P-2-AIs by sponges in the genera *Agelas*, *Stylissa* and *Ptilocaulis*.

4.2 Synthesis of ^{15}N-Oroidin

Our retrosynthetic analysis (Scheme 4.2) of ^{15}N-oroidin starts with cleavage of the amide bond to yield the known 4,5-dibromo-2-trichloroacetylpyrrole **4.2**,[20b,c] readily prepared by bromination of commercially available 2-trichloroacetylpyrrole, and 2-azidoimidazole allylic amine **4.3**, which could be accessed ultimately from the natural synthon urocanic acid **4.6**. The amino group at the 2-position of the imidazole ring will be introduced via a lithiation/azidation sequence, while the ^{15}N label will be introduced by Gabriel synthesis employing the potassium salt of commercially available ^{15}N-phthalimide **4.4**.

Scheme 4.2

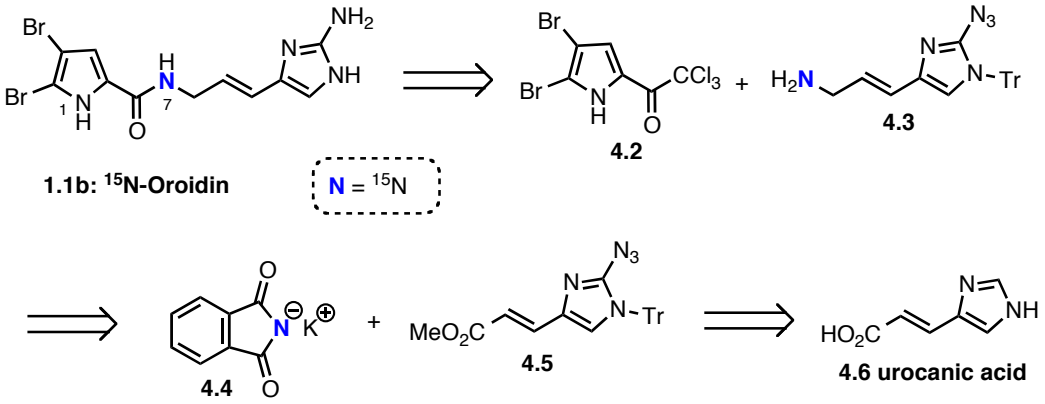

The synthesis commenced with a Fisher esterification of urocanic acid with anhydrous methanolic HCl and subsequent protection gave the known *N*-trityl imidazole derivative **4.7** (Scheme 4.3). Reduction of ester **4.7** with DIBAL-H afforded the corresponding alcohol in excellent yield. Initial attempts to execute a direct azidation of alcohol **11** at the 2-imidazole position with the unprotected alcohol using known procedures gave none of the desired azido product. Instead, the product obtained was tentatively assigned the structure of a triazene-imidazole derivative based on ^{1}H NMR and mass spectrometric analysis. When the TBS protected alcohol **4.8** was subjected to the previously employed conditions for azido-transfer, the corresponding azide was obtained in excellent yield. Deprotection with TBAF afforded alcohol **4.9,** which was then subjected to mesylation (MsCl, Et_3N). Without purification, the mesylate was treated with the potassium salt of ^{15}N-phthalimide (>98% atom ^{15}N) to provide the ^{15}N-labeled pthalimide **4.10**. Cleavage of phthalimide **4.10** with NH_2NH_2 (hydrazine) furnished the requisite ^{15}N-allylic amine which was acylated with 4,5-dibromo-2-trichloroacetylpyrrole (**4.2**) to provide ^{15}N-pyrrolecarboxamide **4.11** in good overall yield. Removal of the trityl group from **4.11** with anhydrous methanolic HCl, generated in situ from acetyl chloride and MeOH, afforded the corresponding 2-azido imidazole that was hydrogenated in the presence of Lindlar's catalyst to provide 7-^{15}N-oroidin (**1.1b**, >98% atom ^{15}N).

The ^{1}H, ^{13}C and ^{15}N NMR spectra and mass spectra were fully consistent with the structure and location of the ^{15}N label as depicted. The FTMS of natural oroidin (**1.1**), Figure 4.1) shows the expected 1:2:1 pattern for the pseudomolecular ion $[M+H]^+$

associated with the ^{79}Br and ^{81}Br isotopomers (*m/z* 387.93990, Δmmu = –0.41 mmu). The FTMS spectrum of 7-^{15}N-oroidin (**1.1b**) (Figure 4.1b) shows the same ion pattern, only the distribution is increased by 1 amu (*m/z* 388.93719, Δmmu = –0.16). Less than 2% of the ^{14}N isotopomer was detected which is consistent with the reported purity of the ^{15}N pthalimide (>98% atom ^{15}N) employed in the synthesis.

Scheme 4.3

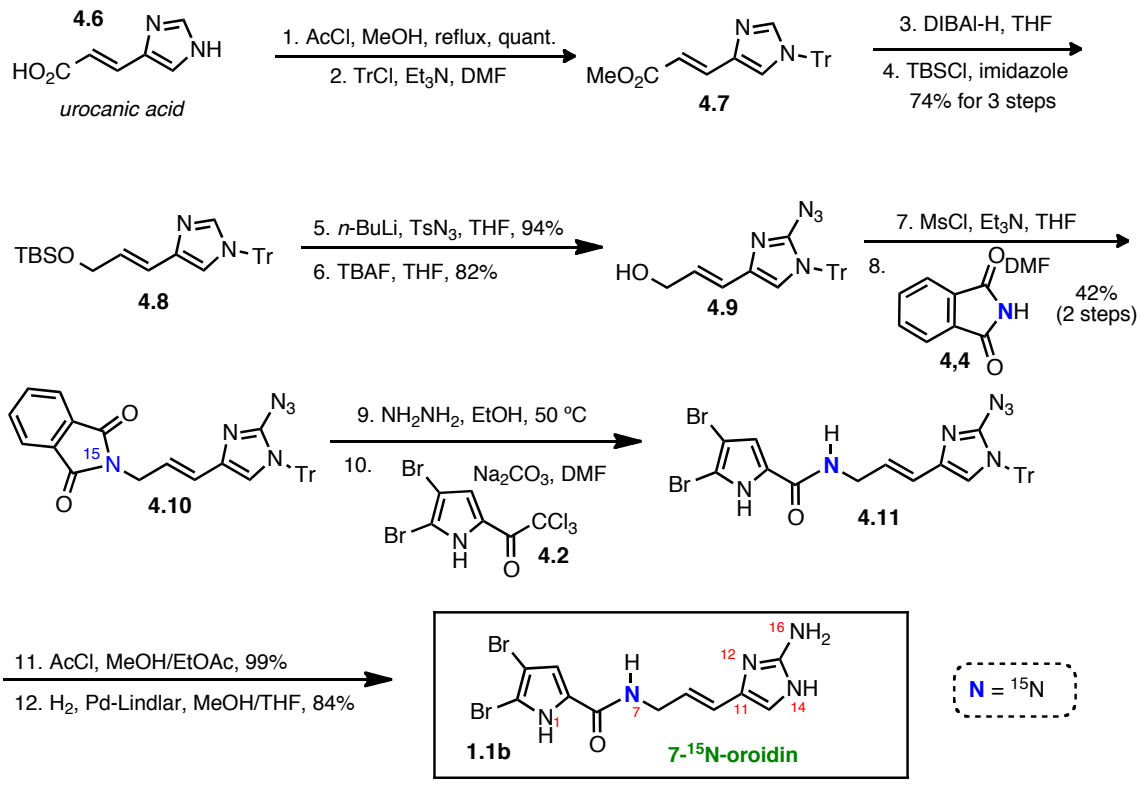

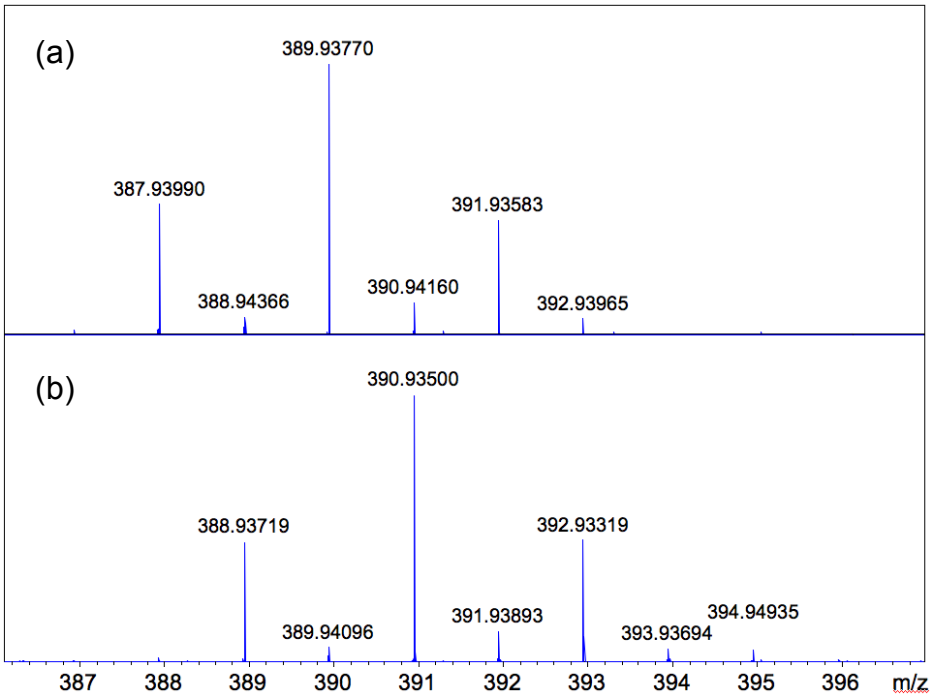

Figure 4.1 MALDI FTMS (7T) expansions of the pseudomolecular ion $[M+H]^+$ of oroidin for (a) natural **1.1** ($C_{11}H_{12}Br_2{}^{14}N_5O$) and (b) 7-^{15}N-oroidin (**1.1b**), $C_{11}H_{12}Br_2{}^{14}N_4{}^{15}NO$, >98% atom ^{15}N. Mass accuracy = 1ppm.

4.3 Synthesis of ^{15}N-Keramadine Analog

Our retrosynthetic analysis of ^{15}N-keramadine analog **2.31a** starts with a Lindlar reduction to introduce the Z-configured olefin with concomitant reduction of the azide group reveling the 2-aminoimidazole moiety (Scheme 4.4). Cleavage of the amide bond then reveals two fragments 5-bromo-2-thrichloroacetylpyrrole **4.2** and propargylic amine derived from **4.13**. The ^{15}N label will be introduced via a Gabriel synthesis employing the potassium salt of commercially available ^{15}N-phthalimide **4.4** and propargyl bromide

4.14. The alkyne moiety will then be coupled with the imidazole **4.15** through a Sonogashira cross coupling reaction.

Scheme 4.4

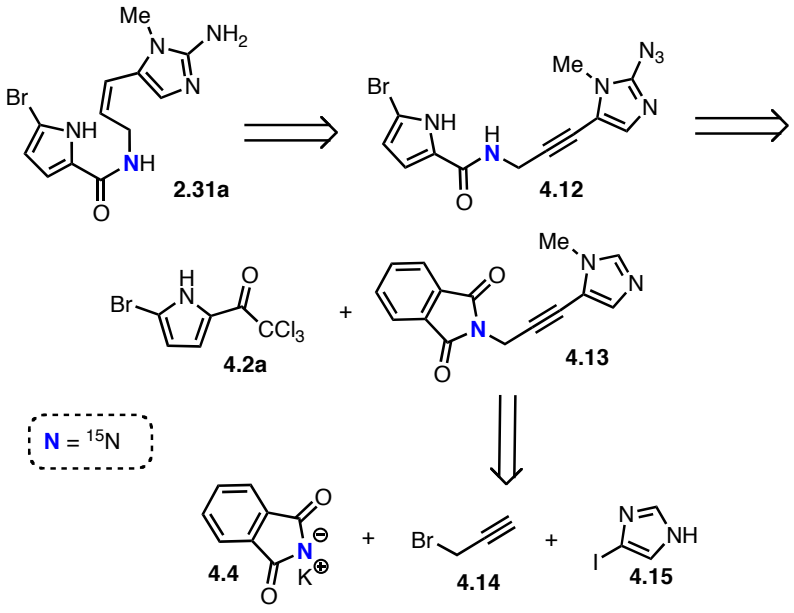

Protection of the nitrogen in **4.15**, distal to the iodine, yields an appropriately protected N-benzenesulfonamide **4.16** (Scheme 4.5). This is then coupled to the substitution product **4.17** of propargyl bromide **4.14** and ^{15}N-phthalimide potassium salt **4.4** through a Sonogashira cross coupling reaction yielding **4.18**. The N-Me is then introduced to the imidazole ring by formation of an N-Me imidazolium salt formed *in situ* by reaction with BF_4OMe_3 (methyl Meerwein salt). In the same pot, addition of methanol leads to the removal of the benzenesulfonyl group through methanolysis

providing **4.13**. The final guanidine nitrogen will then be introduced through a lithiation-azidation sequence followed by phthalimide cleavage to reveal propargyl amine **4.20** that will be coupled to 5-bromo-2trichloroacetylpyrrole **4.2a** to yield **4.12**. A final Lindlar reduction will then deliver the desired ^{15}N-keramadine analog **2.31a** with the Z-configured olefin and the 2-aminoimidazole moiety in place.

Scheme 4.5

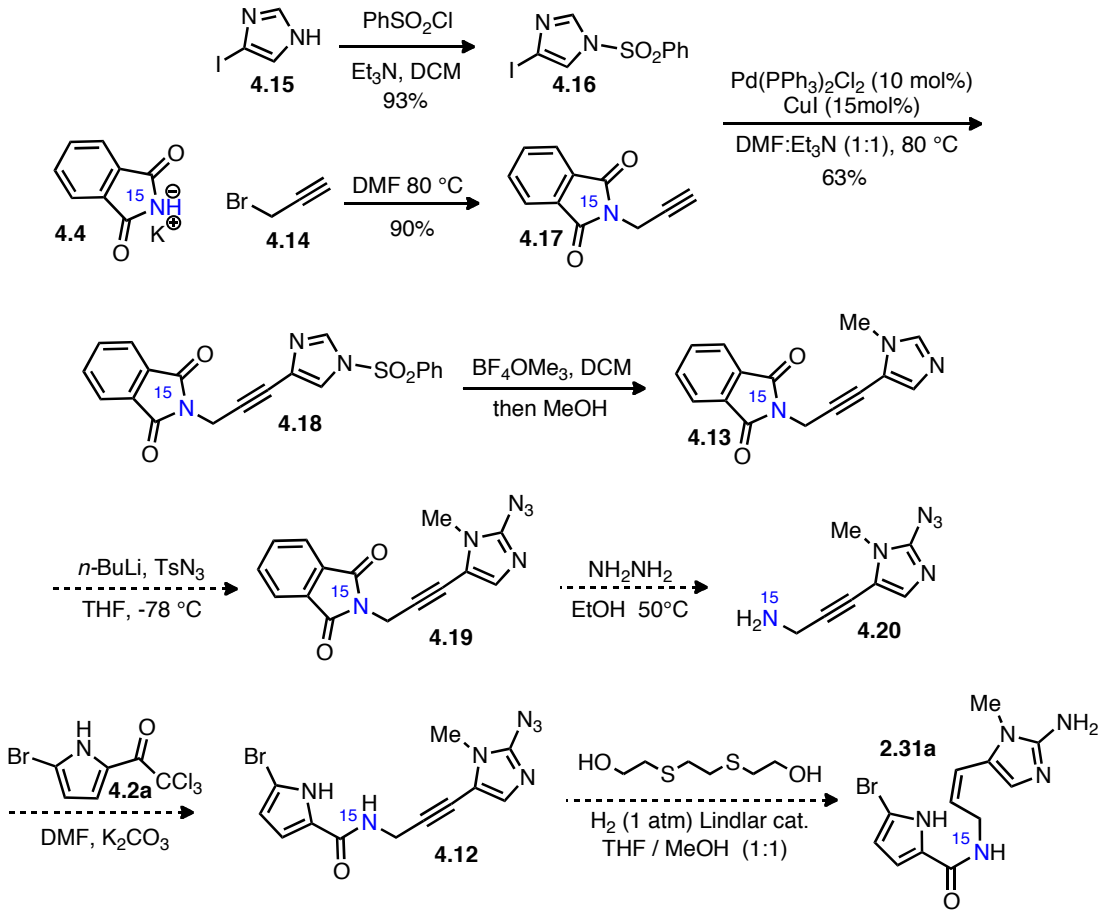

Our interest in the synthesis of ^{15}N-keramadine analog **2.31a** stems from our biosynthetic proposal that it is the ultimate precursor of the agelastatin subfamily of P-2-AI alkaloids. The ^{15}N label will allow us to follow its conversion not only to agelastatatins but quite possibly to other P-2-AIs, isolated or otherwise. The next section details our planned approach on how to ascertain ^{15}N incorporation via mass spectrometry and NMR spectroscopy.

4.4 Evaluation of the Utility of ^{15}N-Oroidin for Biosynthetic Studies by HSQC and FTMS

Two general methods are available for measuring incorporation of the stable isotope ^{15}N into natural products by pulse labeling – mass spectrometry and NMR spectroscopy. In both techniques, the level of isotopic enrichment from *de novo* biosynthesis of derived P-2-AIs must exceed the background ^{15}N present in P-2-AIs already present in the sponge *and*, for MS in particular, any ^{15}N background for other nitrogen atoms in the molecule. As a stable isotope label, ^{15}N is easier to detect and preferable to ^{13}C because the natural abundance of the heavier to lighter isotope for N (~0.3%) is only about 1/4 of C (~1.1%). Ideally for ^{15}N incorporation experiments, mass spectrometry should differentiate the contributions to the M+1 peak from ^{15}N and ^{13}C,[47] a task best-suited to Fourier transform MS (FTMS) with exceptionally high resolution (7T field, R = 240,000) that should be capable of resolving the nominal M+1 peak of the pseudomolecular ion into individual isotopomer contributions from species containing one ^{13}C or one ^{15}N. Baseline separation of the isotopomers was readily achieved by MALDI FTMS (Figure 4.2), allowing quantitation of the ^{15}N isotopomer peak. For

oroidin (**1.1**), the critical *difference* in the mass of ^{12}C-^{15}N containing ions versus the heavier ^{13}C-^{14}N isotopomer amounts to only 0.00632 amu, a baseline separation not readily achievable by high-resolution mass spectrometers with conventional analyzers (e.g. double sector, TOF).

Quantitation of the ^{15}N isotopomer can be made from integration of ion current intensities of the [M+1] components, ^{15}N-^{12}C and ^{14}N-^{13}C (Figure 4.2). Assuming the ^{13}C abundance in *natural* and *synthetic* ^{15}N-labeled oroidin are identical, the ^{13}C peak intensity may be used as the denominator in the ratio h (Equation 4.1), where h_N and h_C are the respective measured peak heights of the ^{15}N-^{12}C and ^{14}N-^{13}C component ions.

$$h = h_N/h_C \qquad \text{(Eqn 4.1)}$$

Consequently, h can be used to reflect small changes in the ^{15}N content.[48] From the ion current peak heights measured in the FTMS spectrum of natural oroidin (**1.1**), h was found to be 0.1487±0.0175. A prepared 'mock' labeled sample ('Mix1'), consisting of a 1.5:0.0075 mixture of oroidin (**1.1**): 7-^{15}N-oroidin (**1.1b**), showed an enhanced h of 0.1881±0.0135 corresponding to a ~4% ^{15}N enrichment. A second sample ('Mix2', 1:0.100, **1.1**:**1.1b**) gave h = 1.024±0.0369, corresponding to ~88% ^{15}N enrichment. We estimate that the limit of detection (LOD, ±3 σ) for ^{15}N incorporation corresponds to an increase in intensity, Δh ~5.2%. Given that natural abundance of ^{15}N is approximately 0.3% atom, this would amount to observation of as little as 10.4 parts per thousand of ^{15}N incorporation per N atom of oroidin (**1.1**) by *de novo* synthesis. Detection of this

small amount will, of course, be made more difficult by the presence of unlabeled oroidin (**1.1**) within the sponge.

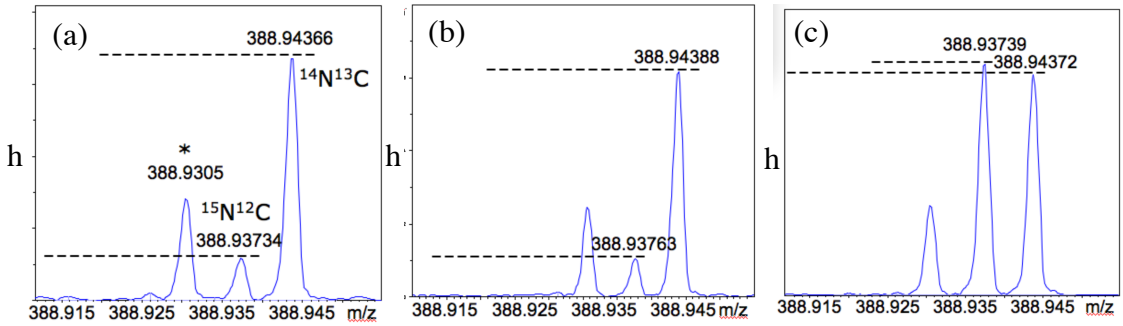

Figure 4.2 MALDI FTMS (7T) expansions of *m/z* and peak height, *h*, for the 'M+1' peak of the pseudomolecular ions of oroidin ($C_{11}H_{11}Br_2N_5O$). Mass accuracy = 1 ppm (*R* = 240,000). (a) natural **1.1**. (b) **1.1** + **1.1b** (0.04 mol equiv). (c) **1.1** + **1.1b** (0.10 mol equiv). Peak assignments of $[M+H]^+$ in (c): *m/z* 388.94372, $^{12}C_{10}{}^{13}CH_{12}Br_2N_5O^+$; *m/z* 388.93739; $^{12}C_{11}H_{12}Br_2N_4{}^{15}NO^+$. The unrelated peak at *m/z* 388.9305 (indicated with an '*') is tentatively assigned to some loss of H from the dominant $^{79}Br/^{81}Br$ isotopomer, $C_{11}H_{10}{}^{79}Br^{81}BrN_5O^+$ ($[M]^+$, Δmmu = –0.5)

The disadvantage of analysis of ^{15}N-content in oroidin and other P-2-AIs by MS is the presence of at least five N atoms, each contributing to the intensity of ^{15}N-^{12}C component of the M+1 peak. Consequently, it may be expected the actual LOD by FTMS will be higher.

Direct detection of ^{15}N incorporation by ^{15}N NMR spectroscopy is impractical due to low natural abundance and severely compromised sensitivity of this *I*=½ nucleus which possesses a low-magnitude, negative magnetogyric ratio (γ = – 4.31726570 MHz

T^{-1}).[49] Conveniently, ^{1}H-^{15}N HSQC circumvents most of these problems by indirect detection of bonded ^{1}H-^{15}N couplets through magnetization transfer from ^{15}N and observation of the more sensitive ^{1}H nucleus. Because four of the five N atoms in oroidin (**1.1**) are bonded to H, 2D ^{1}H-^{15}N HSQC can provide bond-specific information about fractional enrichment at an individual N atom in oroidin and, by extension, more complex P-2-AIs by measurement of the ^{1}H-^{15}N couplet intensity. The intensity of cross peaks in the 2D ^{1}H-^{15}N HSQC spectrum of oroidin will vary for each N-H couplet depending on efficiency of magnetization transfer that largely depends upon the magnitude of the $^{1}J_{NH}$ scalar coupling constant. Nevertheless, the intensity of each crosspeak will scale linearly as a function of ^{15}N abundance.

When put to practice, it is easier and more meaningful to measure ^{15}N enrichment from the 1D projections of 2D HSQC spectra or – best of all – from the 1D version of the HSQC experiment where evolution of the F1 dimension (^{15}N chemical shift) is eliminated and acquisition time is devoted to improving S/N in the detected dimension F2 (^{1}H chemical shift). We define here ΔI as the *difference* of cross peak intensity, I, of the ^{15}N-labeled N-H couplet of interest (in this case, the NH(C=O) signal of **1.1b**) in a sample of oroidin (**1.1**), spiked with a known amount of 7-^{15}N-oroidin (**1.1b**), compared to the intensity, I_0, of oroidin recorded under the same conditions (Equation 4.2). The values of I are normalized to the intensity of the pyrrole N-H couplet of oroidin (I_p = 1.00) in each experiment.

$$\Delta I = (I - I_0)/I_0 \qquad \text{(Eqn. 4.2)}$$

We elected to use the pyrrole N-H couplet of oroidin (**1.1**) (δ_H = 13.14, s; δ_N169.1) as the control because of its ready assignment from ^{1}H-^{15}N HMBC, lack of tautomerism, and likely origination in a different biosynthetic pathway unaffected by biosynthetic incorporation of ^{15}N into the amino-imidazole fragment. The exquisite mass-sensitivity of the triple-tuned [^{13}C,^{15}N]^{1}H 1.7 mm 600 MHz microcryoprobe was used to full advantage in this work for characterization of the ^{15}N content of oroidin samples. This low-volume, high-mass sensitivity cryoprobe allowed measurements of samples of only ~1.5 mg in 30 μL (acquisition times, ~4 h). Figure 4.3 shows the 2D ^{1}H-^{15}N HSQC experiment for oroidin (**1.1**) with respective N assignments (also, see the Experimental for accurate δ's). A single dominant cross peak was observed in the 2D ^{1}H-^{15}N HSQC of 7-^{15}N-oroidin (**1.1b**) (not shown), confirming the location of the ^{15}N label at the amide group N-H (δ_H = 8.75, t, $^3J_{HH}$ = 6.0 Hz, H7; δ_N = 107.8, N7), as expected.

Figure 4.4a-c shows 1D ^{1}H-^{15}N HSQC experiments of oroidin (**1.1**) spiked with different amounts of 7-^{15}N-oroidin (**1.1b**) and the integrals of each N-H couplet, normalized to the N1-pyrrole couplet are reported in Table 4.1 (note that the integrals are not exactly proportional to the stoichiometric ratios of attached H's). As predicted, the value of ΔI increases linearly with the amount of added 7-^{15}N-oroidin (**1.1b**) and the slope of this 'standards addition' linear regression (Figure 4.5) gives the proportionality constant c = 0.34 for ΔI per μg of added **1.1b**.

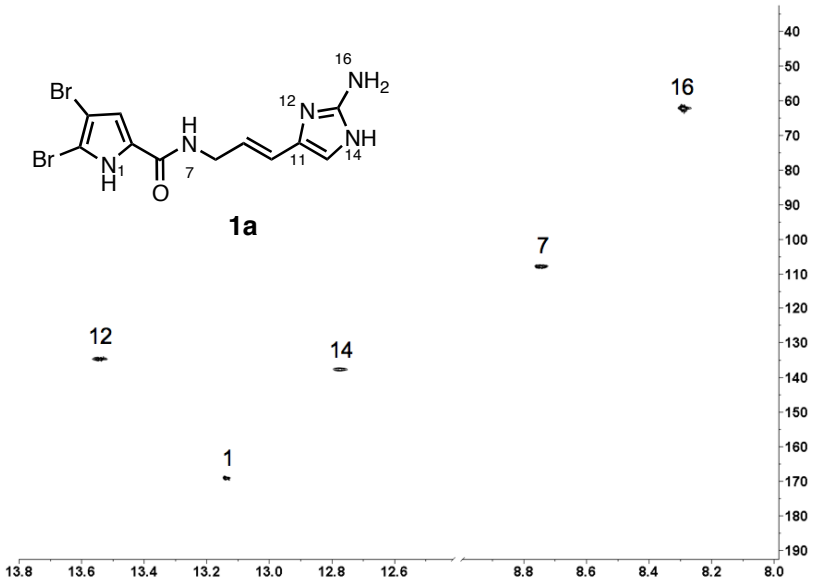

Figure 4.3 2D ^{1}H-^{15}N HSQC (600 MHz, 1:1 DMSO-d_6/benzene-d_6) of natural oroidin (**1.1**, depicted tautomer is arbitrary). N locants are labeled following the numbering scheme of Assman and Köck[50]. ns = 16, T2, T1 = 2K x 256; F2, F1 = 2K x 1K; d1 =1.5s

Table 4.1 Integrals from ^{1}H-^{15}N 1D HSQC of natural oroidin (**1.1**, 1.5 mg/ 30 μL) and **1.1** 'spiked ' with **1.1b**. Integrals of H-N couplets corresponding to N-12, N-14 and N-16 vary due to tautomerism.

Aliquot µg **1.1b**	N(12)	N(1)	N(14)	N(7)	N(16)
0.0	1.26	1.00	1.05	2.17	2.14
2.5	1.03	1.00	0.48	2.57	2.23
5.0	1.65	1.00	1.18	3.83	2.55
10.0	0.63	1.00	0.00	5.74	3.02

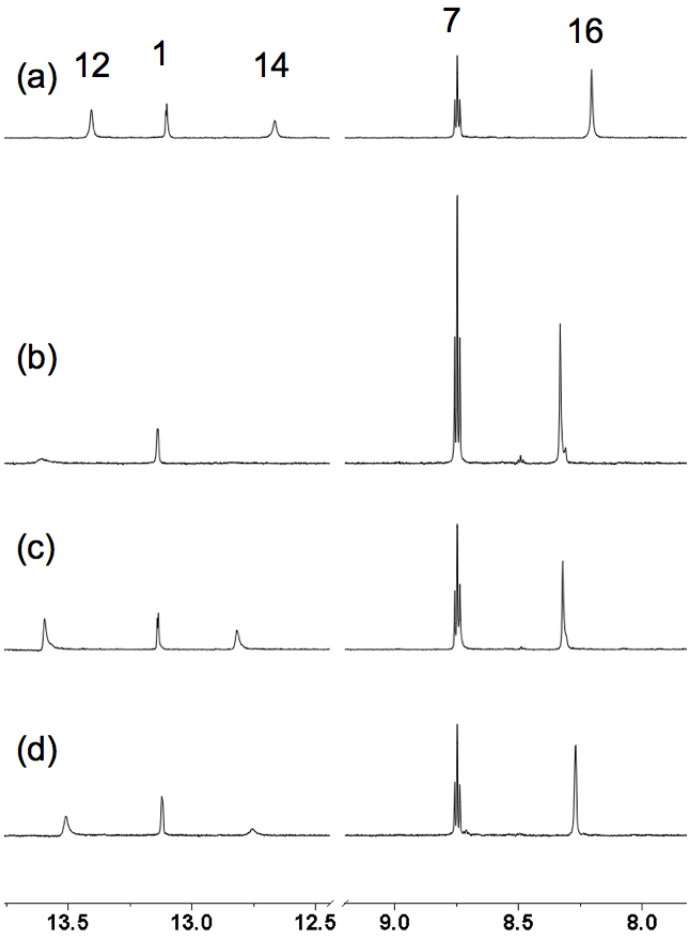

Figure 4.4 1D ^{1}H-^{15}N HSQC experiments (^{1}H δ, 1.7 mm microcryoprobe, 600 MHz) of **1.1** with N-H assignments. Labels indicate N atom assignments made from a separate ^{1}H-^{15}N HMBC experiment (not shown). (a) 1500 μg of **1.1**, no added [^{15}N]-**1.1b**. (b) 1500 μg **1.1** + 10 μg **1.1b**. (c) 1500 μg **1.1** + 5.0 μg **1.1b**. (d) 1500 μg **1.1** + 2.5 μg. Relaxation delay, d1 = 1.50 s, optimized for $^{1}J_{N\text{-}H}$ = 90 Hz; ^{1}H π/2 pulse = 12 μS, ^{15}N π/2 pulse = 34 μS; NA = 6K; dummy scans = 16; NI = 1; T2 = F2= 8K points (no zero fill).

Constant *c* will be useful for estimation of absolute %N incorporations in P-2-AIs labeled during in-field incorporation experiments of secondary metabolism within living sponges. Although it is advisable to measure the relative HSQC intensities of pyrrole N-H couplet and NH(C=O) couplets of the specific P-2-AI in question, it may be reasonably expected that the magnetic properties of these couplets in more complex P-2-AIs are comparable to those of oroidn (**1.1**). We estimate the limit of detection (LOD) for ^{15}N enrichment by HSQC in **1.1** to be approximately 1.5 parts per thousand (based on ±3 SD). This is *more sensitive* than the LOD of ^{15}N-enrichment by FTMS, the reason being HSQC detection of couplet ^{15}N-^{1}H at each N atom and eliminates background 'dilution' by other ^{15}N's, however the precision is inferior to FTMS replicate measurements.

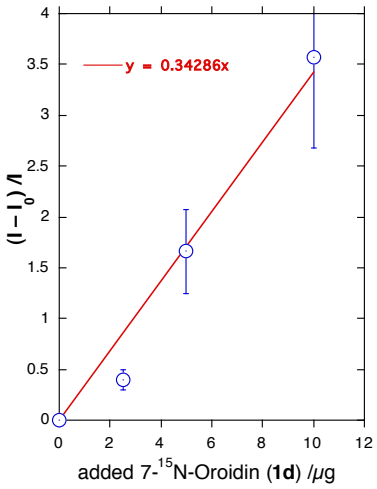

Figure 4.5 Linear regression of ^{1}H-^{15}N HSQC NH(C=O) cross-peak integral ratio, $(I–I_0)/I_0$, of 'mock' pulse labeling experiments with natural abundance **1.1** (1500 μg, I_0) spiked with measured aliquots of **1.1b** (μg, 'x-scale'). Observed I' values for the NH-C=O ^{1}H-^{15}N couplet are normalized to the intensity of the pyrrole N-H cross peak, $I_0 = 1.00$ (I or $I_0 = I'/I_p$). Error bars are ± SD.

4.5 Biosynthetic Feeding Experiments and 'Metabiosynthetic' Studies

Two phases of P-2-AI biosynthesis can be considered: the assembly of oroidin (**1.1**), and downstream conversion of the latter to monomeric and more complex dimeric P-2-AIs. Despite much speculation, on the biosynthesis of P-2-AIs, only two experimental studies in living marine sponges have appeared (Scheme 4.6). Kerr and co-workers found that cultured cells of *Teichaxinella morchella* (*Styllisa caribica*) produced ^{14}C-labeled stevensine (**4.24**)[51] – the simplest monomeric P-2-AI related to oroidin (**---**)– upon exposure to U-^{14}C-labeled histidine or C5-^{14}C-ornithine, but not U-^{14}C-arginine (Scheme 4.6).[52] Incorporation of radiolabeled histidine, ornithine, and proline were reported to be 0.026%, 0.024%, and 0.022%, respectively. Paradoxically, U-^{14}C-histidine was incorporated into **4.24**, but this would require an additional C_1 unit from an unidentified source to complete the imidazole ring and a non-intuitive substitution of NH_2 at C-2 of the imidazole ring. No simple mechanism for this scenario presents itself. In 2011, Al Morabit and co-workers have performed similar studies and corroborated that proline is indeed the precursor of the acylpyrrole group found in P-2-AIs. In contrast with Kerr and co-workers' results, histidine incorporation was not observed. Their experiments have strongly suggested lysine as the precursor of the 2-aminoimidazole moiety of oroidin. Lysine incorporation was measured as 0.031% while proline incorporation was slightly lower at 0.025%. Noticeably lower rates of incorporation was observed for radiolabelled arginine and ornithine, which are known precursors to proline itself.

Scheme 4.7

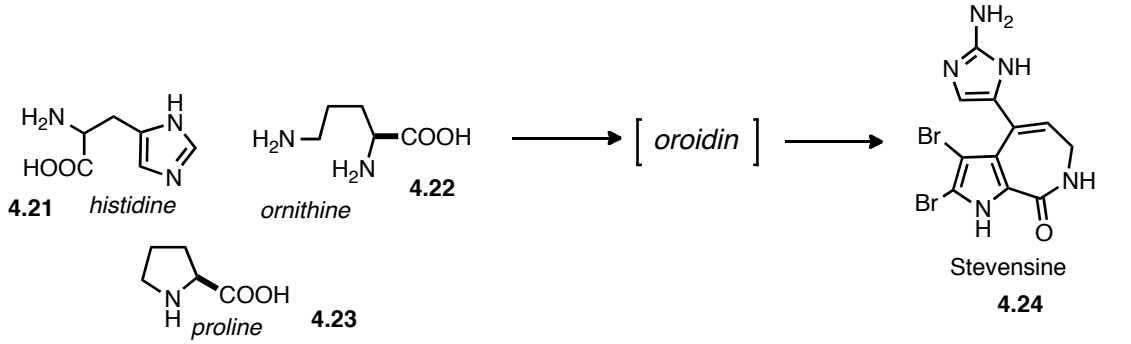

Kerr, Pomponi, and co-workers (1999)

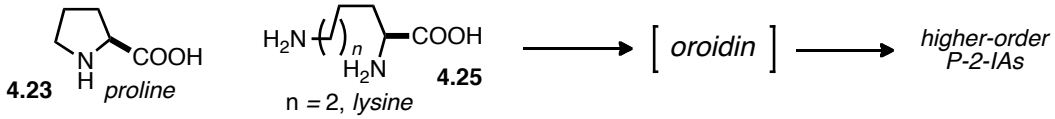

Al Mourabit, Thomas, and co-workers (2011)

Uncertainties in the origin of oroidin (**1.1**) are, in theory, addressable by suitable ^{15}N labeled amino acid incorporation experiments. Unfortunately, low levels of radioactivity and percent incorporation, detection of ^{15}N incorporation into P-2-AIs using ^{15}N-labeled amino acids may be precluded by the limits of detection. For the above reasons, late-stage precursors (*e.g.* 7-^{15}N-oroidin (**1.1b**), sceptrin (**4.1**) and ageliferin (**1.12**) are attractive for mapping the origin of downstream polycyclic P-2-AIs since these molecules should be committed intermediates. Measurement of their rates of incorporation into P-2-AIs in living sponges of the genera *Agelas*, *Stylissa* and *Ptilocaulis* may also provide critical data on the rates of marine alkaloid secondary metabolism for which there is no current information.

The use of precursors labeled with the spin I=1/2 stable isotope ^{15}N is particularly attractive as it provides bond-specific information regarding the flow of intermediates in biosynthesis of complex P-2-AIs. Judicious design and placement of the label in ^{15}N-labeled oroidin is important. Because the primary NH_2 group of the aminoimidazole group is potentially metabolically labile through deamination reactions, we chose to label the amide bond in ^{15}N-oroidin. Quantitation of ^{15}N incorporation into proteins has been made from integration of cross peak volumes of 2D HSQC experiments;[53] however, in the present work with natural products we show that it is far simpler to integrate the corresponding 1D HSQC spectra.

Finally, although the ratio of sceptrin to ageliferin found in one sample of *Agelas conifera* is ~10:1, the ratios of mono-brominated and dibrominated analogs of sceptrin and ageliferin vary slightly from approximately 1:1 ~ 3:4; however, these data do not clearly indicate an ordering for a bromination-dimerization sequence in the biosynthesis of dimeric P-2-AIs. Propagation of 7-^{15}N-oroidin (**1.1b**) along the biosynthetic pathway to complex P-2-AIs will carry the ^{15}N label through symmetrical and non-symmetrical intermediates and detection of residual ^{15}N in strategically chosen N-H bonds in the molecule should reveal timing, ordering and molecularity of the C-C bond-forming events and the extent of coupling of *de novo* enzymatic reactions. HPLC analysis of P-2-AI-containing extracts from *A. conifera* (Agelasidae), collected in the Florida Keys show the presence of sceptrin (**2**) and ageliferin (**3**) along with hymenidin (**1b**), but some specimens of *Agelas sceptrum* collected by us contained sceptrin (**2**) but were devoid of the expected precursors **1.1-1.3**. If **1.1-1.3** are precursors to other P-2-AIs, as is highly

probable, this implies that the *rates* of conversion of **1.1-1.3** to higher-order P-2-AIs are highly dependent upon the sponge species, their biosynthetic capacities, and possibly the habitats they occupy. 7-^{15}N-Oroidin and ^{15}N-keramadine find great value in systematic studies of the time-dependent biosynthesis of P-2-AI natural products by pulse labeling in live sponges to answer some of these questions.

Scheme 4.7

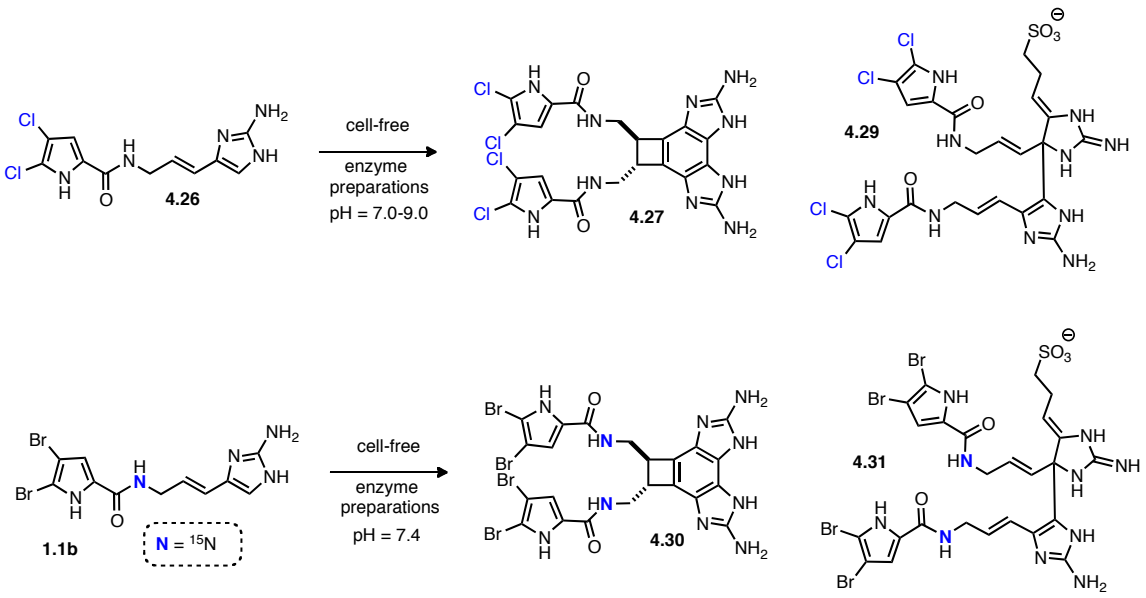

Our group, in collaboration with the Molinski group have recently described an alternative method of probing the biosynthesis of higher order P-2-AIs (Scheme 4.7).[54] Named "metabiosynthesis", this experiment employs cell-free enzyme extracts from marine sponges *Stylissa caribica, Agelas conifera, and Agelas sceptrum*. Freshly collected live sponges were converted to cell-free preparations (CFP). The CFPs, which

contain active enzymes as an aqueous-organic suspension (0.2 mg protein/mL in 1:9 CH_3CN:0.1M sodium phosphate buffer), converts either dichloroclathrodin **4.26** and ^{15}N-oroidin **1.1b** to higher order dimeric P-2-AIs benzosceptrin C **4.30** and nagelamide H **4.29** (or their chlorinated derivatives, tetrachlorobenzosceptrin C **4.27** and tetrachloronagelamide H **4.29** for dichloroclathrodin incubation with CFPs).

Scheme 4.8

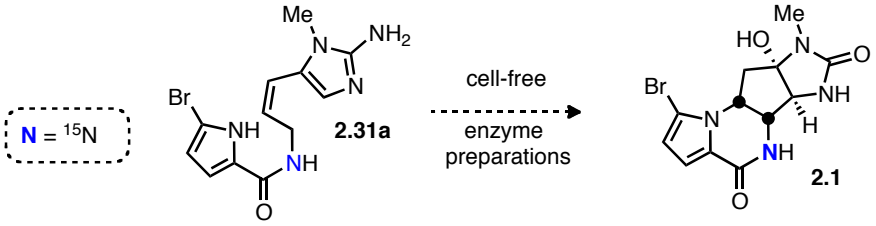

These two seminal publications from our group and the Molinski group show the utility of CFPs of active enzymes can be used to study the biosynthesis of complex P-2-AIs from oroidin and other proposed precursors. Our interest in ^{15}N-keramadine is to investigate its viability as the biosynthetic precursor to the tetracyclic core of agelastatins as we described in our revised biosynthetic proposal detailed in chapter 3.

CHAPTER V

CONCLUSIONS

The pyrrole 2-aminoimidazole (P-2-AI) family of nitrogen rich alkaloids is among the most challenging targets in the synthetic community. With well over one hundred and fifty members, new metabolites continue to be isolated from various marine sources revealing a myriad of biological activities. Approaches towards the synthesis of P-2-AIs have inspired chemists to develop synthetic strategies aimed at efficiency and rapid construction of chemical motifs. Premised on the isolation of keramadine and nagelamide J, a retrobiosynthesis of agelastatin A was devised. This ultimately led to a bioinspired approach to a concise synthesis of the natural product *via* two sequential, potentially biomimetic cyclizations. A carbinolamide precursor to an *N*-acyliminium mediated cyclization was designed. Crucial to the success of synthesizing this precursor was the use of an *N*-methoxy amide as a coupling partner to an imidazolone alkynyl acetal fragment. While the proposed *N*-acyliminium biscyclization cascade failed to deliver all the rings in the tetracyclic natural product, it efficiently formed the C-ring setting three contiguous centers in a highly diastereoselective fashion. This cyclization event was accompanied by an intense red color that we propose involves a $\pi \rightarrow \pi^*$ transition between the HOMO and LUMO of an *N*-acyliminium intermediate which is supported by TD-DFT calculations. Investigations of the diastereoselectivity of this transformation revealed the importance of a protecting group at the N3 of the imidazolone moiety. An enantioselective version of this transformation was developed

using a chiral BINOL-derived phosphoric acid. The final B-ring closure was uniquely successful and occurs on the surface of silica gel with uniform heating assistance of toluene. The reaction sequence leading from an oxidized keramadine analog through a nagelamide J–like intermediate to agelastatin A is a provocative proposal for the biosynthesis of the agelastatins. The described sequential assembly of the C and B rings provides evidence for the proposed reactivity of a linear alkenyl imidazolone pyrrole leading to the agelastatins and complements other approaches to agelastatins involving initial B ring followed by C ring formation.

Towards gaining a better understanding of the biosynthesis of monomeric and dimeric P-2-AIs, a concise synthesis of ^{15}N-oroidin was devised and a direct method for measurement of ^{15}N incorporation by pulse labeling and analysis by 1D ^{1}H-^{15}N HSQC NMR and FTMS was developed. With the use of ^{15}N labeled oroidin being validated through the use of active cell-free enzymes for metabiosynthetic studies, the utility of a ^{15}N-keramadine analog to be converted to agelastatin A and other P-2AIs should shed light on the exciting biomachinery of this family of alkalods.

REFERENCES

(1) (a) H. Hoffmann; T. Lindel, "Synthesis of the pyrrole-imidazole alkaloids", *Synthesis* **2003**, 1753-1783. (b) S. M. Weinreb, "Some recent advances in the synthesis of polycyclic imidazole-containing marine natural products", *Natural Product Reports* **2007**, *24*, 931-948. (c) A. Al-Mourabit; M. A. Zancanella; S. Tilvi; D. Romo, "Biosynthesis, asymmetric synthesis, and pharmacology, including cellular targets, of the pyrrole-2-aminoimidazole marine alkaloids", *Nat. Prod. Rep.* **2011**, *28*, 1229-1260.

(2) K. G. Poullennec; D. Romo, "Enantioselective total synthesis of (+)-dibromophakellstatin", *J. Am. Chem. Soc.* **2003**, *125*, 6344-6345.

(3) S. Wang; D. Romo, "Enantioselective synthesis of (+)-monobromophakellin and (+)-phakellin: a concise phakellin annulation strategy applicable to palau'amine", *Angew. Chem., Int. Ed.* **2008**, *47*, 1284-1286, S1284/1281-S1284/1216.

(4) (a) G. T. Anderson; C. E. Chase; Y.-h. Koh; D. Stien; S. M. Weinreb; M. Shang, "Studies on total synthesis of the cytotoxic marine alkaloid agelastatin A", *J. Org. Chem.* **1998**, *63*, 7594-7595. (b) D. Stien; G. T. Anderson; C. E. Chase; Y.-h. Koh; S. M. Weinreb, "Total synthesis of the antitumor marine sponge alkaloid agelastatin A", *J. Am. Chem. Soc.* **1999**, *121*, 9574-9579. (c) K. S. Feldman; J. C. Saunders; M. L. Wrobleski, "Alkynyliodonium salts in organic synthesis: development of a unified strategy for the syntheses of (-)-agelastatin A and (-)-agelastatin B", *J. Org. Chem.* **2002**, *67*, 7096-7109. (d) K. S. Feldman; J. C.

Saunders, "Alkynyliodonium salts in organic synthesis. Application to the total synthesis of (-)-agelastatin A and (-)-agelastatin B", *J. Am. Chem. Soc.* **2002**, *124*, 9060-9061. (e) E. Baron; P. O'Brien; T. D. Towers, "Synthesis and reactions of cyclopentadiene monoaziridine: a concise approach to the core of agelastatin A", *Tetrahedron Lett.* **2002**, *43*, 723-726. (f) K. J. Hale; M. M. Domostoj; D. A. Tocher; E. Irving; F. Scheinmann, "Enantiospecific formal total synthesis of the tumor and GSK-3β inhibiting alkaloid, (-)-agelastatin A", *Org. Lett.* **2003**, *5*, 2927-2930. (g) M. J. Porter; N. J. White; G. E. Howells; D. D. P. Laffan, "Unusual oxidation behavior of a propargylic alcohol", *Tetrahedron Lett.* **2004**, *45*, 6541-6543. (h) M. M. Domostoj; E. Irving; F. Scheinmann; K. J. Hale, "New total synthesis of the marine antitumor alkaloid (-)-agelastatin A", *Org. Lett.* **2004**, *6*, 2615-2618. (i) F. A. Davis; J. Deng, "Asymmetric total synthesis of (-)-agelastatin A using sulfinimine (N-sulfinyl imine) derived methodologies", *Org. Lett.* **2005**, *7*, 621-623. (j) B. M. Trost; G. Dong, "New class of nucleophiles for palladium-catalyzed asymmetric allylic alkylation. Total synthesis of agelastatin A", *J. Am. Chem. Soc.* **2006**, *128*, 6054-6055. (k) Y. Ichikawa; T. Yamaoka; K. Nakano; H. Kotsuki, "Synthesis of (-)-agelastatin A by [3.3] sigmatropic rearrangement of allyl cyanate", *Org. Lett.* **2007**, *9*, 2989-2992. (l) T. Yoshimitsu; T. Ino; T. Tanaka, "Total synthesis of (-)-agelastatin A", *Org. Lett.* **2008**, *10*, 5457-5460. (m) B. M. Trost; G. Dong, "A stereodivergent strategy to both product enantiomers from the same enantiomer of a stereoinducing catalyst: agelastatin A", *Chem. Eur. J.* **2009**, *15*, 6910-6919. (n) T. Yoshimitsu; T. Ino; N.

Futamura; T. Kamon; T. Tanaka, "Total synthesis of the β-catenin inhibitor, (-)-agelastatin A: a second-generation approach based on radical aminobromination", *Org. Lett.* **2009**, *11*, 3402-3405. (o) N. Hama; T. Matsuda; T. Sato; N. Chida, "Total synthesis of (-)-agelastatin A: the application of a sequential sigmatropic rearrangement", *Org. Lett.* **2009**, *11*, 2687-2690. (p) F. A. Davis; J. Zhang; Y. Zhang; H. Qiu, "Improved synthesis of (-)-agelastatin A", *Synth. Commun.* **2009**, *39*, 1914-1919. (q) D. P. Dickson; D. J. Wardrop, "Total synthesis of (±)-agelastatin A, a potent inhibitor of osteopontin-mediated neoplastic transformations", *Org. Lett.* **2009**, *11*, 1341-1344. (r) P. M. Wehn; B. J. Du, "A stereoselective synthesis of the bromopyrrole natural product (-)-agelastatin A", *Angew. Chem., Int. Ed.* **2009**, *48*, 3802-3805. (s) M. Movassaghi; D. S. Siegel; S. Han, "Total synthesis of all (-)-agelastatin alkaloids", *Chem. Sci.* **2010**, *1*, 561-566. (t) Y. Menjo; A. Hamajima; N. Sasaki; Y. Hamada, "Asymmetric aziridination of cyclic enones using chiral diamine catalysts and its application to the total synthesis of (-)-agelastatin A", *Org. Lett.* **2011**, *13*, 5744-5747.

(5) E. Fattorusso; O. Taglialatela-Scafati, "Two novel pyrrole-imidazole alkaloids from the Mediterranean sponge *Agelas oroides*", *Tetrahedron Lett.* **2000**, *41*, 9917-9922.

(6) M. D'Ambrosio; A. Guerriero; M. Ripamonti; C. Debitus; J. Waikedre; F. Pietra, "The active centers of agelastatin A, a strongly cytotoxic alkaloid of the Coral

sea axinellid sponge *Agelas dendromorpha*, as determined by comparative bioassays with semisynthetic derivatives", *Helv. Chim. Acta* **1996**, *79*, 727-735.

(7) (a) A. Padwa, "Application of cascade processes toward heterocyclic synthesis", *Pure Appl. Chem.* **2003**, *75*, 47-62. (b) B. E. Maryanoff; H.-C. Zhang; J. H. Cohen; I. J. Turchi; C. A. Maryanoff, "Cyclizations of *N*-acyliminium ions", *Chem. Rev. (Washington, DC, U. S.)* **2004**, *104*, 1431-1628. (c) S. N. Gaskell; L. J. Duffy; S. M. Allin, "Asymmetric *N*-acyliminium cyclization as an approach to heterocyclic natural product synthesis", *Nat. Prod. Commun.* **2008**, *3*, 1825-1838. (d) A. Yazici; S. G. Pyne, "Intermolecular addition reactions of *N*-acyliminium ions (Part I)", *Synthesis* **2009**, 339-368. (e) A. Yazici; S. G. Pyne, "Intermolecular addition reactions of *N*-acyliminium ions (Part II)", *Synthesis* **2009**, 513-541. (f) U. Martinez-Estibalez; A. Gomez-SanJuan; O. Garcia-Calvo; E. Aranzamendi; E. Lete; N. Sotomayor, "Strategies based on aryllithium and *N*-acyliminium ion cyclizations for the stereocontrolled synthesis of alkaloids and related systems", *Eur. J. Org. Chem.* **2011**, *2011*, 3610-3633.

(8) Y. Wang; L. Zhu; Y. Zhang; R. Hong, "Bioinspired and concise synthesis of (±)-stemoamide", *Angewandte Chemie International Edition* **2011**, *50*, 2787-2790.

(9) (a) D. J. Hart; N. Magomedov, "Synthesis of (-)-alantrypinone", *Tetrahedron Lett.* **1999**, *40*, 5429-5432. (b) D. J. Hart; N. A. Magomedov, "Synthesis of ent-alantrypinone", *J. Am. Chem. Soc.* **2001**, *123*, 5892-5899.

(10) (a) M. D'Ambrosio; A. Guerriero; C. Debitus; O. Ribes; J. Pusset; S. Leroy; F. Pietra, "Agelastatin A, a new skeleton cytotoxic alkaloid of the oroidin family.

Isolation from the axinellid sponge *Agelas dendromorpha* of the Coral Sea", *J. Chem. Soc., Chem. Commun.* **1993**, 1305-1306. (b) M. D'Ambrosio; A. Guerriero; G. Chiasera; F. Pietra, "Conformational preferences and absolute configuration of agelastatin A, a cytotoxic alkaloid of the axinellid sponge *Agelas dendromorpha* from the Coral Sea, via combined molecular modeling, NMR, and exciton splitting for diamide and hydroxyamide derivatives", *Helv. Chim. Acta* **1994**, *77*, 1895-1902.

(11) T. W. Hong; D. R. Jimenez; T. F. Molinski, "Agelastatins C and D, new pentacyclic bromopyrroles from the sponge *Cymbastela sp.*, and potent arthropod toxicity of (-)-agelastatin A", *J. Nat. Prod.* **1998**, *61*, 158-161.

(12) S. Tilvi; C. Moriou; M.-T. Martin; J.-F. Gallard; J. Sorres; K. Patel; S. Petek; C. Debitus; L. Ermolenko; A. Al-Mourabit, "Agelastatin E, agelastatin F, and benzosceptrin C from the marine sponge *Agelas dendromorpha*", *J. Nat. Prod.* **2010**, *73*, 720-723.

(13) K. J. Hale; M. M. Domostoj; M. El-Tanani; F. Charles Campbell; C. K. Mason, in *Strategies and tactics in organic synthesis, Vol. Volume 6* (Ed.: H. Michael), Academic Press, **2005**, pp. 352-394.

(14) G. R. Pettit; S. Ducki; D. L. Herald; D. L. Doubek; J. M. Schmidt; J.-C. Chapuis, "Antineoplastic agents 470. Absolute configuration of the marine sponge bromopyrrole agelastatin A", *Oncol. Res.* **2005**, *15*, 11-20.

(15) C. K. Mason; S. McFarlane; P. G. Johnston; P. Crowe; P. J. Erwin; M. M. Domostoj; F. C. Campbell; S. Manaviazar; K. J. Hale; M. El-Tanani,

"Agelastatin A: a novel inhibitor of osteopontin-mediated adhesion, invasion, and colony formation", *Mol. Cancer Ther.* **2008**, *7*, 548-558.

(16) L. Meijer; A. M. W. H. Thunnissen; A. W. White; M. Garnier; M. Nikolic; L. H. Tsai; J. Walter; K. E. Cleverley; P. C. Salinas; Y. Z. Wu; J. Biernat; E. M. Mandelkow; S. H. Kim; G. R. Pettit, "Inhibition of cyclin-dependent kinases, GSK-3β and CK1 by hymenialdisine, a marine sponge constituent", *Chem. Biol.* **2000**, *7*, 51-63.

(17) A. A. Mourabit; P. Potier, "Sponge's molecular diversity through the ambivalent reactivity of 2-aminoimidazole: a universal chemical pathway to the oroidin-based pyrrole-imidazole alkaloids and their palau'amine congeners", *Eur. J. Org. Chem.* **2001**, 237-243.

(18) A. Araki; M. Tsuda; T. Kubota; Y. Mikami; J. Fromont; J. i. Kobayashi, "Nagelamide J, a novel dimeric bromopyrrole alkaloid from a sponge *Agelas* species", *Org. Lett.* **2007**, *9*, 2369-2371.

(19) Y.-G. Wang; B. I. Morinaka; J. C. P. Reyes; J. J. Wolff; D. Romo; T. F. Molinski, "Synthesis of 7-^{15}N-oroidin and evaluation of utility for biosynthetic studies of pyrrole-imidazole alkaloids by microscale ^{1}H-^{15}N HSQC and FTMS", *J. Nat. Prod.* **2010**, *73*, 428-434.

(20) E. Fattorusso; O. Taglialatela-Scafati, "Two novel pyrrole-imidazole alkaloids from the Mediterranean sponge *Agelas oroides*", *Tetrahedron Lett.* **2000**, *41*, 9917-9922.

(21) A. S. Dilley; D. Romo, "Enantioselective strategy to the spirocyclic core of palau'amine and related bisguanidine marine alkaloids", *Org. Lett.* **2001**, *3*, 1535-1538.

(22) H. Nakamura; Y. Ohizumi; J. Kobayashi; Y. Hirata, "Physiologically active marine natural products from Porifera. III. Keramadine, a novel antagonist of serotonergic receptors isolated from the Okinawan sea sponge *Agelas sp*", *Tetrahedron Lett.* **1984**, *25*, 2475-2478.

(23) (a) G. E. Hilbert, "Synthesis of 2-imidazolone-4-carboxylic acid and 2-imidazolone", *J. Am. Chem. Soc.* **1932**, *54*, 3413-3419. (b) B. A. Otter; E. A. Falco; J. J. Fox, "Nucleosides. LXI. Transformations of pyrimidine nucleosides in alkaline media. IV. Conversion of 5-hydroxyuridines into imidazoline nucleosides", *J. Org. Chem.* **1969**, *34*, 2636-2642.

(24) (a) S. Ohira, "Methanolysis of dimethyl (1-diazo-2-oxopropyl)phosphonate: generation of dimethyl (diazomethyl)phosphonate and reaction with carbonyl compounds", *Synth. Commun.* **1989**, *19*, 561-564. (b) S. Mueller; B. Liepold; G. J. Roth; H. J. Bestmann, "An improved one-pot procedure for the synthesis of alkynes from aldehydes", *Synlett* **1996**, 521-522.

(25) K. C. Nicolaou; Y. Li; K. C. Fylaktakidou; H. J. Mitchell; H.-X. Wei; B. Weyershausen, "Total synthesis of apoptolidin: part 1. retrosynthetic analysis and construction of building blocks", *Angew. Chem., Int. Ed.* **2001**, *40*, 3849-3854.

(26) A. Gorgues, "Conjugated polyacetylenic aldehydes and acids. II. Preparation and properties of conjugated polyacetylenic aldehydes", *Ann. Chim. (Paris)* **1972**, *7*, 373-385.

(27) G. M. Konig; A. D. Wright, "Two new naturally occurring pyrrole derivatives from the tropical marine sponge *Agelas oroides*", *Natural Product Letters* **1994**, *5*, 141-146.

(28) CCDC 849248 (10) contains the supplementary crystallographic data for this paper. These data can be obtained free of charge from The Cambridge Crystallographic Data Centre via www. ccdc.cam.ac.uk/data_request/cif.

(29) D. A. Peters; R. L. Beddoes; J. A. Joule, "Alternative synthesis of 6-(3-methoxybenzyl)pyrazin-2(1H)-one. Synthesis of indeno[1,2-b]pyrazin-2-ones. Crystal structures of 5-acetoxy-1-benzyl-4-tert-butoxycarbonyl-6-(3-methoxybenzylidene)piperazin-2-one, 1-benzyl-4-tert-butoxycarbonyl-7-methoxy-1,3,4,4a-tetrahydroindeno[1,2-b]pyrazin-2-one and 1-benzyl-4-tert-butoxycarbonyl-7-methoxy-1,3,4,9-tetrahydroindeno[1,2-b]pyrazin-2-one", *J. Chem. Soc., Perkin Trans. 1* **1993**, 1217-1224.

(30) Molecular mechanics calculations were performed using Avogadro 1.0.0 software package (MMFF94s forcefield).

(31) DFT calculations on the products arising from nucleophilic capture at C7 were performed using the Gaussian 09 program package (B3LYP/6-31+G(d))

(32) Please see appendix A for computational details.

(33) (a) G. Gondos; I. Szecsenyi; L. Gera, "Silica gel-assisted reversible ring-opening and ring-closure reactions on a thin layer silica gel chromatographic plate", *J. Planar Chromatogr.--Mod. TLC* **1989**, *2*, 163-164. (b) I. Paterson; M. V. Perkins, "Total synthesis of the marine polypropionate (+)-muamvatin. A configurational model for siphonariid metabolites", *J. Am. Chem. Soc.* **1993**, *115*, 1608-1610. (c) S. Minakata; M. Komatsu, "Organic reactions on silica in water", *Chem. Rev. (Washington, DC, U. S.)* **2009**, *109*, 711-724. (d) Q. Ding; B. Cao; Z. Zong; Y. Peng, "Silica gel-promoted tandem addition-cyclization reactions of 2-alkynylbenzenamines with isothiocyanates", *J. Comb. Chem.* **2010**, *12*, 370-373.

(34) X. Liu; J.-M. Yang; S. S. Zhang; X.-Y. Liu; D. X. Liu, "Induction of cell cycle arrest at G1 and S phases and cAMP-dependent differentiation in C6 glioma by low concentration of cycloheximide", *BMC Cancer* **2010**, *10*, 684.

(35) T. Schneider-Poetsch; J. Ju; D. E. Eyler; Y. Dang; S. Bhat; W. C. Merrick; R. Green; B. Shen; J. O. Liu, "Inhibition of eukaryotic translation elongation by cycloheximide and lactimidomycin", *Nat. Chem. Biol.* **2010**, *6*, 209-217.

(36) Y. Dang; T. Schneider-Poetsch; D. E. Eyler; J. C. Jewett; S. Bhat; V. H. Rawal; R. Green; J. O. Liu, "Inhibition of eukaryotic translation elongation by the antitumor natural product mycalamide B", *RNA* **2011**, *17*, 1578-1588.

(37) G. A. Otto; J. D. Puglisi, "The pathway of HCV IRES-mediated translation initiation", *Cell (Cambridge, MA, U. S.)* **2004**, *119*, 369-380.

(38) G. Dong, "Recent advances in the total synthesis of agelastatins", *Pure Appl. Chem.* **2010**, *82*, 2231-2246.

(39) (a) R. P. Walker; D. J. Faulkner; E. D. Van; J. Clardy, "Sceptrin, an antimicrobial agent from the sponge Agelas sceptrum", *J. Am. Chem. Soc.* **1981**, *103*, 6772-6773. (b) J. Appenzeller; S. Tilvi; M.-T. Martin; J.-F. Gallard; H. El-bitar; E. T. H. Dau; C. Debitus; D. Laurent; C. Moriou; A. Al-Mourabit, "Benzosceptrins A and B with a unique benzocyclobutane skeleton and nagelamide S and T from Pacific sponges", *Org. Lett.* **2009**, *11*, 4874-4877.

(40) (a) J. Kobayashi; M. Tsuda; T. Murayama; H. Nakamura; Y. Ohizumi; M. Ishibashi; M. Iwamura; T. Ohta; S. Nozoe, "Ageliferins, potent actomyosin ATPase activators from the Okinawan marine sponge *Agelas sp*", *Tetrahedron* **1990**, *46*, 5579-5586. (b) P. A. Keifer; R. E. Schwartz; M. E. S. Koker; R. G. Hughes, Jr.; D. Rittschof; K. L. Rinehart, "Bioactive bromopyrrole metabolites from the Caribbean sponge *Agelas conifera*", *J. Org. Chem.* **1991**, *56*, 2965-2975. (c) D. H. Williams; D. J. Faulkner, "*N*-methylated ageliferins from the sponge Astrosclera willeyana from Pohnpei", *Tetrahedron* **1996**, *52*, 5381-5390.

(41) S. Nishimura; S. Matsunaga; M. Shibazaki; K. Suzuki; K. Furihata; S. R. W. M. Van; N. Fusetani, "Massadine, a novel geranylgeranyltransferase type I inhibitor from the marine sponge Stylissa aff. massa", *Org. Lett.* **2003**, *5*, 2255-2257.

(42) (a) R. B. Kinnel; H. P. Gehrken; P. J. Scheuer, "Palau'amine: a cytotoxic and immunosuppressive hexacyclic bisguanidine antibiotic from the sponge *Stylotella agminata*", *J. Am. Chem. Soc.* **1993**, *115*, 3376-3377. (b) R. B. Kinnel; H.-P. Gehrken; R. Swali; G. Skoropowski; P. J. Scheuer, "Palau'amine and its

congeners: A family of bioactive bisguanidines from the marine sponge *Stylotella aurantium*", *J. Org. Chem.* **1998**, *63*, 3281-3286.

(43) (a) K. C. Bascombe; S. R. Peter; W. F. Tinto; S. M. Bissada; S. McLean; W. F. Reynolds, "Axinellamines A and B, new pyrrole alkaloids of the marine sponge *Axinella sp*", *Heterocycles* **1998**, *48*, 1461-1464. (b) S. Urban; P. d. A. Leone; A. R. Carroll; G. A. Fechner; J. Smith; J. N. A. Hooper; R. J. Quinn, "Axinellamines A-D, novel imidazo-azolo-imidazole alkaloids from the Australian marine sponge *Axinella sp*", *J. Org. Chem.* **1999**, *64*, 731-735.

(44) A. Grube; M. Koeck, "Stylissadines A and B: The first tetrameric pyrrole-imidazole alkaloids", *Org. Lett.* **2006**, *8*, 4675-4678.

(45) (a) L. H. Foley; G. Büchi, "Biomimetic synthesis of dibromophakellin", *J. Am. Chem. Soc.* **1982**, *104*, 1776-1777. (b) N. G. De; A. Ahond; J. Guilhem; C. Poupat; H. D. E. Tran; P. Potier; M. Pusset; J. Pusset; P. Laboute, "Marine invertebrates from the New Caledonian lagoon. V. Isolation and identification of metabolites of a new species of sponge, *Pseudaxinyssa cantharella*", *Tetrahedron* **1985**, *41*, 6019-6033.

(46) P. S. Baran; D. P. O'Malley; A. L. Zografos, "Natural product synthesis: sceptrin as a potential biosynthetic precursor to complex pyrrole-imidazole alkaloids: the total synthesis of ageliferin", *Angew. Chem., Int. Ed.* **2004**, *43*, 2674-2677.

(47) Deuterium ^{2}H (~0.02%) and ^{17}O (~0.04%) also contribute to M+1, but are much lower in natural abundance (~0.02% and 0.04%, respectively) and may be ignored in the first approximation.

(48) The $^{13}C/^{15}N$ isotope ratio of synthetic and natural oroidin samples may differ slightly due to differences in fractionation of ^{13}C (or ^{15}N) in compounds derived by "modern" biosynthesis compared to chemical precursors derived from petrochemical-based feedstock. In practice, this will be inconsequential, since corrections can be made with the appropriate normalization.

(49) R. K. Harris; E. D. Becker; D. M. S. M. Cabral; R. Goodfellow; P. Granger, "NMR nomenclature. Nuclear spin properties and conventions for chemical shifts (IUPAC recommendations 2001)", *Pure Appl. Chem.* **2001**, *73*, 1795-1818.

(50) M. Assmann; S. Zea; M. Koeck, "Sventrin, a new bromopyrrole alkaloid from the Caribbean sponge *Agelas sventr*es", *J. Nat. Prod.* **2001**, *64*, 1593-1595.

(51) K. F. Albizati; D. J. Faulkner, "Stevensine, a novel alkaloid of an unidentified marine sponge", *J. Org. Chem.* **1985**, *50*, 4163-4164.

(52) P. Andrade; R. Willoughby; S. A. Pomponi; R. G. Kerr, "Biosynthetic studies of the alkaloid, stevensine, in a cell culture of the marine sponge Teichaxinella morchella", *Tetrahedron Lett.* **1999**, *40*, 4775-4778.

(53) J. Englander; L. Cohen; B. Arshava; R. Estephan; J. M. Becker; F. Naider, "Selective labeling of a membrane peptide with ^{15}N-amino acids using cells grown in rich medium", *Biopolymers* **2006**, *84*, 508-518.

(54) (a) E. P. Stout; Y.-G. Wang; D. Romo; T. F. Molinski, "Pyrrole aminoimidazole alkaloid metabiosynthesis with marine sponges *Agelas conifera* and *Stylissa caribica*", *Angew Chem Int Ed Engl* **2012**, *51*, 4877-4881. (b) E. P. Stout; B. I. Morinaka; Y.-G. Wang; D. Romo; T. F. Molinski, "De novo synthesis of

benzosceptrin C and nagelamide H from 7-^{15}N-oroidin: implications for pyrrole-aminoimidazole alkaloid biosynthesis", *J. Nat. Prod.* **2012**, *75*, 527-530.

APPENDIX A

EXPERIMENTAL AND SELECTED SPECTRAL DATA

General Procedures

All reactions were performed under a nitrogen atmosphere in oven-dried glassware. Dichloromethane was dried by passing through activated molecular sieves or alumina (MBraun solvent purification system). Tetrahydrofuran was distilled over sodium and benzophenone. Methanol was distilled from Mg turnings. Triethylamine was distilled from calcium hydride. Other solvents and reagents were used as received from commercially available sources. Deuterated solvents were purchased from either Aldrich or Cambridge Isotopes and used as received. ^{1}H NMR and ^{13}C NMR spectra were recorded on an 500 MHz spectrometer. ^{1}H NMR chemical shifts are reported as δ values in ppm relative to residual solvent signals: $CDCl_3$ (7.26 ppm), DMSO-d_6 (2.50 ppm), acetone-d_6 (2.05 ppm), CD_3OD (3.31 ppm). ^{1}H NMR coupling constants (*J*) are reported in Hertz (Hz) and multiplicity is indicated as follows: s (singlet), d (doublet), t (triplet), q (quartet), m (multiplet), br s (broad singlet), dd (doublet of doublet), dt (doublet of triplet), dq (doublet of quartet), tq (triplet of quartet), app dt (apparent doublet of triplet), app t (apparent triplet), app q (apparent quartet). ^{13}C NMR chemical shifts are reported as δ values in ppm relative to residual solvent signals: $CDCl_3$ (77.16 ppm), DMSO-d_6 (39.52 ppm), acetone-d_6 (29.84 ppm), CD_3OD (49.00ppm). Flash column chromatography was performed with 60Å Silica Gel (230-400 mesh) as a stationary phase. High resolution mass spectra (ESI or MALDI) were obtained through the Center for Chemical Characterization and Analysis (Texas A&M University). Thin Layer Chromatography (TLC) was performed using glass-backed silica gel F254

(Merck, 250 μm thickness). Visualization of developed plates was performed by fluorescence quenching or by staining with ceric ammonium molybdate followed by heating. Infrared spectra were obtained as thin film on NaCl plates on a FTIR spectrometer.

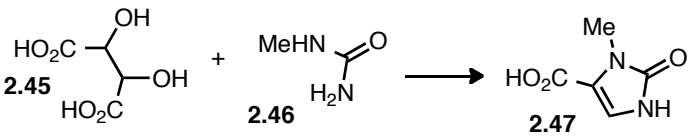

Acid 2.47. Imidazolone acid **2.47** was synthesized using a modified literature procedure[1]. A solid mixture of (±)-tartaric acid **2.45** (100 g, 0.66 mol, 1.0 equiv) and *N*-methyl urea **2.45** (55.69 g, 0.73 mol, 1.1 equiv) was added in 6 portions via a scoopula (waiting 10-15 min before addition of another portion) to a stirred solution of 440 mL concentrated sulfuric acid maintaining the temperature below 45 °C without external cooling. The mixture was then heated to 80 °C and stirred for 3 h at this temperature. The dark brown homogeneous reaction mixture was allowed to cool to 23 °C, poured onto ice, and the resulting tan solids were filtered. The solids were washed with cold water (200 mL) and acetone (~50mL) to give 50.43 g (54%) of acid **2.47** as a tan amorphous solid: R_f = 0.27 (20% MeOH/CH_2Cl_2); IR (thin film): 3159, 3100, 1638 cm^{-1}; ^{1}H NMR (500 MHz; DMSO-d_6): δ 10.85 (br s, 1H), 7.28 (d, *J* = 2.0 Hz, 1H), 3.28 (s,

[1] (a) Hilbert, G. E. *J. Am. Chem. Soc.* **1932**, *54,* 3413-3419. (b) Otter, B. A.; Falco, E. A.; Fox, J. J. *J. Org. Chem*. **1968**, *33*, 3593-3600.

3H); ^{13}C NMR (125 MHz; DMSO-d_6): δ 160.9, 153.8, 118.5, 115.0, 28.5 ppm; HRMS (+ESI) Calcd. for $C_5H_7N_2O_3$ $[M+H]^+$: 143.0457, found: 143.0454.

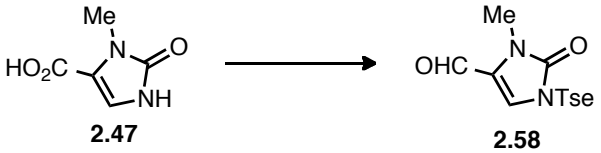

Aldehyde 2.58. To a solution of acid **2.47** (10.00 g, 70.4 mmol, 1.0 equiv) in anhydrous *N,N*-dimethylformamide (700 mL) was added K_2CO_3 (19.45 g, 140.7 mmol, 2.0 equiv). After stirring for 10 min, methyl iodide (4.4 mL, 70.4 mmol, 1.0 equiv) was then added dropwise and the resulting mixture was stirred for 2 h at 23°C and 1 h at 60 °C. Another portion of K_2CO_3 (19.45 g, 140.7 mmol, 2.0 equiv) was then added followed by addition of tosylethyl mesylate (19.59 g, 70.4 mmol, 1.0 equiv). The reaction mixture was stirred for 6 h at 60 °C then cooled to 23 °C and concentrated *in vacuo*. The residue was partitioned between 700 mL EtOAc and 700 mL water. The layers were separated and the organic layer was washed with 700 mL water, dried over Na_2SO_4 and concentrated *in vacuo* to give the crude ester as a light yellow residue. To a solution of the crude ester in 350 mL anhydrous CH_2Cl_2 at -78 °C was added DIBAl-H (31.4 mL, 175.9 mmol, 2.5 equiv) dropwise. The reaction was stirred for 30 min then quenched with 7 mL methanol and then a saturated aqueous solution of Rochelle's salt (350 mL). The mixture was stirred vigorously for 5 h at 23 °C. The aqueous layer was extracted with CH_2Cl_2 (2 x 350 mL) and the pooled organic layer was dried over Na_2SO_4 and

concentrated *in vacuo* to give the crude alcohol as a light yellow residue. To a solution of crude alcohol in 350 mL anhydrous CH_2Cl_2 was added manganese (IV) oxide (34.76 g, 351.8 mmol, 5 equiv) and stirred vigorously for 8 h at 23 °C. The mixture was then filtered through a pad of Celite and the filtrate was concentrated *in vacuo*. The residue was purified by flash column chromatography (SiO_2, 70→80% EtOAc/hexanes) providing 18.49 g (85% over 3 steps) of aldehyde **2.58** as a white solid: R_f = 0.19 (70% EtOAc/hexanes); IR (thin film): 3103, 2931, 2819, 1709, 1655 cm^{-1}; ^1H NMR (500 MHz; $CDCl_3$): δ 9.19 (s, 1H), 7.69 (d, *J* = 8.0 Hz, 2H), 7.30 (d, *J* = 8.0 Hz, 2H), 7.16 (s, 1H), 4.14 (t, *J* = 6.0 Hz, 2H), 3.55 (t, *J* = 6.0 Hz, 2H), 3.37 (s, 3H), 2.39 (s, 3H); ^{13}C NMR (125 MHz; $CDCl_3$): δ 177.2, 152.7, 145.4, 135.9, 130.0 (2C), 127.82, 127.66 (2C), 123.5, 53.6, 39.1, 29.5, 21.7; HRMS (+ESI) Calcd. for $C_{14}H_{17}N_2O_4S$ $[M+H]^+$: 309.0909, found: 309.0906.

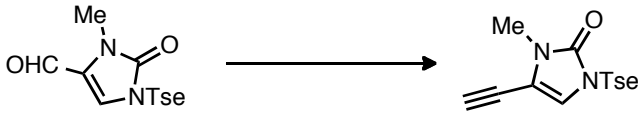

2.58 **2.58a**

Alkyne 2.58a. To a stirred solution of aldehyde **2.58** (5.00 g, 16.2 mmol, 1.0 equiv) in 48 mL anhydrous MeOH and 85 mL anhydrous CH_2Cl_2 at -40 °C was added Ohira-Bestmann reagent **20**[2] (6.23 g, 32.4 mmol, 2.0 equiv) dropwise as an oily liquid and 1.0

[2] S. Mueller, B. Liepold, G. J. Roth, H. J. Bestmann, *Synlett* **1996**, 521-522.

M NaOMe in MeOH (37.3 mL, 37.3 mmol, 2.3 equiv) dropwise ~5 min later. The reaction was stirred for 60 h at –40 °C then allowed to warm to 23 °C over 1 h before addition of 150 mL of a saturated aqueous solution of $NaHCO_3$. The aqueous layer was extracted with CH_2Cl_2 (2 x 150 mL). The organic layer was dried over Na_2SO_4, filtered, and concentrated *in vacuo*. The residue was purified by flash column chromatography (SiO_2, 70→80% EtOAc/hexanes) to give 2.76 g (56%) of alkyne **2.58a** as a light yellow solid: R_f = 0.28 (70% EtOAc/hexanes); IR (thin film): 3257, 3124, 2928, 2108, 1685 cm^{-1}; ^1H NMR (500 MHz; $CDCl_3$): δ 7.73 (d, *J* = 8.5 Hz, 2H), 7.34 (d, *J* = 8.5 Hz, 2H), 6.54 (s, 1H), 4.02 (t, *J* = 6.5 Hz, 2H), 3.55 (t, *J* = 6.5 Hz, 2H), 3.35 (s, 1H), 3.10 (s, 3H), 2.44 (s, 3H); ^{13}C NMR (125 MHz; $CDCl_3$): δ 151.6, 145.1, 136.0, 129.9 (2C), 127.8 (2C), 117.1, 106.6, 83.8, 71.7, 54.0, 38.8, 28.2, 21.7; HRMS (+ESI) Calcd. for $C_{15}H_{17}N_2O_3S$ $[M+H]^+$: 305.0960, found: 305.0949.

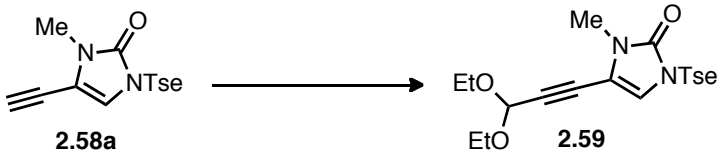

Alkynyl acetal 2.59. To a suspension of alkyne **2.58a** (5.94 g, 19.5 mmol, 1.0 equiv) in 300 mL triethyl orthoformate was added ZnI_2 (6.35 g, 19.5 mmol, 1.0 equiv). The reaction mixture was heated to 110 °C with stirring for 6 h, and then allowed to cool to 23 °C. Filtration through a pad of Celite was followed by washing with 100 mL CH_2Cl_2 and concentration *in vacuo* to give a brown residue. The residue was purified by flash

column chromatography (SiO_2, 20% to 30% acetone/hexanes) to provide 6.65 g (84%) of alkynyl acetal **2.59** as a light yellow oil. R_f = 0.35 (40% acetone/hexanes); IR (thin film): 3121, 2979, 2928, 2238, 2173, 1685 cm^{-1}; ^1H NMR (500 MHz; $CDCl_3$): δ 7.69 (d, *J* = 8.5 Hz, 2H), 7.30 (d, *J* = 8.5 Hz, 2H), 6.51 (s, 1H), 5.42 (s, 1H), 3.97 (t, *J* = 6.5 Hz, 2H), 3.72 (dq, *J* = 9.5, 7.0 Hz, 2H), 3.59 (dq, *J* = 9.5, 7.0 Hz, 2H), 3.50 (t, *J* = 6.5 Hz, 2H), 3.06 (s, 3H), 2.40 (s, 3H), 1.22 (t, *J* = 7.0 Hz, 6H); ^{13}C NMR (125 MHz; $CDCl_3$): δ 151.6, 145.0, 136.0, 129.9 (2C), 127.8 (2C), 117.0, 106.2, 91.3, 90.7, 73.1, 61.2 (2C), 54.0, 38.7, 28.2, 21.7, 15.1 (2C); HRMS (+ESI) Calcd. for $C_{20}H_{27}N_2O_5S$ $[M+H]^+$: 407.1641, found: 407.1648.

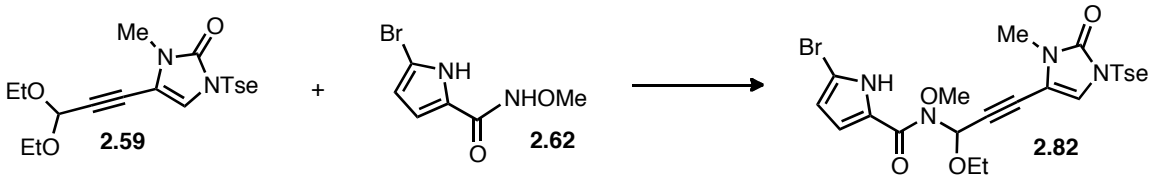

Pyrrole Imidazolone 2.82. To a solution of alkynyl acetal **2.59** (2.58 g, 6.35 mmol, 1.0 equiv) and pyrrole carboxamide **2.62** (1.53 g, 6.98 mmol, 1.1 equiv) in 200 mL CH_2Cl_2 was added 1.9 g of oven-dried powdered 4Å molecular sieves. The suspension was then cooled to –78 ºC followed by addition of 1.0 M $SnCl_4$ in CH_2Cl_2 (1.59 mL, 1.59 mmol, 0.25 equiv). The reaction mixture was removed from the cold bath and allowed to warm to 23 °C and stirred for 2.5 h. A saturated aqueous solution of $NaHCO_3$ (100 mL) was then added and the mixture was stirred vigorously and filtered through a pad of Celite. The organic layer was separated and the aqueous layer was extracted with EtOAc (2 x

100 mL) and the combined organic layer was dried over Na_2SO_4, and concentrated *in vacuo*. The residue was purified by flash column chromatography (SiO_2, 0→12% acetone/CH_2Cl_2) to deliver 852 mg (23%) of adduct **2.82** along with recovered starting materials (961 mg (37%) alkynyl acetal **2.59** and 988 mg (65%) pyrrole carboxamide **2.62**): R_f = 0.36 (3% acetone/CH_2Cl_2); IR (thin film): 3236, 3129, 2982, 2934, 2241, 1697, 1614 cm^{-1}; ^1H NMR (500 MHz; acetone-d_6): δ 7.74 (d, *J* = 8.5 Hz, 2H), 7.40 (d, *J* = 8.5 Hz, 2H), 7.00 (d, *J* = 4.0 Hz, 1H), 6.84 (s, 1H), 6.58 (s, 1H), 6.31 (d, *J* = 4.0 Hz, 1H), 4.03 (s, 3H), 3.99 (t, *J* = 6.5 Hz, 2H), 3.74 (dq, *J* = 9.5, 7.0 Hz, 1H), 3.69 (t, *J* = 6.5 Hz, 2H), 3.66 (dq, *J* = 9.5, 7.0 Hz, 1H), 3.03 (s, 3H), 2.42 (s, 3H), 1.22 (t, *J* = 7.0 Hz, 3H); ^{13}C NMR (125 MHz; acetone-d_6): δ 161.3, 152.2, 145.5, 137.5, 130.4 (2C), 128.7 (2C), 125.8, 118.5, 118.0, 113.7, 106.5, 106.1, 89.9, 78.0, 74.8, 65.8, 64.4, 54.1, 39.1, 28.2, 21.5, 15.2; HRMS (+MALDI) Calcd. for $C_{24}H_{28}BrN_4O_6S$ $[M+H]^+$: 579.0913, found: 579.0890.

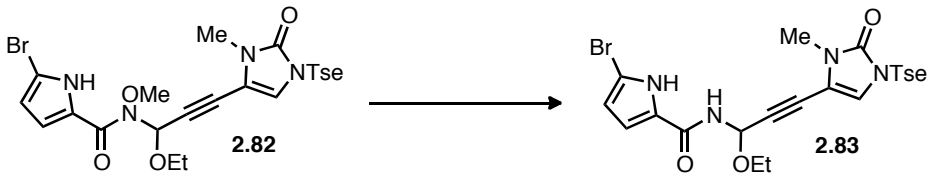

Amide Pyrrole Imidazolone 2.83. To a solution of pyrrole imidazolone **2.82** (632 mg, 1.09 mmol, 1.0 equiv) in 60 mL anhydrous THF at -20 °C was added 0.1 M SmI_2 in THF (21.8 mL, 2.18 mmol, 2.0 equiv). The reaction was stirred for 20 min and allowed to warm to 23 °C. A 0.1 M solution of $Na_2S_2O_3$ (100 mL) was then added and the

mixture was extracted with EtOAc (3 x 70 mL). The organic layer was dried over Na_2SO_4, filtered, and concentrated *in vacuo* leaving a light yellow residue. The residue was purified by flash column chromatography (SiO_2, 80→90% EtOAc/hexanes) to provide 471 mg (79%) of amide **2.83** as a white solid. R_f = 0.19 (80% EtOAc/hexanes); IR (thin film): 3204, 3127, 2976, 2928, 2235, 1682, 1640 cm^{-1}; ^1H NMR (500 MHz; CD_3OD): δ 7.71 (d, *J* = 8.0 Hz, 2H), 7.38 (d, *J* = 8.0 Hz, 2H), 6.89 (d, *J* = 4.0 Hz, 1H), 6.75 (s, 1H), 6.23 (s, 1H), 6.17 (d, *J* = 4.0 Hz, 1H), 4.02 (t, *J* = 6.0 Hz, 2H), 3.69 (t, *J* = 6.0 Hz, 2H), 3.70-3.63 (m, 2H), 3.08 (s, 3H), 2.42 (s, 3H), 1.23 (t, *J* = 7.0 Hz, 3H).; ^{13}C NMR (125 MHz; CD_3OD): δ 161.4, 153.0, 146.5, 137.5, 130.8 (2C), 128.9 (2C), 127.7, 118.4, 114.6, 112.8, 107.7, 105.7, 92.6, 73.1, 71.2, 63.8, 54.3, 39.7, 28.6, 21.6, 15.4; HRMS (-ESI) Calcd. for $C_{23}H_{24}BrN_4O_5S$ $[M-H]^-$: 547.0651, found: 547.0664.

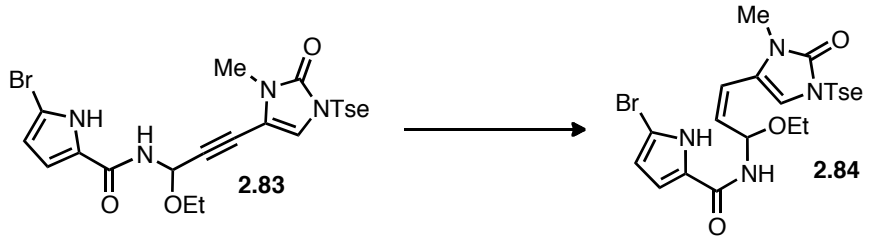

(*Z*)-Alkenyl Pyrrole Imidazolone 2.84. To a solution of amide **2.83** (144 mg, 0.26 mmol, 1.0 equiv) in a 1:1 mixture of anhydrous THF and methanol was added Lindlar catalyst (278 mg, 0.13 mmol, 0.5 equiv). Following three evacuations/purge cycles with H_2, the heterogenous mixture was stirred under 1 atm H_2 for 4 h and then filtered through a pad of Celite. The filtrate was concentrated *in vacuo* yielding a yellow

residue. The residue was purified by flash column chromatography (SiO_2 pretreated with 10% Et_3N in hexanes then washed with CH_2Cl_2), 80→90% EtOAc/hexanes) providing 121 mg (84%) of (*Z*)-alkene **2.84** as a white solid: R_f = 0.27 (90% EtOAc/hexanes); IR (thin film): 3189, 3121, 2925, 1667, 1623 cm^{-1}; ^1H NMR (500 MHz; $CDCl_3/CD_3OD$): δ 7.70 (d, *J* = 8.0 Hz, 2H), 7.28 (d, *J* = 8.0 Hz, 2H), 6.81 (d, *J* = 4.0 Hz, 1H), 6.50 (s, 1H), 6.15 (d, *J* = 4.0 Hz, 1H), 6.01 (d, *J* = 12.0 Hz, 1H), 6.00 (d, *J* = 8.0 Hz, 1H) 5.78 (dd, *J* = 12.0, 8.0 Hz, 1H), 4.05-3.96 (m, 2H), 3.66-3.50 (m, 4H), 3.06 (s, 3H), 2.40 (s, 3H), 1.18 (t, *J* = 7.0 Hz, 3H); ^{13}C NMR (125 MHz; $CDCl_3/CD_3OD$): δ 160.8, 152.8, 145.6, 136.1, 130.2 (2C), 129.3, 128.3 (2C), 126.8, 119.7, 116.7, 113.9, 112.3, 112.0, 104.9, 76.2, 63.0, 54.2, 38.7, 27.6, 21.7, 15.3; HRMS (+ESI) Calcd. for $C_{23}H_{28}BrN_4O_5S$ $[M+H]^+$: 551.0964, found: 551.0945.

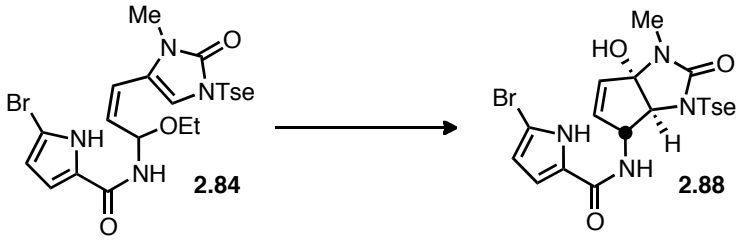

Monocyclized adduct 2.88. To a suspension of cyclization precursor **2.84** (51.0 mg, 92.5 μmol, 1.0 equiv) in 4 mL CH_2Cl_2 at -78 ºC was added trifluoroacetic acid (212 μL, 2.77 mmol, 30.0 equiv). The reaction was immediately warmed to –30 ºC and stirred for 5 min to give a dark red solution. A 10 mL saturated aqueous solution of $NaHCO_3$ was then added and the mixture was removed from the cold bath and allowed to warm to 23

°C while stirring vigorously. The crude mixture was extracted with EtOAc (3 x 10 mL) and the combined organic layers were dried over Na_2SO_4, filtered, and concentrated *in vacuo* to give a yellow residue. The residue was purified by flash column chromatography (SiO_2, 80→85% EtOAc/hexanes) providing 38.5 mg (80%) of cyclized adduct **2.88** as an off-white solid: R_f = 0.20 (80% EtOAc/hexanes); IR (thin film): 3207, 3067, 2928, 1682, 1626 cm^{-1}; ^1H NMR (500 MHz; CD_3OD): δ 7.80 (d, *J* = 8.0 Hz, 2H), 7.33 (d, *J* = 8.0 Hz, 2H), 6.79 (d, *J* = 4.0 Hz, 1H), 6.17 (d, *J* = 4.0 Hz, 1H), 6.16 (dd, *J* = 6.0, 2.0 Hz, 1H), 5.91 (dd, *J* = 6.0, 2.0 Hz, 1H), 4.74 (app q, *J* = 2.0 Hz, 1H), 3.84-3.73 (m, 2H), 3.65 (d, *J* = 2.0 Hz, 1H), 3.63-3.51 (m, 2H), 2.78 (s, 3H), 2.40 (s, 3H); ^{13}C NMR (125 MHz; CD_3OD): δ 161.7, 158.7, 146.5, 137.3, 134.7, 133.5, 131.0 (2C), 129.2 (2C), 128.3, 113.7, 112.6, 104.7, 98.2, 74.2, 61.1, 54.4, 38.3, 25.4, 21.6; HRMS (-ESI) Calcd. for $C_{21}H_{22}BrN_4O_5S$ $[M-H]^-$: 521.0494, found: 521.0470.

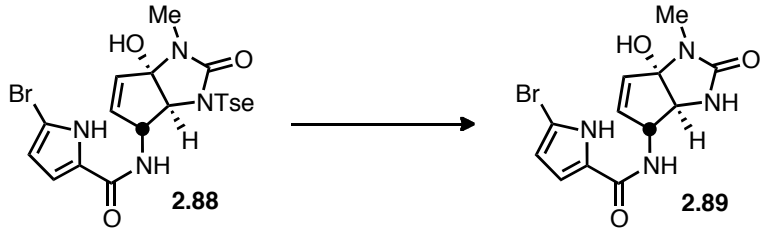

pre-Agelastatin A 2.89. To a solution of cyclized adduct **2.88** (38.5 mg, 0.07 mmol, 1.0 equiv) in anhydrous THF (5 mL) was added 1.0 M KHMDS in THF (221 μL, 0.22 mmol, 3.0 equiv). The mixture was stirred for 0.5 h at 60 °C and was allowed to cool to 23 °C. A saturated aqueous solution of NH_4Cl (10 mL) was then added followed by

extraction with EtOAc (3 x 10 mL). The combined organic layers were dried over Na_2SO_4, filtered, and concentrated *in vacuo* to give a yellow residue. The residue was purified by flash column chromatography (SiO_2, EtOAc) providing 15.6 mg (62%) of pre-agelastatin A **2.88** as a white solid: R_f = 0.14 (EtOAc); IR (thin film): 3287, 2925, 1682, 1632 cm^{-1}; ^1H NMR (500 MHz; CD_3OD): δ 6.79 (d, *J* = 4.0 Hz, 1H), 6.20 (dd, *J* = 6.0, 2.0 Hz, 1H), 6.13 (d, *J* = 4.0 Hz, 1H), 5.99 (dd, *J* = 6.0, 2.0 Hz, 1H), 4.66 (app q, *J* = 2.0 Hz, 1H), 3.67 (d, *J* = 2.0 Hz, 1H), 2.79 (s, 3H); ^{13}C NMR (125 MHz; CD_3OD): δ 162.2, 160.7, 134.5, 133.8, 128.2, 113.9, 112.5, 104.8, 100.5, 70.0, 63.9, 25.1; HRMS (+ESI) Calcd. for $C_{12}H_{14}BrN_4O_3$ $[M+H]^+$: 341.0249, found: 341.0239.

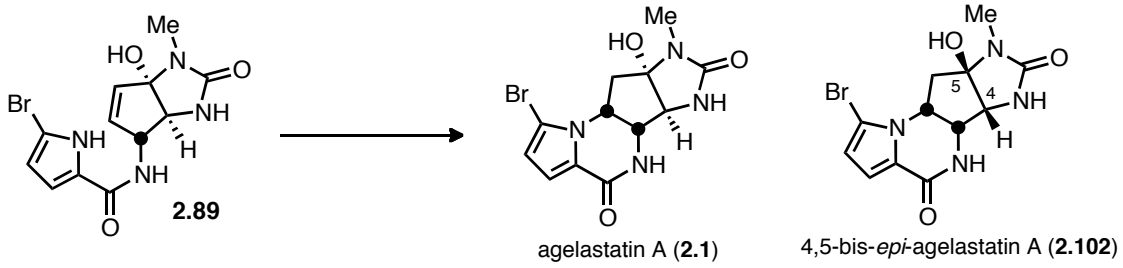

Agelastatin A and 4,5-bis-*epi*-agelastatin A. Pre-Agelastatin A (**2.89**) (3.8 mg, 11.1μmol) was loaded onto four 10 cm x 5 cm TLC plates (pre-treated with 10% Et_3N in hexanes and dried extensively with a heat gun). The plates were then eluted with 10% MeOH in CH_2Cl_2 to ensure uniform adsorption onto silica gel particles, dried using a heat gun for 1 min, then heated with a hot plate (surface temperature 45 ºC) for 50 minutes. (Note: Monitoring of the reaction was done by scraping off a small amount of silica gel and adding a drop of methanol followed by TLC analysis). The product band

was then scraped off from the entire TLC plate and eluted with 30% MeOH in CH_2Cl_2 (15mL). The organics were concentrated *in vacuo* and purified by preparative TLC eluting and washing with 10% MeOH in CH_2Cl_2 to give 2.6 mg (68%) agelastatin A (**2.1**) as a white solid and 0.5 mg (13%) 4,5-bis-*epi*-agelastatin A (**2.102**) as a thin film.

Agelastatin A (**2.1**); R_f = 0.17 (10% methanol/CH_2Cl_2); IR (thin film): 3257, 2916, 2851, 1652, 1555 cm^{-1}; ^1H NMR (500 MHz; CD_3OD): δ 6.91 (d, *J* = 4.0 Hz, 1H), 6.33 (d, *J* = 4.0 Hz, 1H), 4.60 (app dt, *J* = 12.0, 6.0 Hz, 1H), 4.09 (d, *J* = 5.5 Hz, 1H), 3.88 (s, 1H), 2.81 (s, 3H), 2.65 (dd, *J* = 13.0, 6.5 Hz, 1H), 2.10 (app t, *J* = 13.0 Hz, 1H); ^{13}C NMR (125 MHz; CD_3OD): δ 161.4, 161.1, 124.1, 116.0, 113.8, 107.3, 95.7, 67.4, 62.2, 54.4, 40.0, 24.2; HRMS (+ESI) Calcd. for $C_{12}H_{14}BrN_4O_3$ $[M+H]^+$: 341.0249, found: 341.0257.

4,5-bis-*epi*-agelastatin A (**2.102**); R_f = 0.20 (10% methanol/CH_2Cl_2); IR (thin film): 3292, 2922, 2848, 1691, 1555 cm^{-1}; ^1H NMR (500 MHz; CD_3OD): δ 6.90 (d, *J* = 4.0 Hz, 1H), 6.33 (d, *J* = 4.0 Hz, 1H), 5.00 (ddd, *J* = 10.5, 7.0, 5.0 Hz, 1H), 4.42 (app t, *J* = 5.5 Hz, 1H), 4.01 (d, *J* = 6.0 Hz, 1H), 2.73 (s, 3H), 2.52 (dd, *J* = 13.0, 7.0 Hz, 1H), 2.26 (dd, *J* = 13.0, 10.5 Hz, 1H); HRMS (+ESI) Calcd. for $C_{12}H_{14}BrN_4O_3$ $[M+H]^+$: 341.0249, found: 341.0236

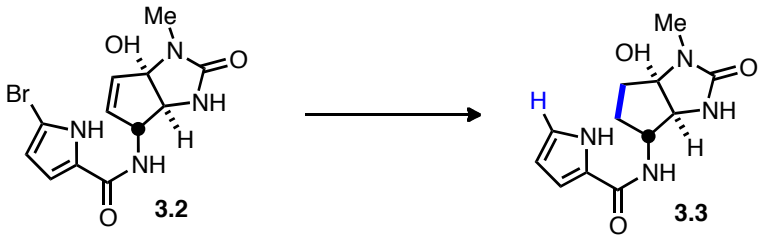

Debromo Dihydro Pre-Agelastatin A (3.3). To a solution of cyclized adduct **3.2** (3.1 mg, 0.009 mmol, 1.0 equiv) in 2:1 THF:H_2O (0.75 mL) was added triethylamine (7 µL, 0.05 mmol, 5.5 equiv) and 20 wt.% $Pd(OH)_2$ on carbon (1.3 mg, 0.002 mmol, 0.2 equiv). The reaction was purged with H_2 stirred under this atmosphere for 4h. The reaction mixture was then filtered through a celite plug washing with 20% methanol in DCM. The filtrate was concentrated *in vacuo* to give a white residue. The residue was purified by preparative TLC eluting and washing with 10% MeOH in CH_2Cl_2 to give 2.1 mg (87%) of **3.3** as a white solid: R_f = 0.32 (10% MeOH in DCM); IR (thin film): 3281, 2928, 1676, 1626 cm^{-1}; ^1H NMR (500 MHz; CD_3OD): δ 6.91 (dd, *J* = 2.5, 1.5 Hz, 1H), 6.87 (dd, *J* = 3.5, 1.5 Hz, 1H), 6.16 (dd, *J* = 3.5, 2.5 Hz, 1H), 3.95 (td, *J* = 6.0, 3.0 Hz, 1H), 3.59 (d, *J* = 3.5 Hz, 1H), 2.77 (s, 3H), 2.14 (dt, *J* = 13.5, 7.5 Hz, 1H), 2.03 (dt, *J* = 13.5, 6.0 Hz, 1H), 1.93-1.99 (m, 1H), 1.86-1.93 (m, 1H); ^{13}C NMR (125 MHz; CD_3OD): δ 164.0, 161.4, 126.6, 123.0, 112.3, 110.2, 97.8, 69.8, 60.1, 35.5, 29.5, 24.2; HRMS (+ESI) Calcd. for $C_{12}H_{17}N_4O_3$ $[M+H]^+$: 265.1301, found: 265.1309

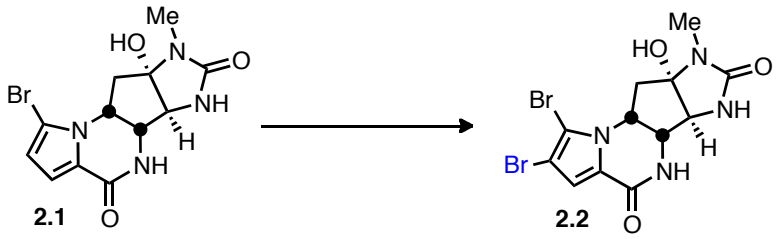

Agelastatin B (2.2). To a solution of agelastatin A **2.1** (1.9 mg, 5.6 µmol, 1.0 equiv) in 2:1 THF:H_2O (0.5 mL) was added 2,6-di-*t*-butyl-pyridine (1.9 µL, 8.4 µmol, 1.5 equiv) followed by *N*-bromosuccinimide (1.2 mg, 6.7µmol, 1.2 equiv) as a solid. After stirring for 1h, the reaction mixture was quenched by addition of a small crystal of sodium thiosulfate. The mixture was concentrated to give a white residue. The residue was purified by preparative TLC eluting and washing with 10% MeOH in CH_2Cl_2 to give 2.1 mg (90%) of agelastatin B **2.2** as a white solid: R_f = 0.19 (10% MeOH in DCM); IR (thin film): 3407, 1652, 1122 cm^{-1}; ^1H NMR (500 MHz; CD_3OD): δ 6.97 (s, 1H), 4.60 (dt, *J* = 12.0, 6.0 Hz, 1H), 4.11 (d, *J* = 5.5 Hz, 1H), 3.87 (m, 1H), 2.81 (s, 3H), 2.67 (dd, *J* = 13.0, 6.5 Hz, 1H), 2.12 (app t, *J* = 13.0 Hz, 1H); ^{13}C NMR (125 MHz; CD_3OD): δ 161.4, 160.0, 124.8, 116.9, 108.7, 101.7, 95.6, 67.4, 62.0, 55.4, , 39.9, 24.22; HRMS (+ESI) Calcd. for $C_{12}H_{13}Br_2N_4O_3$ $[M+H]^+$: 420.9323, found: 420.9323

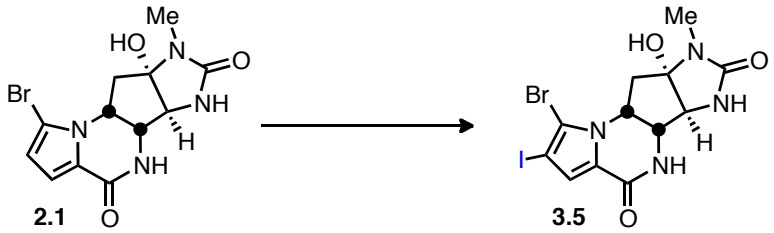

14-Iodo Agelastatin A (3.5). To a solution of agelastatin A **2.1** (3.1 mg, 9.1 μmol, 1.0 equiv) in 2:1 THF:H_2O (1.0 mL) was added 2,6-di-*t*-butyl-pyridine (3.1 μL, 13.6 μmol, 1.5 equiv) followed by *N*-iodosuccinimide (2.5 mg, 10.9 μmol, 1.2 equiv) as a solid, and $In(OTf)_3$ (0.5 mg, 0.9 μmol, 0.1 equiv). After stirring for 1h, the reaction mixture was quenched by addition of a small crystal of sodium thiosulfate. The mixture was concentrated to give a white residue. The residue was purified by preparative TLC eluting and washing with 10% MeOH in CH_2Cl_2 to give 4.2 mg (99%) of **3.5** as a white solid: R_f = 0.19 (10% MeOH in DCM); IR (thin film): 3290, 2916, 2848, 1697, 1655 cm^{-1}; ^1H NMR (500 MHz; CD_3OD): 7.03 (s, 1H), 4.62 (dt, *J* = 12.0, 6.0 Hz, 1H), 4.10 (d, *J* = 6.0 Hz, 1H), 3.87 (s, 1H), 2.81 (s, 3H), 2.67 (dd, *J* = 13.0, 6.5 Hz, 1H), 2.11 (app t, *J* = 13.0 Hz, 1H); ^{13}C NMR (125 MHz; CD_3OD): δ 161.4, 160.0, 126.2, 122.4, 113.7, 95.5, 69.0, 67.4, 62.1, 55.9, 39.9, 24.2; HRMS (+ESI) Calcd. for $C_{12}H_{12}BrICIN_4O_3$ $[M+Cl]^+$: 500.8826, found: 500.8803

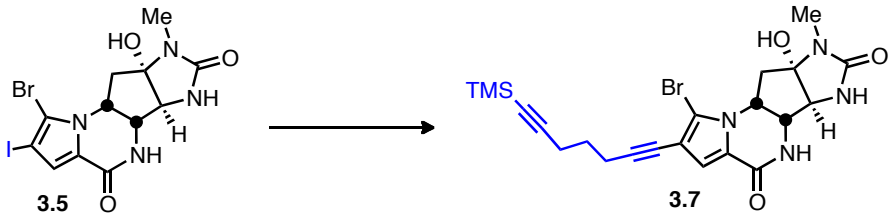

14-Alkynyl Agelastatin A (3.7). A solution of 14-iodo agelastatin A **3.5** (5.0 mg, 10.7 µmol, 1.0 equiv) in DMF/Et_3N (0.75 mL) was degassed by bubbling argon for 15 minutes. $Pd(PPh_3)_4$ (3.7 mg, 3.2 µmol, 0.3 equiv) was then added followed by bis-alkyne **3.6** (3.5 mg, 21.4 µmol, 2.0 equiv). The reaction was sealed in argon, stirred at 60 °C for 2h and concentrated *in vacuo* to give a yellow residue. The residue was purified by pipette flash column chromatography (SiO_2, 10→15% MeOH/DCM) providing 2.3 mg (43%) of 14-alkynyl agelastatin A **3.7** as a thin film: R_f = 0.24 (10% MeOH in DCM); IR (thin film): 3275, 2848, 1700, 1650 cm^{-1}; ^1H NMR (500 MHz; CD_3OD): δ 6.91 (s, 1H), 4.58 (dt, *J* = 12.0, 6.0 Hz, 1H), 4.09 (d, *J* = 5.5 Hz, 1H), 3.87 (s, 1H), 2.81 (s, 3H), 2.67 (dd, *J* = 13.0, 6.5 Hz, 1H), 2.51 (t, *J* = 7.0 Hz, 2H), 2.40 (t, *J* = 7.0 Hz, 2H), 2.12 (app t, *J* = 13.0 Hz, 1H), 1.76 (quintet, *J* = 7.0 Hz, 2H), 0.13 (s, 9H).; ^{13}C NMR (125 MHz; CD_3OD): δ 161.4, 160.5, 123.6, 117.6, 111.3, 110.6, 107.5, 95.6, 92.5, 85.6, 74.1, 67.4, 62.0, 54.9, 39.9, 29.0, 24.2, 19.5, 19.1, 0.2; HRMS (+ESI) Calcd. for $C_{22}H_{28}BrN_4O_3Si$ $[M+H]^+$: 503.1114, found: 503.1135

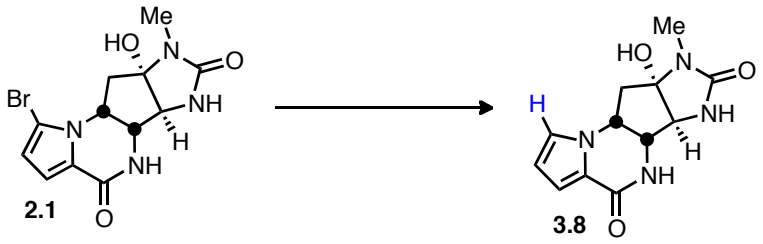

13-Debromo Agelastatin A (3.8). To a solution of agelastatin A **2.1** (6.7 mg, 19.6 µmol, 1.0 equiv) in 2:1 THF:H_2O (2.0 mL) was added triethylamine (15 µL, 108 µmol, 5.5 equiv) and 20 wt.% $Pd(OH)_2$ on carbon (4.1 mg, 5.9 µmol, 0.3 equiv). The reaction was purged with H_2 stirred under this atmosphere for 6h. The reaction mixture was then filtered through a celite plug washing with 20% methanol in DCM. The filtrate was concentrated *in vacuo* to give a white residue. The residue was purified by preparative TLC eluting and washing with 10% MeOH in CH_2Cl_2 to give 5.0 mg (97%) of **3.8** as a white solid: R_f = 0.12 (10% MeOH in DCM); IR (thin film): 3183, 2916, 1706, 1646 cm^{-1}; ^1H NMR (500 MHz; CD_3OD): δ 7.03 (dd, *J* = 2.5, 1.5 Hz, 1H), 6.89 (dd, *J* = 4.0, 1.5 Hz, 1H), 6.24 (dd, *J* = 4.0, 2.5 Hz, 1H), 4.66 (dt, *J* = 10.0, 6.0 Hz, 1H), 4.00 (dd, *J* = 5.0, 1.0 Hz, 1H), 3.81 (d, *J* = 1.0 Hz, 1H), 2.80 (s, 3H), 2.63 (dd, *J* = 13.0, 6.0 Hz, 1H), 2.28 (dd, *J* = 13.0, 10.0 Hz, 1H); ^{13}C NMR (125 MHz; CD_3OD): δ 162.1, 161.3, 125.6, 122.8, 115.4, 111.1, 95.8, 68.0, 62.9, 55.6, 41.6, 24.2; HRMS (+ESI) Calcd. for $C_{12}H_{15}N_4O_3$ $[M+H]^+$: 263.1144, found: 263.1130

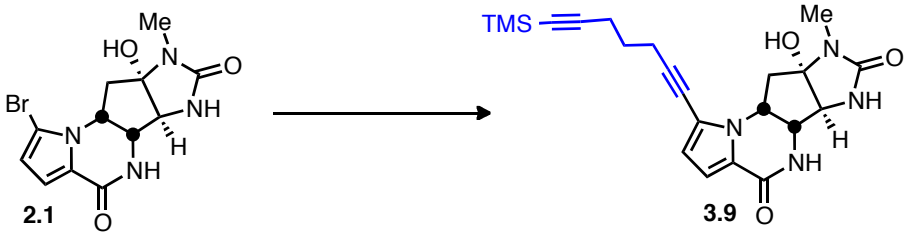

13-Alkynyl Agelastatin A (3.9). A solution of agelastatin A **3.5** (3.1 mg, 9.1 μmol, 1.0 equiv) in DMF/Et_3N (1.0 mL) was degassed by bubbling argon for 15 minutes. $Pd(PPh_3)_4$ (6.4 mg, 5.5 μmol, 0.6 equiv) was then added followed by bis-alkyne **3.6** (4.5 mg, 27.3 μmol, 3.0 equiv). The reaction was sealed under argon, stirred at 60 °C for 6h and concentrated *in vacuo* to give a yellow residue. The residue was purified by pipette flash column chromatography (SiO_2, 10→15% MeOH/DCM) providing 2.9 mg (75%) of 13-alkynyl agelastatin A **3.9** as a thin film: R_f = 0.22 (10% MeOH in DCM); IR (thin film): 3274, 2922, 1699, 1652 cm^{-1}; ^1H NMR (500 MHz; CD_3OD): δ 6.83 (d, *J* = 4.0 Hz, 1H), 6.37 (d, *J* = 4.0 Hz, 1H), 4.65 (dt, *J* = 12.0, 6.0 Hz, 1H), 4.07 (d, *J* = 5.5 Hz, 1H), 3.87 (s, 1H), 2.82 (s, 3H), 2.63 (dd, *J* = 13.5, 7.0 Hz, 1H), 2.61 (t, *J* = 7.0 Hz, 2H), 2.39 (t, *J* = 7.0 Hz, 2H), 2.13 (app t, *J* = 12.6 Hz, 1H), 1.79 (quintet, *J* = 7.0 Hz, 2H), 0.13 (s, 9H).; ^{13}C NMR (125 MHz; CD_3OD): δ 161.5, 161.3, 123.0, 119.9, 115.7, 114.8, 107.1, 96.5, 95.7, 86.0, 71.8, 67.5, 62.4, 53.8, 40.3, 28.9, 24.4, 19.7, 19.1, 0.2 (3C); HRMS (+ESI) Calcd. for $C_{22}H_{28}N_4O_3SiNa$ $[M+Na]^+$: 447.1828, found: 447.1845

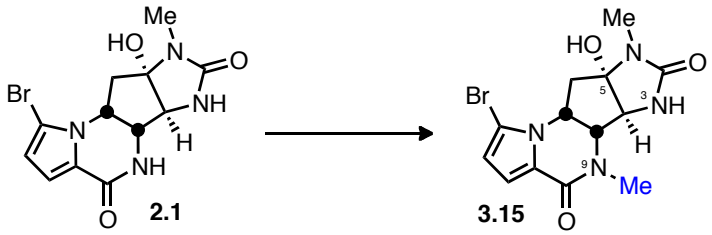

9-Methyl Agelastatin A (3.15). To a solution of agelastatin A **2.1** (2.0 mg, 5.9 μmol, 1.0 equiv) in anhydrous DMF (0.5 mL) was added LiHMDS (6.4 μL of 1.0 M solution in THF, 6.4 μmol, 1.1 equiv). After 30 min, TMSCl (5.9 μL of 1.0 M solution in THF, 5.9 μmol, 1.0 equiv) was added to the reaction mixture. After another 30 min of stirring, LiHMDS (6.4 μL of 1.0 M solution in THF, 6.4 μmol, 1.1 equiv) was added followed by MeI (11.7 μL of 0.5 M solution in THF, 5.9 μmol, 1.0 equiv) 30 minutes later. The reaction mixture was stirred for another 30 min before addition TBAF (41 μL, 41.0 μmol, 7.0 equiv). A 0.5 mL of saturated NH_4Cl solution was added 30 minutes later. The reaction mixture was then filtered through a short silica gel plug washing with 20% methanol in DCM. The filtrate was concentrated *in vacuo* to give a white residue. The residue was purified by preparative TLC eluting and washing with 10% MeOH in CH_2Cl_2 to give 1.5 mg (72%) of **3.15** as a white solid: R_f = 0.26 (10% MeOH in DCM); IR (thin film): 3248, 2925, 1691, 1632 cm^{-1}; ^1H NMR (500 MHz; CD_3OD): δ 6.89 (d, *J* = 4.0 Hz, 1H), 6.33 (d, *J* = 4.0 Hz, 1H), 4.70 (dt, *J* = 12.0, 6.0 Hz, 1H), 4.16 (s, 1H), 4.02 (d, *J* = 6.0 Hz, 1H), 3.14 (s, 3H), 2.81 (s, 3H), 2.66 (dd, *J* = 13.0, 6.5 Hz, 1H), 2.10 (dd, *J* = 13.0, 12.0 Hz, 1H); ^{13}C NMR (125 MHz; CD_3OD): δ 124.3, 116.1, 114.1,

106.4, 94.8, 68.6, 66.0, 54.2, 41.0, 24.2 (carbonyls missing); HRMS (-ESI) Calcd. for $C_{13}H_{14}BrN_4O_3$ [M-H]$^-$: 353.0249, found: 353.0233

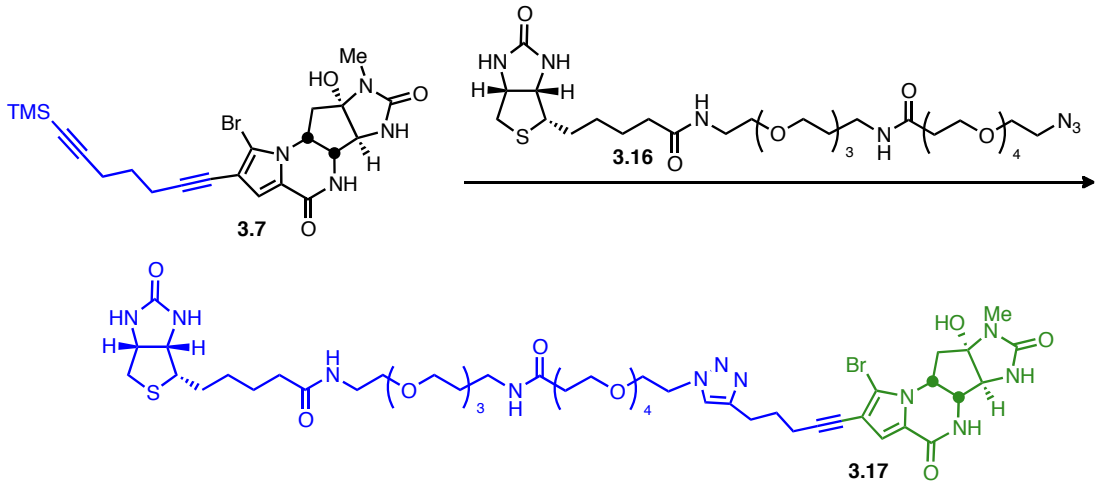

14-Alkynyl biotin Agelastatin A (3.17). To a solution of 14-alkynyl agelastatin A **3.7** (2.0 mg, 4.0 µmol, 1.0 equiv) in 2:1 THF:H_2O (1.0 mL) was added TBAF (20 µL, 20 µmol, 5.0 equiv) and stirred for 1 hour. A $CuSO_4$/sodium ascorbate stock solution (20µL, 1 µmol $CuSO_4$, 10 µmol sodium ascorbate, 0.25 equiv $CuSO_4$, 2.5 equiv sodium ascorbate) was then added. (The stock solution was made from mixing equal volumes of 0.1 M $CuSO_4 5H_2O$ and 1.0 M sodium ascorbate aqueous solutions, until the initial black color turned light yellow.) After stirring for 24h, the reaction mixture was filtered through a cotton plug washing with 2:1 THF:water. The filtrate was concentrated *in vacuo* to give a yellow residue. The residue was purified by preparative TLC eluting and washing with 20% MeOH in DCM to give 1.3 mg (28%) of **3.17** as a thin film: R_f = 0.21 (20% MeOH in DCM); ^{1}H NMR (500 MHz; CD_3OD): δ 7.86 (s, 1H), 6.92 (s, 1H),

4.61-4.56 (m, 1H), 4.55 (t, *J* = 5.0 Hz, 2H), 4.49 (dd, *J* = 8.0, 4.0 Hz, 1H), 4.30 (dd, *J* = 8.0, 4.5 Hz, 1H), 4.10 (d, *J* = 5.5 Hz, 1H), 3.88 (s, 1H) 3.88 (t, *J* = 5.0 Hz, 2H), 3.69 (t, *J* = 6.0 Hz, 2H) 3.65-3.61 (m, 4H), 3.61-3.55 (m, 16H), 3.51 (td, *J* = 6.0, 3.0 Hz, 4H), 3.25 (t, *J* = 7.0 Hz, 4H), 3.22-3.17 (m, 1H), 2.92 (dd, *J* = 13.0, 5.0 Hz, 1H), 2.90 (t, *J* = 8.0 Hz, 2H), 2.81 (s, 3H), 2.69 (s, 1H), 2.70 (d, *J* = 13.0 Hz, 1H), 2.67 (dd, *J* = 12.0, 6.0 Hz, 1H), 2.46 (t, *J* = 6.0 Hz, 2H), 2.41 (t, *J* = 6.0 Hz, 2H), 2.20 (t, *J* = 7.0 Hz, 2H), 2.11 (app t, *J* = 13.0 Hz, 2H), 2.03 (m, 1H), 2.07 (quintet, *J* = 7.5 Hz, 2H), 1.75 (app ddt, *J* = 13.0, 6.5, 2.0 Hz, 4H), 1.55-1.71 (m, 4H), 1.43 (m, 2H); ^{13}C NMR (125 MHz; CD_3OD): δ 176.0, 173.9, 161.4, 160.4, 148.1, 124.3, 123.7, 117.6, 111.3, 110.6, 95.6, 92.9, 74.3, 71.59, 71.54, 71.51, 71.47, 70.4, 69.98, 69.88, 68.3, 67.4, 63.4, 62.0, 61.6, 57.0, 54.9, 51.4, 41.1, 39.9, 37.86, 37.83, 37.77, 36.9, 30.8, 30.4, 30.3, 29.8, 29.5, 26.9, 25.3, 24.3, 19.5; HRMS (-ESI) Calcd. for $C_{50}H_{76}BrN_{11}O_{13}K$ $[M+K]^+$: 1188.4165, found: 1188.4216

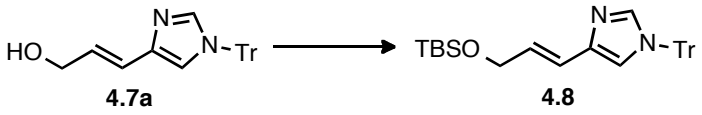

4.7a **4.8**

Silyl ether (4.8): To a solution of alcohol **4.7a** (3.0 g, 8.19 mmol) in 40 mL of DMF were added imidazole (5.58 g, 81.9 mmol) and TBSCl (1.60 g, 10.64 mmol) at 0 °C. The resulting solution was stirred for 30 min at 0 °C and allowed to warm to 25 °C for another 30 min, then it was diluted with 100 mL of Et_2O and 100 mL of H_2O. The organic phase was separated and the aqueous layer was extracted with 50 mL of Et_2O twice. The combined organic layer was dried over $MgSO_4$ and concentrated *in vacuo* to

leave a residue, which was purified by column chromatography on silica gel (gradient elution: 15:1→5:1 hexanes/EtOAc) to afford silyl ether **4.8** (3.09 g, 78%): IR (thin film): 3059, 3029, 2955, 2931, 2854, 2360, 1495, 1445, 1247, 1111 cm^{-1}; ^1H NMR (500 MHz, $CDCl_3$) δ 0.08 (s, 6H), 0.91 (s, 9H), 4.31 (d, J = 3.5 Hz, 2H), 6.40 (dt, J = 16, 4.5 Hz, 1H), 6.44 (d, J = 16 Hz, 1H), 6.74 (d, J = 1.5 Hz, 1H), 7.12–7.18 (m, 6H), 7.30–7.36 (m, 9H), 7.39 (d, J = 1 Hz, 1H); ^{13}C NMR (125 MHz, $CDCl_3$) δ –4.9, 18.8, 26.3, 64.0, 75.5, 119.3, 121.4, 127.9, 128.4, 130.1, 139.3, 139.4, 142.6; HRMS (ESI): Calcd for $C_{31}H_{36}N_2OSi$ [M+H]: 481.2675. Found: 481.2670.

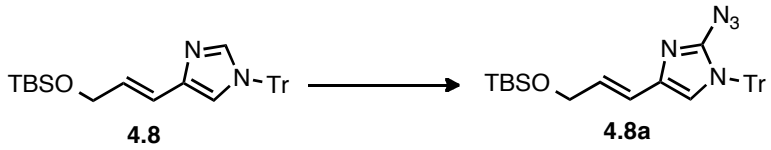

Azidoimidazole (4.8a): To a solution of **4.8** (6.30 g, 13.11 mmol) in 200 mL of THF was added *n*-BuLi (2.50 M in hexane, 6.29 mL) dropwise at –78 °C. After being stirred at the same temperature for 1 h, TsN_3 (3.88 mg, 19.67 mmol) in 20 mL of THF was added dropwise. The reaction was stirred for another 20 min at –78 °C, and diluted with 400 mL of EtOAc and 400 mL of saturated NH_4Cl. The organic layer was separated and the aqueous phase was extracted with 100 mL of EtOAc twice. The combined organic phase was dried over $MgSO_4$ and concentrated *in vacuo* to leave a residual oil, which was purified by column chromatography on silica gel (gradient elution: 20:1→10:1 hexanes/EtOAc) to furnish azidoimidazole **4.8a** (6.43 g, 94%): IR (thin film): 2955, 2366, 21334, 1495, 1418, 1250 cm^{-1}; ^1H NMR (500 MHz, $CDCl_3$) δ 0.09 (s, 6H), 0.93

(s, 9H), 4.31 (d, J = 3 Hz, 2H), 6.32–6.42 (m, 2H), 6.58 (s, 1H), 7.12–7.18 (m, 6H), 7.29–7.36 (m, 9H); ^{13}C NMR (125 MHz, $CDCl_3$) δ –4.9, 18.8, 26.3, 63.8, 75.3, 118.2, 120.6, 128.0, 128.1, 128.2, 130.0, 136.2, 142.1, 142.6; HRMS (ESI): Calcd for $C_{31}H_{35}N_5OSi$ [M+H]: 522.2689. Found: 522.2610.

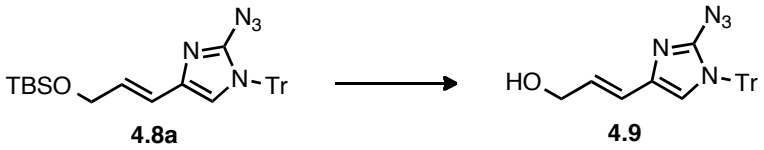

Alcohol (4.9): To a solution of **4.8a** (30 mg, 0.058 mmol) in 1.0 mL of THF was added TBAF (1.0 M in THF, 0.17 mL) at 0°C. The resulting solution was stirred for 1 h and diluted with 5 mL of EtOAc and 5 mL of saturated NH_4Cl. The organic phase was separated and the aqueous phase was extracted with 10 mL of EtOAc twice. The combined organic phase was dried over $MgSO_4$ and concentrated *in vacuo* to leave a residual oil, which was purified by column chromatography on silica gel (gradient elution: 10:1→3:1 hexanes/EtOAc) to provide alcohol **14** (24 mg, quant.): IR (thin film): 3062, 3032, 2925, 2360, 2132, 1489, 1415 cm^{-1}; ^{1}H NMR (500 MHz, $CDCl_3$) δ 1.90 (br s, 1H), 4.27 (d, J = 5.5 Hz, 2H), 6.37 (dt, J = 15.5, 1 Hz, 1H), 6.45 (dt, J = 15.5, 5,5 Hz, 1H), 6.61 (s, 1H), 7.13–7.19 (m, 6H), 7.31–7.37 (m, 9H); ^{13}C NMR (125 MHz, $CDCl_3$) δ 63.7, 75.4, 118.7, 122.4, 127.6, 128.1, 128.2, 130.0, 135.7, 141.9, 142.8; HRMS (ESI): Calcd for $C_{25}H_{21}N_5O$ [M+Li]: 414.1906. Found: 414.1900.

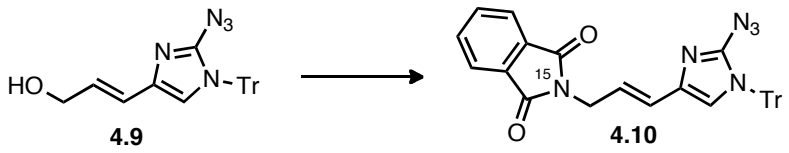

Phthalimide (4.10): To a solution of alcohol **4.9** (1.25 g, 3.07 mmol) and LiCl (0.65 g, 15.34 mmol) in 20 mL of THF were added Et_3N (4.31 mL, 30.7 mmol) and MsCl (0.285 mL, 3.68 mmol) dropwise sequentially at –50 °C. The resulting solution was stirred for 1 h at the same temperature and diluted with 30 mL of EtOAc and 30 mL of saturated $NaHCO_3$. The organic phase was separated and the aqueous phase was extracted with 30 mL of EtOAc twice. The combined organic phase was dried over $MgSO_4$ and concentrated *in vacuo* to provide a crude product, which was used for the next reaction without further purification.

A solution of allylic chloride prepared above and ^{15}N potassium phthalimide (572 mg, 3.07 mmol) in 8.0 mL of DMF was stirred for 10 h at 25 °C. Then 20 mL of Et_2O and 30 mL of H_2O were added to dilute the reaction mixture. The organic phase was separated and the aqueous layer was extracted with 20 mL of Et_2O twice. The combined organic layer was dried over $MgSO_4$ and concentrated *in vacuo* to leave a residue, which was purified by column chromatography on silica gel (gradient elution: 10:1→3:1 hexanes/EtOAc) to furnish phthalimide **4.10** (692 mg, 42% from **4.9**): IR (thin film): 2363, 2342, 2132, 1712, 1489, 1418 cm^{-1}; ^1H NMR (500 MHz, $CDCl_3$) δ 4.39 (d, J = 6 Hz, 2H), 6.29 (dt, J = 15.5, 5.5 Hz, 1H), 6.39 (d, J = 15.5 Hz, 1H), 6.57 (s, 1H), 7.08–7.18 (m, 15H), 7.64–7.85 (m, 4H); ^{13}C NMR (125 MHz, $CDCl_3$) δ 39.6 (d, $J_{C\text{-}N}$ = 95

Hz), 78.4, 119.2, 121.3, 123.9, 125.5(d, $J_{C\text{-}N}$ = 21 Hz), 128.1, 128.2, 129.9, 132.4 (d, $J_{C\text{-}N}$ = 75 Hz), 134.2, 134.6, 135.2, 141.9, 168.2 (d, $J_{C\text{-}N}$ = 133 Hz) ; HRMS (ESI): Calcd for $C_{33}H_{24}N_5{}^{15}NO_2$ [M+Li]: 544.2091. Found: 544.2131.

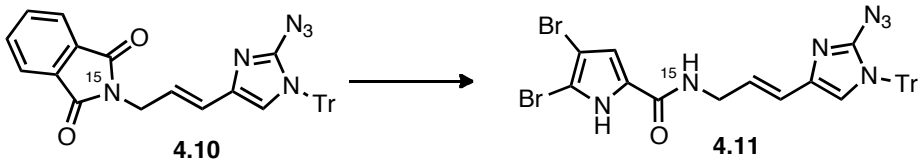

4.10 **4.11**

Pyrrole-2-carboxylate ester (4.11): To a solution of **4.10** (30 mg, 0.056 mmol) in 2.0 mL of EtOH was added NH_2NH_2 (0.035 mL, 1.12 mmol). The resulting solution was stirred for 2 h at 50 °C during which time a white precipitate appeared. The reaction mixture was cooled to 25 °C and diluted with 10 mL CH_2Cl_2. The mixture was filtered with CH_2Cl_2 through a pad of Celite. The filtrate was concentrated *in vacuo* to obtain crude amine **4.10a**, which was used for the next reaction without further purification.

To a solution of crude allyl amine **4.10a** prepared above in 0.5 mL of DMF were added Na_2CO_3 (30 mg, 0.28 mmol) and 4,5-dibromo-2-trichloroacetylpyrrole (62 mg, 0.17 mmol). The resulting mixture was stirred for 6 h at 25 °C and diluted with 20 mL of Et_2O and 30 mL of H_2O. The organic phase was separated and the aqueous layer was extracted with 20 mL of Et_2O twice. The combined organic layer was dried over $MgSO_4$ and concentrated *in vacuo* to leave a residue, which was purified by column chromatography on silica gel (gradient elution: 10:1→3:1 hexanes/EtOAc) to obtain **4.11** (29 mg, 78% from **4.10**): IR (thin film) 2339, 2132, 1632, 1429, 1421 cm^{-1}; ^1H

NMR (500 MHz, $CDCl_3$) δ 4.16 (s, 2H), 6.32 (S, 1H), 6.52 (s, 1H), 6.58 (s, 1H), 7.10–7.18 (m, 6H), 7.28–7.38 (m, 9H), 11.0 (br s, 1H); ^{13}C NMR (125 MHz, $CDCl_3$) δ 41.7 (d, $J_{C\text{-}N}$ = 106 Hz), 75.5, 99.9, 106.2, 112.2, 119.0, 123.5, 124.3 (d, $J_{C\text{-}N}$ = 15 Hz), 128.2, 128.3, 129.9, 135.3, 141.9. 143.1, 159.6 (d, $J_{C\text{-}N}$ = 175 Hz); HRMS (ESI): Calcd for $C_{30}H_{23}N_6{}^{15}NO$ [M+Li]: 665.0441. Found: 665.0499.

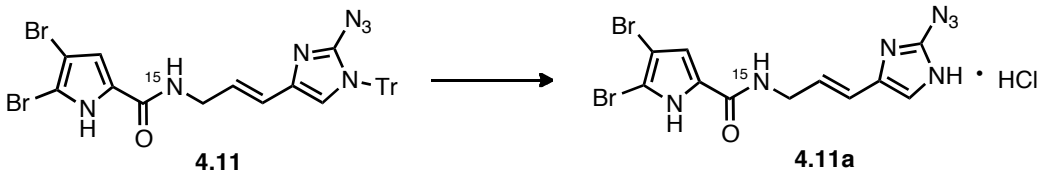

^{15}N-azido-oroidin (4.11a): To a solution of **4.11** (380 mg, 0.58 mmol) in 20 mL of EtOAc was added HCl, which was prepared by addition of AcCl (2.06 mL, 28.9 mmol) to MeOH (1.17 mL, 28.9 mmol) dropwise at 0 °C. The solution was stirred for 1.5 h at 25 °C and during that time there was some precipitate formed. The reaction mixture was filtered to separate the solid product of azidoimidazole hydrochloride salt (240 mg, quant.), which was of sufficient pure for the next reaction: IR (thin film) 3115, 233, 2150, 1611, 1555, 1439 cm^{-1}; ^1H NMR (500 MHz, CD_3OD) δ 4.11 (d, J = 5 Hz, 2H), 6.35 (dt, J = 16, 3.5 Hz, 1H), 6.43 (d, J = 16 Hz, 1H), 6.89 (d, J = 2 Hz, 1H), 7.31 (s, 1H); ^{13}C NMR (125 MHz, CD_3OD) δ 42.3 (d, $J_{C\text{-}N}$ = 114 Hz), 100.8, 107.3, 115.2, 116.3, 117.5 (d, $J_{C\text{-}N}$ = 22.5 Hz), 129.4 (d, $J_{C\text{-}N}$ = 106 Hz), 131.8, 132.3, 142.6, 162.4 (d, $J_{C\text{-}N}$ = 174 Hz); HRMS (ESI): Calcd for $C_{11}H_9Br_2N_6{}^{15}NO$ [M+H]: 416.9163. Found: 416.9171.

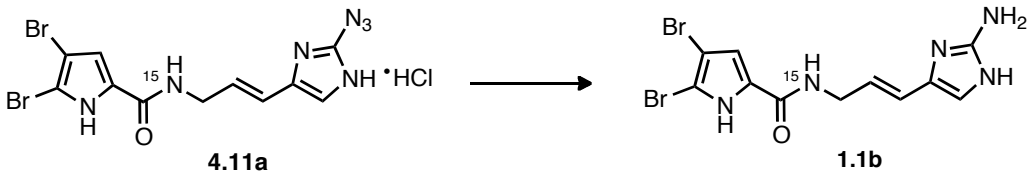

^{15}N-oroidin (1.1b): To a solution of azidoimidazole hydrochloride salt **4.11a** (210 mg, 0.50 mmol) in 30 mL of MeOH/EtOAc (1 : 1) was added Lindlar catalyst (100 mg, 5% Pd on $CaCO_3$, poisioned with Pb). The resulting mixture was stirred under atmospheric hydrogen at 25 °C for 6 h then filtered with MeOH through a pad of Celite. The filtrate was concentrated *in vacuo* to leave a residue, which was purified on column chromatography on silica gel (gradient elution: 10:1:0→1:1:0.01 CH_2Cl_2/MeOH/NH_4OH) to furnish ^{15}N-oroidin **1.1b** (165 mg, 84%): IR (thin film): 3304, 2363, 2339, 1620, 1507, 1415 cm^{-1}; ^{1}H NMR (500 MHz, CD_3OD) δ 4.00 (d, J = 6 Hz, 2H), 5.87 (dt, J = 16, 6 Hz, 1H), 6.30 (d, J = 16 Hz, 1 H), 6.47 (s, 1H), 6.83 (d, J = 1 Hz, 1H); ^{13}C NMR (125 MHz, CD_3OD) δ 43.1 (d, $J_{C\text{-}N}$ = 106 Hz), 100.7, 107.0, 115.1, 118.5, 122.2, 123.6 (d, $J_{C\text{-}N}$ = 15 Hz), 129.7 (d, $J_{C\text{-}N}$ = 99 Hz), 132.2, 152.8, 162.4 (d, $J_{C\text{-}N}$ = 175 Hz); ^{15}N NMR (CD_3SOCD_3) δ –272.8 (relative to $MeNO_2$); HRMS (ESI): Calcd for $C_{11}H_{11}Br_2N_4{}^{15}NO$ [M+H]: 390.9258. Found: 390.9289.

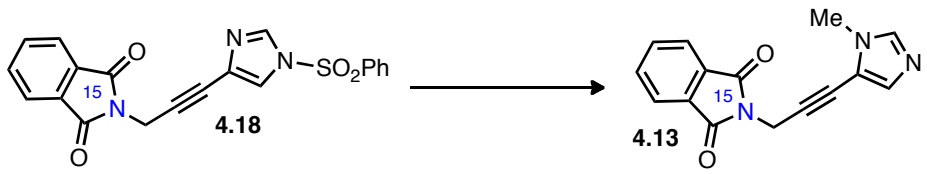

N-Methyl Propargyl phthalimide (4.13). To a solution of **4.18** (970 mg, 2.47 mmol, 1.0 equiv) in DCM was added BF_4OMe_3 (404 mg, 2.60 mmol, 1.05 equiv) in a glove box. The reaction mixture was stired for 3.5 h followed by addition of 15mL of methanol. After 30 min, the mixture was concentrated *in vacuo* to give a yellow residue. The residue was purified by flash column chromatography (SiO_2, 30→50% EtOAc/Hexanes) to deliver 343.6 mg (52%) of adduct **4.13** as off-white solids: ^{1}H NMR (500 MHz; $CDCl_3$): δ 7.89 (dd, J = 5.5, 3.0 Hz, 2H), 7.75 (dd, J = 5.5, 3.0 Hz, 2H), 7.40 (s, 1H), 7.23 (s, 1H), 4.71 (d, J = 1.0 Hz, 2H), 3.65 (s, 3H).; ^{13}C NMR (125 MHz; CD_3OD): δ 167.2 (d, $J_{C\text{-}N}$ = 12.5 Hz), 138.5, 135.1, 134.4, 132.1 (d, $J_{C\text{-}N}$ = 8.1 Hz),, 123.8, 115.4, 90.3, 71.6, 32.2, 28.1 (d, $J_{C\text{-}N}$ = 11.6 Hz)

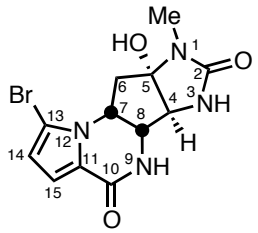

agelastatin A (**2.1**)

Table S1. Comparison of ^{1}H NMR data of natural and synthetic agelastatin A in CD_3OD.

Assignment	**natural**[3] (300 MHz) δ (ppm) (multiplicity, *J* in Hz, #H)	**synthetic** (500 MHz, this work) δ (ppm) (multiplicity, *J* in Hz, #H)
C15-H	6.92 (br d, *J* = 4.2 Hz, 1H)	6.91 (d, *J* = 4.0 Hz, 1H)
C14-H	6.33 (d, *J* = 4.2 Hz, 1H)	6.33 (d, *J* = 4.0 Hz, 1H)
C7-H	4.60 (m, *J* = 12.3, 6.6, 5.4 Hz, 1H)	4.60 (app dt, *J* = 12.0, 6.0 Hz, 1H)
C8-H	4.09 (br d, *J* = 5.4 Hz, 1H)	4.09 (d, *J* = 5.5 Hz, 1H)
C4-H	3.89 (br s, 1H)	3.88 (s, 1H)
N1-Me	2.81 (s, 3H)	2.81 (s, 3H)
C6-Hα	2.65 (br dd, *J* = 12.9, 6.6 Hz, 1H)	2.65 (dd, *J* = 13.0, 6.5 Hz, 1H)
C6-Hβ	2.10 (br t, *J* = 12.9 Hz, 1H)	2.10 (app t, *J* = 13.0 Hz, 1H)

[3] D'Ambrosio, A. Guerriero, C. Debitus, O. Ribes, J. Pusset, S. Leroy, F. Pietra, *J. Chem. Soc., Chem. Commun*. **1993**, *16*, 1305-1306.

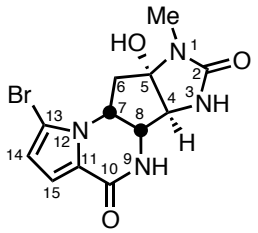

agelastatin A (**2.1**)

Table S2. Comparison of ^{13}C NMR data of natural and synthetic agelastatin A in CD_3OD.

	natural[3] (δ in ppm, 75MHz)	**synthetic** (Hale)[4] (δ in ppm, 125 MHz)	**synthetic** (Du Bois)[5] (δ in ppm, 125 MHz)	**synthetic** (this work) (δ in ppm, 125 MHz)
C2	163.00	161.4	161.4	161.4
C10	162.65	161.1	161.1	161.1
C11	125.71	124.1	124.1	124.1
C15	117.59	116.0	116.0	116.0
C14	115.37	113.8	113.8	113.8
C13	108.80	107.2	107.3	107.3
C5	97.24	95.6	95.6	95.7
C4	68.98	67.4	67.4	67.4
C8	63.76	62.2	62.2	62.2
C7	55.96	54.3	54.4	54.4
C6	41.58	40.0	40.0	40.0
N1-Me	25.79	24.2	24.2	24.2

[4] M. M. Domostoj, E. Irving, F. Scheinmann, K. J. Hale, *Org. Lett.* **2004**, *6*, 2615-2618.

[5] P. M. Wehn, B. J. Du Bois, *Angew. Chem., Int. Ed.* **2009**, *48*, 3802-3805

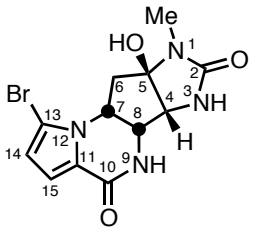

4,5-bis-*epi*-agelastatin A (**2.102**)

Table S3. Comparison of ^{1}H NMR data of 4,5-bis-*epi*-agelastatin A in CD_3OD.

Assignment	**Pietra's report**[6] (300 MHz) δ (ppm) (multiplicity, *J* in Hz, #H)	**this work** (500 MHz) δ (ppm) (multiplicity, *J* in Hz, #H)
C15-H	6.90 (d, *J* = 4.2 Hz, 1H)	6.90 (d, *J* = 4.0 Hz, 1H)
C14-H	6.33 (d, *J* = 4.2 Hz, 1H)	6.33 (d, *J* = 4.0 Hz, 1H)
C7-H	5.00 (ddd, *J* = 10.5, 6.9, 5.4 Hz, 1H)	5.00 (ddd, *J* = 10.5, 7.0, 5.0 Hz, 1H)
C8-H	4.43 (t, *J* = 5.4 Hz, 1H)	4.42 (app t, *J* = 5.5 Hz, 1H),
C4-H	4.02 (d, *J* = 5.4 Hz, 1H)	4.01 (d, *J* = 6.0 Hz, 1H)
N1-Me	2.73 (s, 3H)	2.73 (s, 3H)
C6-H'	2.53 (dd, *J* = 13.2, 6.9 Hz, 1H)	2.52 (dd, *J* = 13.0, 7.0 Hz, 1H)
C6-H''	2.26 (dd, *J* = 13.2, 10.5 Hz, 1H)	2.26 (dd, *J* = 13.0, 10.5 Hz, 1H)

[6] M. D'Ambrosio, A. Guerriero, M. Ripamonti, C. Debitus, J. Waikedre, F. Pietra, *Helv. Chim. Acta* **1996**, *79*, 727-735.

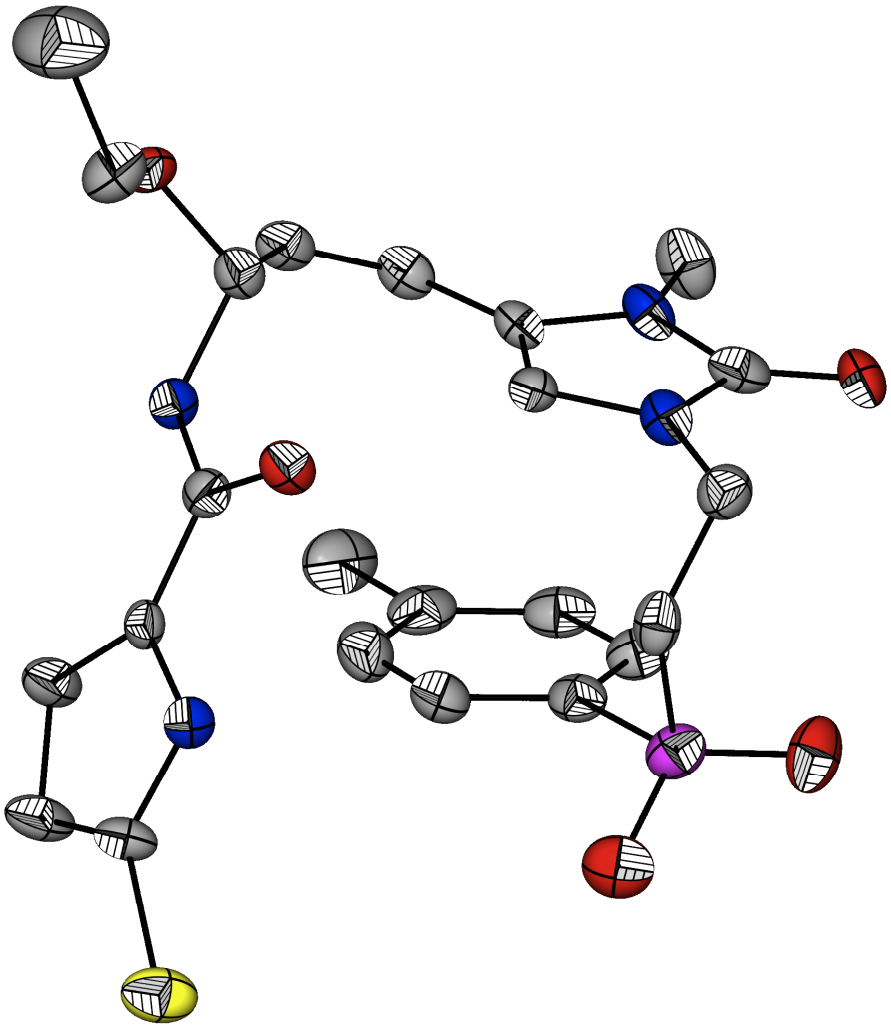

Figure S1. Single crystal X-ray structure (ORTEP) of cyclization precursor **2.84**

Crystal data and structure refinement for 2.84.

Identification code	drbm	
Empirical formula	C22 H25 Br N4 O6 S	
Formula weight	553.43	
Temperature	110(2) K	
Wavelength	1.54178 Å	
Crystal system	Monoclinic	
Space group	P2(1)/n	
Unit cell dimensions	a = 14.4647(7) Å	a= 90°.
	b = 11.6582(5) Å	b= 104.740(4)°.
	c = 14.8181(7) Å	g = 90°.
Volume	2416.58(19) $Å^3$	
Z	4	
Density (calculated)	1.521 Mg/m^3	
Absorption coefficient	3.522 mm^{-1}	
F(000)	1136	
Crystal size	0.40 x 0.12 x 0.08 mm^3	
Theta range for data collection	3.81 to 60.00°.	
Index ranges	-15<=h<=15, -11<=k<=12, -15<=l<=16	
Reflections collected	33741	
Independent reflections	3444 [R(int) = 0.0798]	
Completeness to theta = 60.00°	96.4 %	
Absorption correction	Semi-empirical from equivalents	
Max. and min. transmission	0.7659 and 0.3331	
Refinement method	Full-matrix least-squares on F^2	
Data / restraints / parameters	3444 / 17 / 338	
Goodness-of-fit on F^2	1.073	
Final R indices [I>2sigma(I)]	R1 = 0.0708, wR2 = 0.2153	
R indices (all data)	R1 = 0.0932, wR2 = 0.2605	
Extinction coefficient	0.0029(5)	
Largest diff. peak and hole	0.860 and -1.350 $e.Å^{-3}$	

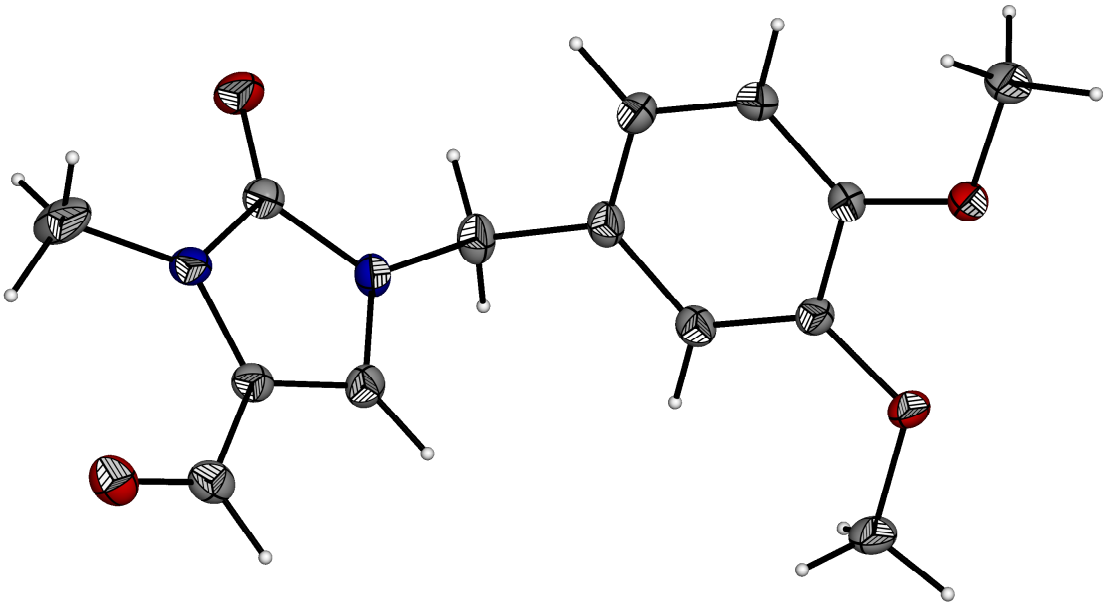

Figure S2. Single crystal X-ray structure (ORTEP) of DMB aldehyde **2.58b**

Crystal data and structure refinement for 2.58b

Identification code	drb1005	
Empirical formula	C14 H16 N2 O4	
Formula weight	276.29	
Temperature	110(2) K	
Wavelength	0.71073 Å	
Crystal system	Monoclinic	
Space group	P2(1)/c	
Unit cell dimensions	a = 11.146(3) Å	a= 90°.
	b = 15.768(5) Å	b= 108.066(4)°.
	c = 8.036(2) Å	g = 90°.
Volume	1342.7(7) $Å^3$	
Z	4	
Density (calculated)	1.367 Mg/m^3	
Absorption coefficient	0.101 mm^{-1}	
F(000)	584	
Crystal size	0.40 x 0.30 x 0.06 mm^3	
Theta range for data collection	1.92 to 27.51°.	
Index ranges	-14<=h<=14, -20<=k<=20, -10<=l<=10	
Reflections collected	15135	
Independent reflections	3075 [R(int) = 0.0435]	
Completeness to theta = 27.51°	99.4 %	
Absorption correction	Semi-empirical from equivalents	
Max. and min. transmission	0.9939 and 0.9606	
Refinement method	Full-matrix least-squares on F^2	
Data / restraints / parameters	3075 / 0 / 181	
Goodness-of-fit on F^2	1.026	
Final R indices [I>2sigma(I)]	R1 = 0.0402, wR2 = 0.0978	
R indices (all data)	R1 = 0.0579, wR2 = 0.1104	
Largest diff. peak and hole	0.270 and -0.226 $e.Å^{-3}$	

TD-DFT Calculations of *N*-acyliminium 2.87

Herein, we aim to provide rationalization of the observed deep red color during the first cyclization event (**2.84→2.88**), which we propose to be due to the formation of *N*-acyliminium **2.87**, the most likely intermediate formed in solution prior to nucleophilic quenching. To this end, we obtained a UV-VIS spectrum of the reaction mixture as illustrated in figure S3. Four absorption bands were identified and for the most part we are interested in band 4, which confirms absorption in the blue-green region of the visible spectrum and accounts for the red color observed.

Figure S3. UV-Vis spectrum of the reaction (**2.84→2.88**) in CH_2Cl_2.

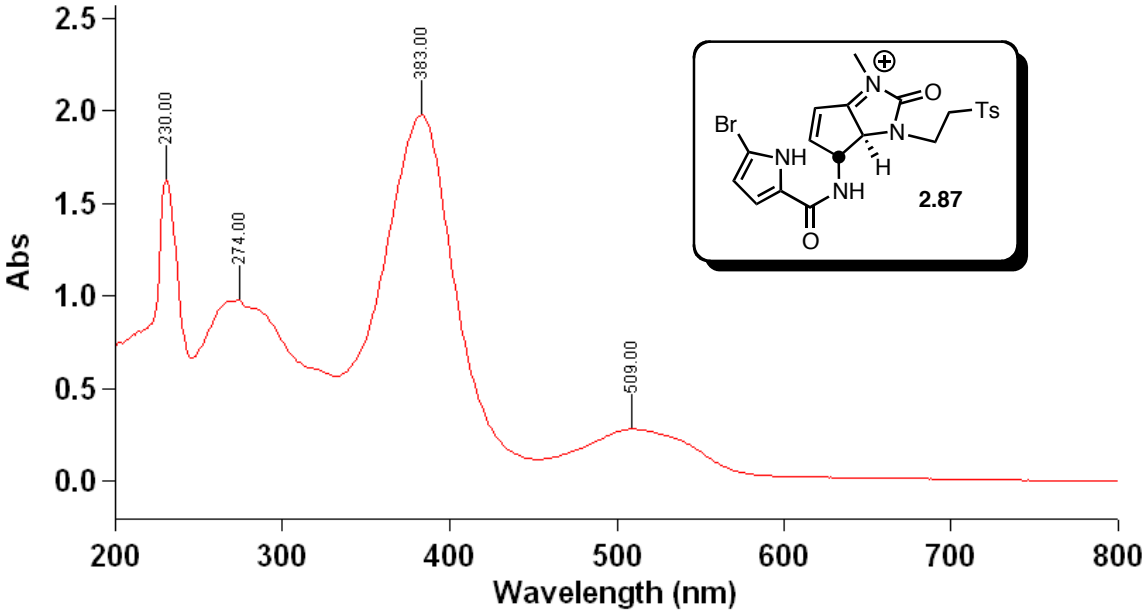

Table S4. Absorbance maxima of tosyl and pyrrole moieties in dichloromethane.

	Compound	Absorbance maxima (nm)	
		Experimental	B3LYP/6-31+G(d)
1	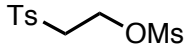	229	224
2	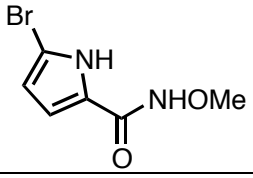	261	261
3	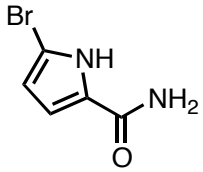	273	273

We then turned to Time-Dependent Density Functional Theory (TD-DFT) to predict the excited states of the proposed intermediate **2.87**. TD-DFT is the most widely used *ab initio* tool for modeling vertical excitations. At the outset, we sought to identify absorption bands due to the aromatic pyrrole and tosyl moieties of **2.87** and assess the utility of TD-DFT. For this purpose, calculations were performed on simpler sub-structures listed in table S4 and the results show remarkable agreement of experimental and calculated absorption maxima. These results allowed us to assign bands 1 and 2 as the corresponding tosyl-ethyl and bromopyrrole amide moieties, respectively, of intermediate **2.87**.

As anticipated, TD-DFT-predicted electronic spectra of proposed intermediate **2.87** also showed four absorption bands that were in good agreement the experimental results (see Table S5). This provides further verification of **2.87** as the intermediate formed in solution during the first cyclization. Figure S4 shows the comparative estimation of the accuracy of the calculated results versus the experimental values. Since the quality of obtained results is highly functional dependent, several functionals were screened. B3LYP and X3LYP hybrid functionals gave the best fit while larger basis sets provided minimal variation. While band 3 was least accurately predicted, it is still within error observed in TD-DFT calculations of other organic systems. Larger deviations are usually observed with charged species. [7]

Table S5. Experimental versus TD-DFT predicted absorption bands.

Absorption maxima (nm)				
	Band 1	**Band 2**	**Band 3**	**Band 4**
experimental	230	274	383	509
B3LYP*	226	281	340	527
X3LYP*	225	280	332	509

*6-31+G(d) (solvent=dichloromethane)

[7] D. Jacquemin, E. A. Perpete, G. E. Scuseria, I. Ciofoni, C. Adamo, *J. Chem. Theory Comput.* **2008**, *4*, 123-135.; D. Jacquemin, V. Wathelet, E. A. Perpete, C. Adamo, *J. Chem. Theory Comput.* **2009**, *5*, 2420-2435.

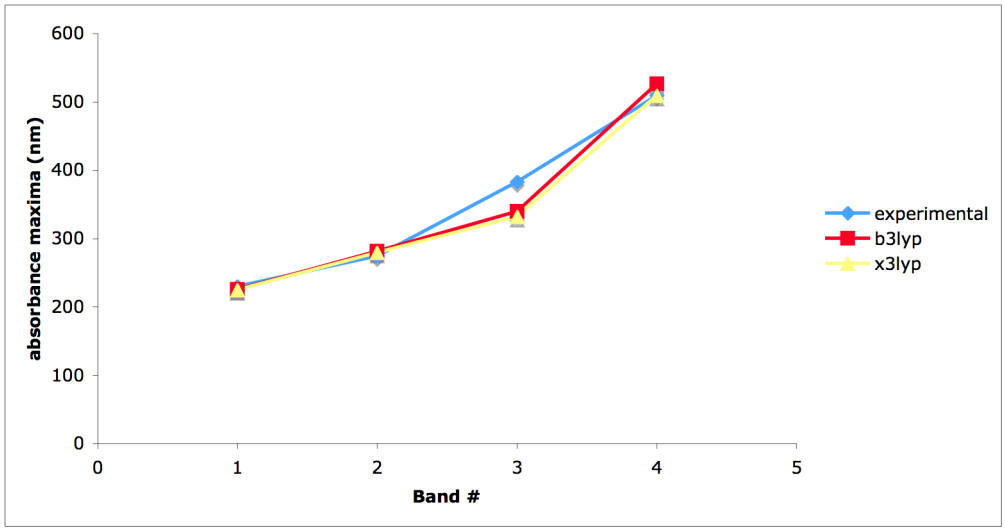

Figure S4. Experimental versus TD-DFT predicted absorption bands.

Visualized in table S6 are the orbital pairs involved in each excited state. These orbital portraits, respectively, further confirm the initial assignment of bands 1 and 2 as the tosyl-ethyl and bromopyrrole amide moieties. Band 3 is shown to be a $\pi \rightarrow \pi^*$ transition involving π orbitals of the amide bond to the π^* orbitals of the acyliminium moiety. Most importantly, band 4, which is responsible for the red color of intermediate **2.87**, is revealed to be a $\pi \rightarrow \pi^*$ transition between the HOMO (composed mostly of orbital contributions from the bromopyrrole amide moiety) and the LUMO (composed mostly of orbital contributions from the acyliminium moiety).

Table S6. Orbital pairs involved in each transition.

	Occupied MO*	Unoccupied MO*
Band 1 (230 nm)	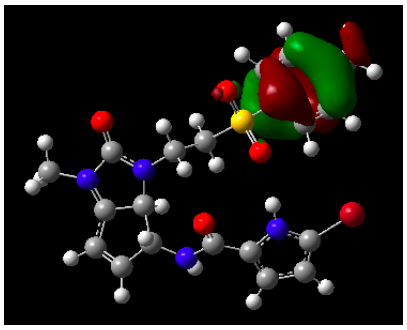	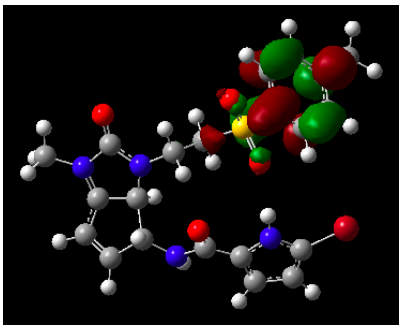
Band 2 (274 nm)	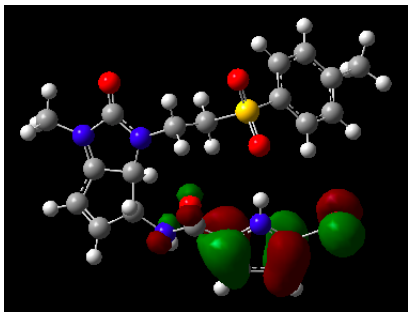	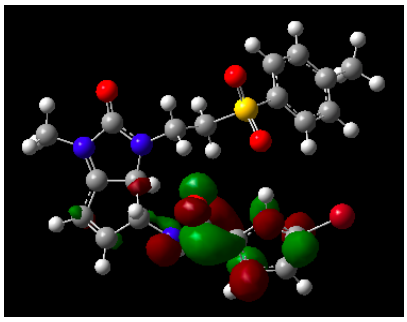
Band 3 (383 nm)	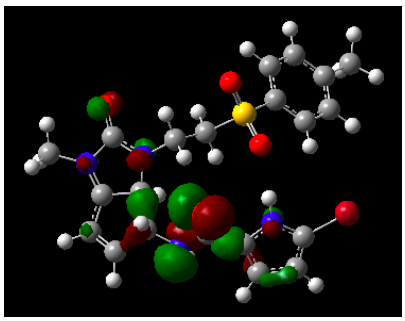	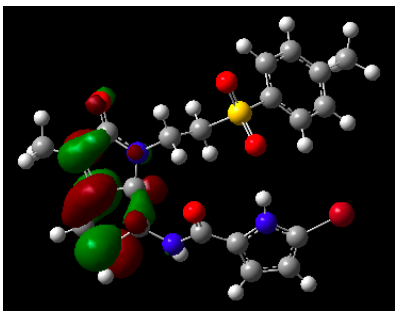

*isovalue for surface = 0.04

Table S6. Continued.

	Occupied MO*	Unoccupied MO*
Band 4 (509 nm)	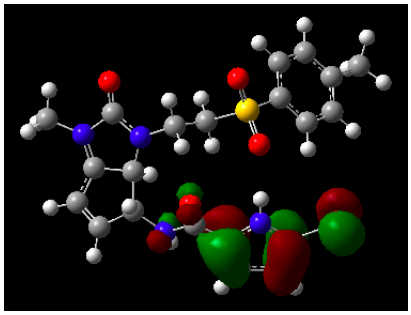	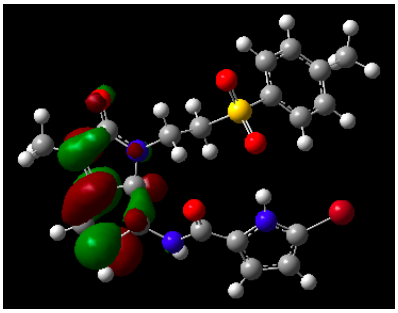

*isovalue for surface = 0.04

Computational Methods

All structures were optimized in the gas phase. For geometry and frequency optimizations, the B3LYP level of theory with the 6-31+G(d) basis set was employed and no symmetry constraints were imposed. Time-Dependent Density Functional Theory (TD-DFT) single point calculations were performed on the optimized structures to obtain calculated absorption bands. Solvation was performed using the scrf keyword which defaults to a Polarizable Continuum Model (PCM) of solvation. Dichloromethane was employed as solvent to closely mimic our experimental results. All calculations were done within the Gaussian 09 program.

The following input files gave the corresponding output below for the excitations within the TD-DFT method.

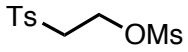

Input File:

%chk=g09.chk
#p td scrf=(solvent=dichloromethane) b3lyp/6-31+G(d) pop=full gfinput

TSeOMs

0 1

C	-8.958866	-2.719394	1.390920
C	-7.459873	-2.730552	1.204949
C	-6.773233	-1.564602	0.831297
C	-5.393169	-1.572841	0.627251
C	-4.689851	-2.766440	0.804783
S	-2.910203	-2.789214	0.559938
C	-2.234929	-2.439050	2.223311
C	-0.706960	-2.495916	2.181412
O	-0.136960	-1.934967	3.394859
S	-0.170957	-2.870394	4.755401
C	1.197378	-2.072719	5.600351
O	0.182065	-4.243714	4.390586
O	-1.412993	-2.610559	5.484296
O	-2.544536	-1.648184	-0.302243
O	-2.505412	-4.162434	0.204370
C	-5.345674	-3.944503	1.171073
C	-6.725569	-3.915702	1.371259
H	-9.469539	-2.968932	0.451046
H	-9.316993	-1.733704	1.706178
H	-9.275283	-3.453675	2.139332
H	-7.325943	-0.638372	0.691909
H	-4.868628	-0.673721	0.318710
H	-2.656634	-3.178957	2.908628
H	-2.581475	-1.440532	2.503370
H	-0.342992	-3.516313	2.042128
H	-0.312208	-1.854689	1.391539
H	1.273950	-2.550126	6.580013
H	2.106305	-2.228618	5.017977
H	0.966868	-1.011464	5.706471
H	-4.785197	-4.867899	1.281167
H	-7.240769	-4.830295	1.655580

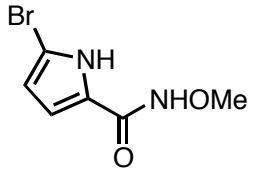

Input File:

%chk=g09.chk
#p td scrf=(solvent=dichloromethane) b3lyp/6-31+G(d) pop=full gfinput

BrPyCONHOMe

0 1

O	5.139733	-0.809091	0.661133
C	4.066531	-0.311128	0.331798
N	2.918015	-1.063406	0.117706
O	2.875902	-2.320402	0.733719
C	3.289795	-3.342566	-0.184046
C	3.939850	1.126779	0.051265
C	2.911856	1.973410	-0.352821
C	3.440908	3.284626	-0.438214
C	4.777024	3.192850	-0.084530
Br	6.077257	4.536525	0.022353
N	5.071460	1.898990	0.205971
H	2.024437	-0.601311	0.251393
H	3.186327	-4.274602	0.377009
H	4.333424	-3.196027	-0.477585
H	2.639053	-3.357137	-1.066429
H	1.892726	1.687737	-0.579090
H	2.922089	4.188460	-0.723933
H	5.962592	1.517063	0.498290

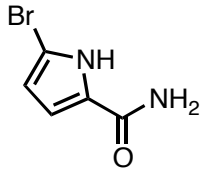

Input File:

%chk=g09.chk
#p td scrf=(solvent=dichloromethane) b3lyp/6-31+G(d) pop=full gfinput

BrPyCOONH2

0 1

O	4.899949	-0.414208	-0.546125
C	3.843533	0.219236	-0.463968
N	2.631482	-0.347352	-0.737374
C	3.847464	1.635680	-0.063344
C	2.878392	2.615620	0.122533
C	3.537474	3.805430	0.520649
C	4.889643	3.508632	0.563712
Br	6.338182	4.609348	1.010580
N	5.069625	2.208495	0.213475
H	1.760095	0.155425	-0.661032
H	2.610247	-1.321359	-1.005370
H	1.810267	2.500600	-0.010852
H	3.091558	4.762828	0.749446
H	5.940980	1.696255	0.148960

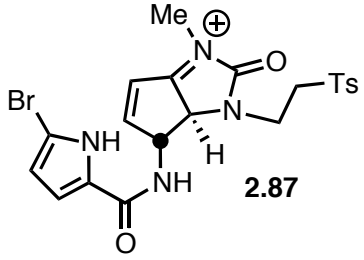

2.87

Input File:

%chk=g09.chk
#p td=(NStates=30) scrf=(solvent=dichloromethane) b3lyp/6-31+G(d) pop=full gfinput

intermediate 2

1 1

O	4.353444	2.515132	-1.202826
C	4.172115	1.515455	-0.559751
N	3.097102	0.677426	-0.471155
C	1.829939	0.950722	-1.169271
C	0.838172	1.757537	-0.315329
S	-0.823715	1.638830	-1.093824
C	-1.846142	2.779398	-0.171366
C	-1.944881	4.106303	-0.604600
C	-2.748407	4.989498	0.113176
C	-3.456663	4.570140	1.252932

C	-4.314195	5.544488	2.023071
C	-3.343542	3.229924	1.654792
C	-2.544795	2.327678	0.951508
O	-1.294616	0.262088	-0.826357
O	-0.668485	2.125634	-2.473774
C	3.303437	-0.326514	0.549246
H	2.690753	-0.113086	1.438531
C	4.749739	-0.165913	0.864433
C	5.299802	-1.364003	1.424898
C	4.426159	-2.364397	1.121401
C	3.218684	-1.909423	0.339063
H	3.359507	-2.105191	-0.733076
N	2.003739	-2.554083	0.728062
C	0.941439	-2.568476	-0.188311
C	-0.338786	-3.033647	0.299496
C	-0.735278	-3.785558	1.409502
C	-2.134628	-3.933442	1.344543
C	-2.552801	-3.254316	0.204002
Br	-4.277295	-3.055987	-0.478023
N	-1.474431	-2.735646	-0.428932
O	1.131983	-2.163605	-1.337788
N	5.225557	0.917829	0.312006
C	6.604388	1.414725	0.277289
H	1.409913	-0.015542	-1.457766
H	2.080082	1.500926	-2.077740
H	1.108325	2.816013	-0.260917
H	0.725144	1.355311	0.696272
H	-1.425498	4.429803	-1.501471
H	-2.839573	6.018534	-0.225899
H	-4.938554	6.142407	1.349916
H	-4.971622	5.030611	2.730695
H	-3.691203	6.245072	2.594252
H	-3.900622	2.881878	2.520926
H	-2.489626	1.285334	1.249703
H	6.272981	-1.470265	1.888733
H	4.574020	-3.412425	1.368102
H	1.783828	-2.630689	1.714444
H	-0.084216	-4.232976	2.150194
H	-2.772949	-4.482136	2.021904
H	-1.491303	-2.072412	-1.197690
H	6.578141	2.404270	-0.181076
H	7.225903	0.747976	-0.328124
H	6.996415	1.481087	1.29385

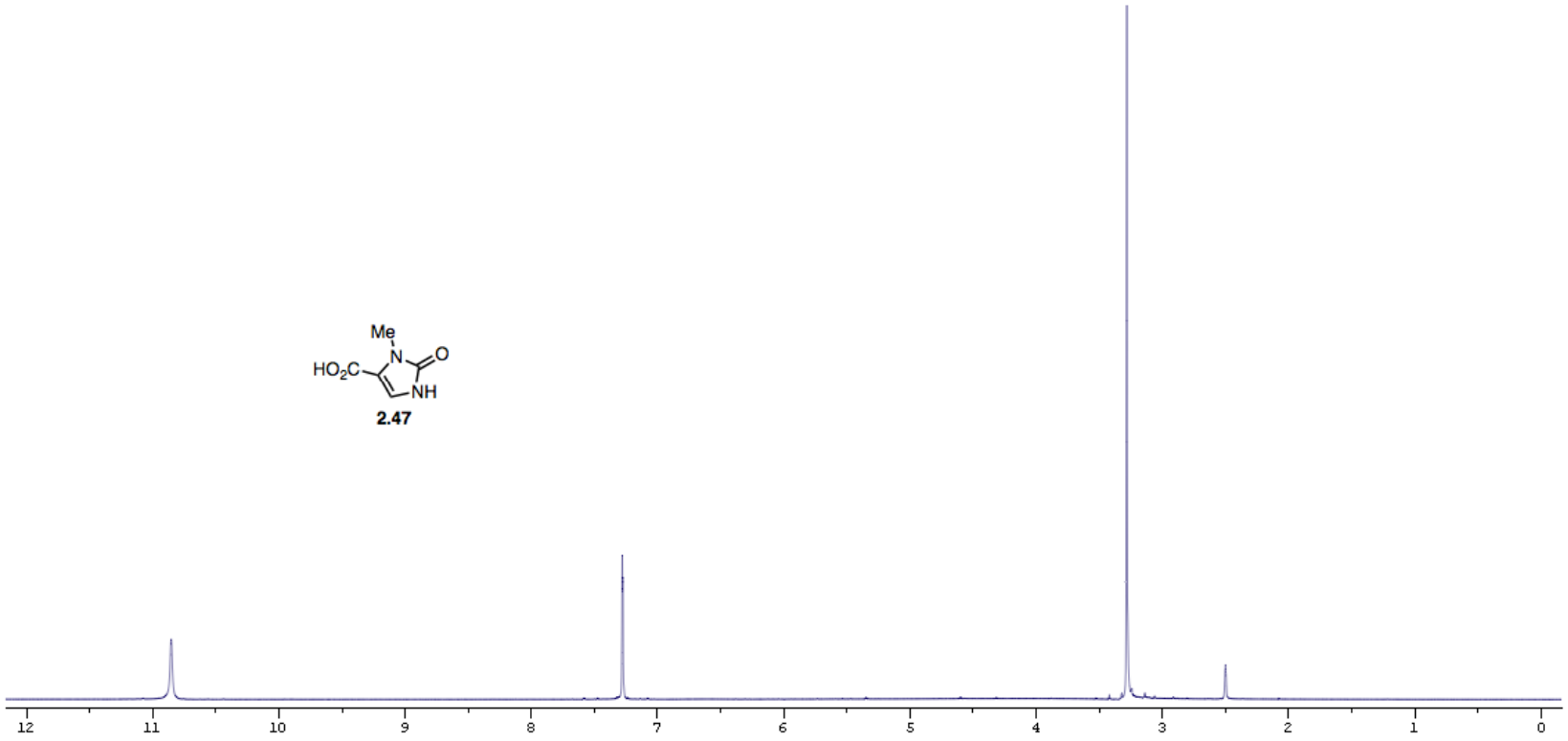

^{1}H NMR (500 MHz) of **2.47** in DMSO-d_6

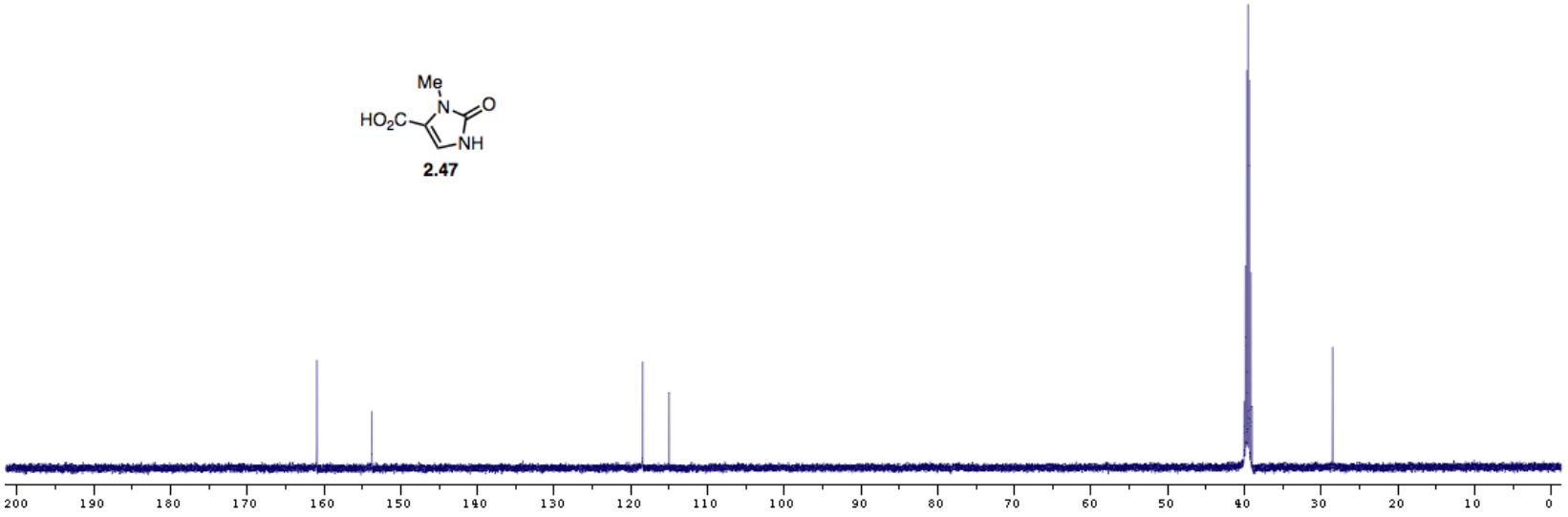

^{13}C NMR (125 MHz) of **2.47** in DMSO-d_6

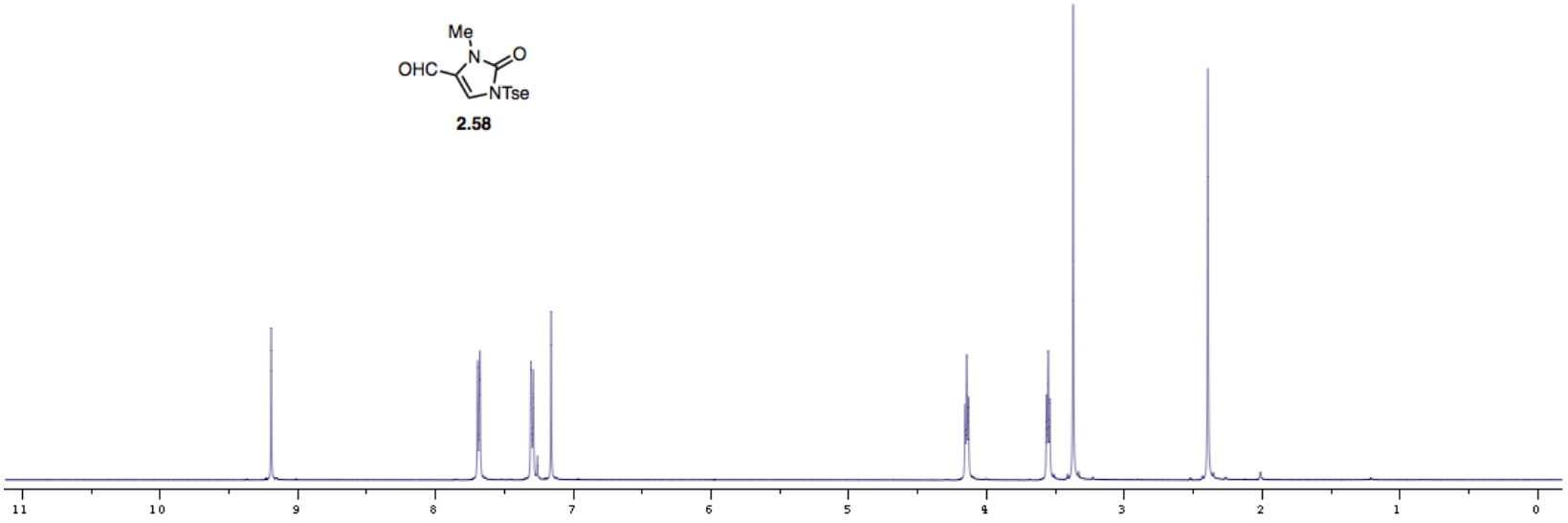

^{1}H NMR (500 MHz) of **2.58** in $CDCl_3$

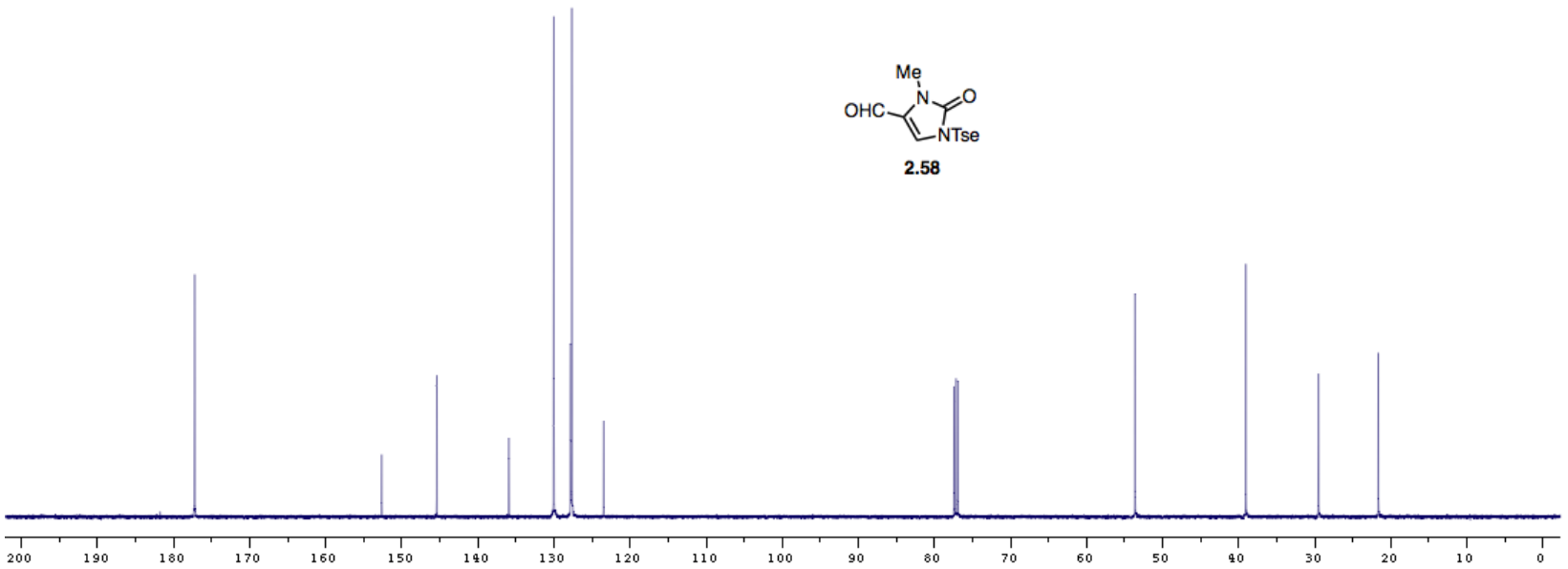

^{13}C NMR (125 MHz) of **2.58** in $CDCl_3$

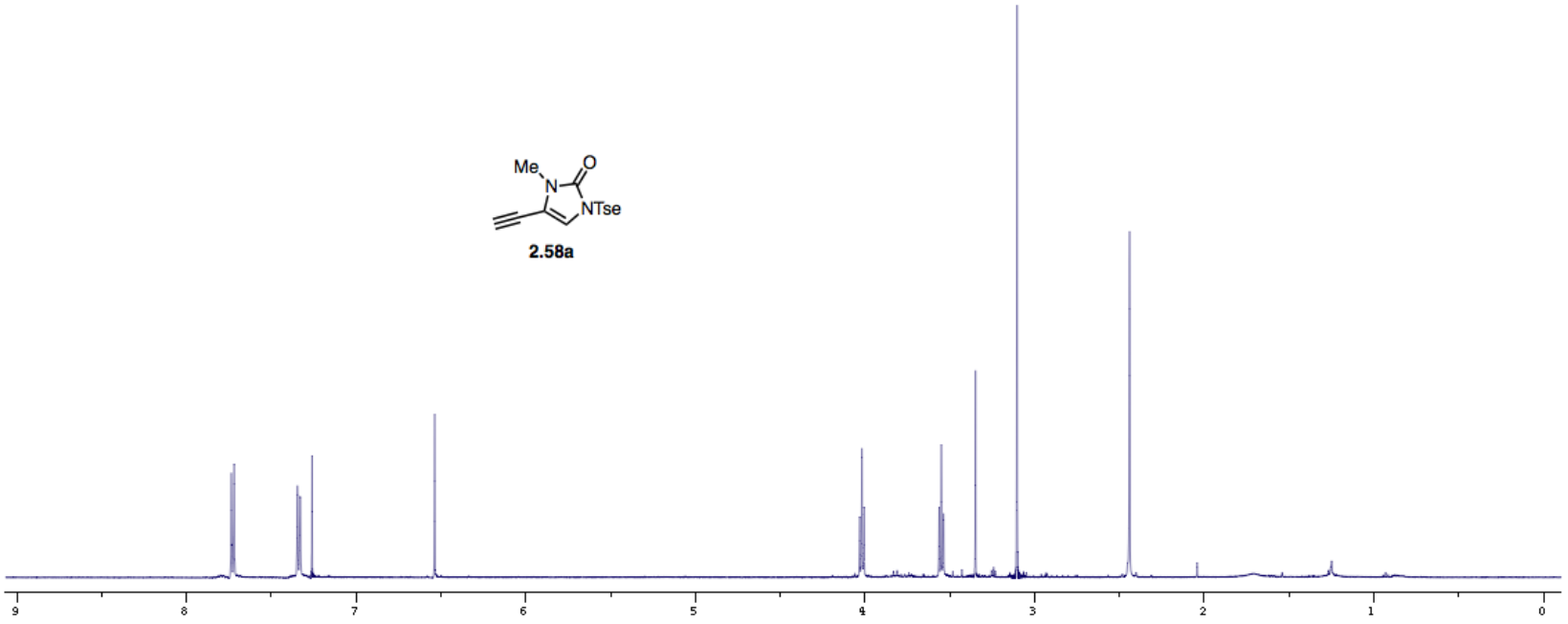

^{1}H NMR (500 MHz) of **2.58a** in $CDCl_3$

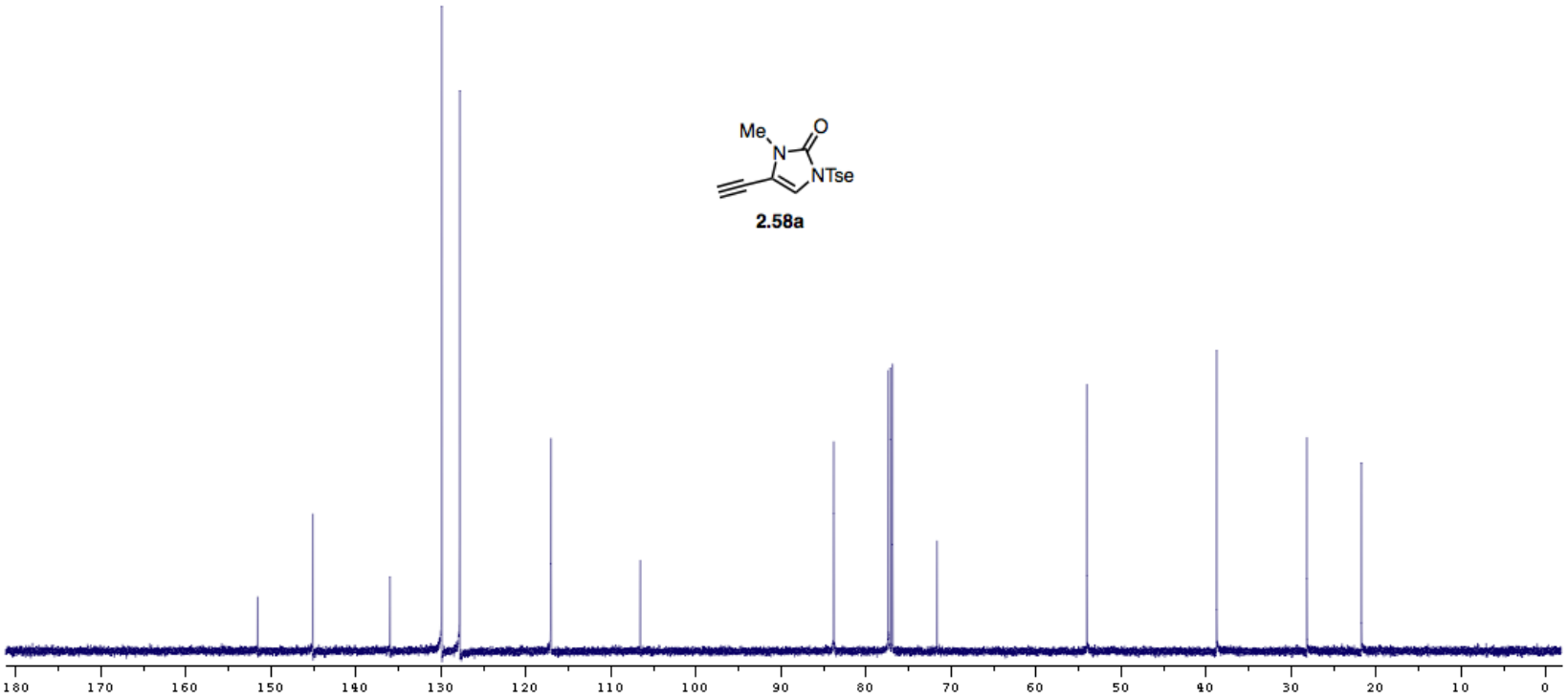

^{13}C NMR (125 MHz) of **2.58a** in $CDCl_3$

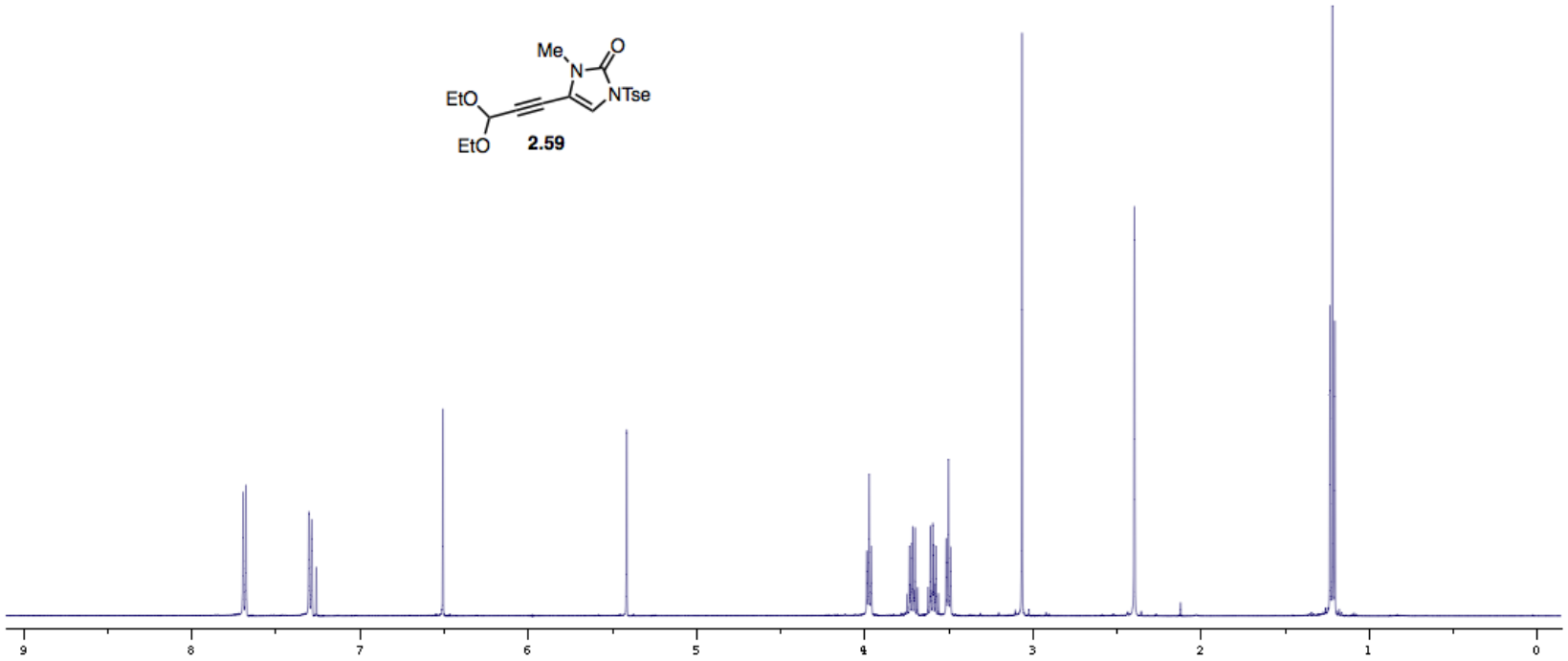

^{1}H NMR (500 MHz) of **2.59** in $CDCl_3$

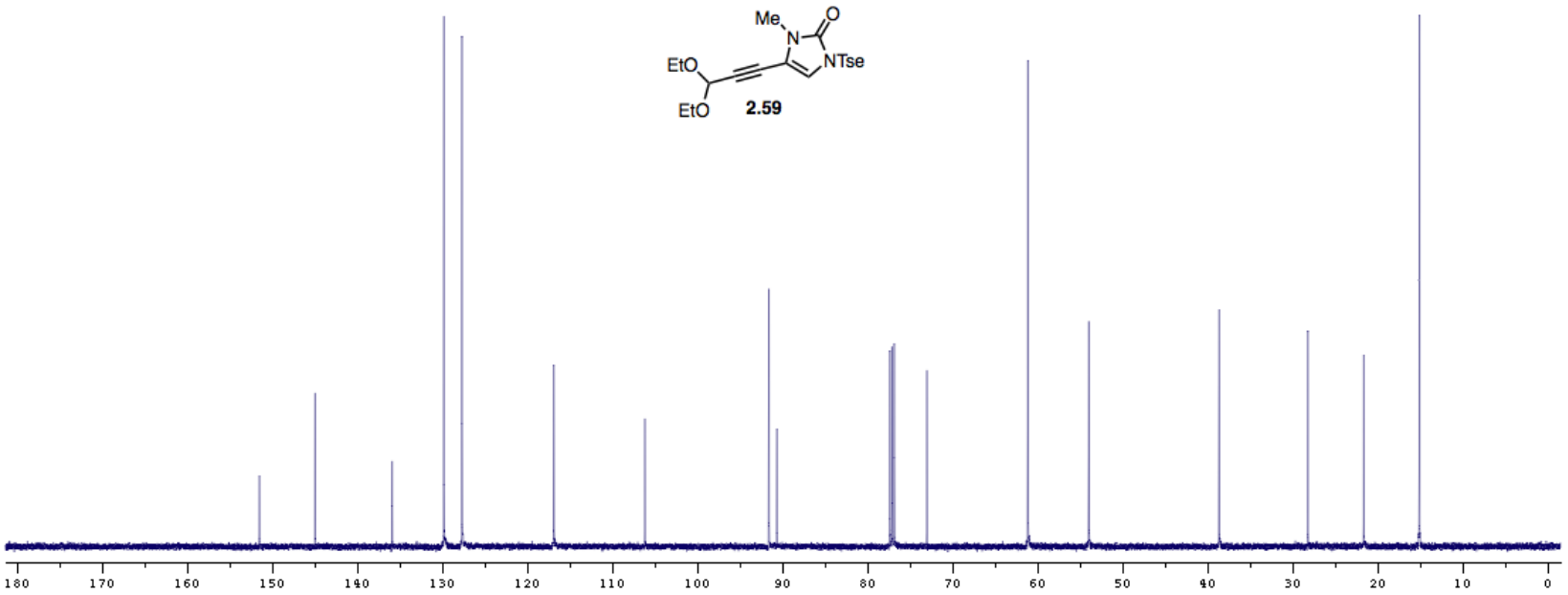

^{13}C NMR (125 MHz) of **2.59** in $CDCl_3$

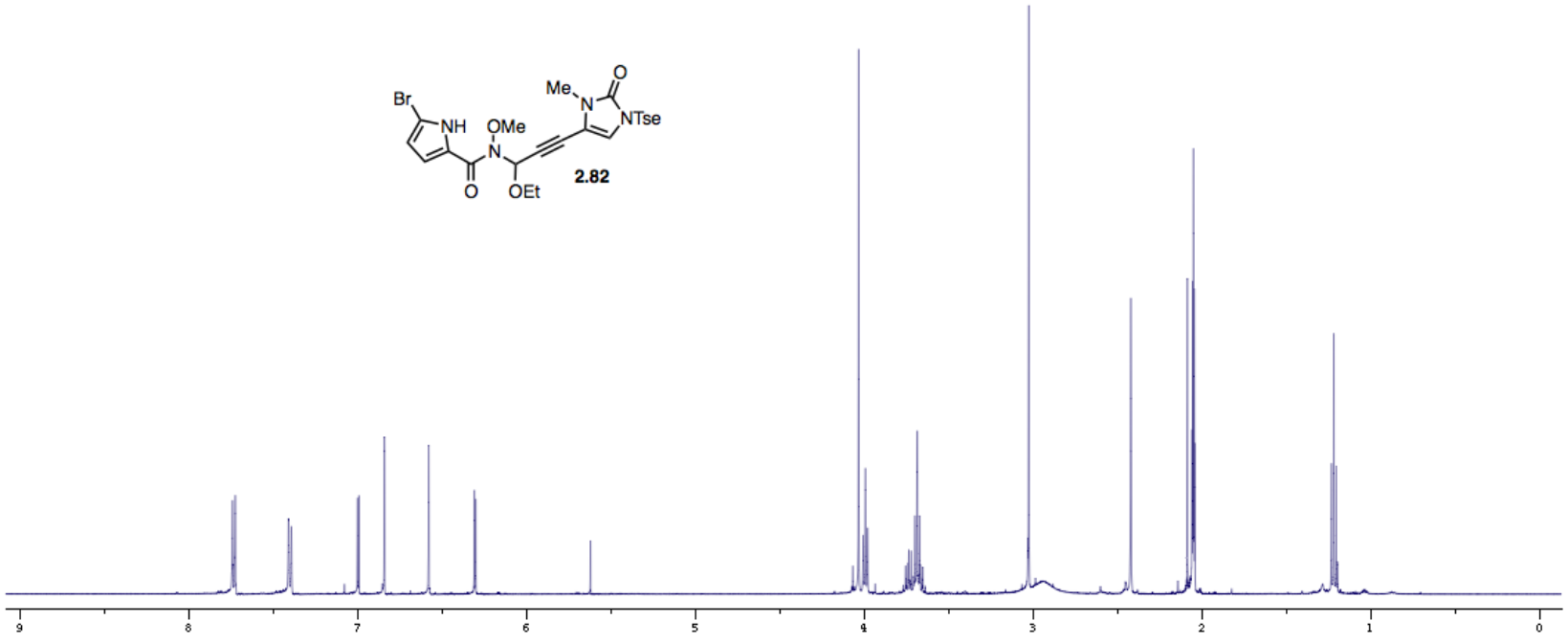

^{1}H NMR (500 MHz) of **2.82** in acetone-d_6

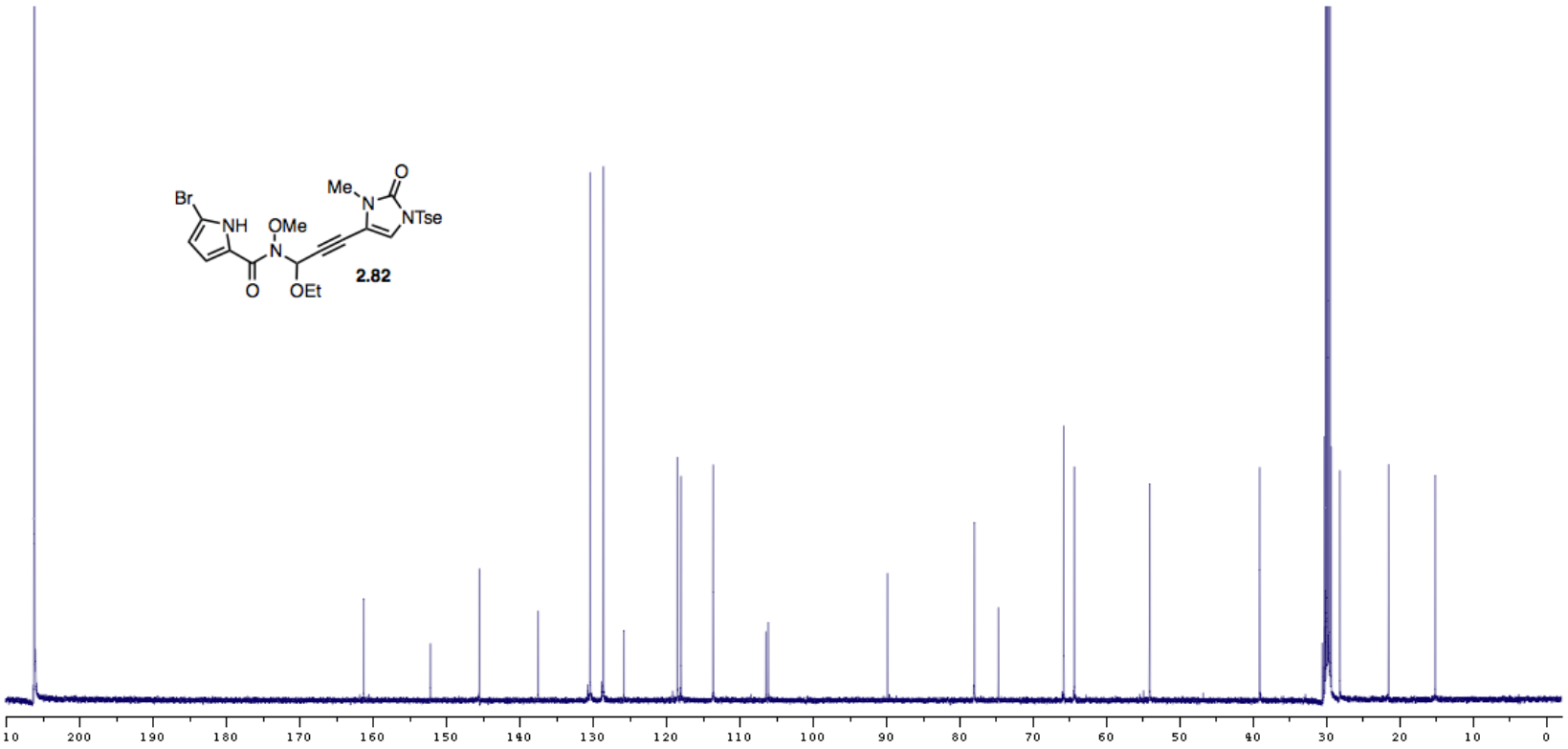

^{13}C NMR (125 MHz) of **2.82** in acetone-d_6

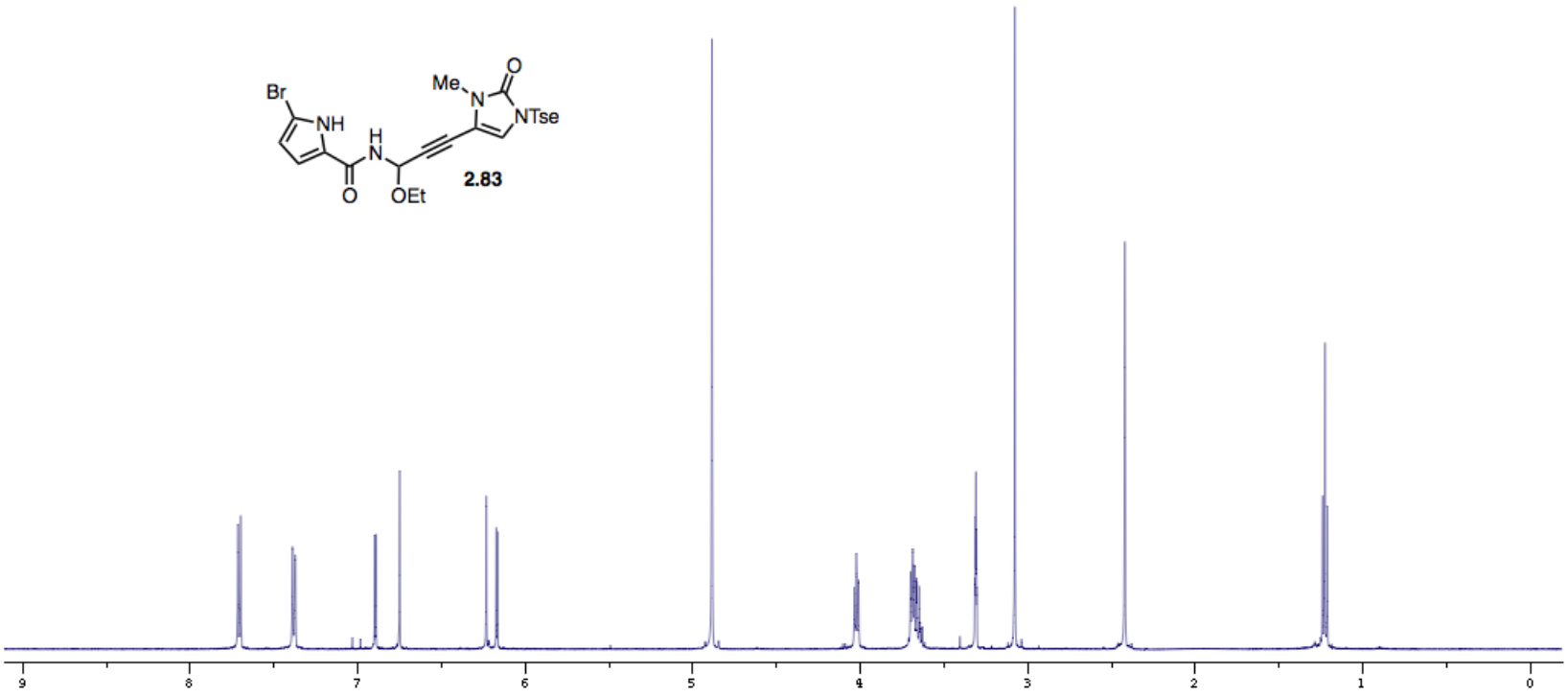

^{1}H NMR (500 MHz) of **2.83** in CD_3OD

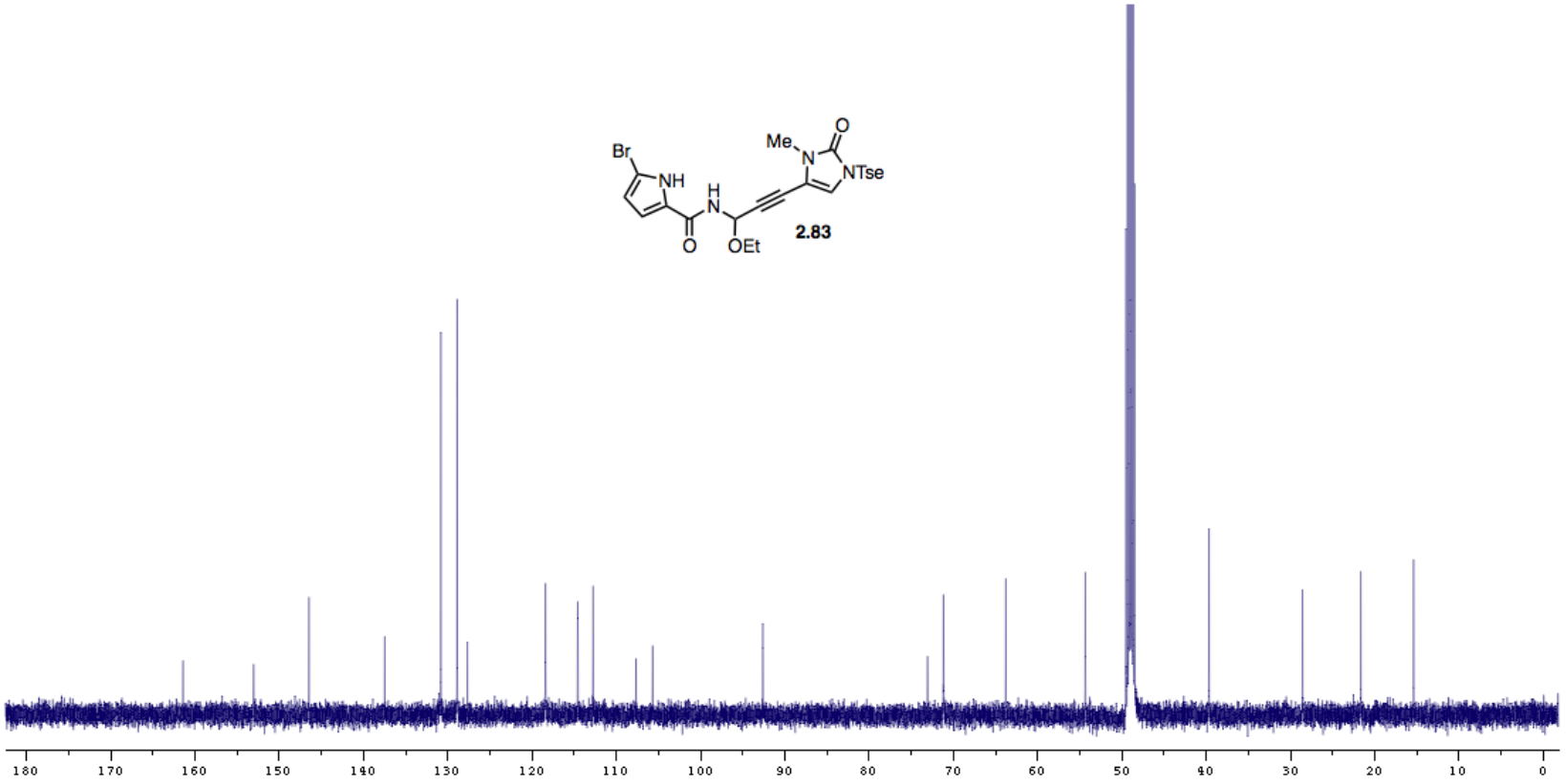

^{13}C NMR (125 MHz) of **2.83** in CD_3OD

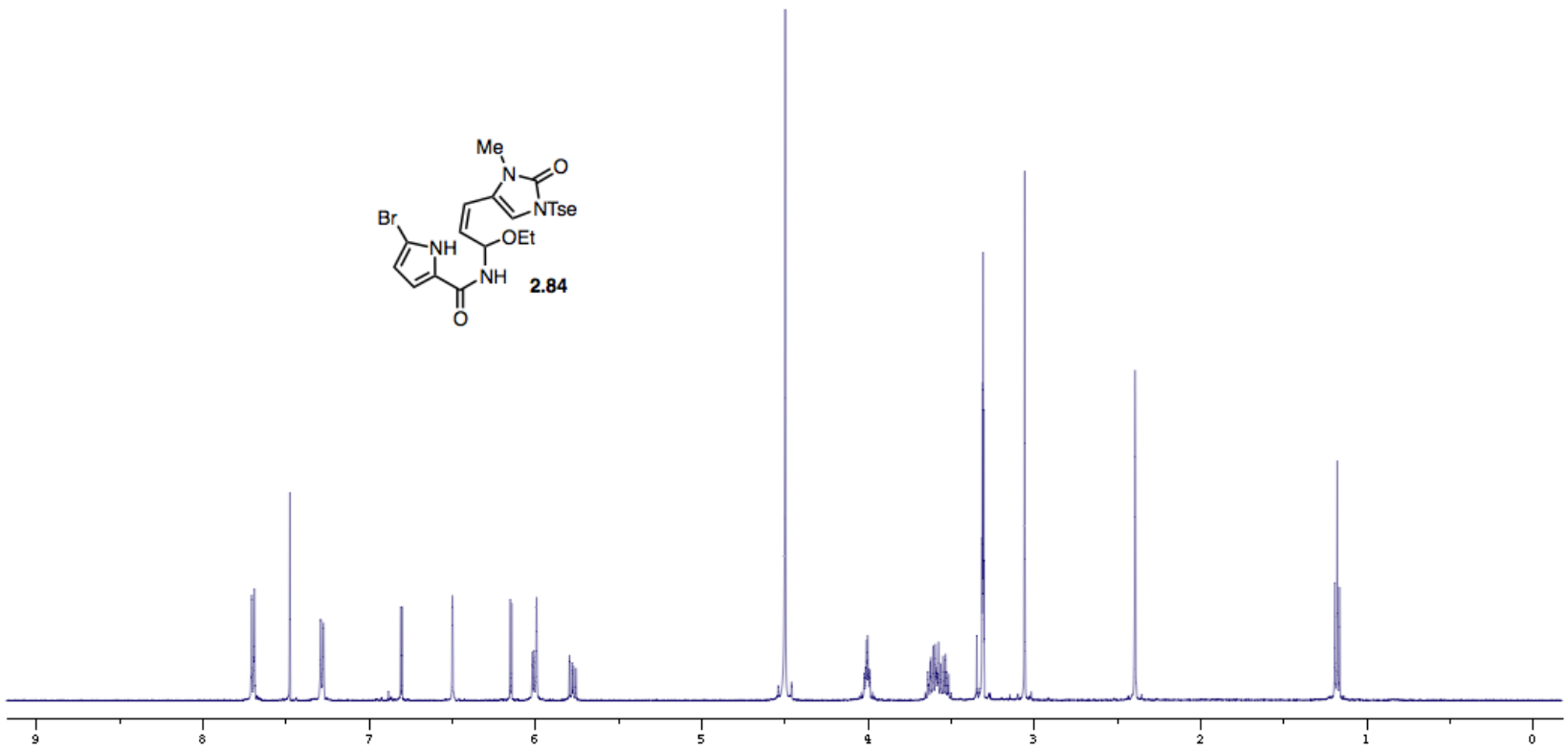

^{1}H NMR (500 MHz) of **2.84** in $CDCl_3/CD_3OD$ (1:1)

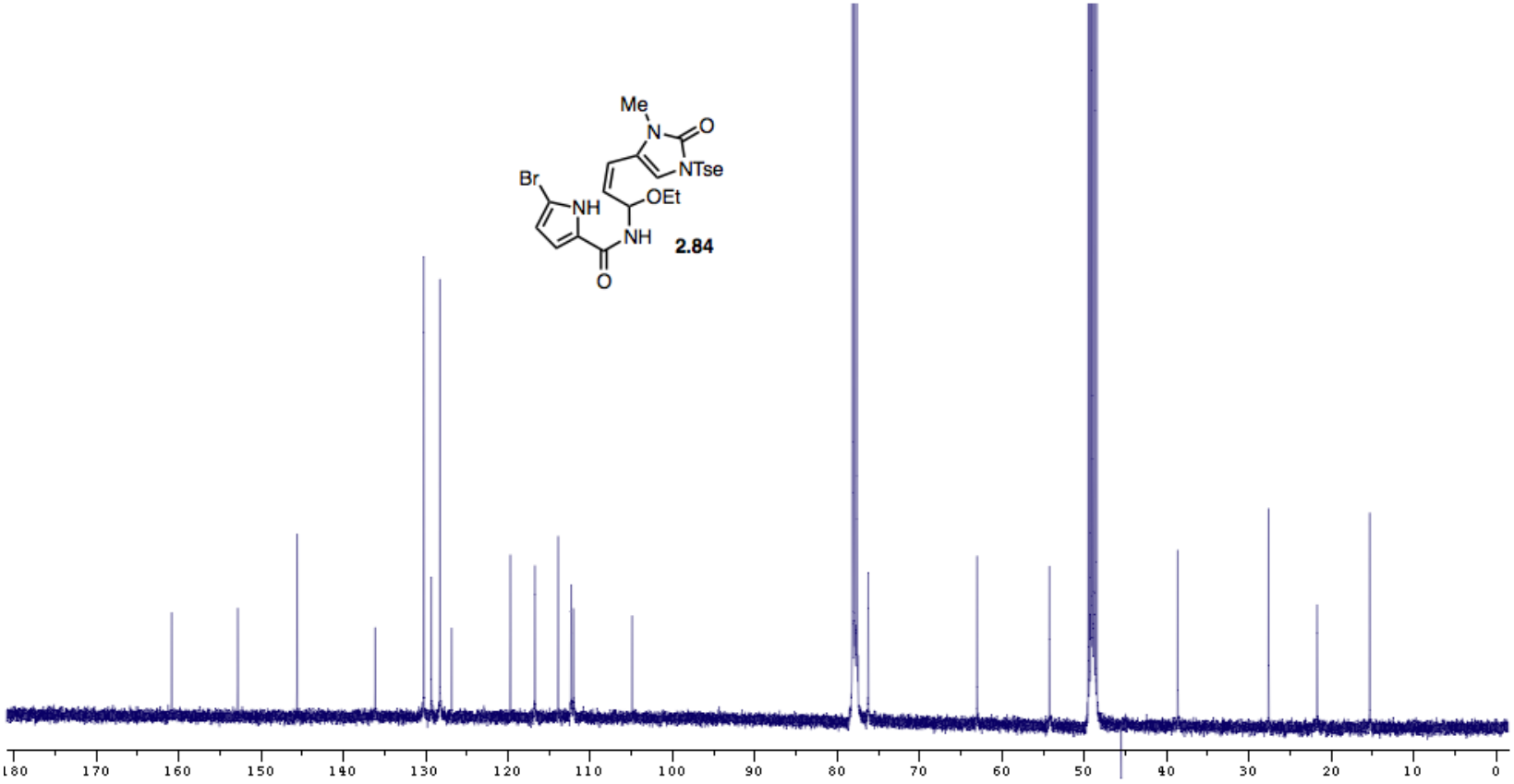

^{13}C NMR (125 MHz) of **2.84** in $CDCl_3/CD_3OD$ (1:1)

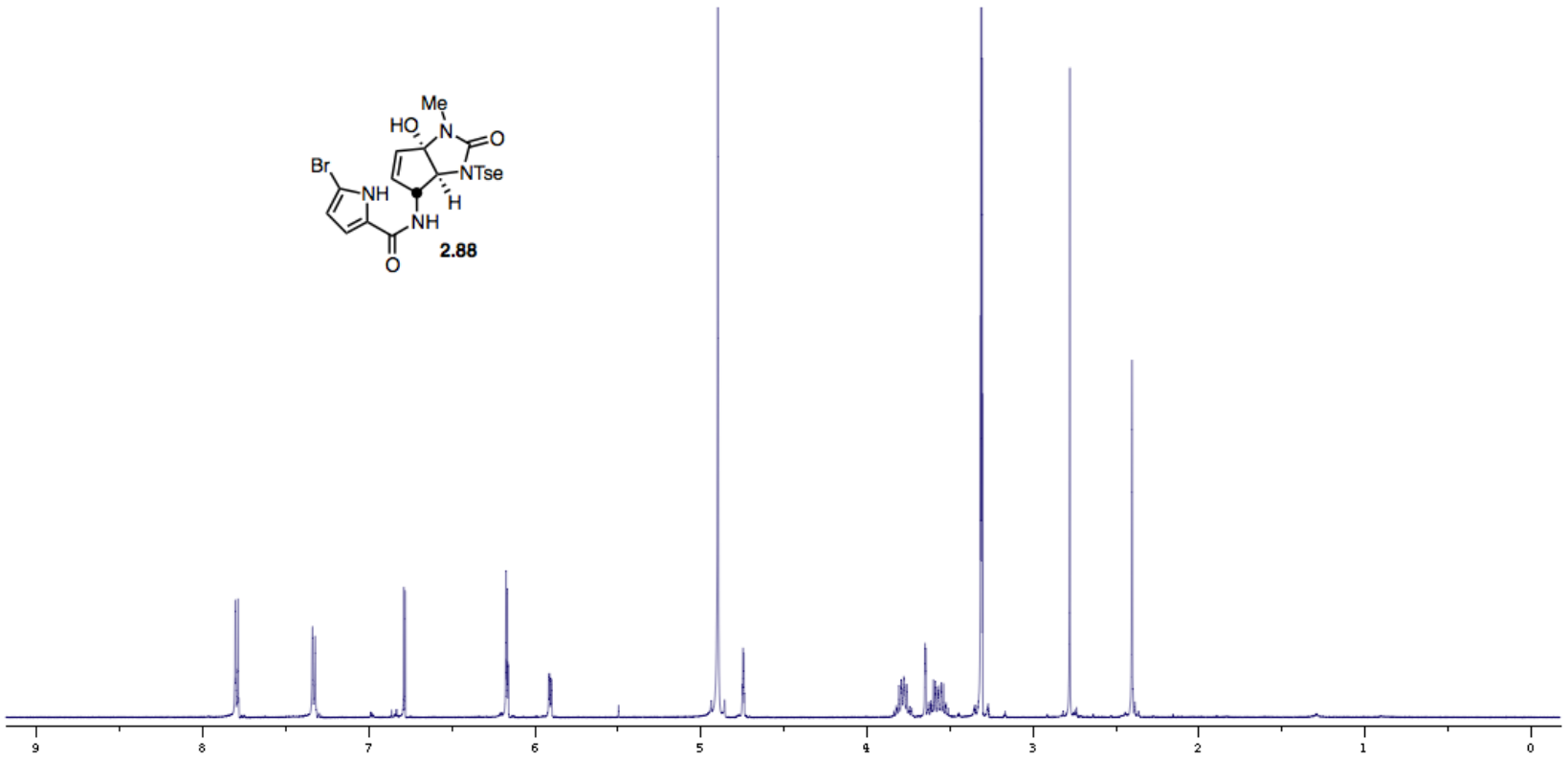

^{1}H NMR (500 MHz) of **2.88** in CD_3OD

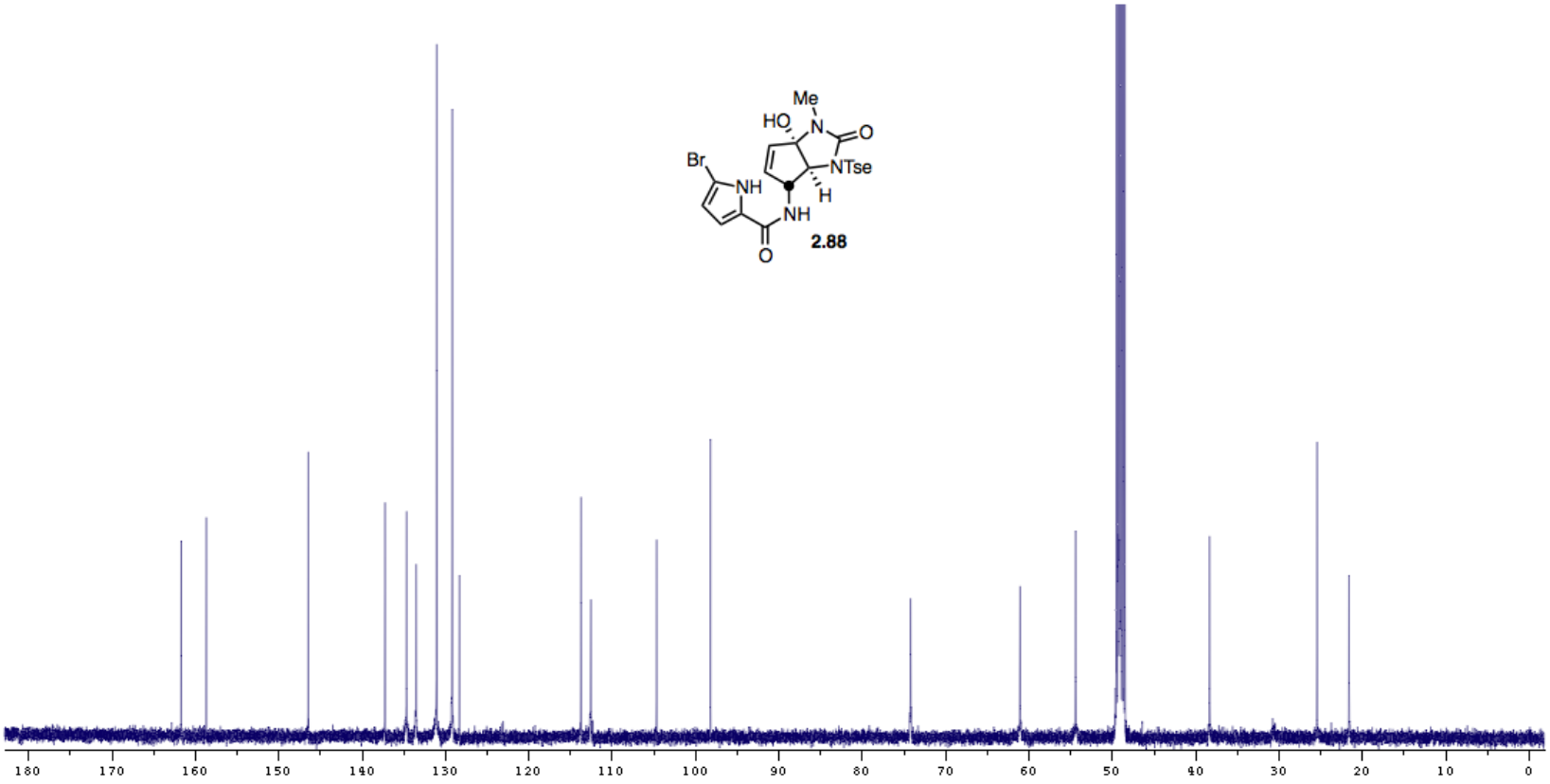

^{13}C NMR (125 MHz) of **2.88** in CD_3OD

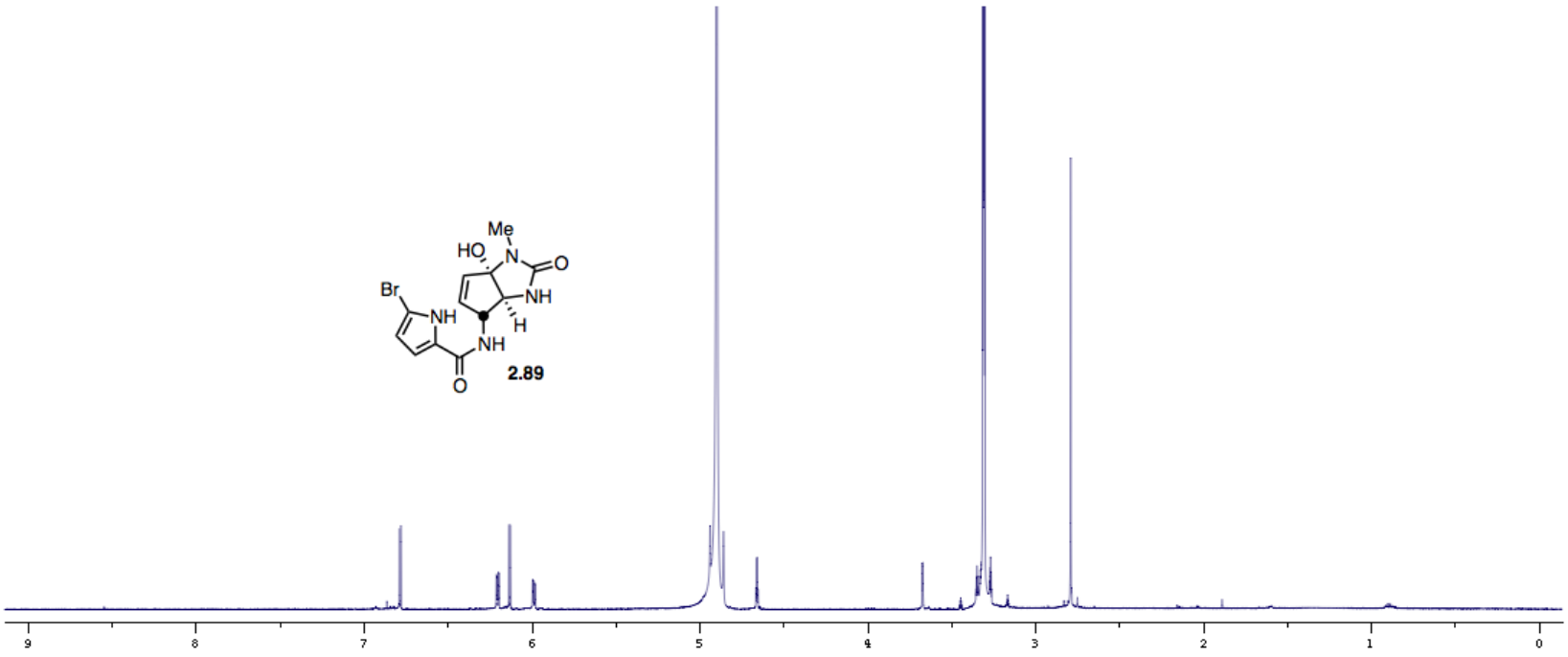

^{1}H NMR (500 MHz) of **2.89** in CD_3OD

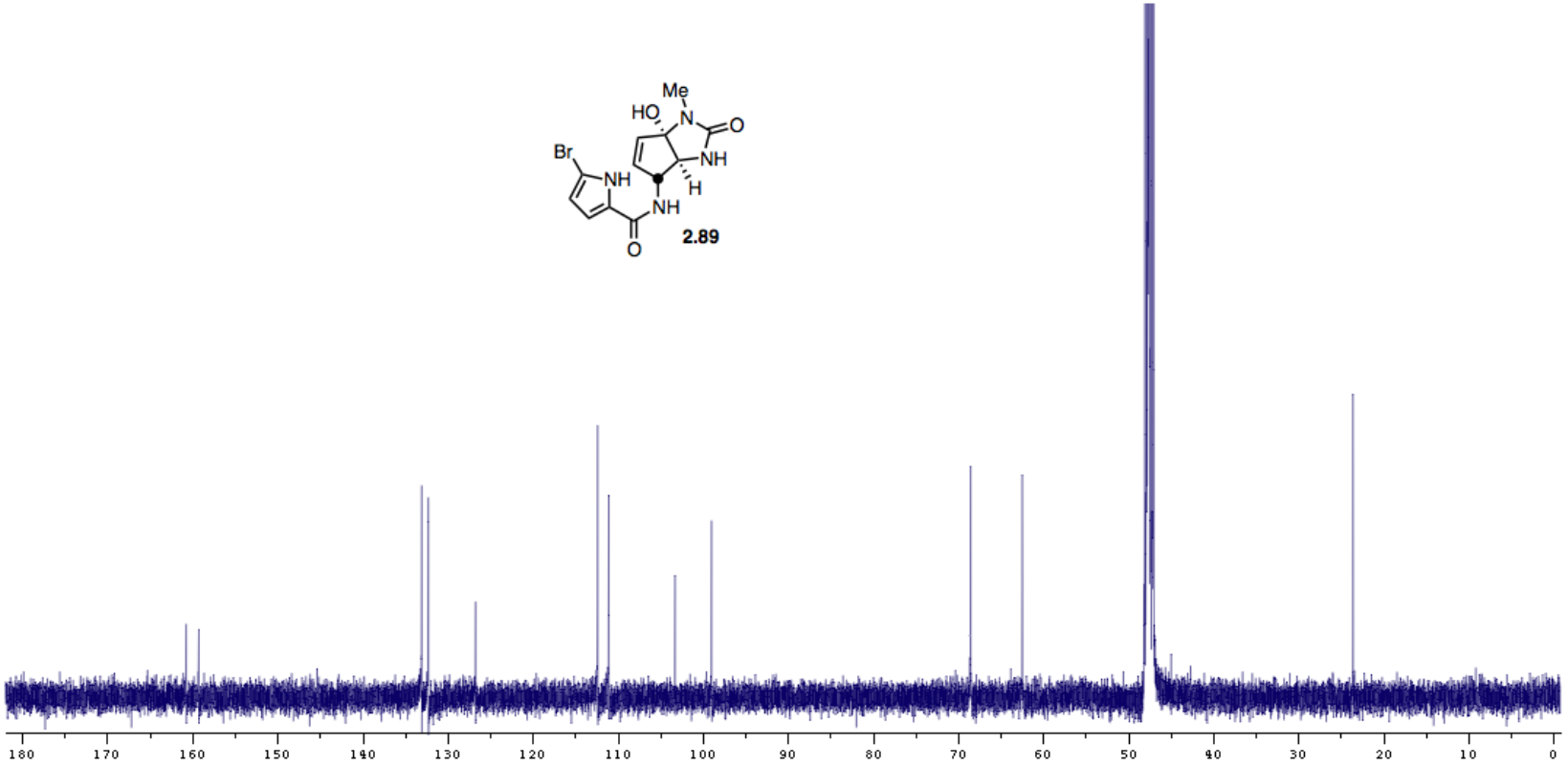

^{13}C NMR (125 MHz) of **2.89** in CD_3OD

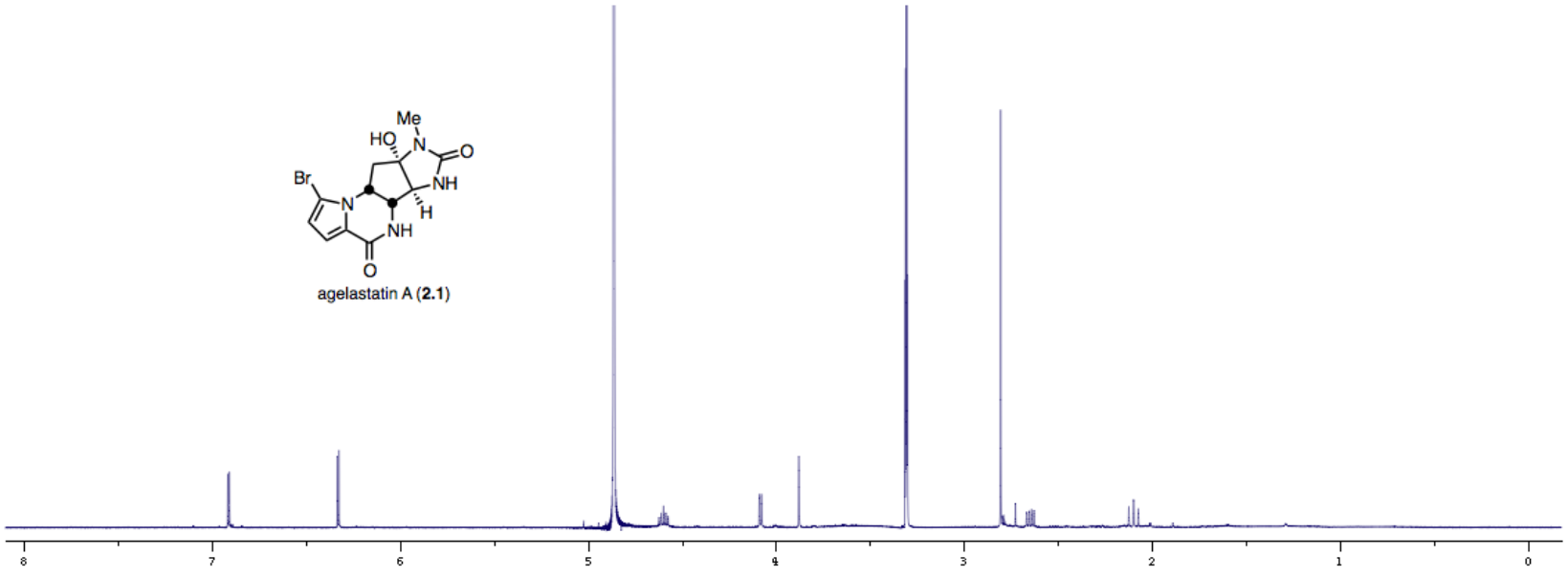

^{1}H NMR (500 MHz) of **2.1** in CD_3OD

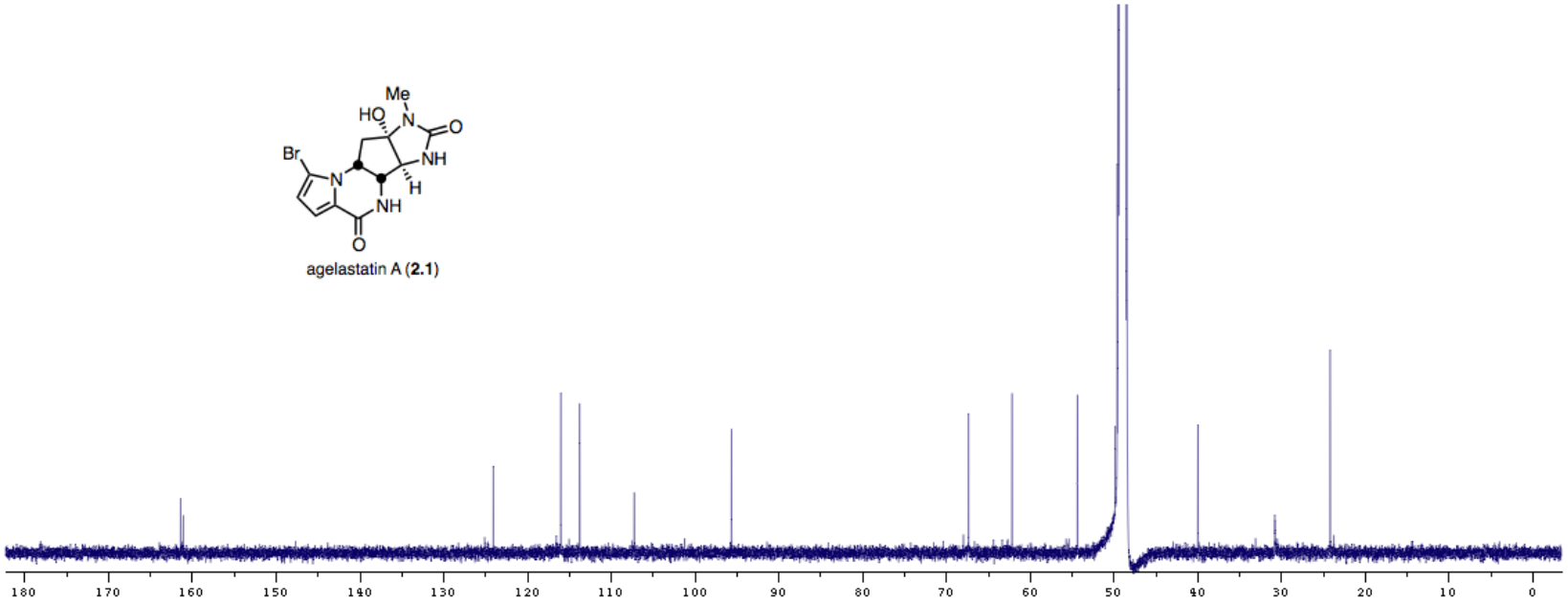

^{13}C NMR (125 MHz) of **2.1** in CD_3OD

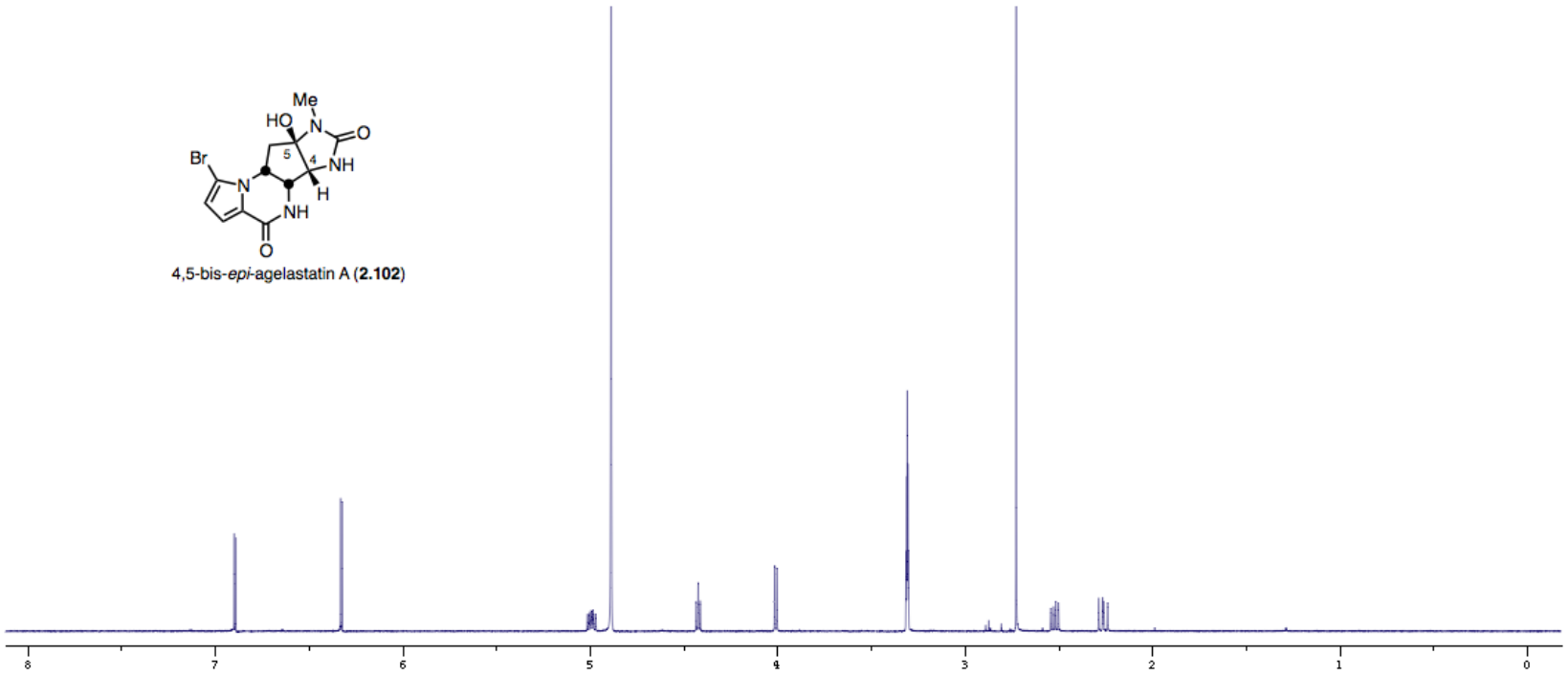

^{1}H NMR (500 MHz) of **2.102** in CD_3OD

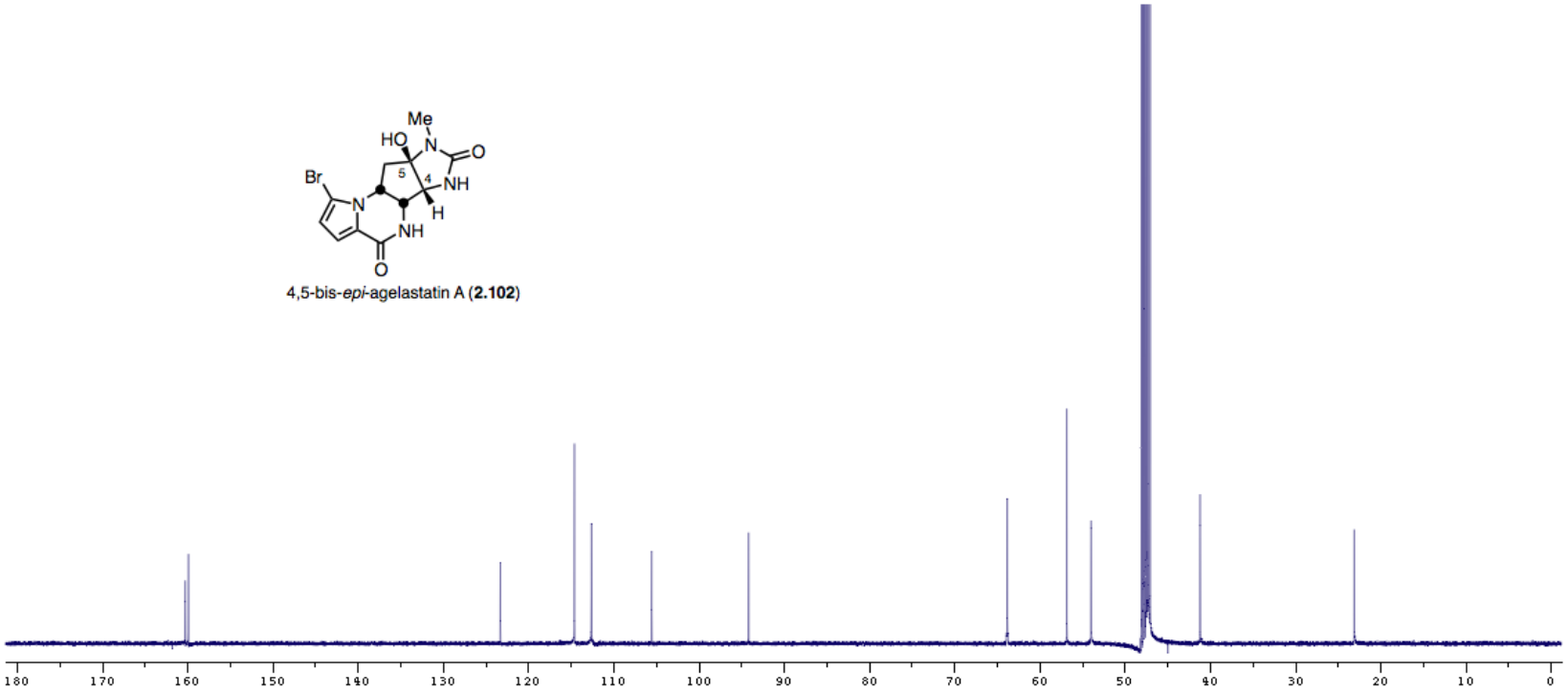

^{13}C NMR (125 MHz) of **2.102** in CD_3OD

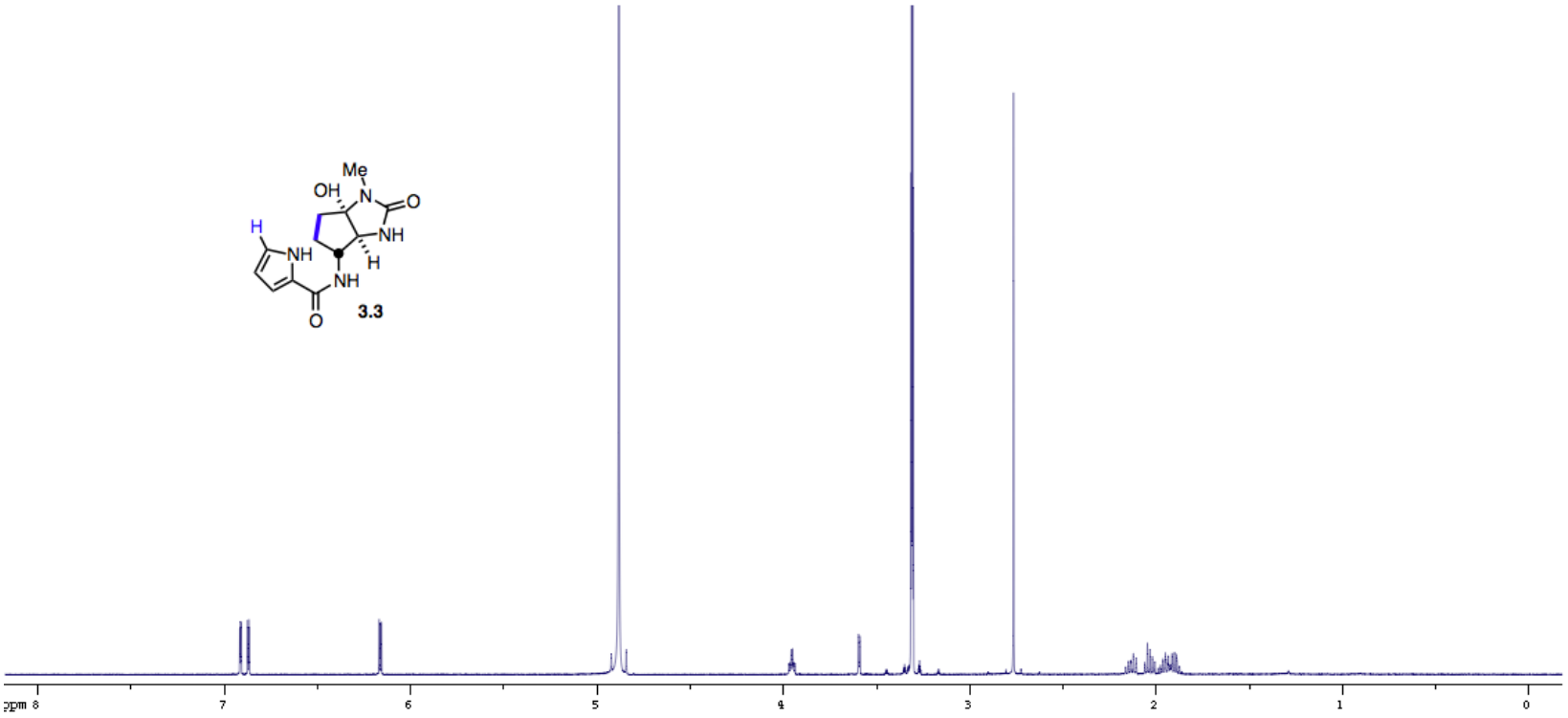

^{1}H NMR (500 MHz) of **3.3** in CD_3OD

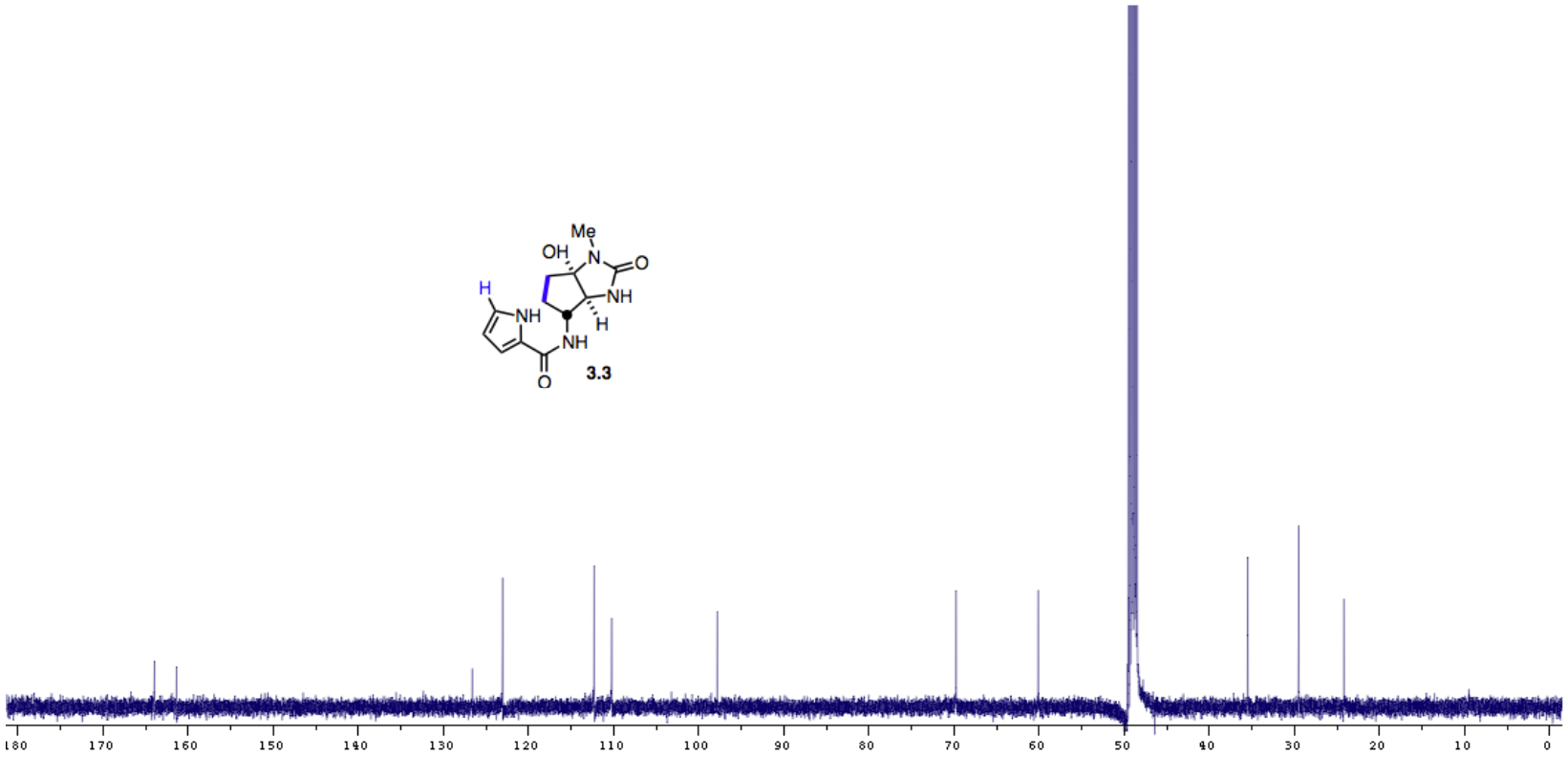

^{13}C NMR (125 MHz) of **3.3** in CD_3OD

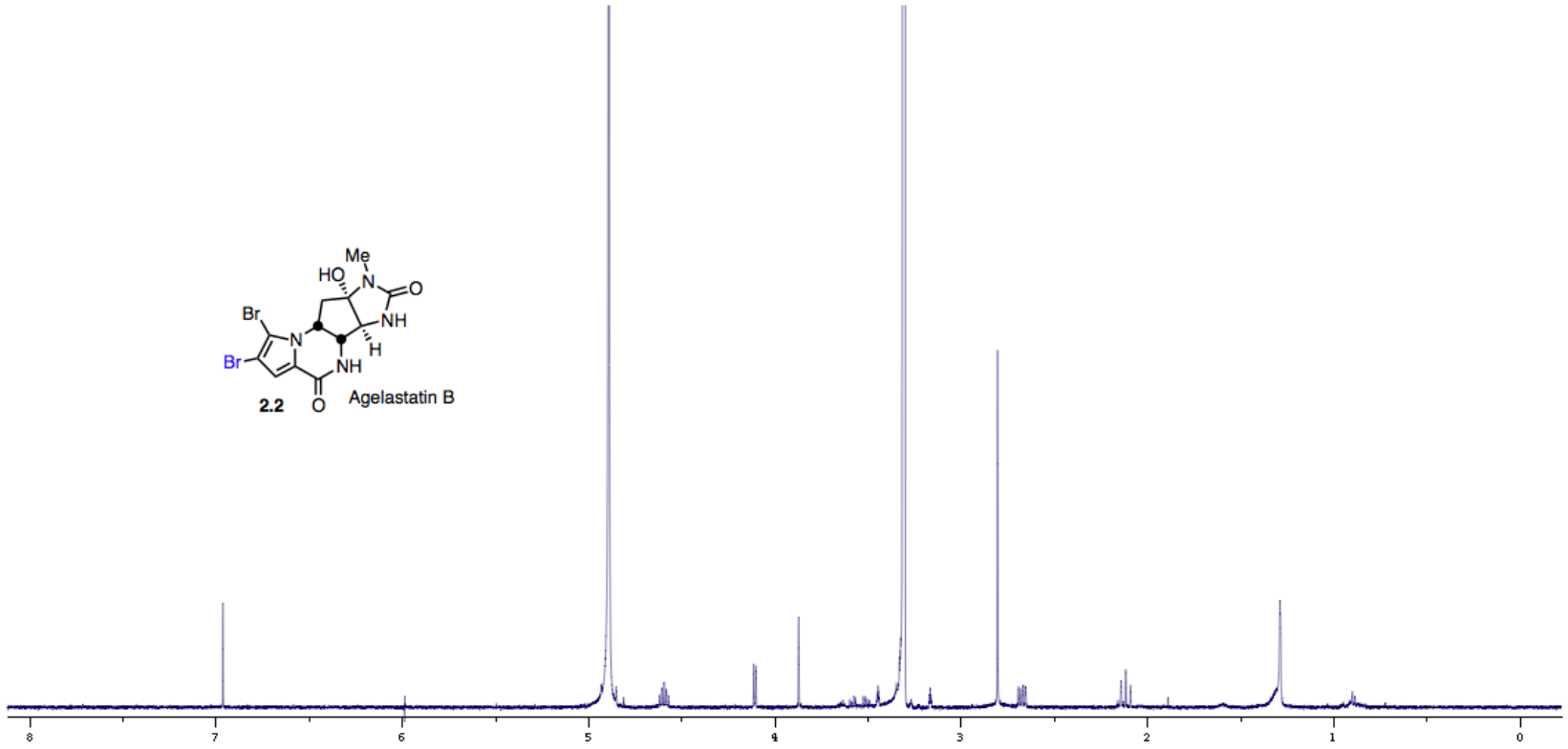

^{1}H NMR (500 MHz) of **2.2** in CD_3OD

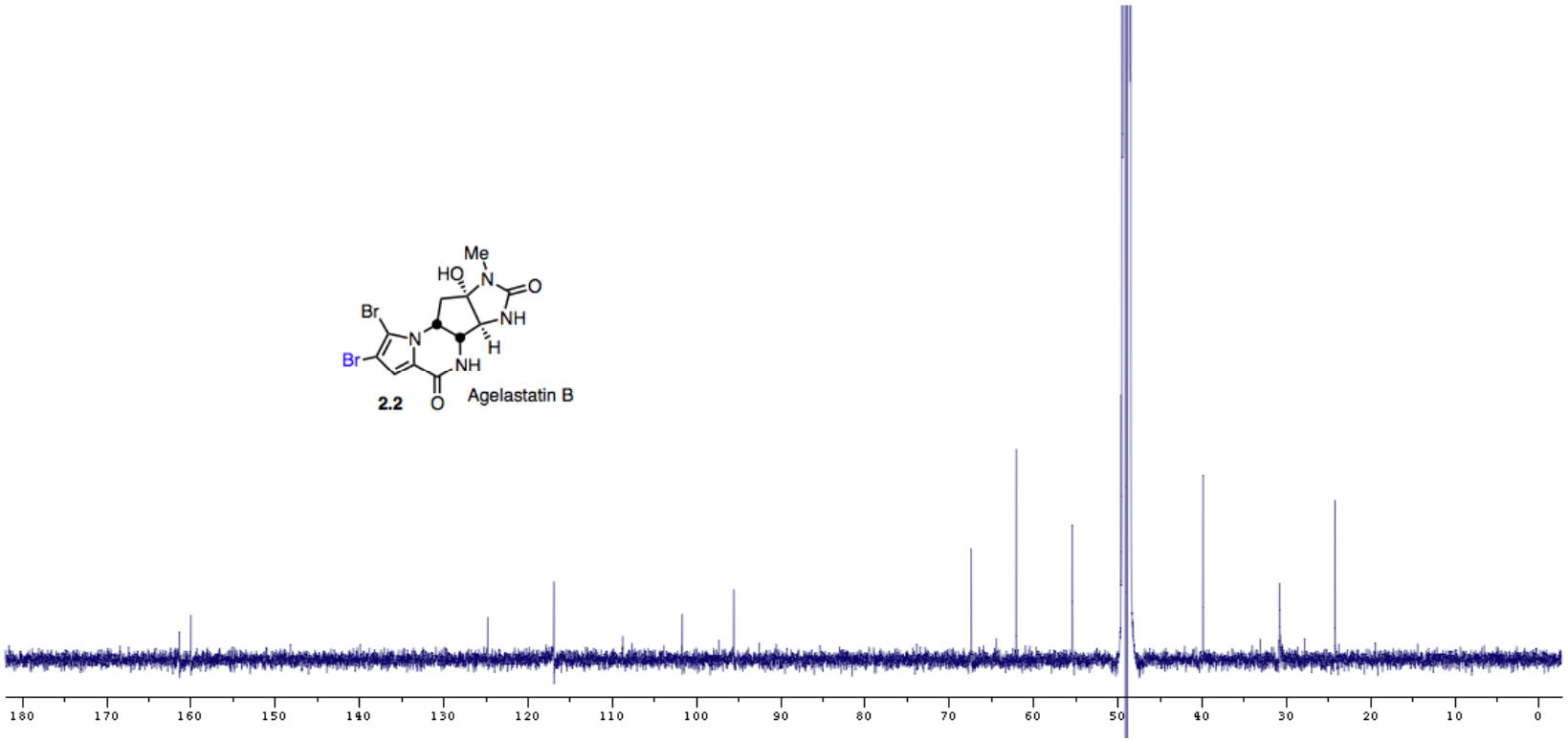

^{13}C NMR (125 MHz) of **2.2** in CD_3OD

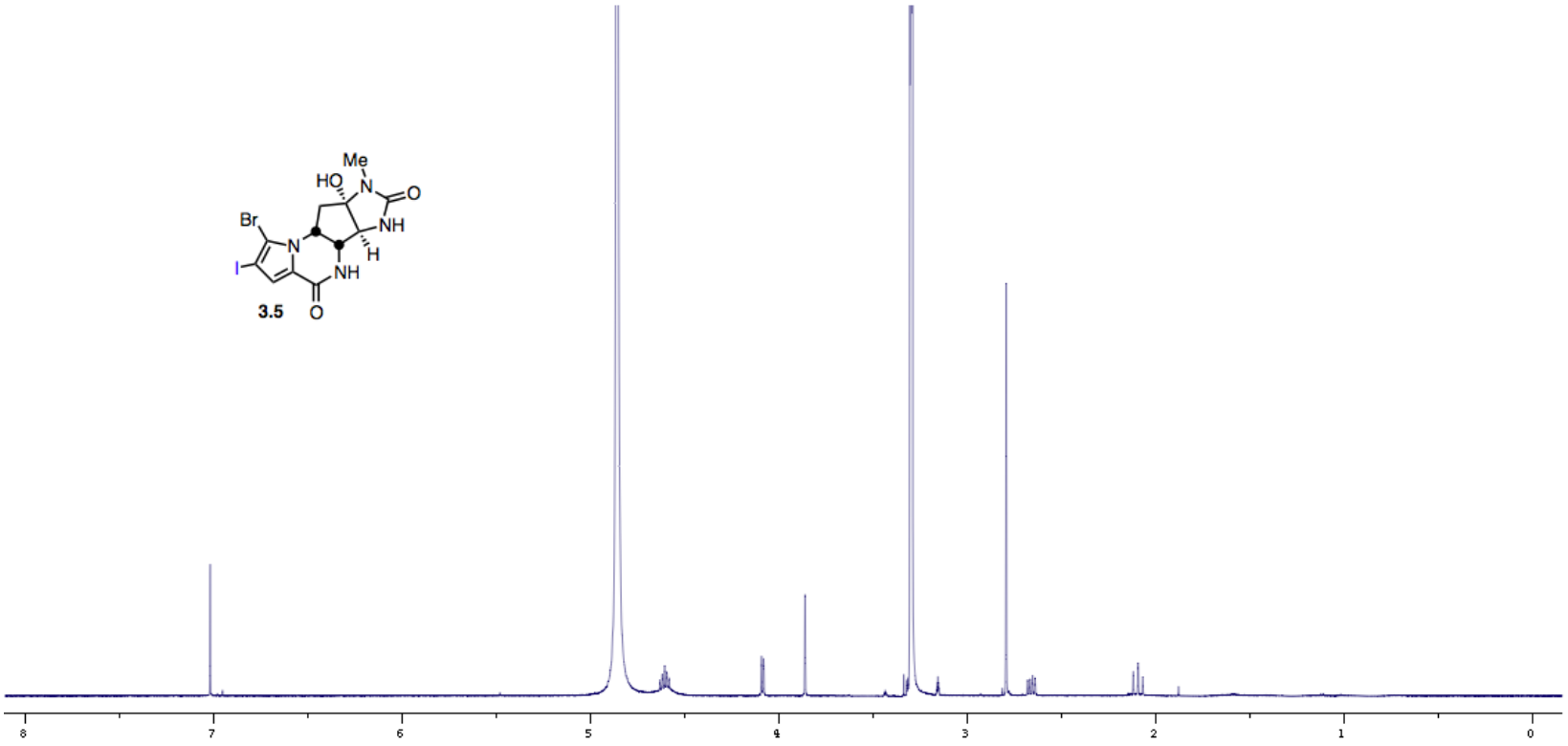

^{1}H NMR (500 MHz) of **3.5** in CD_3OD

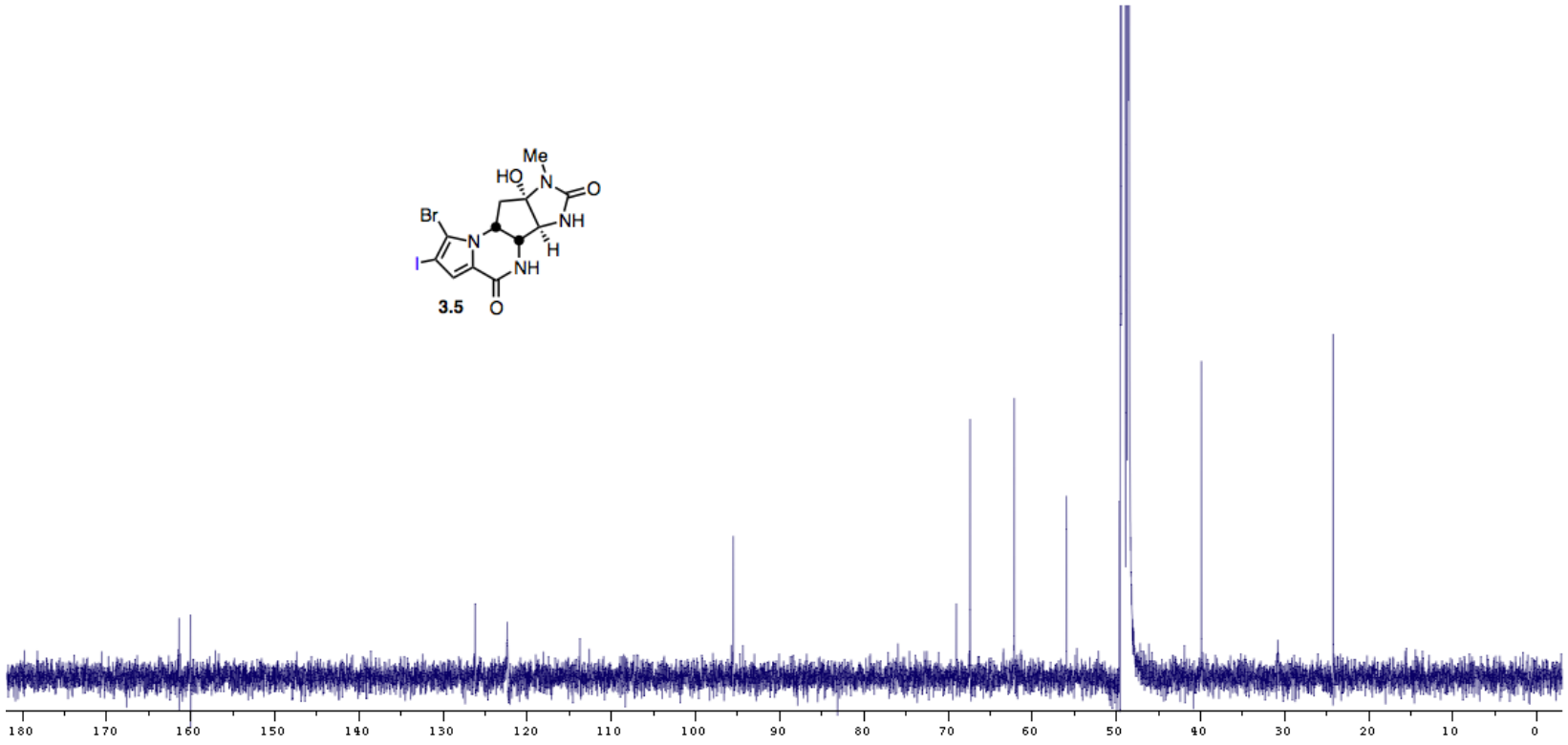

^{13}C NMR (125 MHz) of **3.5** in CD_3OD

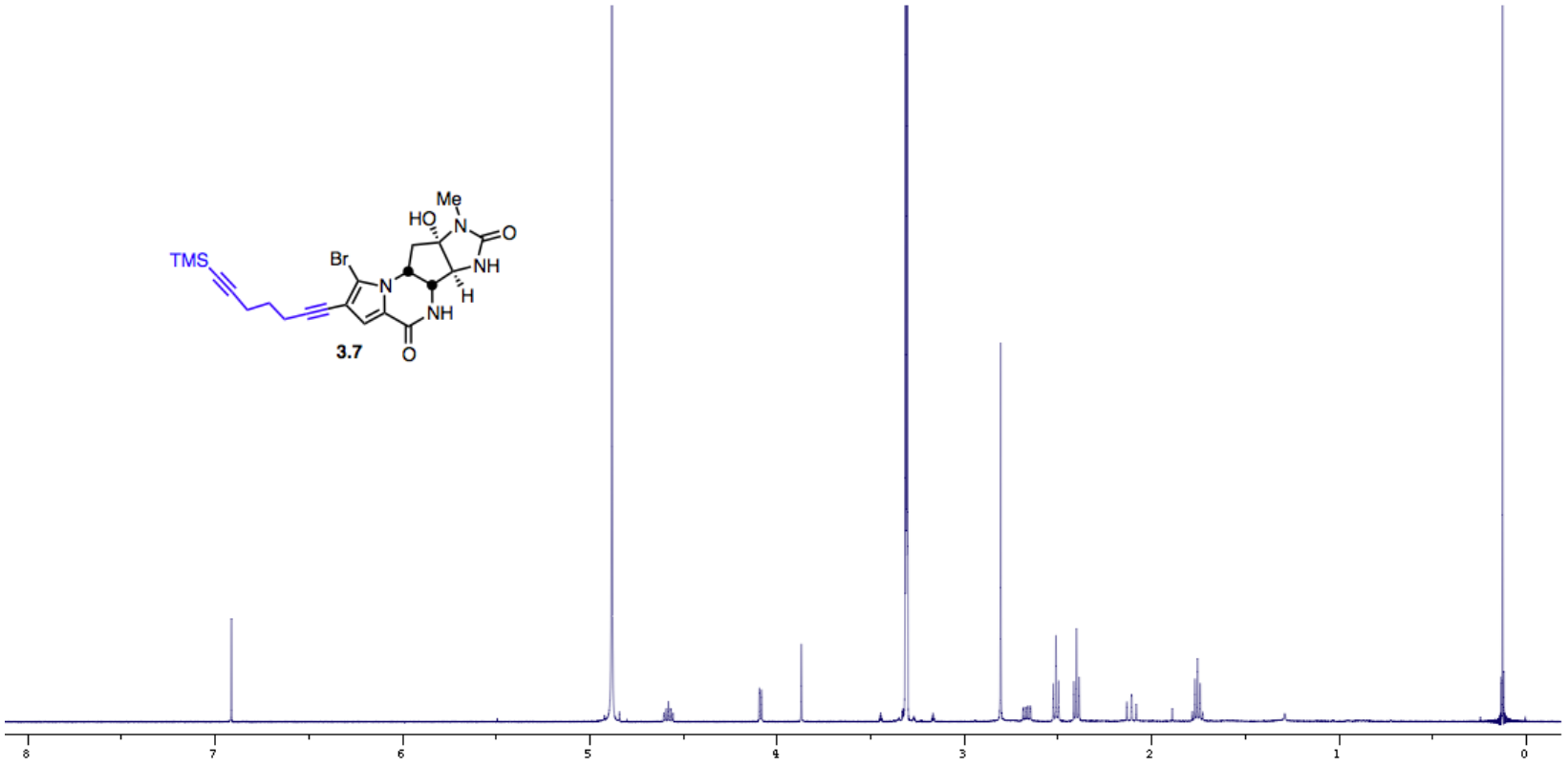

^{1}H NMR (500 MHz) of **3.7** in CD_3OD

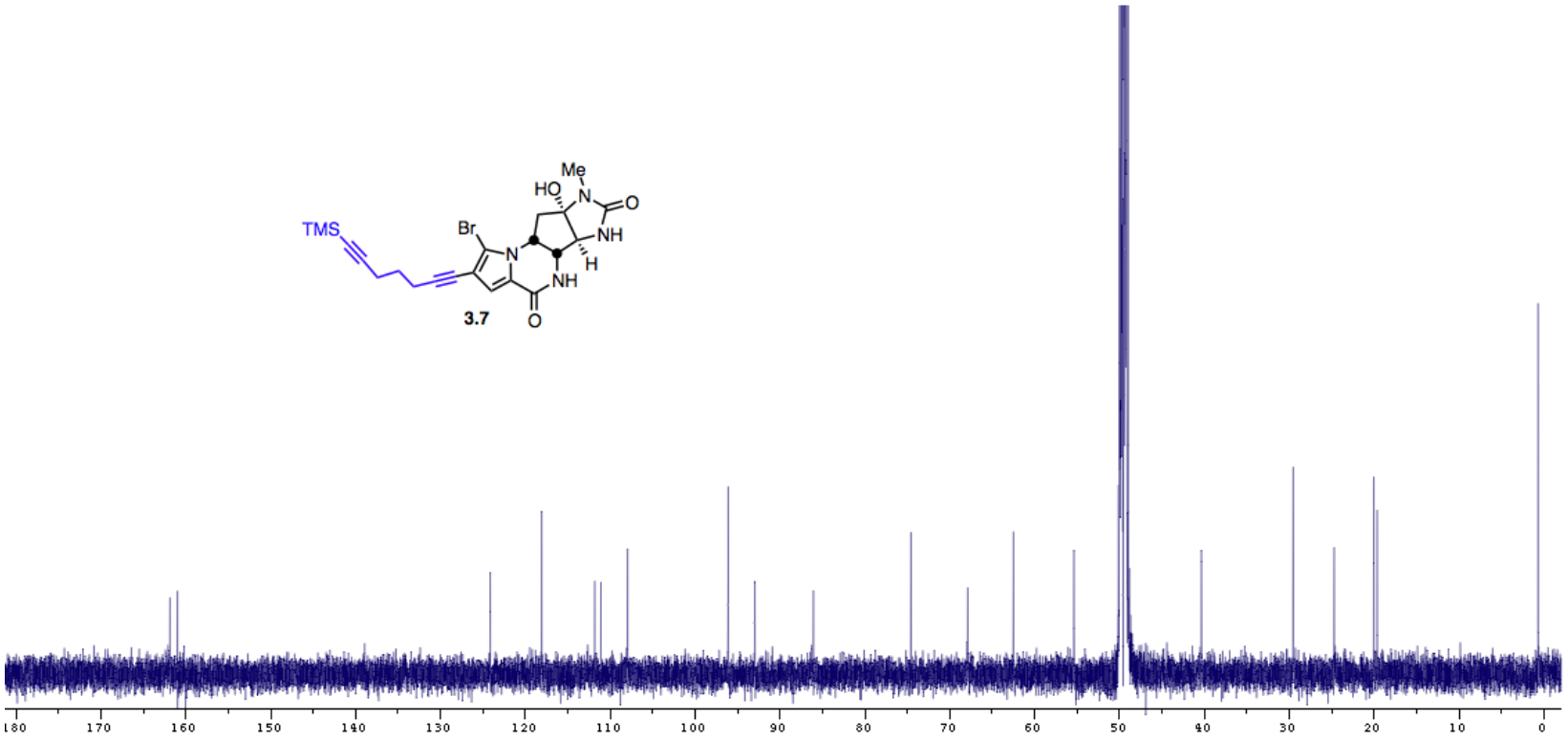

^{13}C NMR (125 MHz) of **3.7** in CD_3OD

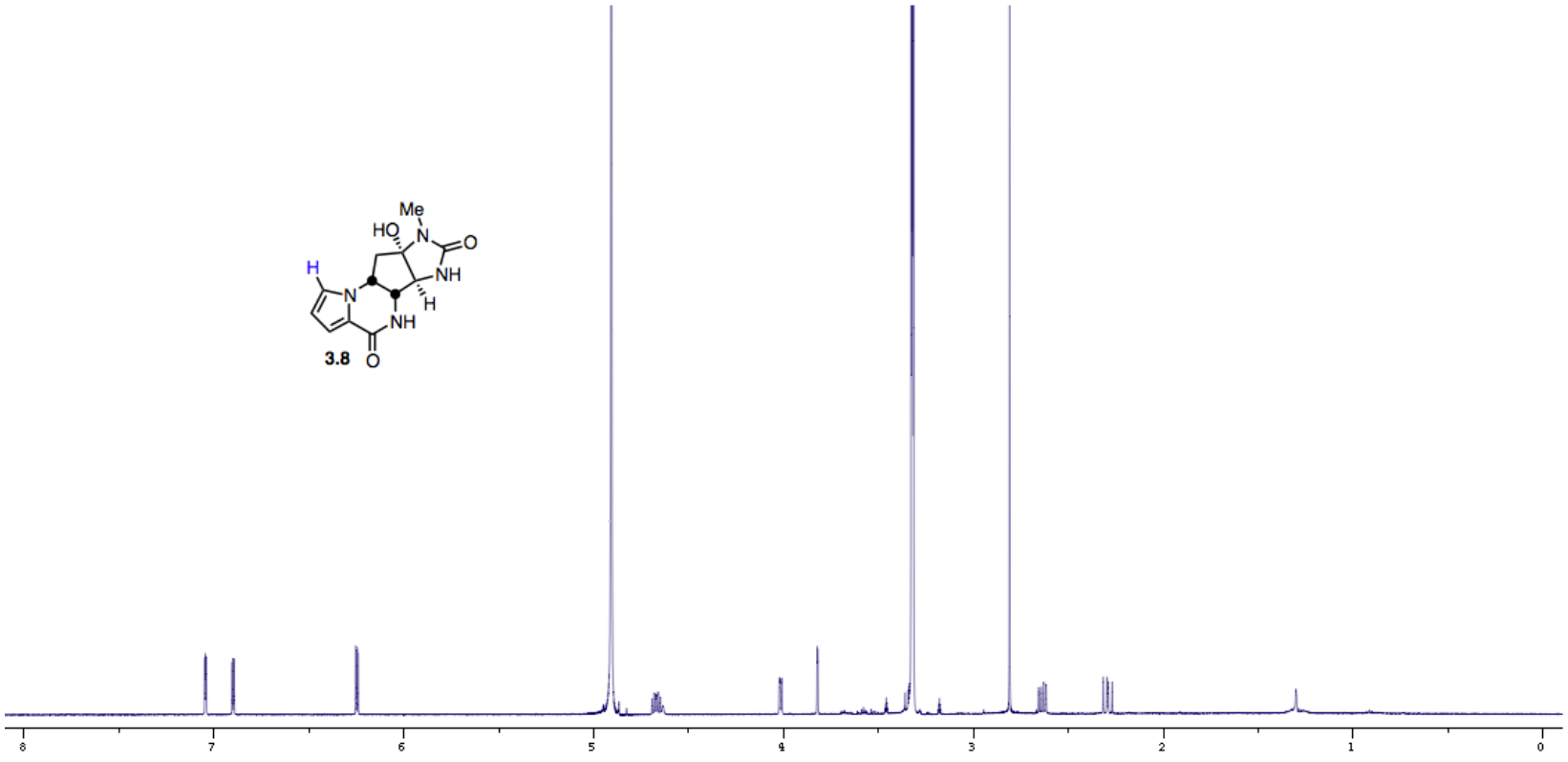

^{1}H NMR (500 MHz) of **3.8** in CD_3OD

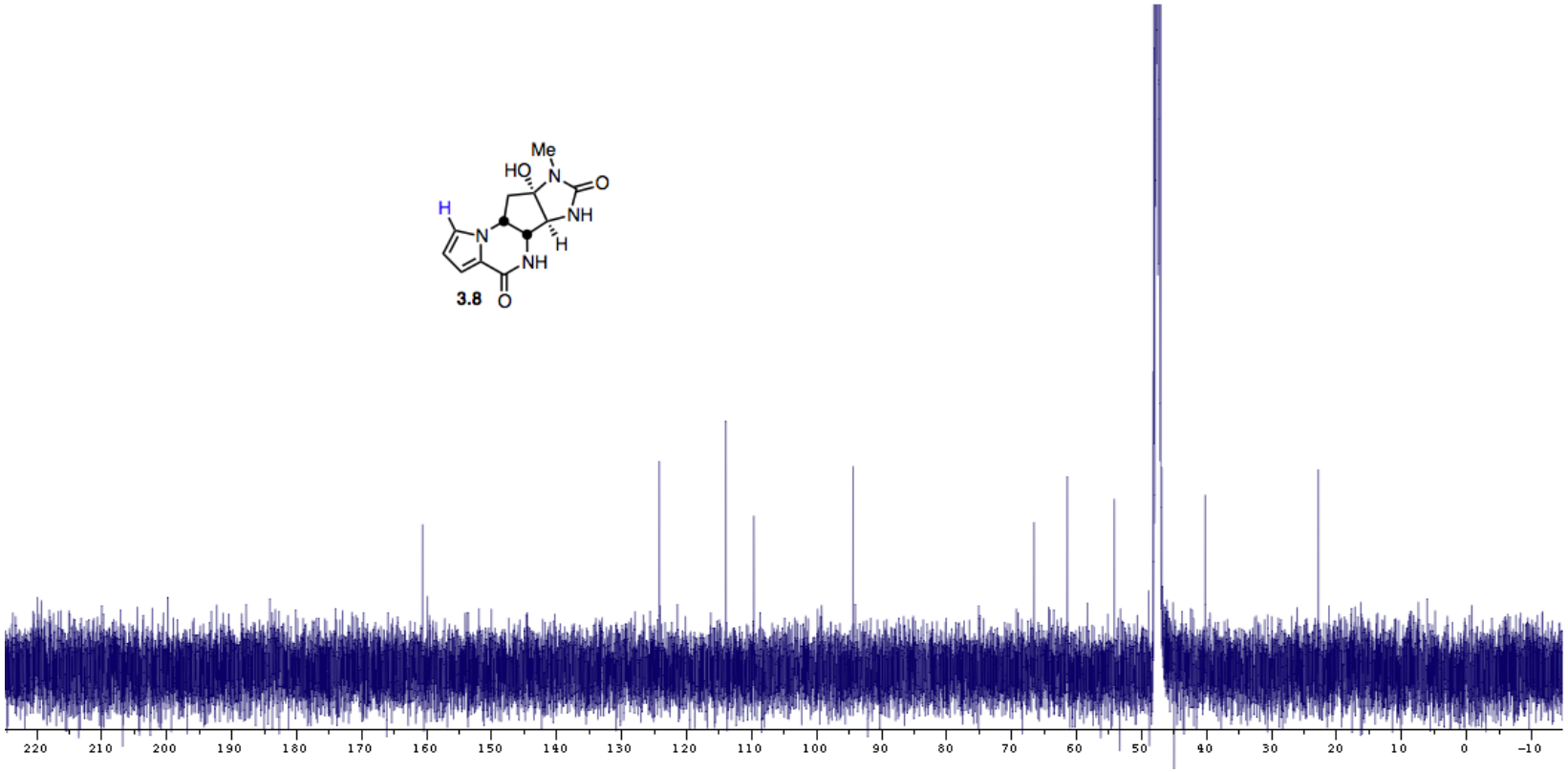

^{13}C NMR (125 MHz) of **3.8** in CD_3OD

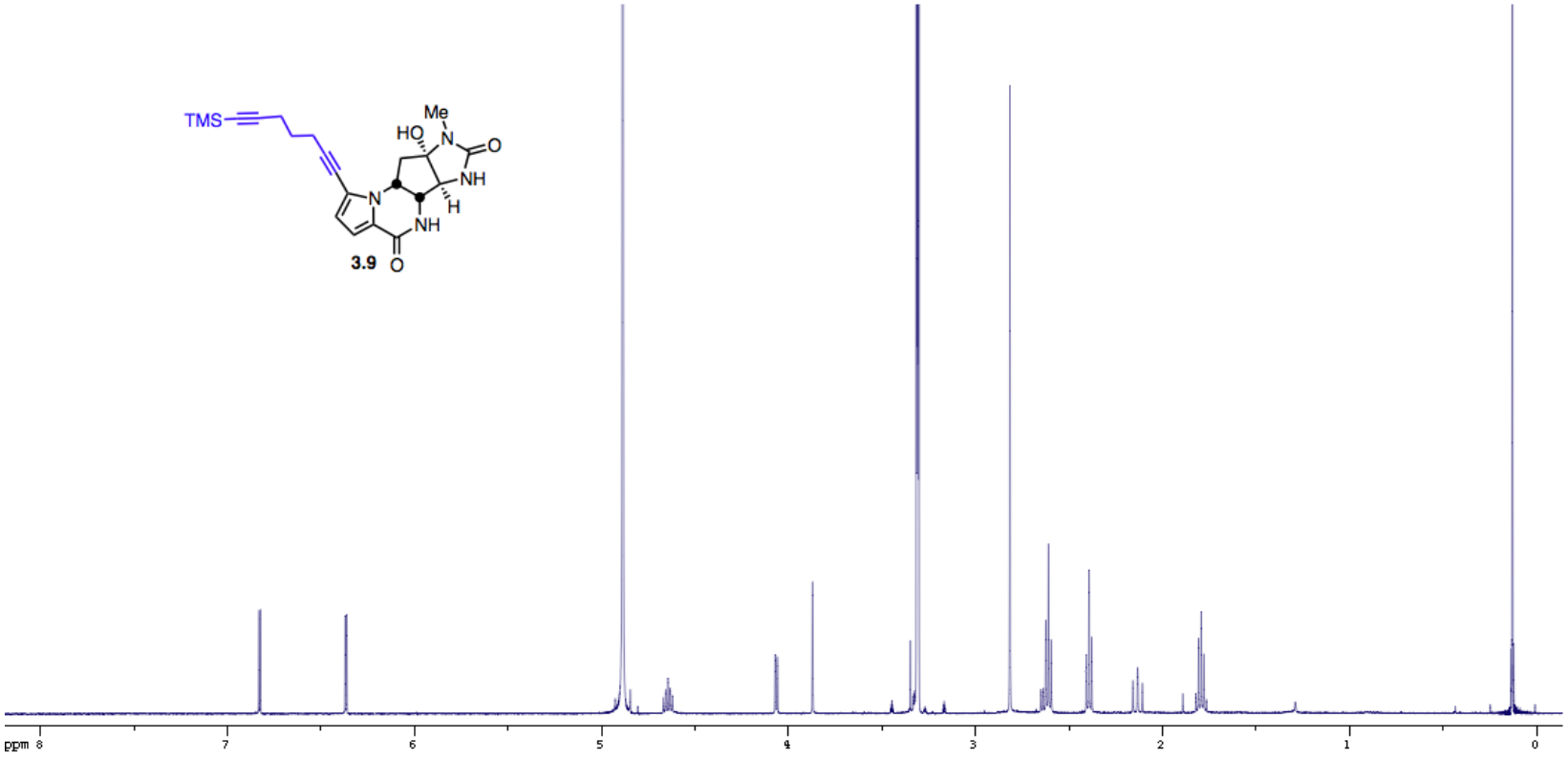

^{1}H NMR (500 MHz) of **3.9** in CD_3OD

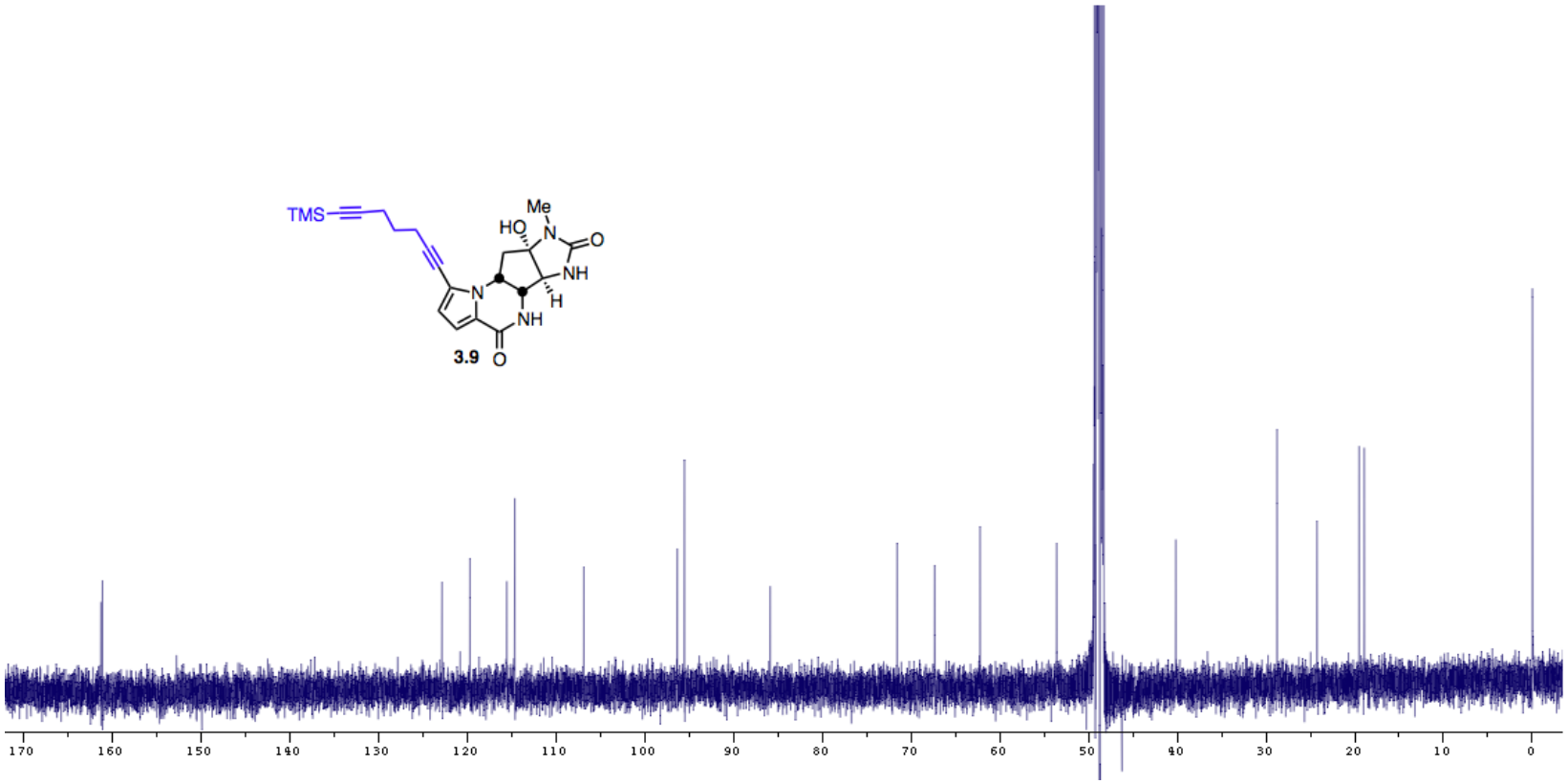

^{13}C NMR (125 MHz) of **3.9** in CD_3OD

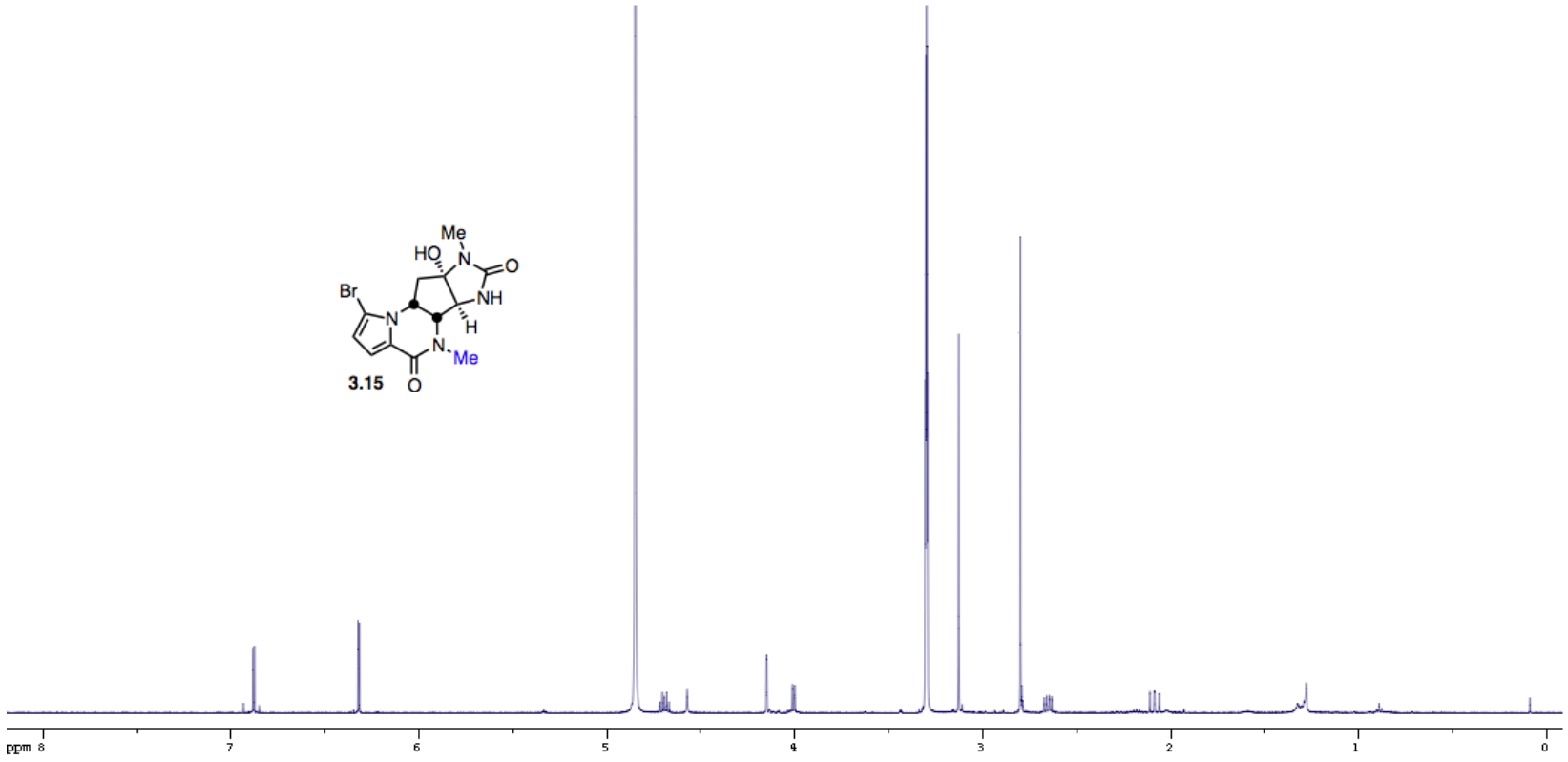

^{1}H NMR (500 MHz) of **3.15** in CD_3OD

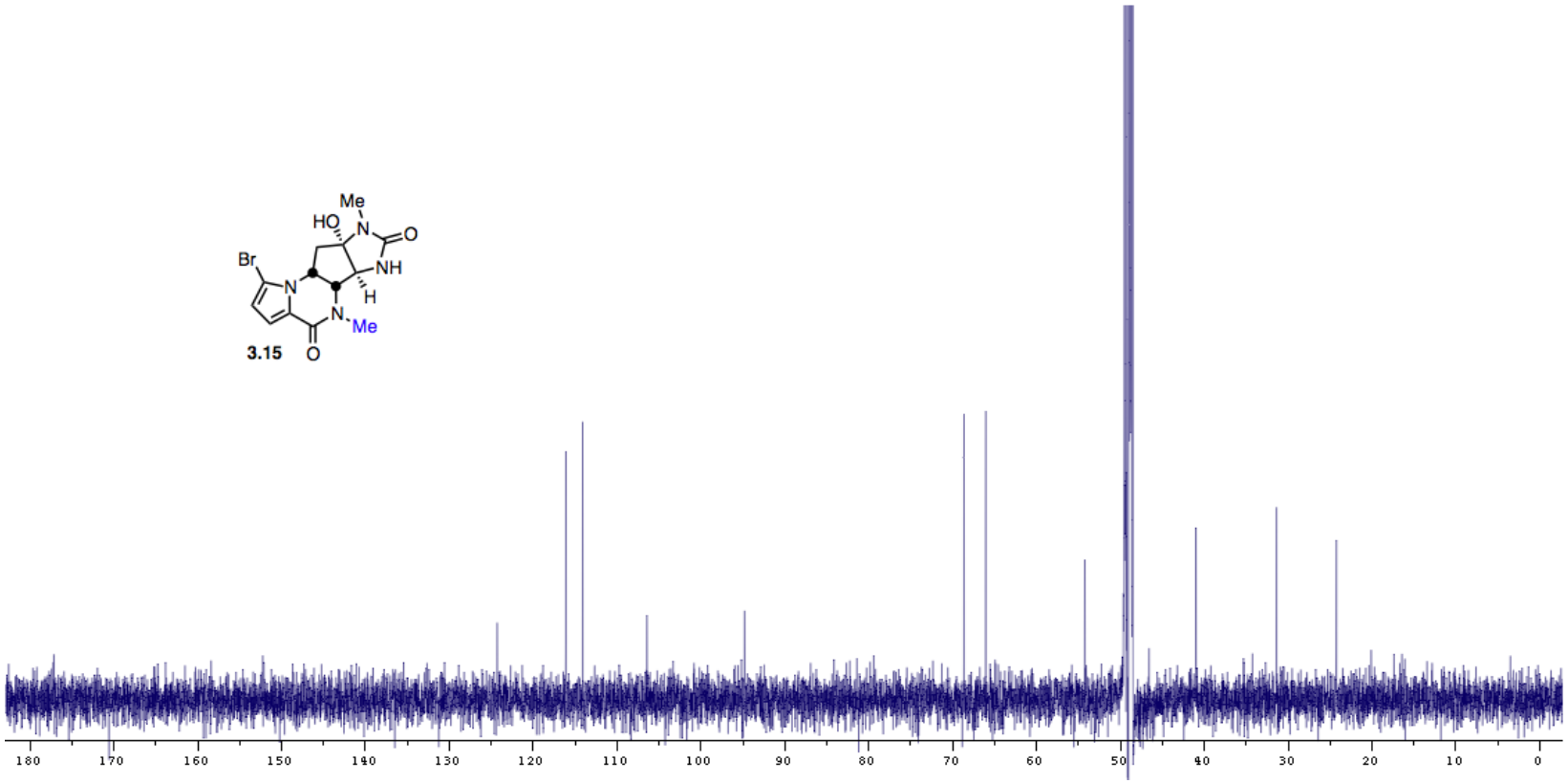

^{13}C NMR (125 MHz) of **3.15** in CD_3OD

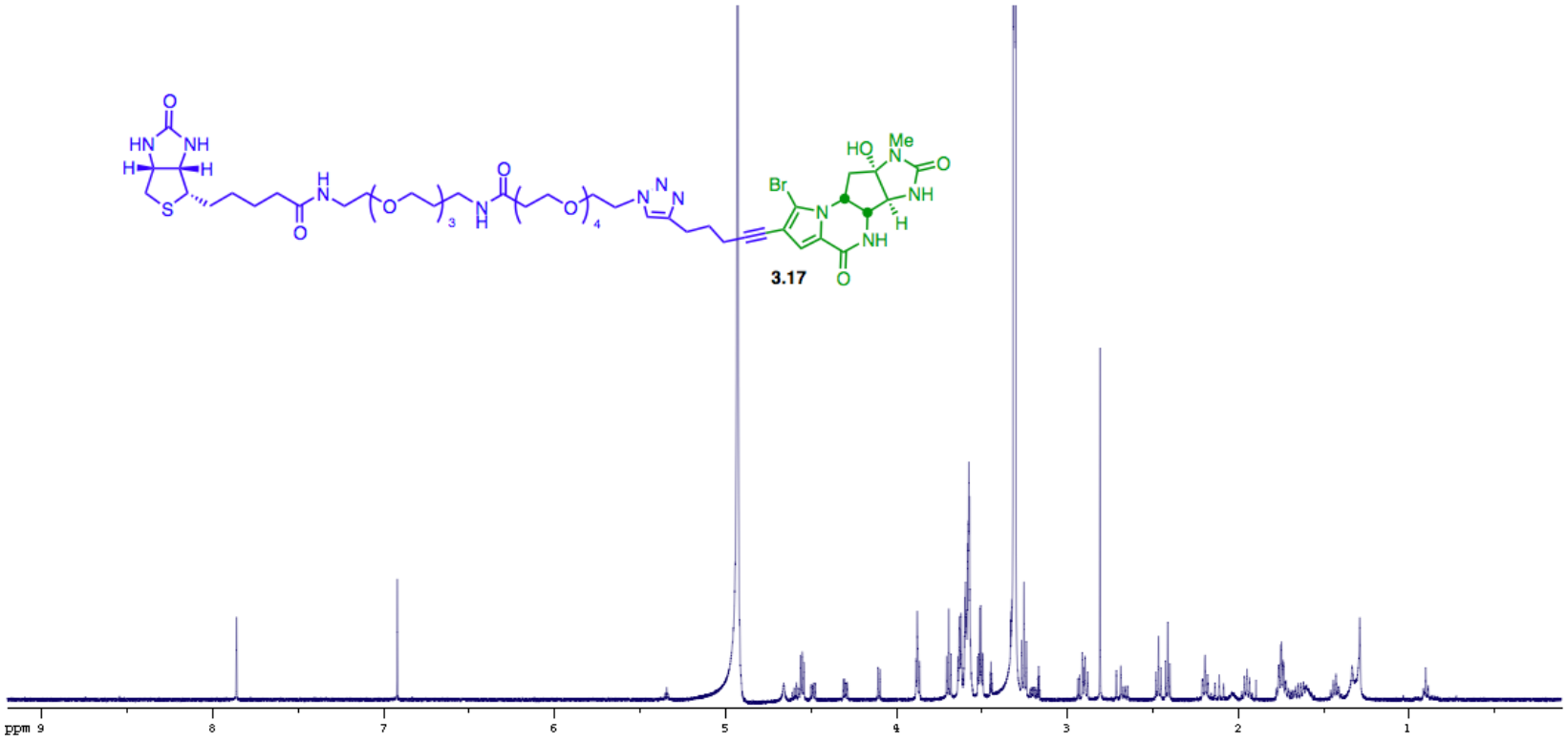

^{1}H NMR (500 MHz) of **3.17** in CD_3OD

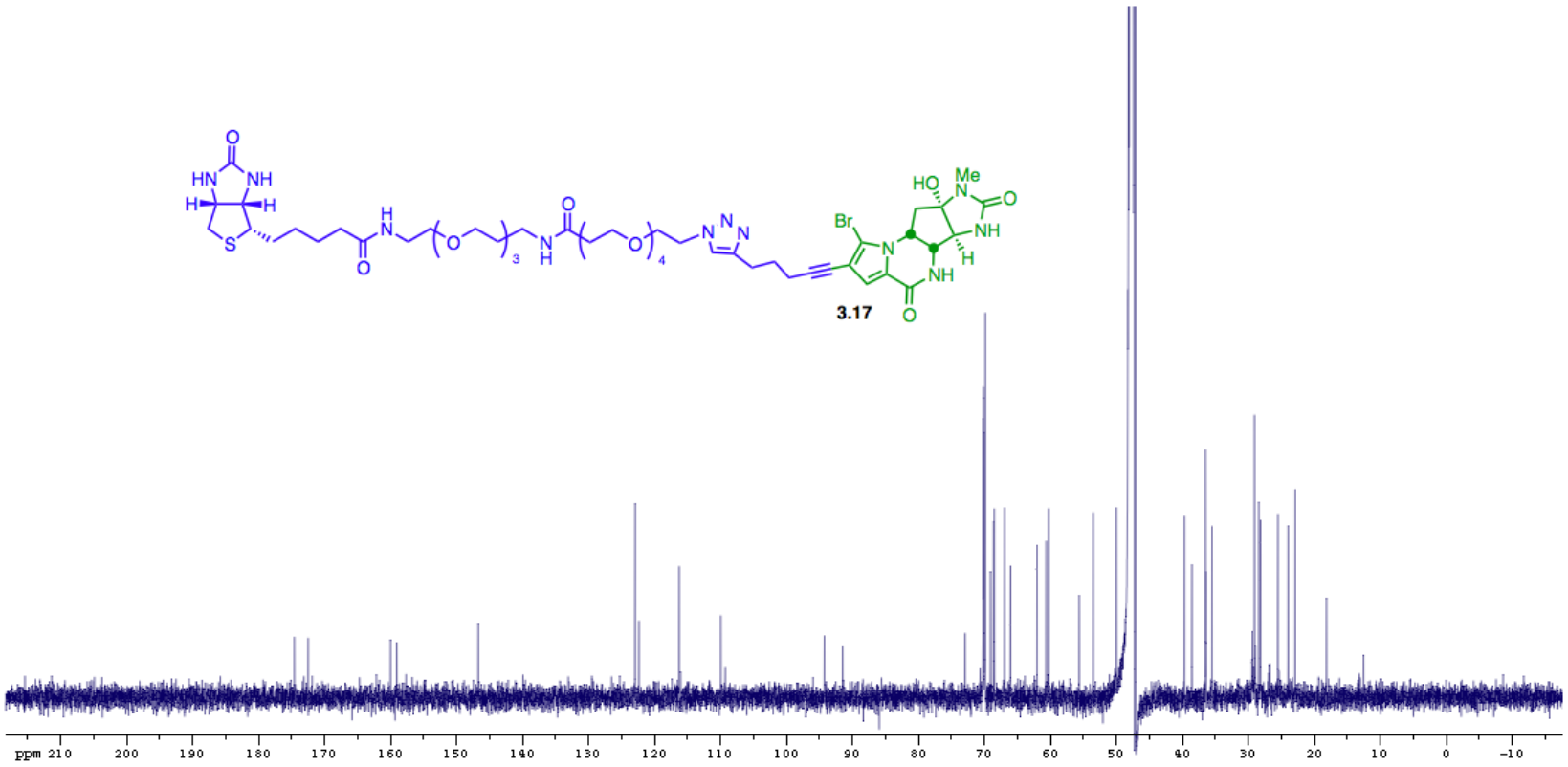

^{13}C NMR (125 MHz) of **3.17** in CD_3OD

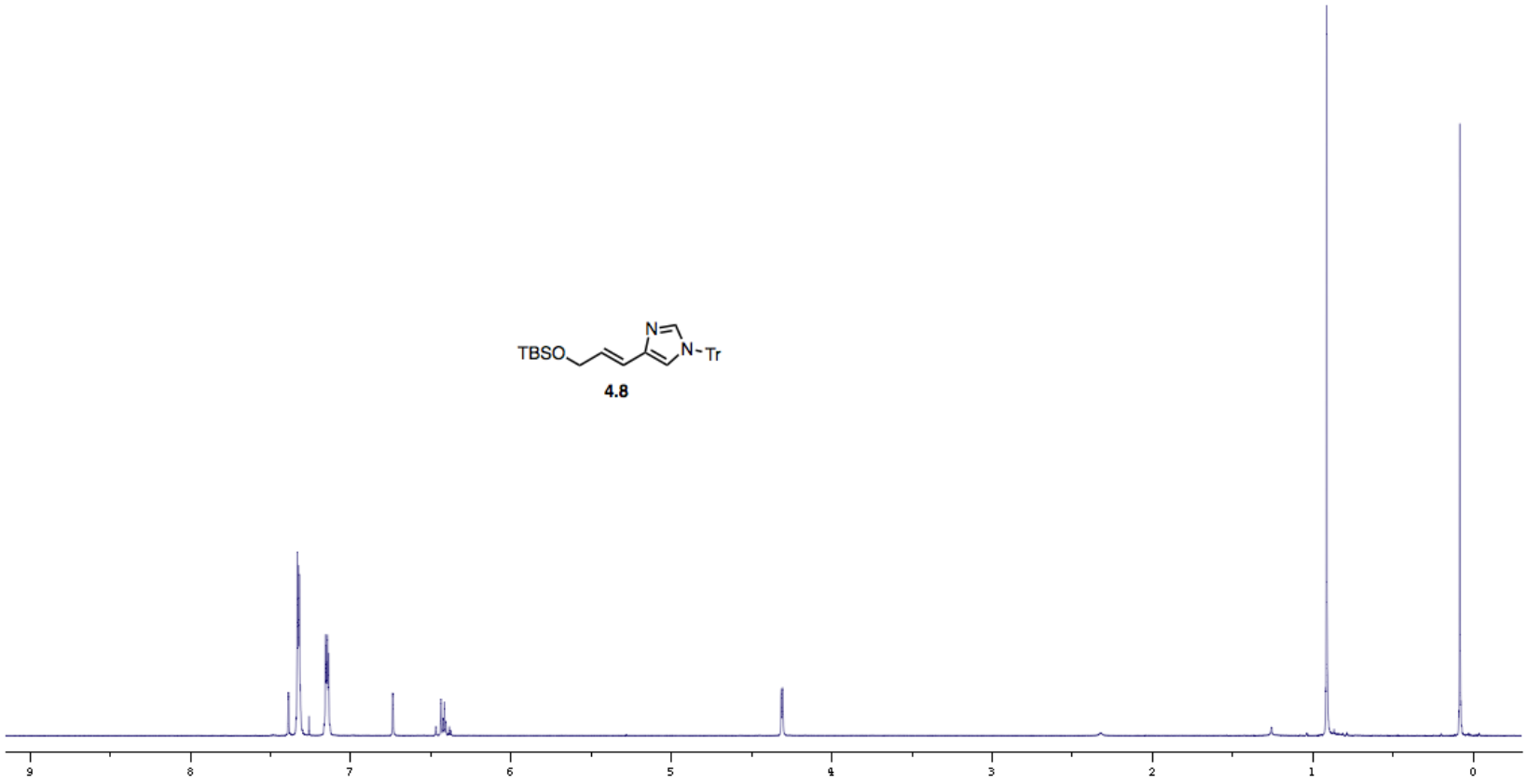

^{1}H NMR (500 MHz) of **4.8** in $CDCl_3$

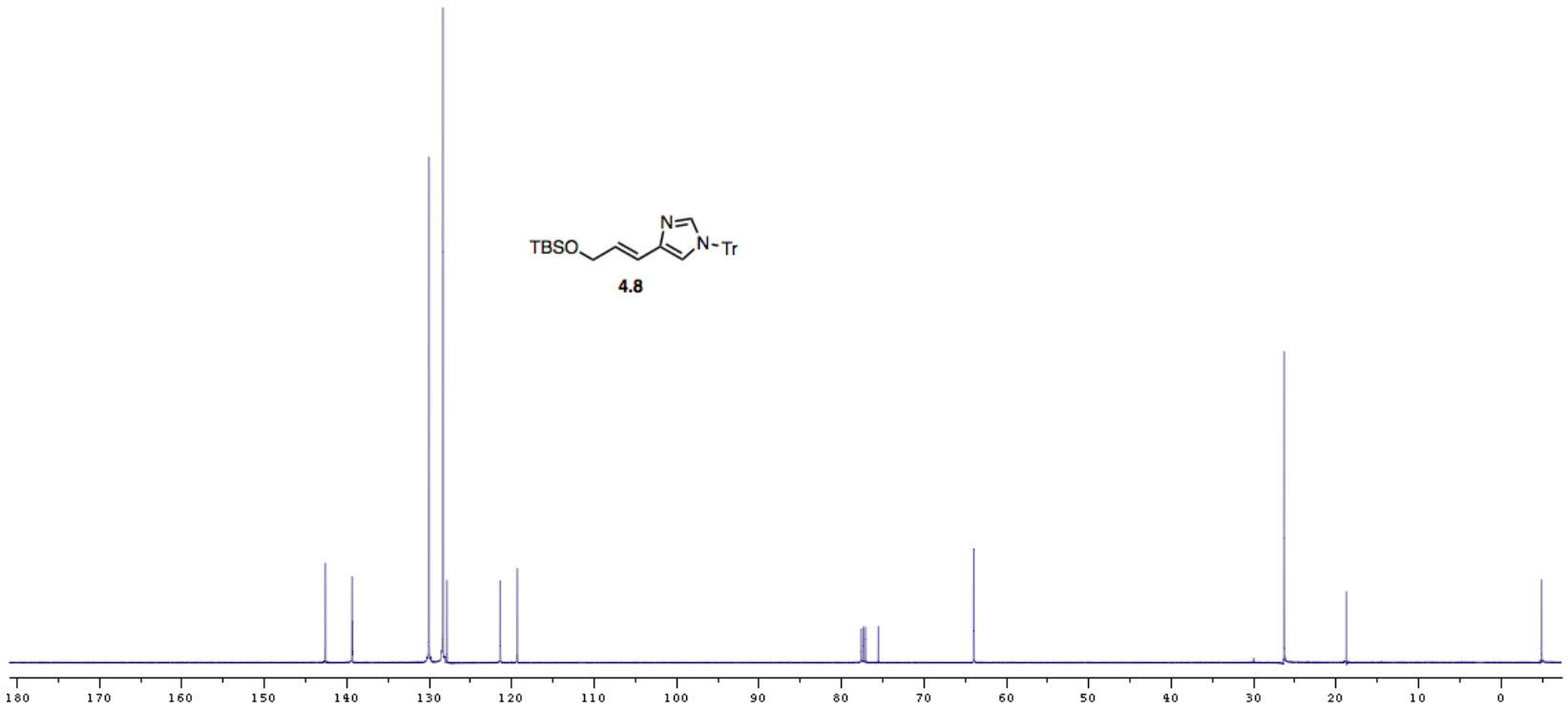

^{13}C NMR (125 MHz) of **4.8** in $CDCl_3$

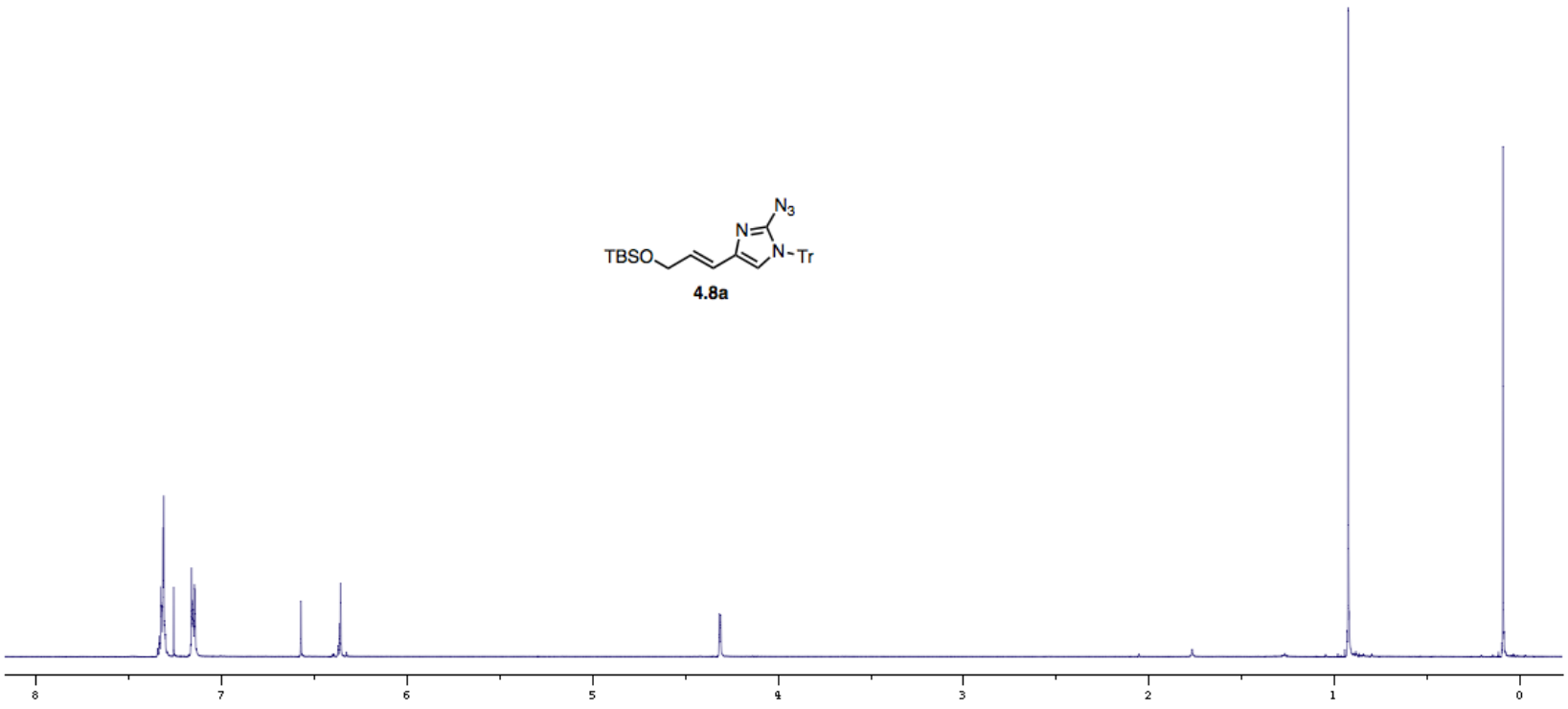

^{1}H NMR (500 MHz) of **4.8a** in $CDCl_3$

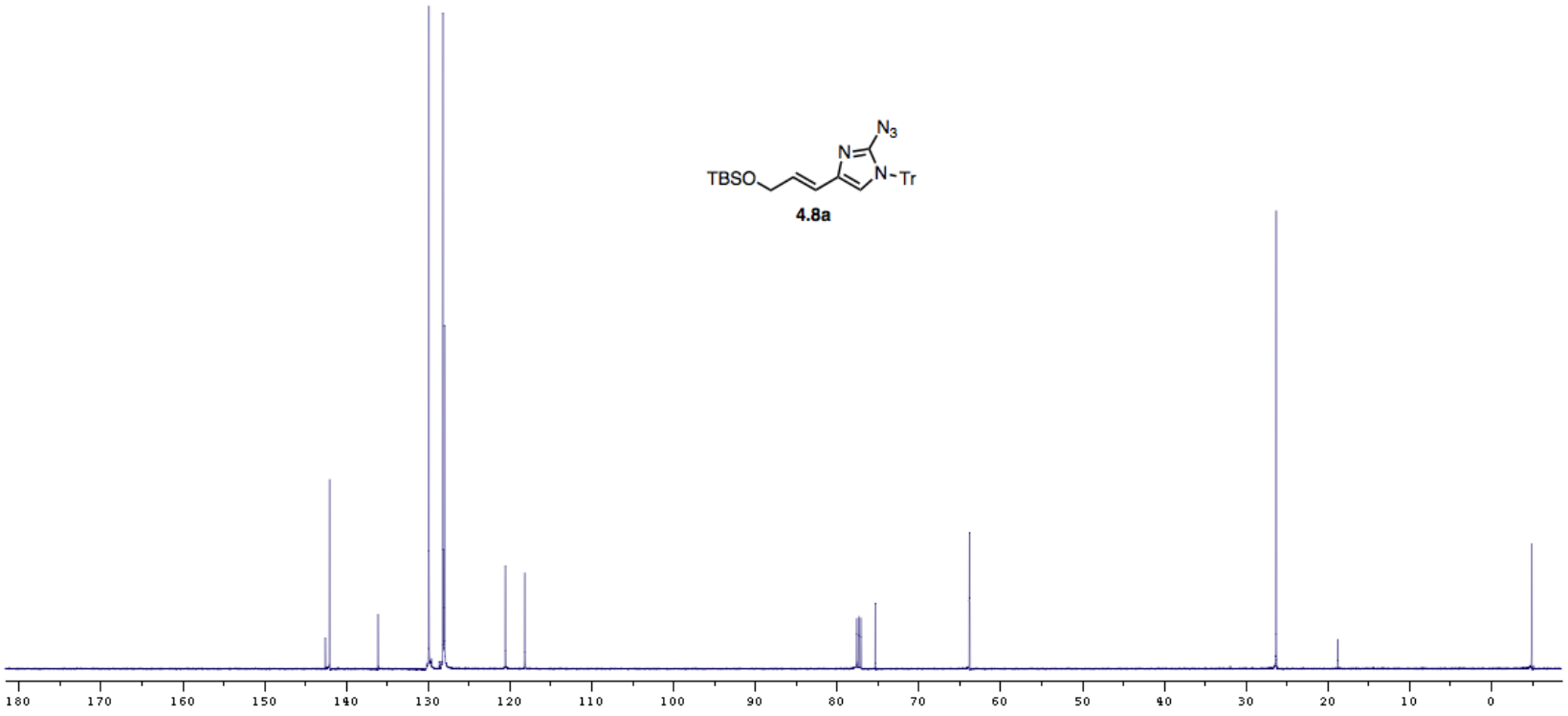

^{13}C NMR (125 MHz) of **4.8a** in $CDCl_3$

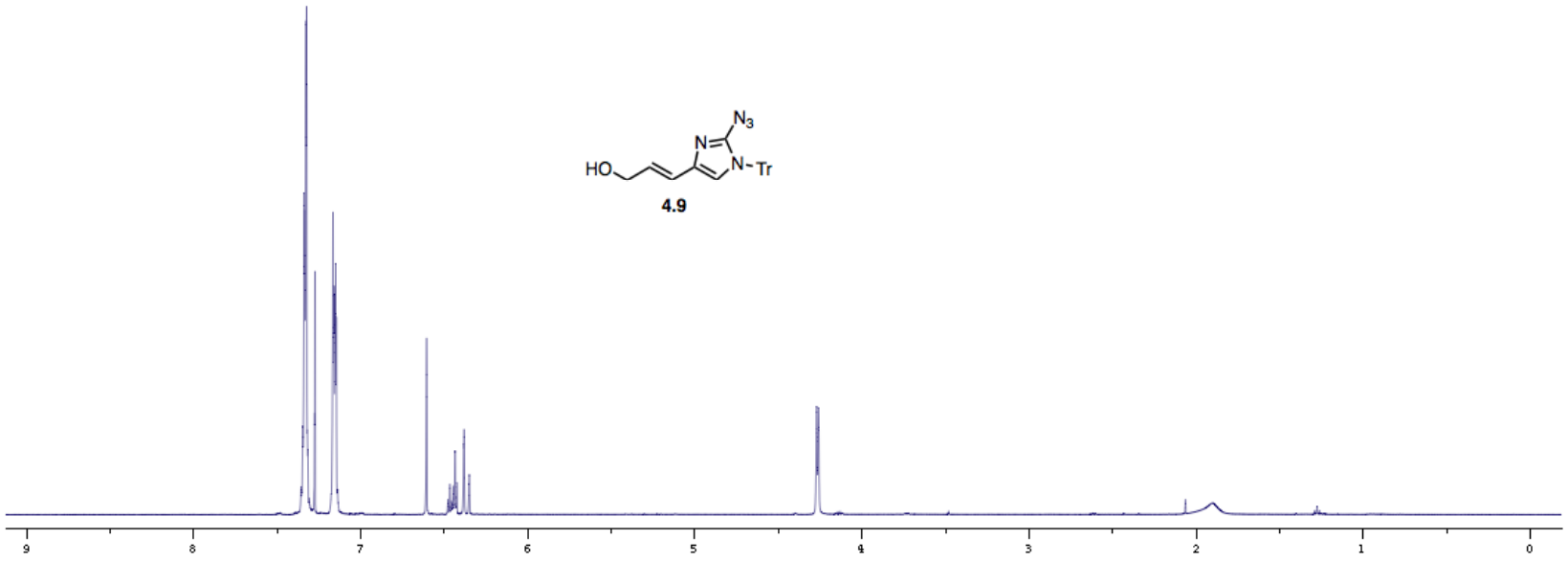

^{1}H NMR (500 MHz) of **4.9** in $CDCl_3$

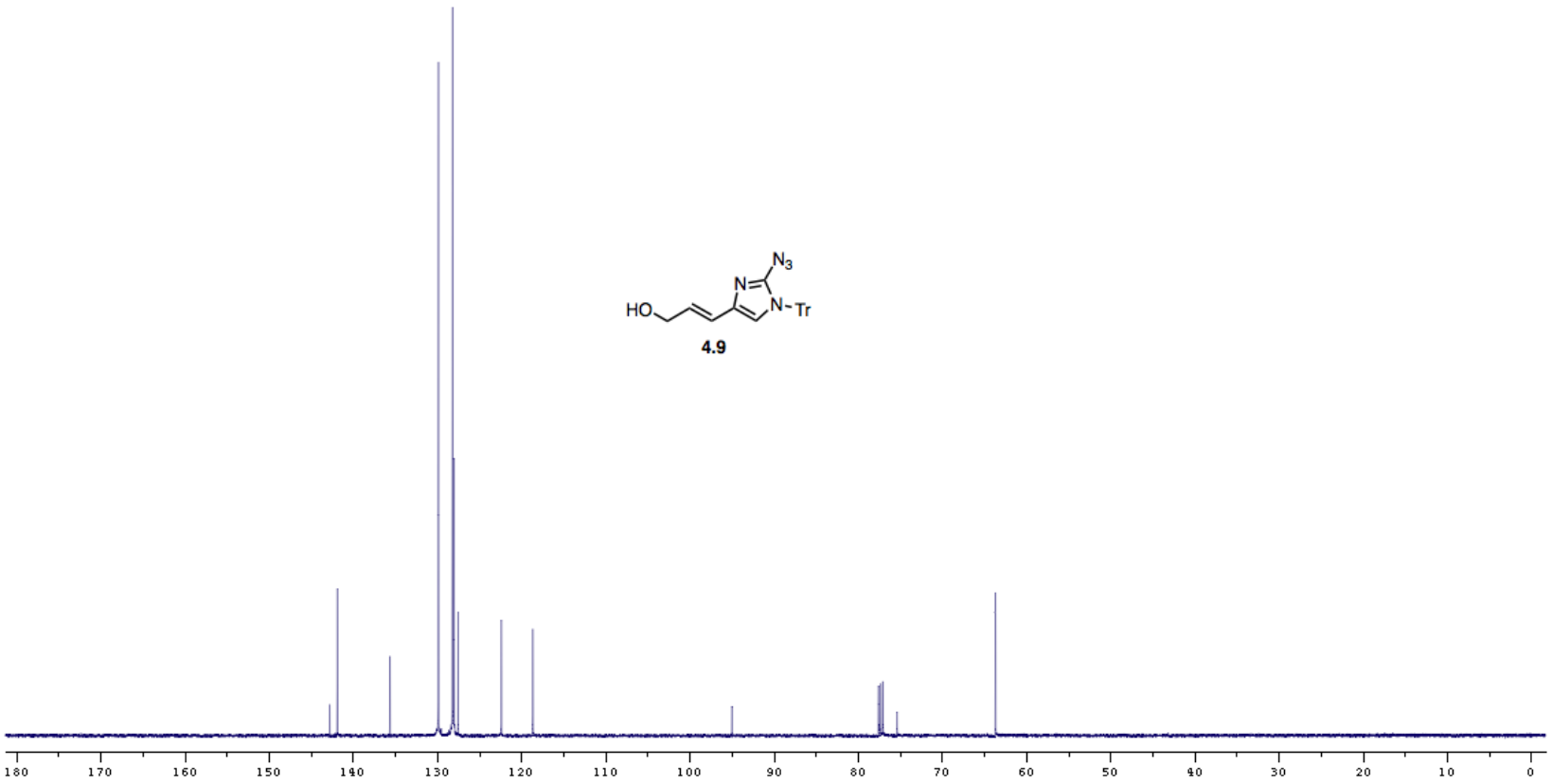

^{13}C NMR (125 MHz) of **4.9** in $CDCl_3$

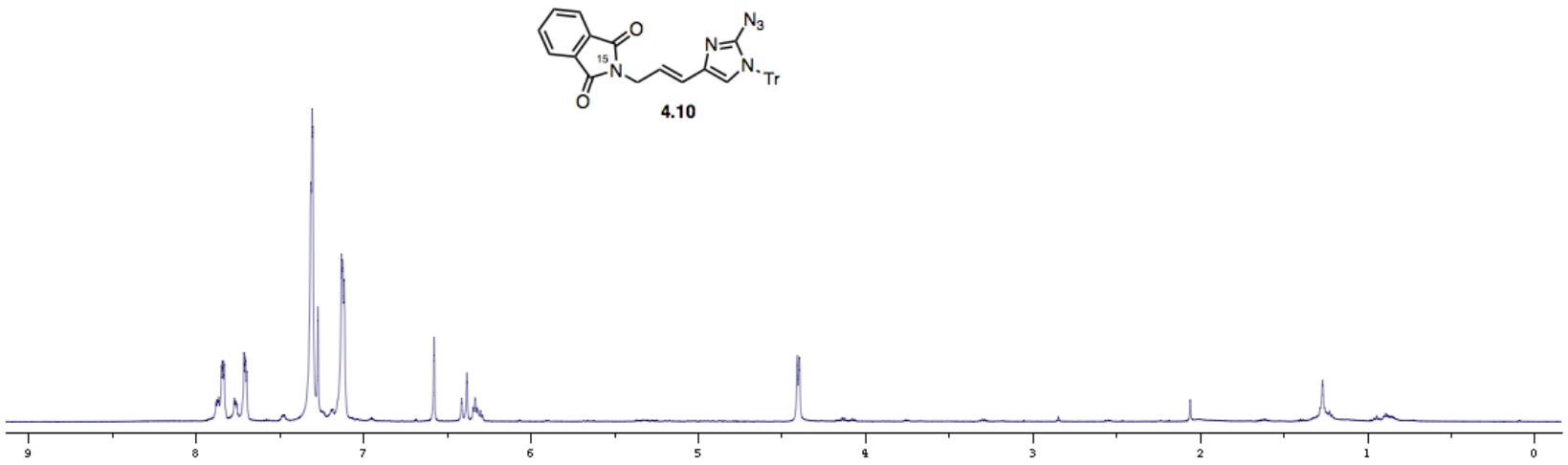

^{1}H NMR (500 MHz) of **4.10** in $CDCl_3$

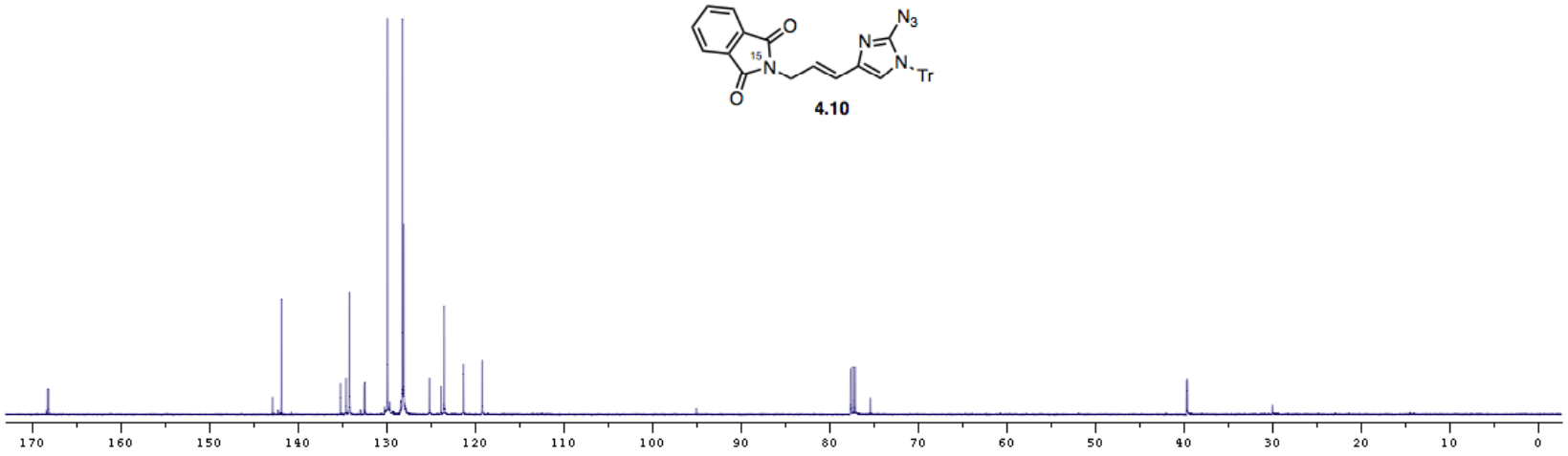

^{13}C NMR (125 MHz) of **4.10** in $CDCl_3$

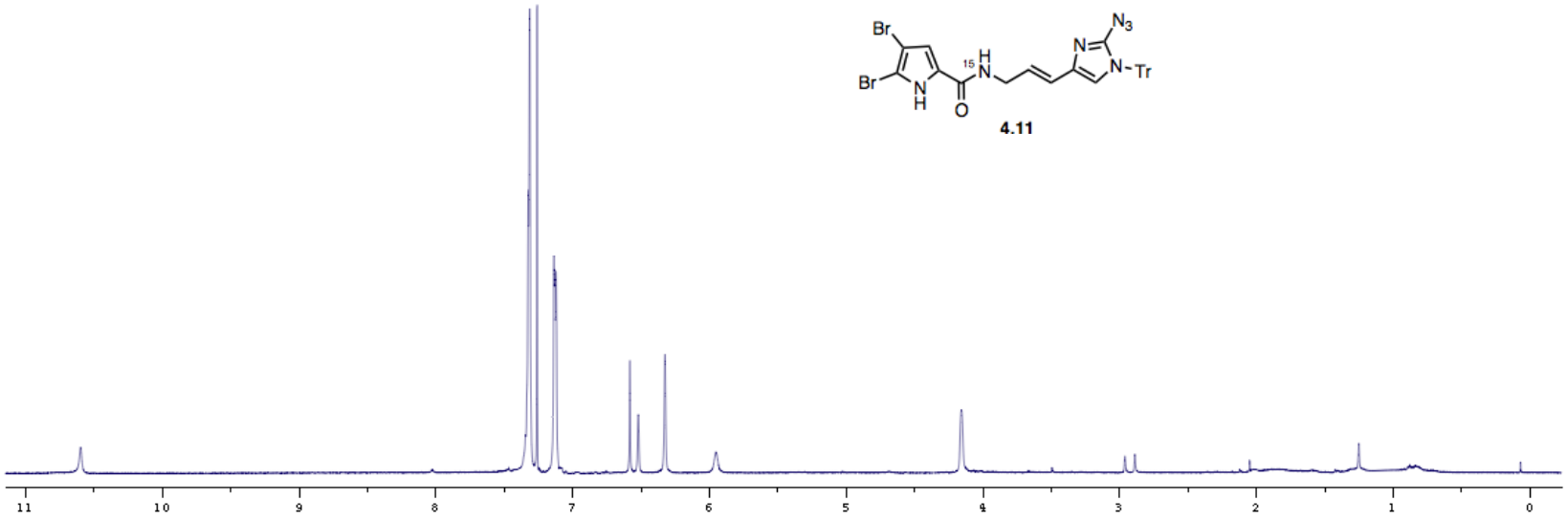

^{1}H NMR (500 MHz) of **4.11** in $CDCl_3$

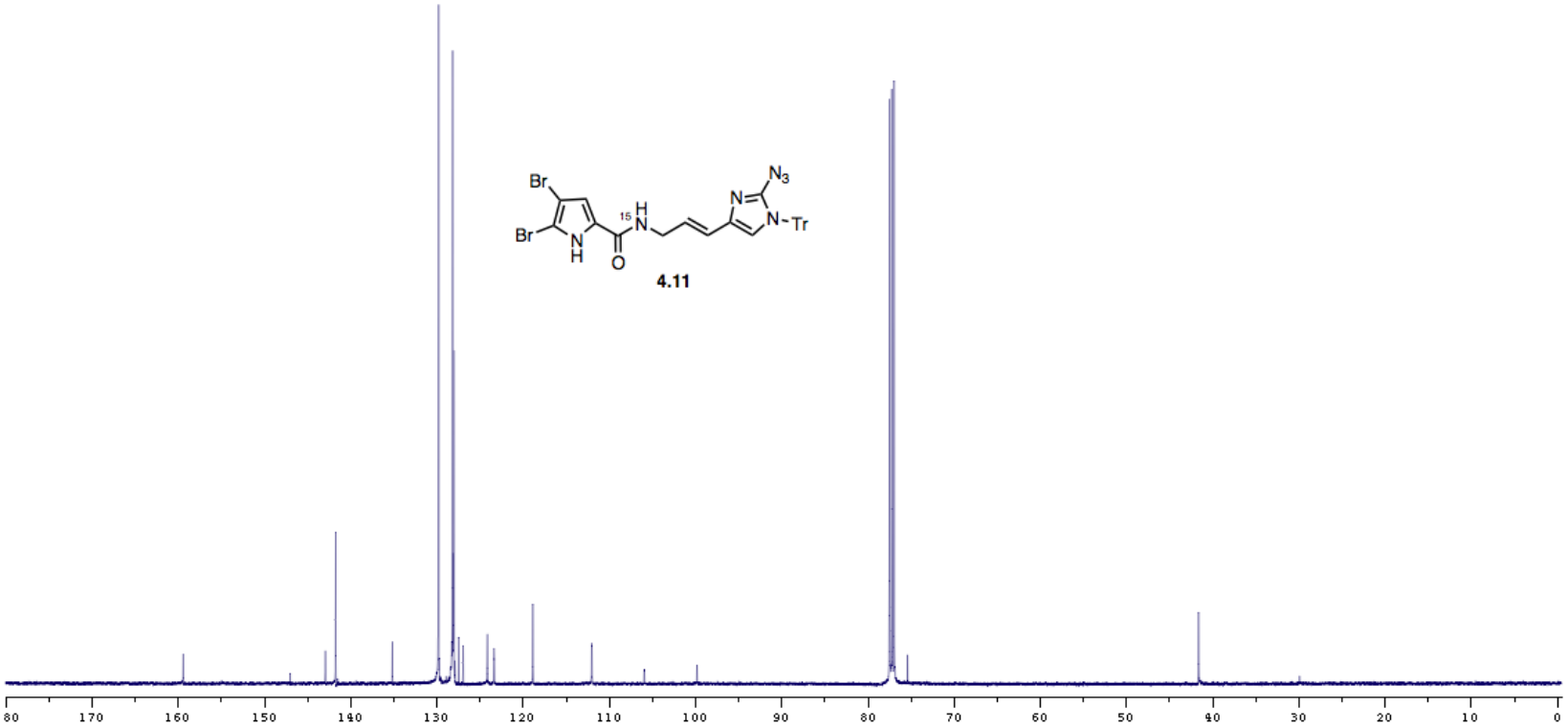

^{13}C NMR (125 MHz) of **4.11** in $CDCl_3$

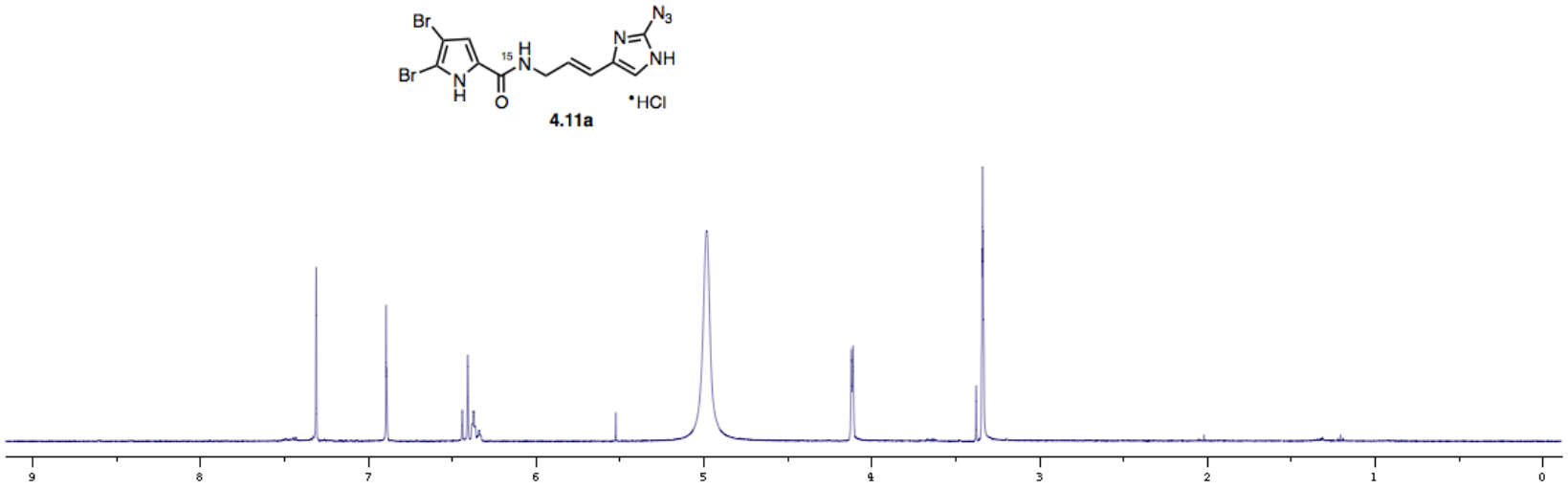

^{1}H NMR (500 MHz) of **4.11a** in CD_3OD

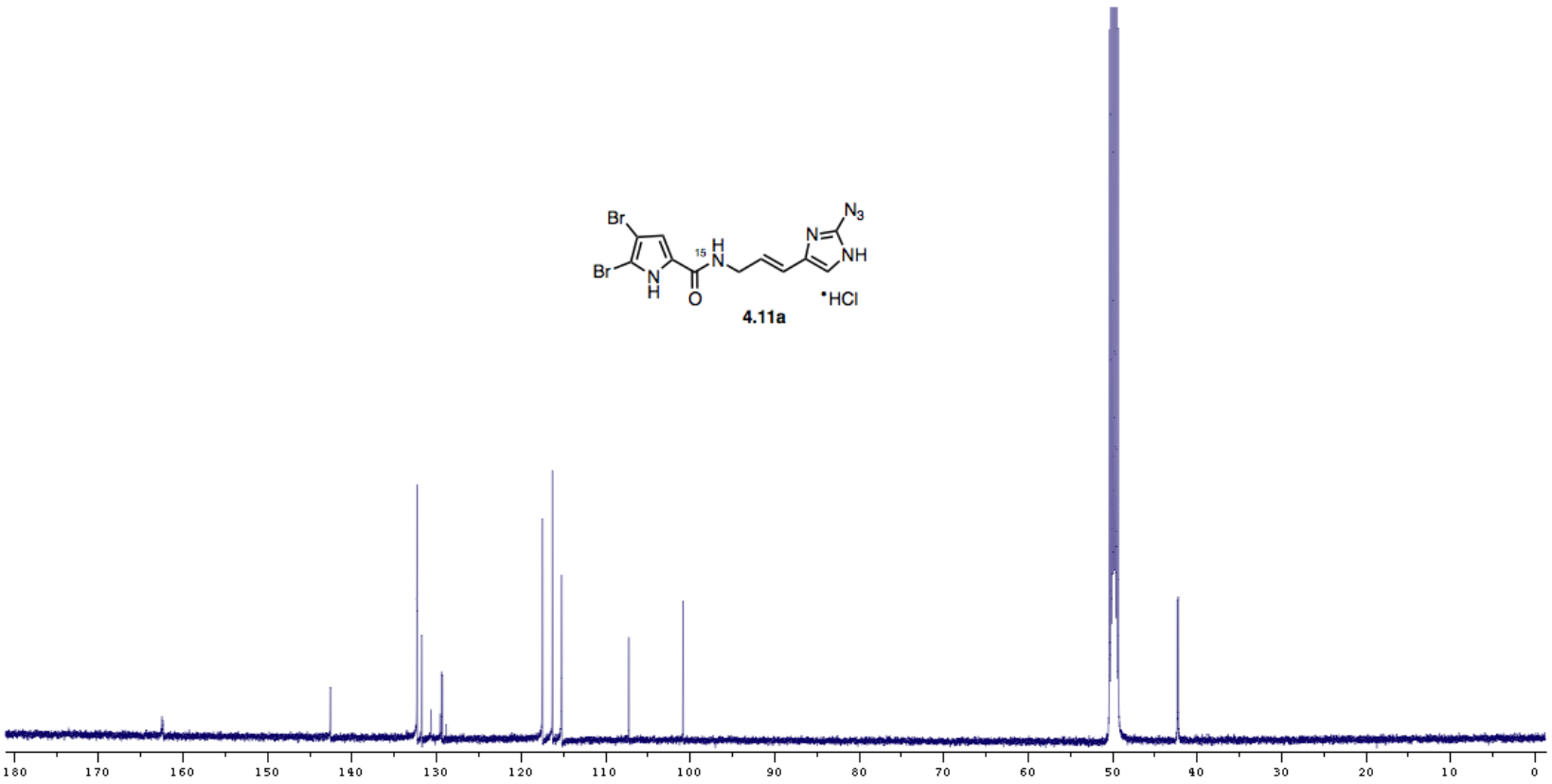

^{13}C NMR (125 MHz) of **4.11a** in CD_3OD

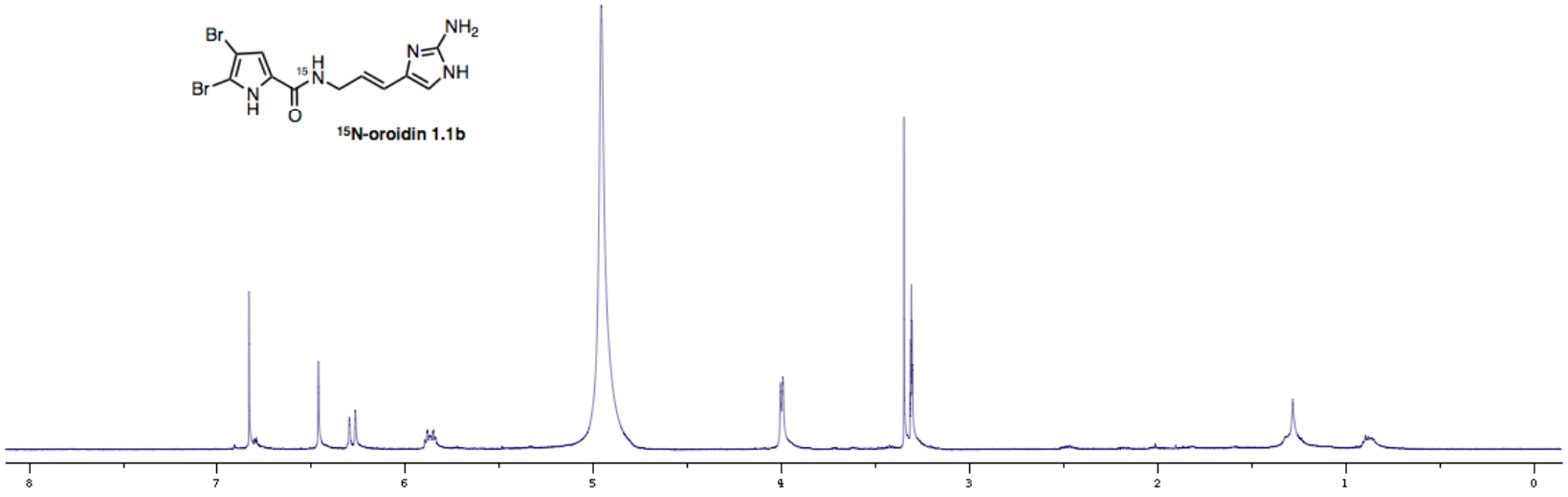

^{1}H NMR (500 MHz) of **1.1b** in CD_3OD

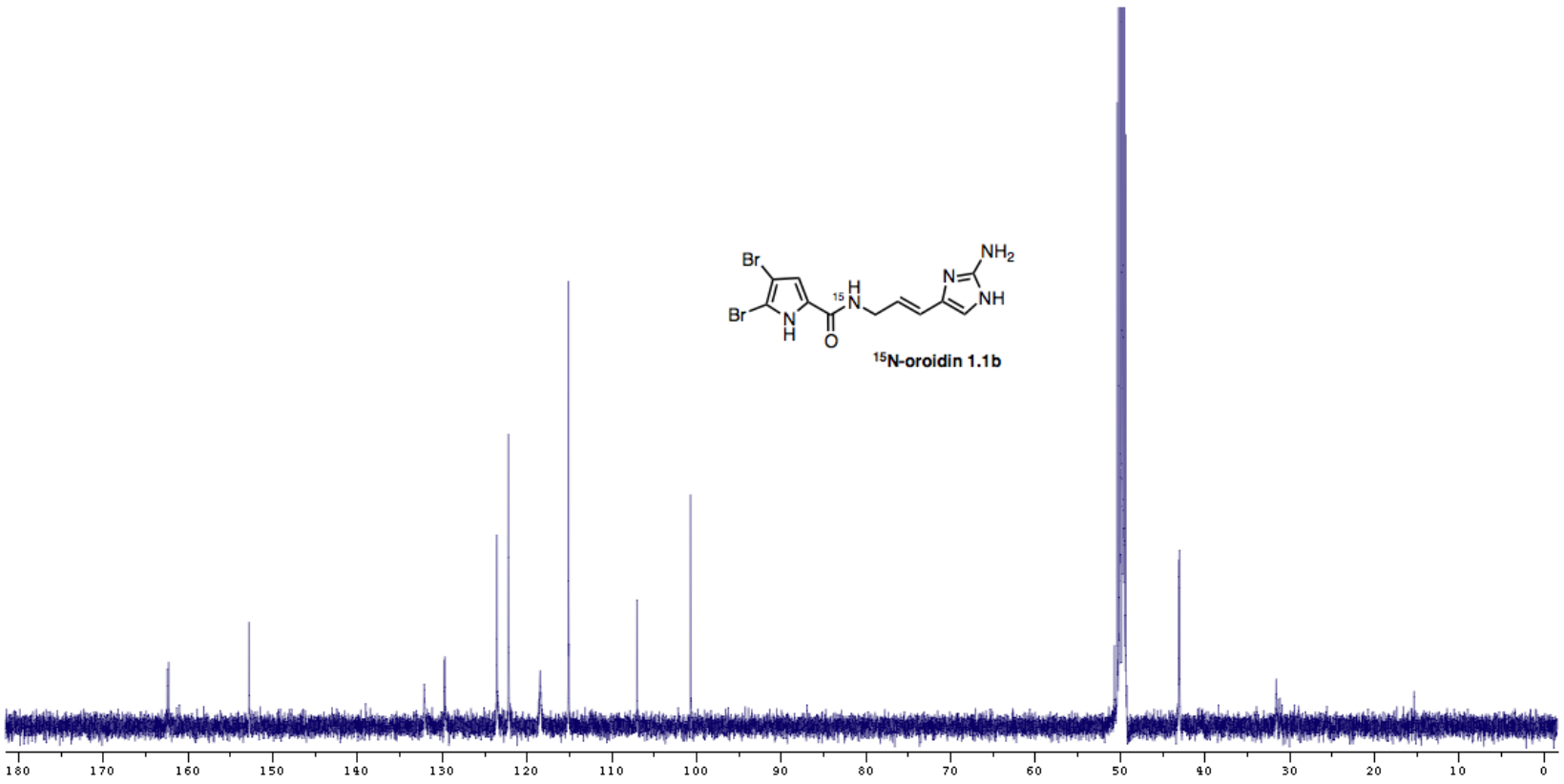

^{13}C NMR (125 MHz) of **1.1b** in CD_3OD

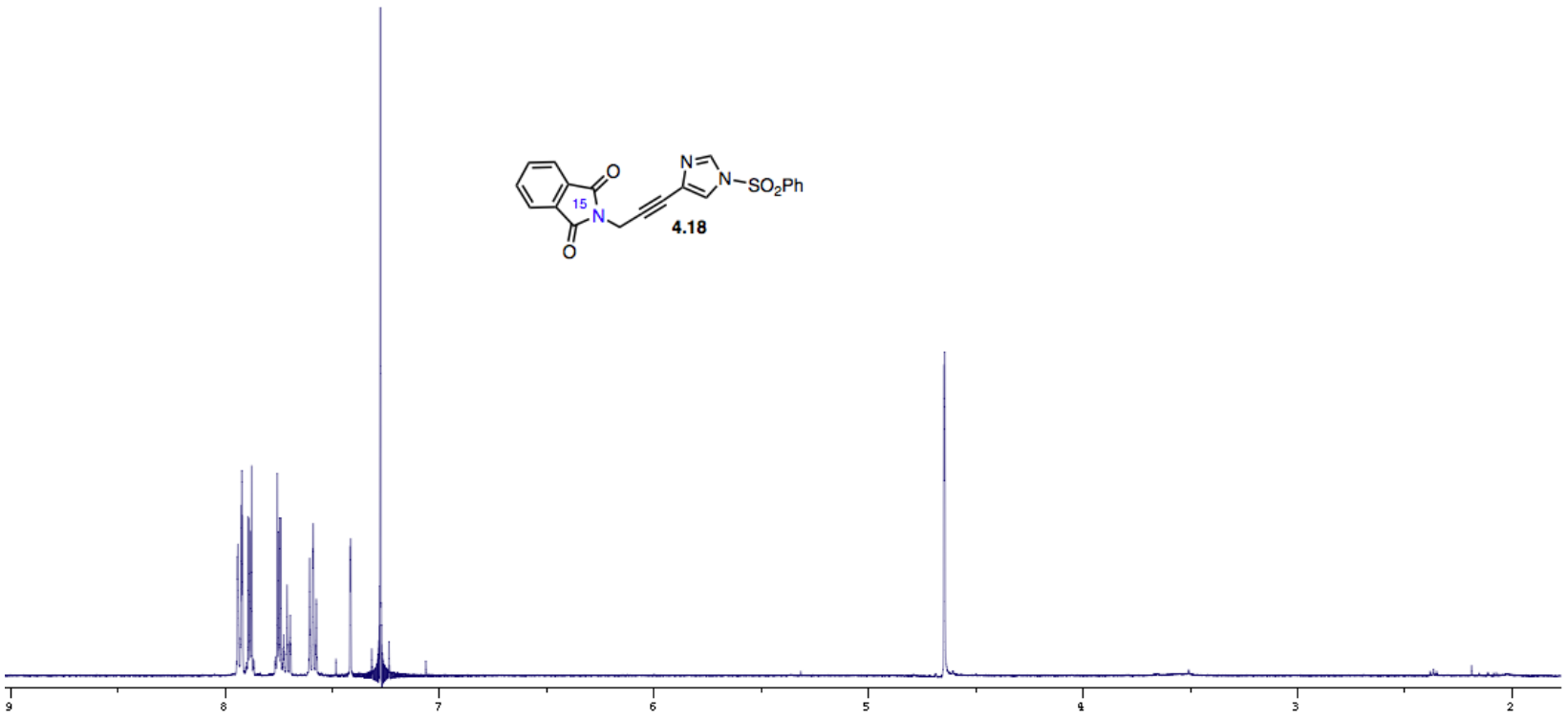

^{1}H NMR (500 MHz) of **4.18** in $CDCl_3$

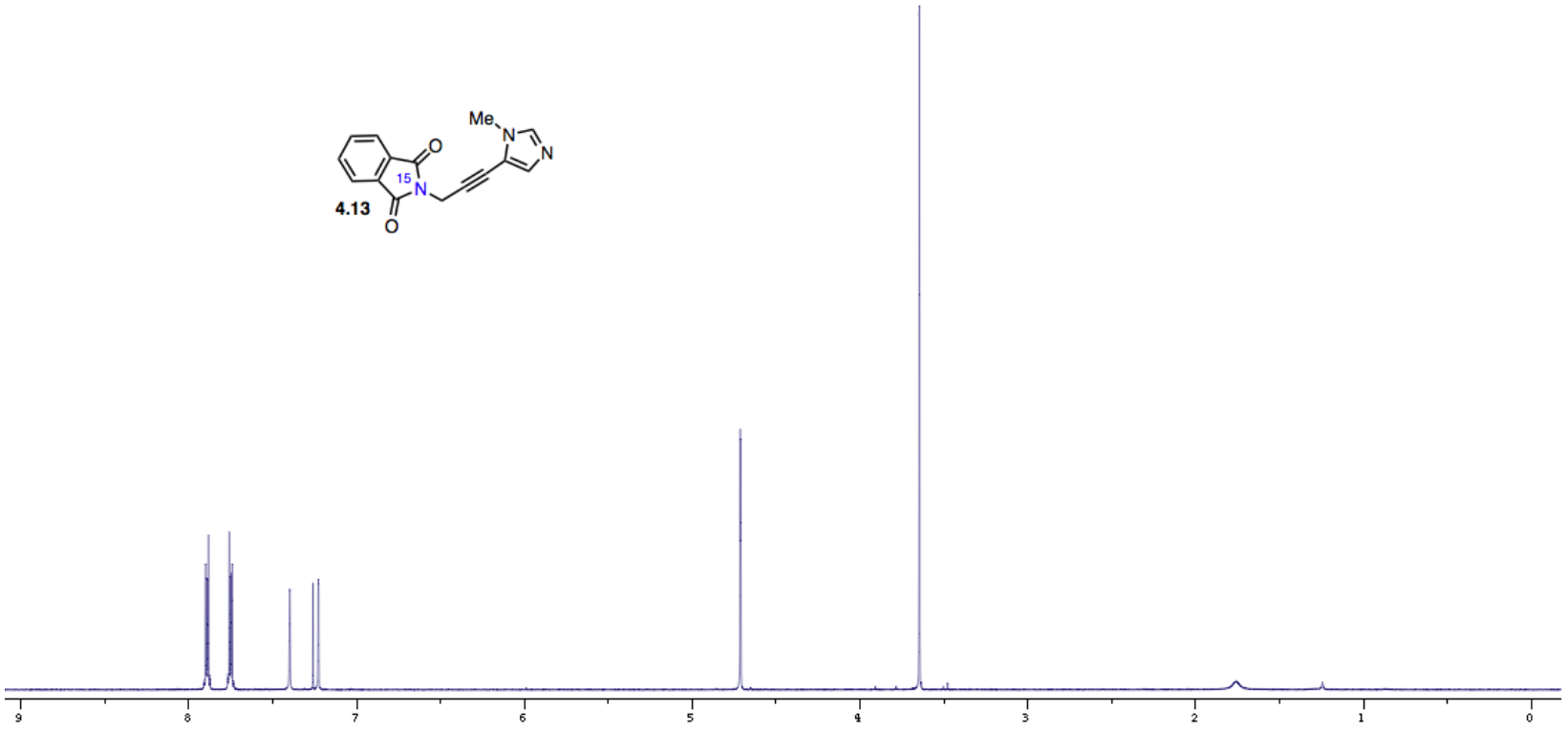

^{1}H NMR (500 MHz) of **4.13** in $CDCl_3$

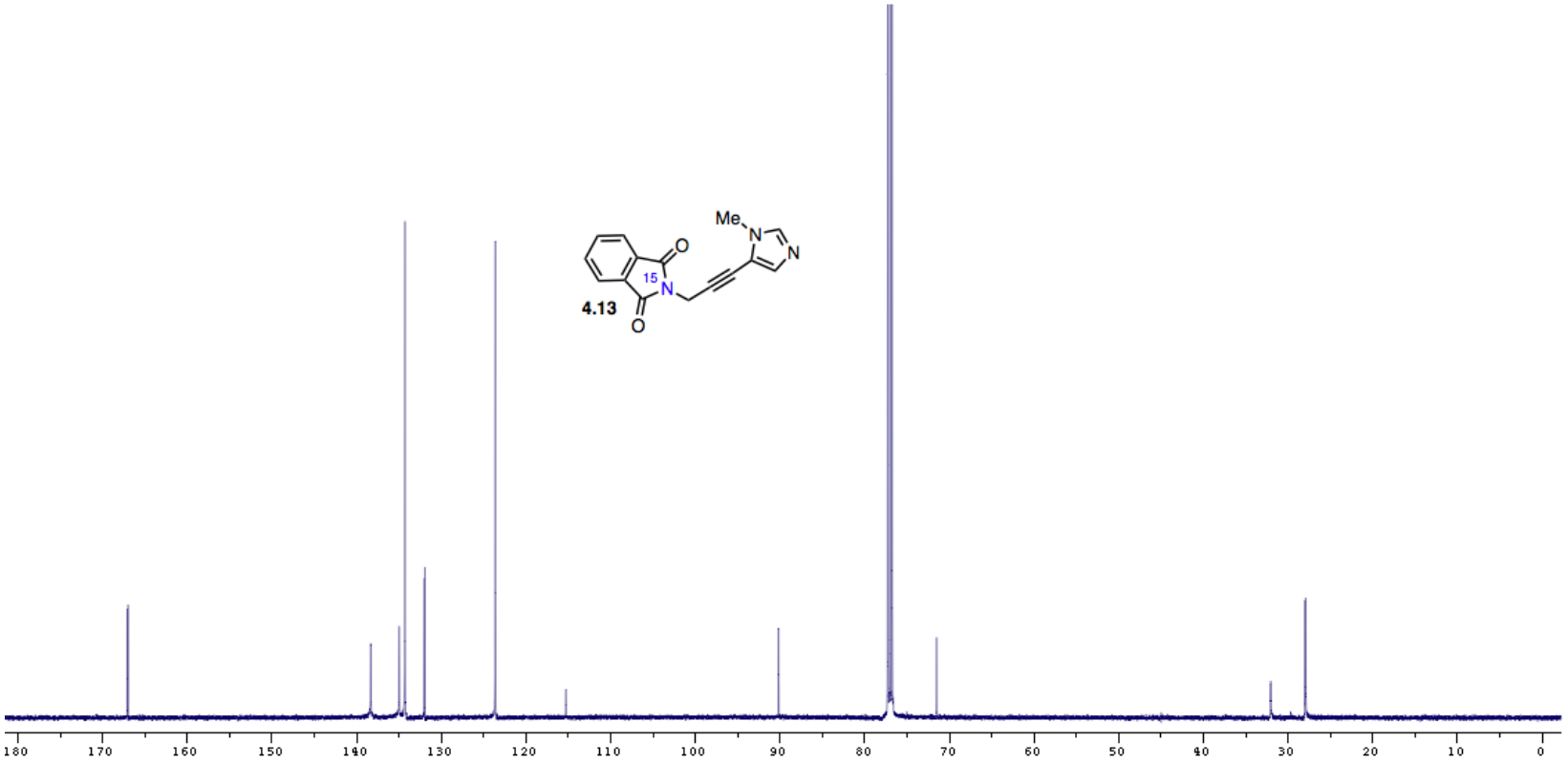

^{13}C NMR (125 MHz) of **4.13** in $CDCl_3$

APPENDIX B

LETTERS OF PERMISSION

American Chemical Society's Policy on Theses and Dissertations

If your university requires a signed copy of this letter see contact information below.

Thank you for your request for permission to include **your** paper(s) or portions of text from **your** paper(s) in your thesis. Permission is now automatically granted; please pay special attention to the implications paragraph below. The Copyright Subcommittee of the Joint Board/Council Committees on Publications approved the following:

> Copyright permission for published and submitted material from theses and dissertations
> ACS extends blanket permission to students to include in their theses and dissertations their own articles, or portions thereof, that have been published in ACS journals or submitted to ACS journals for publication, provided that the ACS copyright credit line is noted on the appropriate page(s).
>
> Publishing implications of electronic publication of theses and dissertation material
> Students and their mentors should be aware that posting of theses and dissertation material on the Web prior to submission of material from that thesis or dissertation to an ACS journal may affect publication in that journal. Whether Web posting is considered prior publication may be evaluated on a case-by-case basis by the journal's editor. If an ACS journal editor considers Web posting to be "prior publication", the paper will not be accepted for publication in that journal. If you intend to submit your unpublished paper to ACS for publication, check with the appropriate editor prior to posting your manuscript electronically.

If your paper has **not** yet been published by ACS, we have no objection to your including the text or portions of the text in your thesis/dissertation in **print and microfilm formats**; please note, however, that electronic distribution or Web posting of the unpublished paper as part of your thesis in electronic formats might jeopardize publication of your paper by ACS. Please print the following credit line on the first page of your article: "Reproduced (or 'Reproduced in part') with permission from [JOURNAL NAME], in press (or 'submitted for publication'). Unpublished work copyright [CURRENT YEAR] American Chemical Society." Include appropriate information.

If your paper has already been published by ACS and you want to include the text or portions of the text in your thesis/dissertation in **print or microfilm formats**, please print the ACS copyright credit line on the first page of your article: "Reproduced (or 'Reproduced in part') with permission from [FULL REFERENCE CITATION.] Copyright [YEAR] American Chemical Society." Include appropriate information.

Submission to a Dissertation Distributor: If you plan to submit your thesis to UMI or to another dissertation distributor, you should not include the unpublished ACS paper in your thesis if the thesis will be disseminated electronically, until ACS has published your paper. After publication of the paper by ACS, you may release the entire thesis (**not the individual ACS article by itself**) for electronic dissemination through the distributor; ACS's copyright credit line should be printed on the first page of the ACS paper.

Use on an Intranet: The inclusion of your ACS unpublished or published manuscript is permitted in your thesis in print and microfilm formats. If ACS has published your paper you may include the manuscript in your thesis on an intranet that is not publicly available. Your ACS article cannot be posted electronically on a publicly available medium (i.e. one that is not password protected), such as but not limited to, electronic archives, Internet, library server, etc. The only material from your paper that can be posted on a public electronic medium is the article abstract, figures, and tables, and you may link to the article's DOI or post the article's author-directed URL link provided by ACS. This paragraph does not pertain to the dissertation distributor paragraph above.

Questions? Call +1 202/872-4368/4367. Send e-mail to copyright@acs.org or fax to +1 202-776-8112. 10/10/03, 01/15/04, 06/07/06

JOHN WILEY AND SONS LICENSE TERMS AND CONDITIONS

Aug 05, 2013

This is a License Agreement between Jeremy Chris P Reyes ("You") and John Wiley and Sons ("John Wiley and Sons") provided by Copyright Clearance Center ("CCC"). The license consists of your order details, the terms and conditions provided by John Wiley and Sons, and the payment terms and conditions.

All payments must be made in full to CCC. For payment instructions, please see information listed at the bottom of this form.

License Number	3202540828331
License date	Aug 05, 2013
Licensed content publisher	John Wiley and Sons
Licensed content publication	Angewandte Chemie International Edition
Licensed content title	Bioinspired Total Synthesis of Agelastatin A
Licensed copyright line	Copyright © 2012 WILEY-VCH Verlag GmbH & Co. KGaA, Weinheim
Licensed content author	Jeremy Chris P. Reyes,Daniel Romo
Licensed content date	Jun 11, 2012
Start page	6870
End page	6873
Type of use	Dissertation/Thesis
Requestor type	Author of this Wiley article
Format	Print and electronic
Portion	Full article
Will you be translating?	No
Total	0.00 USD
Terms and Conditions	

TERMS AND CONDITIONS

This copyrighted material is owned by or exclusively licensed to John Wiley & Sons, Inc. or one of its group companies (each a "Wiley Company") or a society for whom a Wiley Company has exclusive publishing rights in relation to a particular journal (collectively "WILEY"). By clicking "accept" in connection with completing this licensing transaction, you agree that the following terms and conditions apply to this transaction (along with the billing and payment terms and conditions established by the Copyright Clearance Center Inc., ("CCC's Billing and Payment terms and conditions"), at the time that you opened your